NUREG/IA-0533

International Agreement Report

RELAP5, TRACE and APROS Model Benchmark for the IAEA SPE-4 Experiment

Prepared by:
R. Orosz, T. Varju, Á. Aranyosy, V. Holl, T. Hajas & A. Aszódi

Budapest University of Technology and Economics
Institute of Nuclear Techniques
Műegyetem rkp. 3.
1111 Budapest, Hungary

K. Tien, NRC Project Manager

Division of Systems Analysis
Office of Nuclear Regulatory Research
U.S. Nuclear Regulatory Commission
Washington, DC 20555-0001

Manuscript Completed: October 2021
Date Published: September 2022

Prepared as part of
The Agreement on Research Participation and Technical Exchange
Under the Thermal-Hydraulic Code Applications and Maintenance Program (CAMP)

Published by
U.S. Nuclear Regulatory Commission

AVAILABILITY OF REFERENCE MATERIALS IN NRC PUBLICATIONS

NRC Reference Material

As of November 1999, you may electronically access NUREG-series publications and other NRC records at NRC's Library at www.nrc.gov/reading-rm.html. Publicly released records include, to name a few, NUREG-series publications; *Federal Register* notices; applicant, licensee, and vendor documents and correspondence; NRC correspondence and internal memoranda; bulletins and information notices; inspection and investigative reports; licensee event reports; and Commission papers and their attachments.

NRC publications in the NUREG series, NRC regulations, and Title 10, "Energy," in the *Code of Federal Regulations* may also be purchased from one of these two sources.

1. **The Superintendent of Documents**
   U.S. Government Publishing Office
   Washington, DC 20402-0001
   Internet: https://bookstore.gpo.gov/
   Telephone: (202) 512-1800
   Fax: (202) 512-2104

2. **The National Technical Information Service**
   5301 Shawnee Road
   Alexandria, VA 22312-0002
   Internet: https://www.ntis.gov/
   1-800-553-6847 or, locally, (703) 605-6000

A single copy of each NRC draft report for comment is available free, to the extent of supply, upon written request as follows:

Address: **U.S. Nuclear Regulatory Commission**
Office of Administration
Digital Communications and Administrative Services Branch
Washington, DC 20555-0001
E-mail: Reproduction.Resource@nrc.gov
Facsimile: (301) 415-2289

Some publications in the NUREG series that are posted at NRC's Web site address www.nrc.gov/reading-rm/doc-collections/nuregs are updated periodically and may differ from the last printed version. Although references to material found on a Web site bear the date the material was accessed, the material available on the date cited may subsequently be removed from the site.

Non-NRC Reference Material

Documents available from public and special technical libraries include all open literature items, such as books, journal articles, transactions, *Federal Register* notices, Federal and State legislation, and congressional reports. Such documents as theses, dissertations, foreign reports and translations, and non-NRC conference proceedings may be purchased from their sponsoring organization.

Copies of industry codes and standards used in a substantive manner in the NRC regulatory process are maintained at—

The NRC Technical Library
Two White Flint North
11545 Rockville Pike
Rockville, MD 20852-2738

These standards are available in the library for reference use by the public. Codes and standards are usually copyrighted and may be purchased from the originating organization or, if they are American National Standards, from—

American National Standards Institute
11 West 42nd Street
New York, NY 10036-8002
Internet: www.ansi.org
(212) 642-4900

Legally binding regulatory requirements are stated only in laws; NRC regulations; licenses, including technical specifications; or orders, not in NUREG-series publications. The views expressed in contractor prepared publications in this series are not necessarily those of the NRC.

The NUREG series comprises (1) technical and administrative reports and books prepared by the staff (NUREG–XXXX) or agency contractors (NUREG/CR–XXXX), (2) proceedings of conferences (NUREG/CP–XXXX), (3) reports resulting from international agreements (NUREG/IA–XXXX), (4) brochures (NUREG/BR–XXXX), and (5) compilations of legal decisions and orders of the Commission and Atomic and Safety Licensing Boards and of Directors' decisions under Section 2.206 of NRC's regulations (NUREG–0750).

NUREG/IA-0533

International Agreement Report

RELAP5, TRACE and APROS Model Benchmark for the IAEA SPE-4 Experiment

Prepared by:
R. Orosz, T. Varju, Á. Aranyosy, V. Holl, T. Hajas & A. Aszódi

Budapest University of Technology and Economics
Institute of Nuclear Techniques
Műegyetem rkp. 3.
1111 Budapest, Hungary

K. Tien, NRC Project Manager

Division of Systems Analysis
Office of Nuclear Regulatory Research
U.S. Nuclear Regulatory Commission
Washington, DC 20555-0001

Manuscript Completed: October 2021
Date Published: September Year

Prepared as part of
The Agreement on Research Participation and Technical Exchange
Under the Thermal-Hydraulic Code Applications and Maintenance Program (CAMP)

Published by
U.S. Nuclear Regulatory Commission

ABSTRACT

One-dimensional thermal-hydraulic system codes are often used to predict and investigate different transient scenarios of NPPs. Throughout the years, numerous experimental facilities were constructed in order to simulate the accident behavior of different types of reactors. A frequently studied topic is, whether the simulation codes primarily designed to investigate western-type PWRs could describe the processes of the Russian-type reactors properly.

The main objective of this study is to investigate the SPE-4 experiment conducted on the Hungarian PMK-2 test facility with multiple system codes simultaneously. The integral test facility was operated at nominal pressures and temperatures identical of its reference plant (VVER-440/213), while the volume and power scaling ratios were 1:2070. The current experiment deals with a cold leg break of 7.4%.

The obtained results of the calculations performed with RELAP5, TRACE and the Finnish APROS codes were evaluated by comparing them to the measurement data sets. The qualitative assessment showed that each code is capable of predicting the characteristics of the major processes taking place in the reactor. In addition, a detailed quantitative analysis has also been performed with the original and improved FFT and SAR based methods. Finally, several suggestions had been made regarding the models and the methods used.

TABLE OF CONTENTS

LIST OF FIGURES

LIST OF TABLES

ACKNOWLEDGMENTS

We wish to express our gratitude to József Bánáti and Róbert Dániel Rádi for helping and supporting our work with their valuable ideas and comments, especially about the application of RELAP5 and the SNAP environment.

Special thanks are owed to Dr. Andrej Prošek (at the Jožef Stefan Institute, Ljubljana, Slovenia) for providing us with useful material and knowledge about the FFTBM methodology and valuable data sets.

ABBREVIATIONS AND ACRONYMS

AA	Average Amplitude
ACAP	Automated Code Assessment Program
AEKI	Atomic Energy Research Institute
AF	Accuracy Factor
BME	Budapest University of Technology and Economics
CAMP	Code Application and Maintanance Program
CL	Cold Leg
DC	Downcomer
ECCS	Emergency Core Cooling System
EFW	Emergency Feedwater
FFT	Fast Fourier Transform
FFTBM	Fast Fourier Transformation Based Method
HA	Hydroaccumulator
HL	Hot Leg
HPIS	High Pressure Injection System
HS	Heat Structure
HTC	Heat Transfer Coefficient
IAEA	International Atomic Energy Agency
LOFT	Loss Of Fluid Test
LPIS	Low Pressure Injection System
MCP	Main Circulation Pump
ND	Number of Discrepancies
NPP	Nuclear Power Plant
NRC	Nuclear Regulatory Commission
NTI	Intitute of Nuclear Techniques
PMK	Paksi Modell Kísérlet (in Hungarian)
PRZ	Pressurizer
RPV	Reactor Pressure Vessel
SARBM	Stochastic Approximation Ration Based Method
SBLOCA	Small Break Loss Of Coolant Accident
SFT	Sink Fluid Temperature
SG	Steam Generator
SIT	Safety Injection Tank

SPE	Standard problem exercise
SNAP	Symbolic Nuclear Analysis Package
UP	Upper Plenum
VA	Variable Accuracy
VVER	Water-Water Energetic Reactor
WF	Weighted Frequency

1 INTRODUCTION

The criteria for the construction of new nuclear power plant units have been significantly tightened worldwide as a result of the events in Fukushima in 2011. For the territory of the European Union, the Council Directive 2014/87/Euratom of 8 July 2014 amending Directive 2009/71/Euratom establishing a Community framework for the nuclear safety of nuclear installations, imposed obligations on the Member States to ensure that the national framework requires that 'nuclear power plants should be designed, constructed and operated with the objectives of preventing accidents and, should an accident occur, mitigating its effects and avoiding off-site contamination', and 'regulatory authorities should ensure that these objectives are applied in order to identify and implement appropriate safety improvements at existing plants'.

In line with these objectives the Council Directive 2014/87/Euratom of 8 July 2014 in SECTION 2 (Specific obligations) under Article 8a prescribes the following:

> *"Nuclear safety objective for nuclear installations*
>
> *1. Member States shall ensure that the national nuclear safety framework requires that nuclear installations are designed, sited, constructed, commissioned, operated and decommissioned with the objective of preventing accidents and, should an accident occur, mitigating its consequences and avoiding:*
>
> *(a) early radioactive releases that would require off-site emergency measures but with insufficient time to implement them;*
>
> *(b) large radioactive releases that would require protective measures that could not be limited in area or time.*
>
> *2. Member States shall ensure that the national framework requires that the objective set out in paragraph 1:*
>
> *(a) applies to nuclear installations for which a construction licence is granted for the first time after 14 August 2014;*"

Accordingly, the Hungarian nuclear safety regulations have been amended and thus the two new VVER-1200/V-527 nuclear power plant units under design on the Paks site must meet these requirements.

Analyzes performed with various thermo-hydraulic system codes can effectively support the design and operation work and verify compliance with the requirements.

Due to the above, it is really important for Hungary to have a sufficient number of professionals with adequate experience in the use of these kinds of softwares. One of the main goals of this project in the Budapest University of Technology and Economics Institute of Nuclear Techniques (BME NTI) is to get acquainted with the RELAP5 and TRACE codes and gain relevant experience through a well-known benchmark task. Later, based on this experience, our main target is to build a VVER-1200 full plant model and investigate various transients, with which we could effectively support the design and operation of the new units.

The RELAP5/MOD3.3 and TRACE system codes were made available for selected Hungarian institutions in the framework of a CAMP (Code Application and Maintenance Program) agreement signed by the US Nuclear Regulatory Commission (US NRC) and the Hungarian Atomic Energy Authority (HAEA) in August 2019. BME NTI is one of the organizations which were approved by HAEA to get access to the computer codes under the CAMP agreement.

In the Institute there is years of professional experience with the licensed APROS code, developed by the Finnish VTT Technical Research Centre and Fortum Oyj company. Despite the fact that APROS is not a CAMP code, we found it useful to involve it in this project by comparing the simulation results with those of the RELAP5 and TRACE codes.

The current study is primarily based on the findings of our recent article [19] dealing with the SPE-4 experiment. Our report first briefly introduces the PMK-2 facility and the SPE-4 benchmark experiment performed on it. Then, a detailed description is presented for the RELAP5, TRACE and APROS models. Furthermore, an existing RELAP model was provided by Paks II. Ltd [4]. This model served as a guideline in the modeling of more complicated system elements. Following that, a thorough qualitative and quantitative analysis of the obtained results is presented. In the final section of this report, the major findings and suggestions are summarized. A non-exhaustive collection of figures that had proven to be useful in constructing the model geometry are presented in the Appendix.

2 DESCRIPTION OF THE PMK-2 FACILITY

The PMK-2 (AEKI, Budapest, Hungary) is an experimental facility, which served as a full-pressure and full-temperature thermo-hydraulic test rig of the VVER type pressurized water reactors. The design of the test facility started in the early 80's, concurrently to the installation finish of its four reference units (1983-1987) of the Paks NPP in Hungary. Accordingly, majority tests conducted on PMK-2 served the purpose of investigating system response of VVER-440/213 on SBLOCA transients. Both the volume and power scaling ratios across the facility are 1:2070, however, due to the importance of gravitational forces in both single- and two-phase flow, the elevation ratio of 1:1 has been applied (except for the lower plenum and pressurizer). This arrangement (along with the applied control system) assures the near identical initial state to that of the reference power plant.

In the experiments, a vertical pipe parallel to the reactor vessel was used as an external downcomer. Core model is equipped with a bundle of 19 fuel rods, which have a controllable electrical heating for the decay heat modeling. The six loops of the plant are modelled by a single active loop that includes the hot leg, the pressurizer, the steam generator and the cold leg. The primary main circulating pump is accommodated in a by-pass line with the preheater. Pump trip simulation is achieved by controlling flow rate by PV11 valve in the by-pass line in a prescribed manner. Natural circulation takes place in the 'normal' cold leg opened during the by-pass closure.

The instrumentation of the PMK-2 facility is different in nature and much more extensive than that of the real power plant, because it is an experimental facility built to study transients with two-phase flow. In addition to devices that measure coolant pressure and temperature at a number of points, differential pressure and collapsed water level measurements are also connected to the primary circuit to facilitate a better understanding of the process of two-phase transients. The primary circuit also includes several volumetric flow rate meters and thermocouples measuring the temperature of the metal structures. The detailed description of the facility can be found in the literature [1]. Simplified design drawings of main components taken from [1] and [2] are given in the Appendix.

3 THE SPE-4 EXPERIMENT

The Standard Problem Exercise no. 4 (SPE-4) [3] was part of a comprehensive code validation series conducted on the PMK-2 facility organized by the International Atomic Energy Agency (IAEA). The main objectives of such experiments was to create a VVER specific data base and provide a possibility to the interested international community for joint code validation exercises. The 1st (1986), the 2nd (1987) and the 4th (1993) exercises were based on SBLOCA tests, with a cold leg break of 7.4%, considering different availability of ECC systems. The 3rd (1989) exercise was a VVER-specific case namely the opening of the steam generator (SG) hot collector cover.

The SPE-4 experiment can be characterized as follows:

- SBLOCA in the cold leg equivalent to a 7.4% break of the reference NPP
- Transient initiation at nominal operating parameters
- Complete isolation of the secondary side at the beginning of the transient
- Given pump coast-down characteristics
- Secondary side bleeding through valve PV23
- Availability of two hydroaccumulators modeling 3 tanks of the reference plant
- Unavailability of high pressure injection system (HPIS)
- Availability of low pressure injection system (LPIS)
- Availability of emergency feed water system (EFWS)

4 RELAP5 MODEL

4.1 Thermo-Hydraulic Model

The model of the experiment was made using version 3.0.2 of the SNAP (Symbolic Nuclear Analysis Package) environment. Calculations were performed using RELAP5/MOD3.3 Patch 05, version "lb". Parameters regarding the model's geometry and its control systems were set according to the data specified in technical documents [1] and [3]. Initial thermal-hydraulic properties, such as temperatures and pressures have been set close to the nominal ones in order to minimize the required runtime to reach the steady-state. The model development in RELAP5 resulted in many model versions of which the final one is presented below. The nodalization scheme of the PMK-2 facility applied, shown on Figure 4.1 and Figure 4.2, is based mainly on an older APROS model discussed in [2]. The model includes the following subsystems of the test facility, with the single junctions omitted (subsystem abbreviations and component numbers are given in brackets to facilitate identification of components):

- **Cold leg circulation branch (CLEG)**: CLPIP_1(802), CLPIP_2(804), CLPIP_3(806), CLPIP_4(808), MV11_1(17), MV_11(809), MV11_2(29), CLPIP_5(810), CLPIP_6(812), CLPIP_7(814), CLPIP_8(816)
- **Downcomer (DC)**: DC_TIP_1(829), DC_TOP_2(876), DC_MID(1), DC_BOT(2)
- **Lower plenum (LP)**: LOW_PL(826)
- **Core (CORE)**: CORE_IN(4), CORE(5), CORE_OUT(12)
- **Upper plenum + pressure vessel head (RPV)**: UP_BOT(13), UP_L1(971), UP_L2(973), UP_L3(975), UP_MID(15), UP_TOP(16), UH_BOT(970), UH_TOP(18), UH_MID(33)
- **Hydroaccumulator SIT-1 (SIT1)**: SIT_1(46), MV91_1(998), MV91_2(31), MV_91(823), SIT1_P1(882), SIT1_P2(830)
- **Hydroaccumulator SIT-2 (SIT2)**: SIT_1(993), MV92_1(996), MV92_2(30), MV_92(995), SIT2_P1994)
- **Hot leg (HLEG)**: HLPIP_1(827), HLPIP_2(832), HLPIP_3(833), HLPIP_4(842), HLPIP_5(836), HLPIP_6(854)
- **Pressurizer (PRZ)**: SP_PIP1(978), PV12_1(981), PV12(979), PRZ(845), SURGE_PIP(36), PRZ_PMP(39), PRZ_PIP(38), PRZ_VOL(41)
- **ENVIRONMENT (ENV)**: ENV_HEAT(849), ENV_SRC(849), E_PIP(848)
- **BREAK**: MV_31(983), BREAK_P(982), CNTM(987)
- **High-pressure injection system (HPIS)**: MV_77(990), HPIS_PIP(989), HPIS_PMP(35), HPIS_TA(991)
- **Steam generator primary side (SGP)**: SGPIP_1(599), SGPIP_2(611), SGPIP_3(8), SGPIP_4(610), SGPIP_5(606)
- **Steam generator secondary side (SGS)**: SGPIP_6(907), SGPIP_7(904), SGPIP_8(902), SGPIP_9(917), PV_23(918), ATM(919), SEPTR(906), FW_PMP(901), FEEDW(900), SGPIP_11(905), SGPIP_12(912), PV_22(913), PV_22_a(915), SGPIP_10(914), ISO(916), EFS(908), EFS_PMP(42)
- **BYPASS (BYP)**: BY_BR1(748), BY_TA_1(850), MV12_1(14), MV_12(926), MV12_2(27), BY_PIP1(752), BYPIP_2(754), PMK_PUMP(171), BYPIP_3(756), CLHEAT(928), BYPIP_4(927), PV11_1(3), PV_11(925), PV11_2(28), BY_TA_2(762), BY_BR2(764)

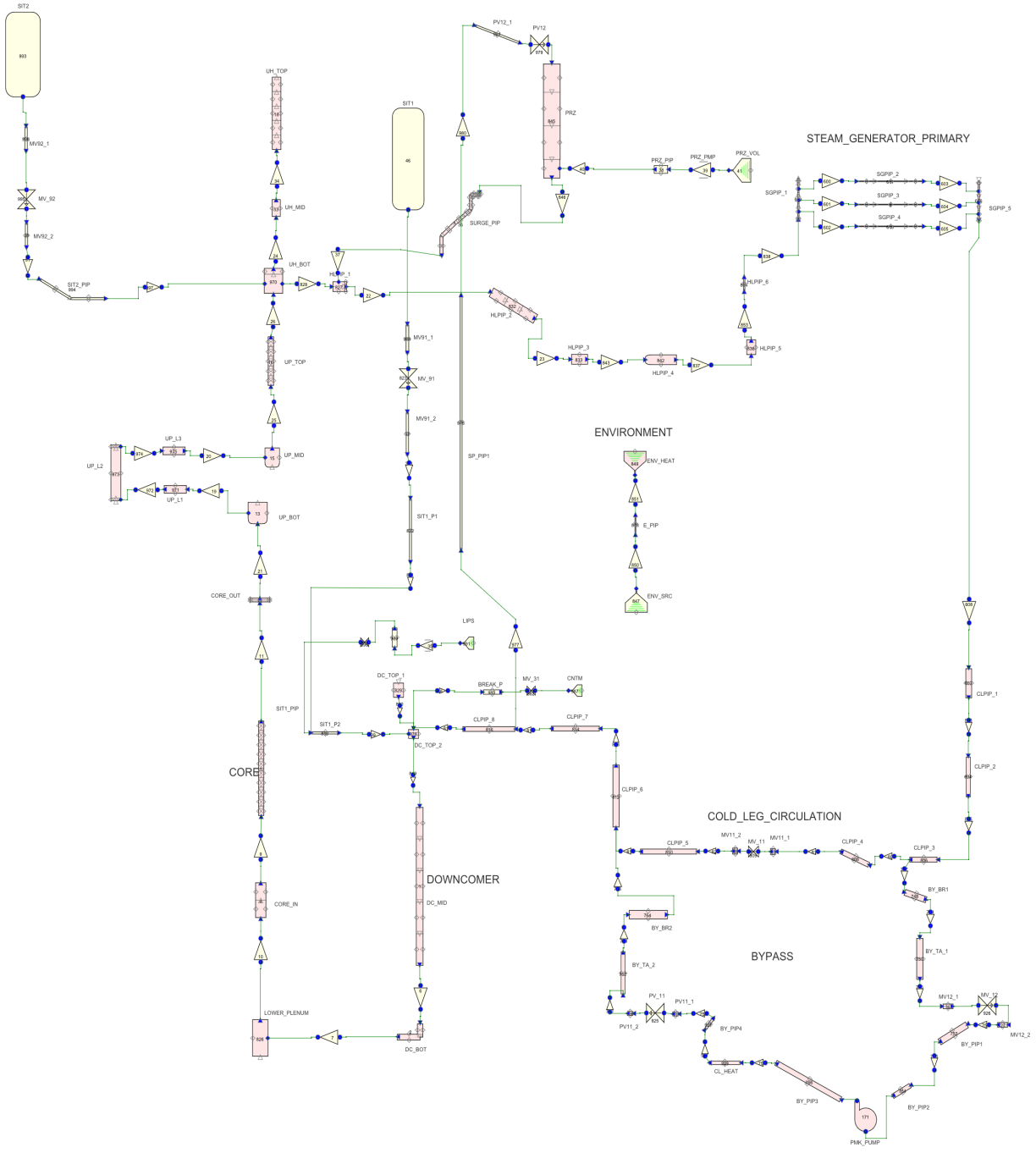

Figure 4.1 Nodalization Scheme of the Primary Circuit in the RELAP5 Model

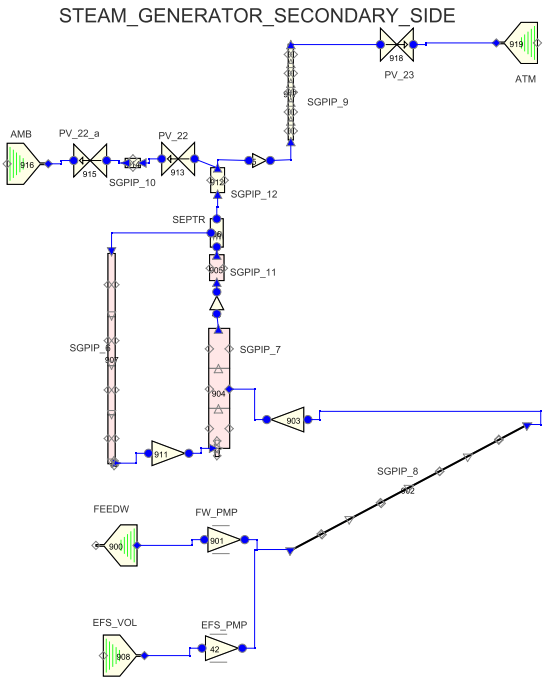

Figure 4.2 Nodalization Scheme of the Secondary Circuit in the RELAP5 Model

Considering the requisites of modeling the system, the following remarks were made:

- In case of a scaled-down facility, the contribution of heat losses to the major processes is a matter of great importance. Therefore, the walls of pipe and branch components has been modeled through heat structures, which are connected to external (ambient) points.
- To ensure that a sufficient amount of coolant was present in the system (the liquid level in the pressurizer reaches its measured initial value) during the steady-state calculation, the pressurizer was equipped with a level-control unit.
- Considering that the connection point elevations of PIPE components can't be given arbitrarily, loop closure was achieved by dividing the components into nodes unevenly, which in some cases resulted in small control volumes.
- The active length of the core was divided into 10 nodes.
- In the steam generator model, a separator component ensures the phase separation. The crossflow connections between the downcomer and the riser chamber were deleted due to problems with numerical stability.
- Considering the amount of data required for the pump component, the pump curves were extracted from the referred RELAP model.
- Hydro-accumulators were modeled using the ACCUMULATOR component of RELAP5; however, the surge lines were modeled independently.
- In steady state, due to the limits of one-dimensional flow simulation some component volumes become stagnant (there is no flow through the volume). Consequently, as a result of the thermal contact the temperature of the aforementioned regions would decrease until it reaches equilibrium with the environment. To avoid that, the heat

transfer coefficients in these volumes were set to zero during the steady-state simulation and were reset to their nominal values at the start of the transient.

- In order to ensure that steady state conditions are attained, the transient starts at 1500 seconds. In steady-state the current flows through the bypass branch, while after the pump coast-down, the flow traverses the circulation branch.
- In the measurement, the pressure limitation function of valve PV23 was not used since its pressure limits were not reached. It was concluded that in order to accurately model the physical phenomena, the limitation function was not implemented, even if the simulations were to indicate its supposed actuation.
- It was found that the used version of SNAP did not support the Ransom-Trapp critical flow model. The model was exported to ASCII format and the subcooled two-phase and overheated discharge coefficients were set to 0.46 in case of PV23. This adjustment was necessary and was made similarly by numerous professionals as shown in [3], with different values for the coefficients.
- For the simulation, a minimum time step of 10 μs was used. The maximum time step allowed was 0.01 s.

4.2 Control Systems and Heat Structure Modeling

Numerous control systems were implemented in the model, of which the functions are described in the following paragraphs. Control systems are presented on Figure 4.3, Figure 4.4 and Figure 4.5.

- **BREAK**: Opens the valve modeling the break at 1500 s. The pressure of the tank downstream of the break valve is not constant as a sudden rise in the first few seconds of the transient is followed by a continuous decrease. This variation is given to the code as a boundary condition as seen in Table 4.14.
- **SCRAM**: In case the value of pressure signal PR21 decreases under 11.15 MPa, the modeling of decay heat is initiated. The decay heat power was given as a function of time. Before the SCRAM, a constant heating power of 665.1 kW is defined. Following the SCRAM, power values are calculated by using the multiplier factors presented in Table 4.13.
- **SIT_1, SIT_2**: The valves isolating accumulators SIT1 and SIT2 open if the pressure reaches their respective set-point (5.90 MPa). The valves are shut when the liquid level in the accumulators reach 0.245 and 1.035 meters.
- **FLOW**: The steady-state flow rate of 4.91 kg/s in the primary circuit was set by a PI controller, controlling the valve stem position of SERVO VALVE PV11.
- **COAST-DOWN**: Pump coast-down was modeled by closing the valve PV11. Coast-down is initiated when pressure PR21 reaches 9.21 MPa. Then, after 150 seconds the simultaneous closing of MOTOR VALVE MV11 and opening of MOTOR VALVE MV12 allows the fluid to flow through in the circulation branch. The valve stem versus time data set for PV11 was discretized from the measured cold leg mass flow curve FL53 and FL54. The rather complicated control scheme is using the scalar and additive constant properties of the sum blocks for linear interpolation and logical trips for bucketing. Interpolation is performed for multiplier values. The purpose of this

arrangement is to achieve the same effect as an else-if structure in a programming language, the interpolation parameters being the variables of which the values change for each case. Due to these cases being mutually exclusive, the signals of each branch weighted by the outputs of each trip can be summed and the final output signal will correspond to the time elapsed since the actuation of the coast-down. Then, the output is multiplied by a factor of 0.129134, which is the valve stem position obtained from steady-state calculations. The time elapsed since the coast-down is obtained in a way that is analogous with a while loop. While the pressure is greater than the given set-point, the dt time step values are summed. Then, with a simple subtraction block, the time difference is calculated. Switching between the steady state and transient control was achieved by weighting the signals of the PI controller and the coast-down block with the trip signals of the set pressure. It should be noted however, that a data table initiated by a timer would have also been sufficient. In order to facilitate the parametrization of the model, the valve stem position multipliers are presented in Table 4.12 as a function of time elapsed after the transient. Control scheme FALSE_TRIP was used to stop the pump.

- **SPRAY**: In steady-state conditions, a constant mass flow of 8.5E-4 kg/s is maintained so that the pressurizer does not become stagnant. When the transient is initiated, the valve PV12 is shut off and the injection from the cold leg terminates. The input for the PI control block is the error of the simulated spray flow rate with respect to its nominal value.
- **PRESSURE_HEATING**: Pressure control of the primary circuit was achieved via a PI control block which adjusts the heating power of the pressurizer. The initiation of the transient disables the heating of the pressurizer. The output of the PI controller serves as the control variable for the heat structure 54 (PRZ). The maximum heating power of the pressurizer is 3200 Watts which is used as a multiplier component in the aforementioned heat structure. The input of this control block was the error of the upper plenum pressure with respect to its nominal value.
- **SG_LEVEL**: The fluid-level on the secondary side of the steam generator is controlled by a PI control block. The feedwater pump and SERVO VALVE PV21 are modelled by a time-dependent junction which supplies a mass flow such as the liquid level in the downcomer reaches the initial measured value of 8.95 m. The control logic was implemented such as under steady state, a minimum of 0.35 kg/s flow rate is maintained. The trip of this unit is initiated by the transient, using the trip function of the time-dependent junction. The input of this block is the collapsed level in the downcomer subtracted from the nominal liquid level.
- **SG_PRESSURE**: The secondary side pressure is levelled by a PI control block controlling the valve stem position of steam valve PV22. After the transient, the secondary side is isolated, PV23 and PV22_a are shut. The input of this control block was the error of the steam generator secondary side pressure with respect to its nominal value.
- **BLEED**: The secondary side relief valve PV23 is opened 150 seconds after the initiation of pump coast-down, realizing the bleed function on the secondary side. Pressure limitation was not implemented in this case since in the measurement, its opening set-point was not reached.

- **CL_HEAT**: Following the instructions in [1], 18.5 kW of thermal power was introduced to hydraulic component CLHEATER which serves to model the heat generated by the pump. The heating power is set to 0 after the transient is initiated, as presented in Table 4.18.
- **LPIS**: The low pressure injection system is actuated at the time pressure signal PR21 reaches 1.04 MPa after which a mass flow of 0.042 kg/s is supplied continuously until the end of the transient. The input was given as data table, provided in Table 4.16. The input for this data is the time elapsed since the actuation of the signal as defined on Figure 4.4. This follows the same principle as presented for the flow control.
- **STAGNANT**: For stagnant components, for the previously mentioned reasons, heat transfer coefficients are set to zero under steady state conditions and are set to 7.5 W/m^2K at the start of the transient using Table 4.19.
- **EFWIS**: The emergency feedwater system starts to inject after the secondary side pressure reaches 0.93 MPa and supplies a mass flow of 0.042 kg/s to the steam generator. The corresponding data table is Table 4.17. The input for this data is the time elapsed since the actuation of the signal as defined on Figure 4.5. This follows the same principle as presented for the flow control.
- **PRZ_LEV**: The measured initial liquid level (1.32 m) in the pressurizer is achieved by pumping liquid into the volume following the output signal of a PI control block. The input to the PI control block is the error of the collapsed level in the pressurizer with respect to the target value.

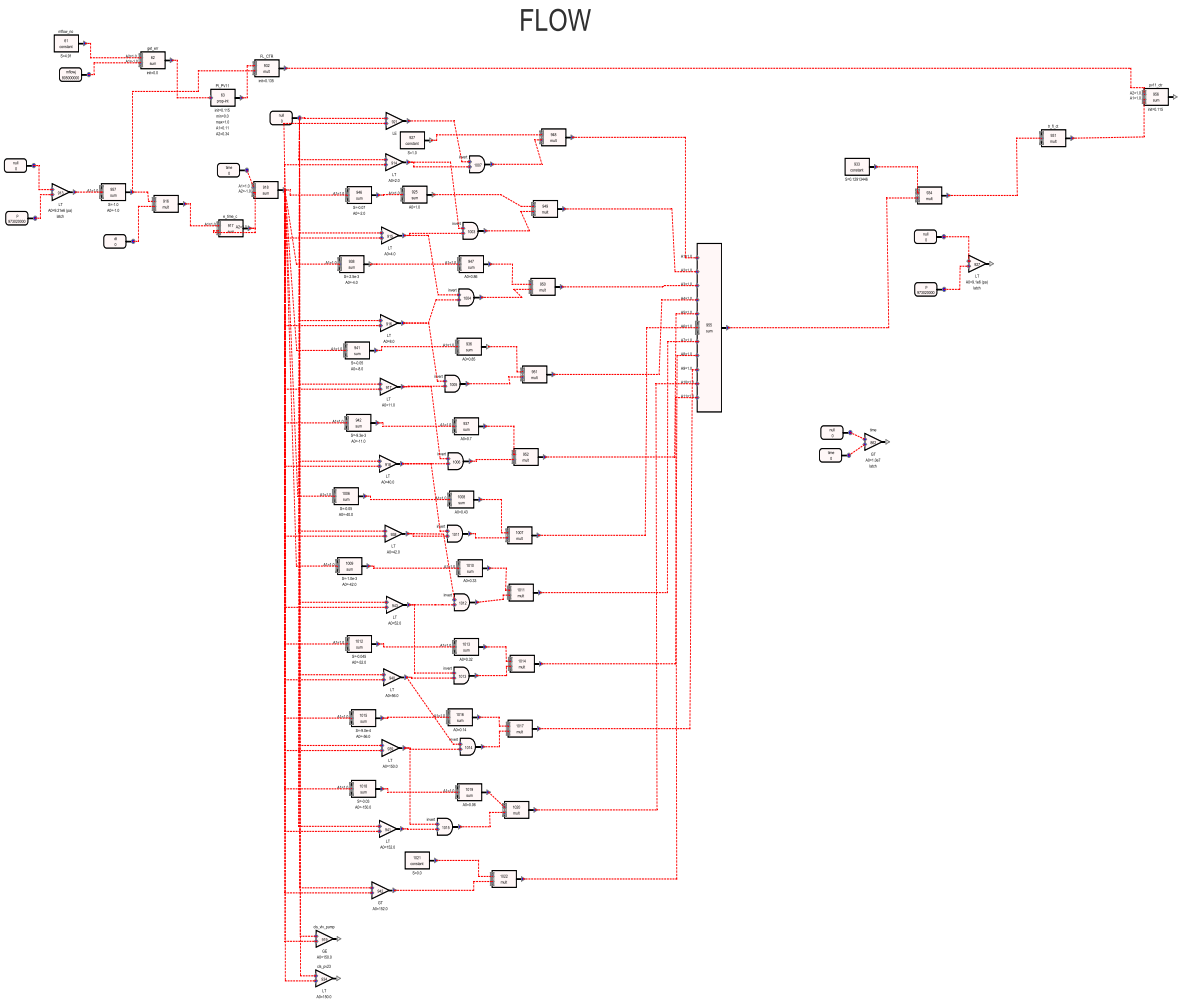

Figure 4.3 Pump Coast Down Control System in the RELAP5 Model

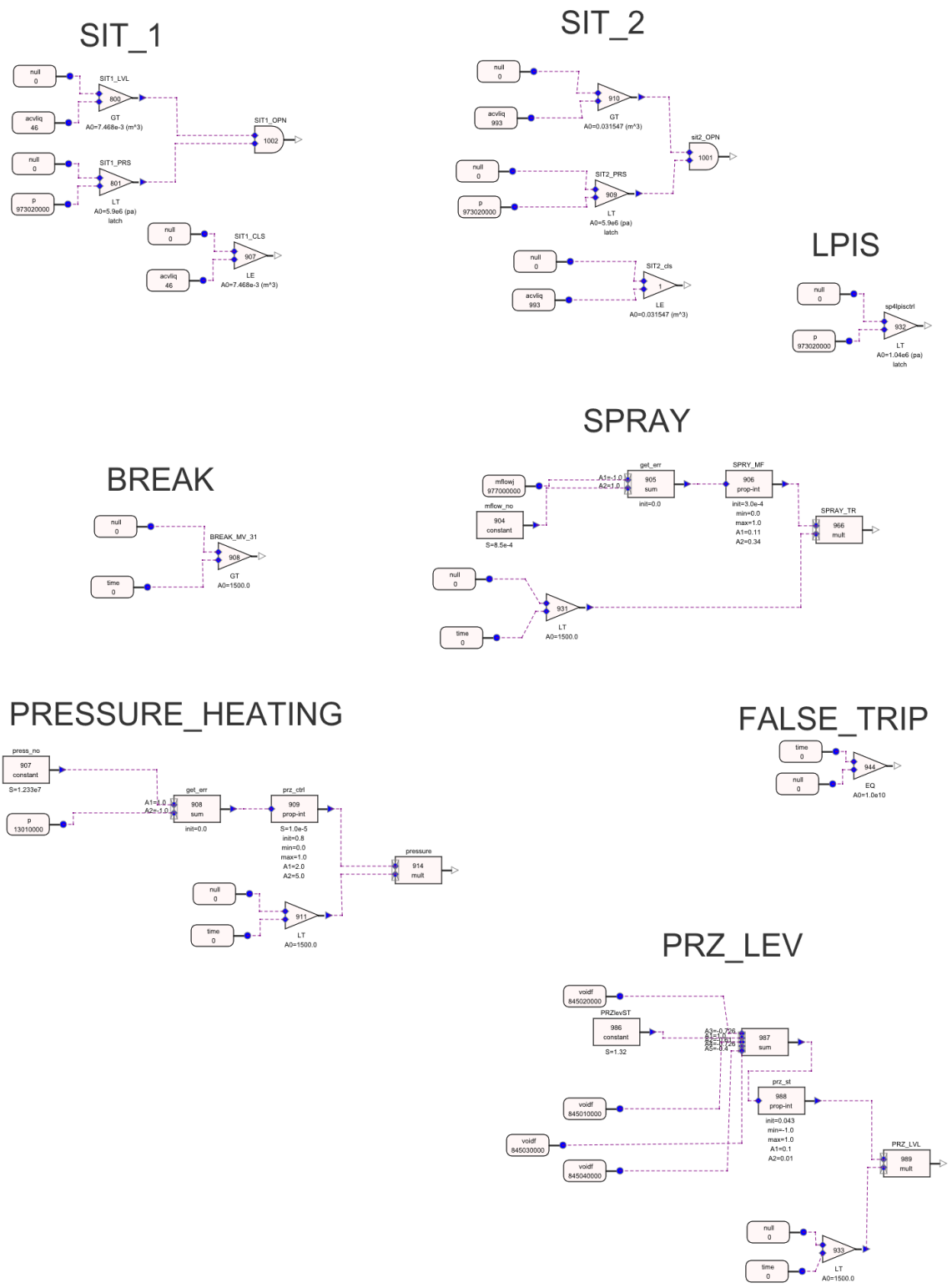

Figure 4.4 Primary Circuit Control Systems in the RELAP5 Model

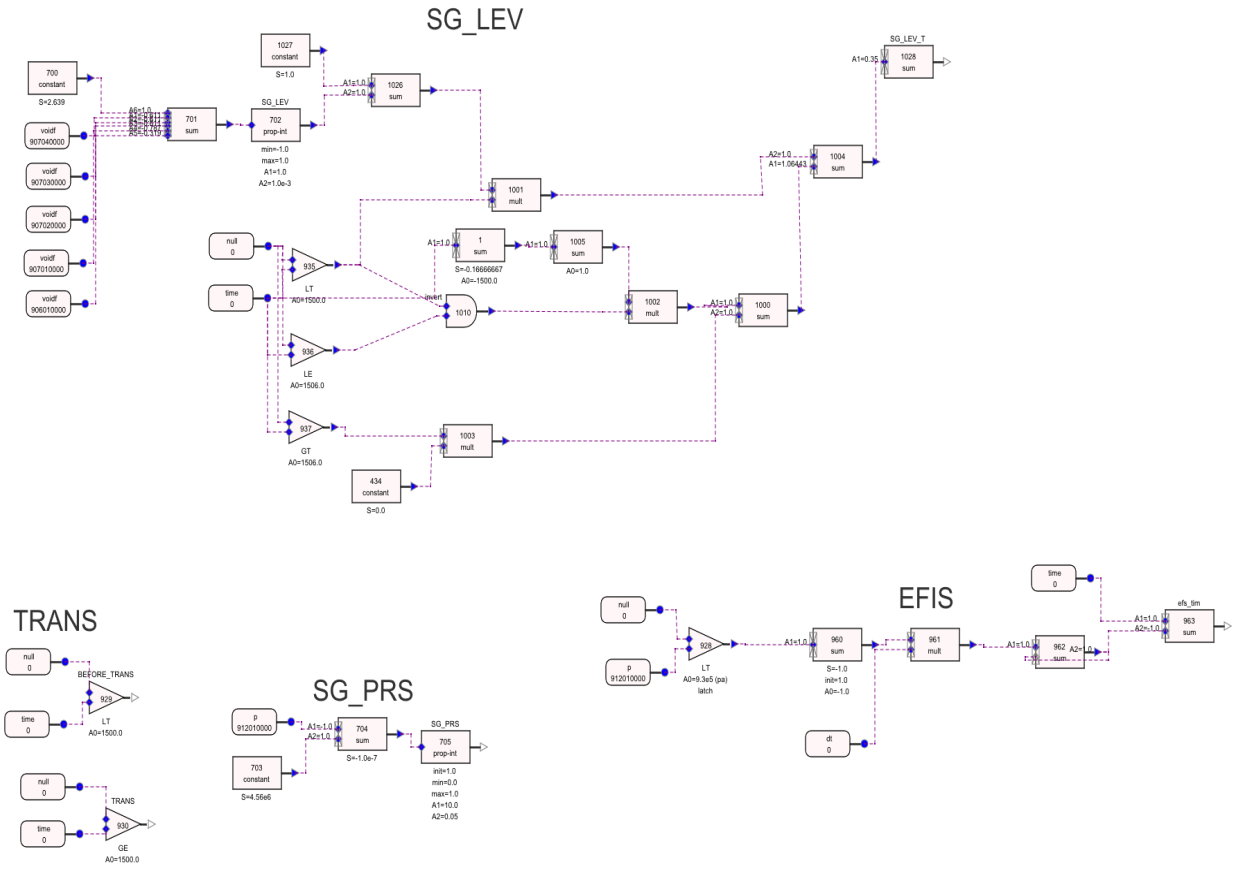

Figure 4.5 Secondary Circuit Control Systems in the RELAP5 Model

Numerous heat structures were defined for the model. Some important aspects of heat structure definitions have already been discussed, the remaining are summarized briefly in this paragraph. When defining the axial structures, in each node the heated length was set to at least 100 in order to ignore the axial profile. Stagnant components were connected to a time-dependent volume with ambient parameters. The two materials used were user-defined Material 1 used for structural components while material 2 used as the fuel bundle material. The corresponding data tables are Table 4.20 and Table 4.21. In case of the CORE, CL_HEAT and PRZ components, definition of heat source was necessary which was achieved by defining General Table components in the first two cases while in the latter case, the output of a PI controller was given in the source definitions. This value was converted into heating power by defining the source multiplier. For correctly defining the decay heat, the first step was to determine the time of SCRAM initiation by simulation and this value was added to the time steps presented in Table 4.13. For the steam generator, the heat structures are rather complex. Apart from the thermal coupling between the tubes and the secondary side it was necessary to define additional thermal connections with the cold and hot leg collectors of the primary side.

4.3 Measurements

For a thorough evaluation and comparison of the models, the measurements listed in Table 4.1 were simulated. The names of individual measurements correspond to those performed on the PMK-2 facility during the SPE-4 experiment. The measurement blocks are shown on Figure 4.6. A brief explanation is due for these blocks. In case of pipe and branch components, water level measurement was performed by calculating the collapsed level in each node between the given points. Then, the elevation from the reference level of the lowest component was added. In some cases where the elevation of the measurement gauges was inside a node, a minimum value was set for the parameters of the node in question. In case of ACCUMULATOR components, since surge lines were modeled independently, component signal ACVLIQ can be used with the inverse area multiplier. Then, the elevation of the accumulator bottom from reference level is added. Measuring pressure drops obviously consists of subtracting the pressures of the boundary nodes of the component in question, keeping in mind that for DP11, hydrostatic pressure needed to be taken into account. The correction to the pressure was calculated using the fluid density in the core multiplied by the geometrical elevation change between the two locations and the gravity. In case of wall temperatures which were extracted from the dataset of the corresponding heat structure, it has to be mentioned that no information was found about the exact radial location of the transducers used in the PMK-2 facility. In case of the steam generator collector temperatures and the secondary side fluid temperatures, the measurement locations were displaced with respect to the measurement because of the nodalization. In case of core temperatures TE12 and TE13, document [3] was ambiguous concerning the positioning of the transducers. Temperatures TE13, TE14 and TE15 were extracted from the same unit of the heat structure corresponding to the uppermost node of the core component. In the RELAP model, TE13 was measured at the uppermost node of the core component, while TE12 was measured 0.5 m lower. It has to be mentioned that only steam generator heater liquid level LE81 was measured, while LE82 was only implemented in the model. The reason for it is the difficulties were encountered with the level control of the steam generator. Due to high initial liquid level, the time-dependent junction component modeling the feedwater pump supplied a higher mass flow to the generator which in turn led to a significant amount of liquid pushed into the separator. To remedy this problem, the level control was implemented using liquid level LE82 in the input signal of the PI control block. Measurement blocks in RELAP are shown on Figure 4.6**.**

Table 4.1 List of Measurement Points and RELAP5 Variable Identifiers (Dependent Data ID Denotes the Identifier of the Data Set from which the Measured Quantity is Extracted)

ID	Measured quantity	Dependent Data ID
DP11	Core pressure drop	cntrlvar-967
DP16	Pump primary pressure drop	cntrlvar-968
DP61	SG primary side pressure drop	cntrlvar-981
FL00	Break mass flow	mflowj-982000000
FL53	Cold leg mass flow	mflowj-815000000
FL54	Cold leg mass flow	mflowj-817000000
LE11	Reactor liquid level	cntrlvar-975
LE21	Upper plenum liquid level	cntrlvar-971
LE22	Upper plenum liquid level	cntrlvar-985
LE23	Upper plenum liquid level	cntrlvar-304

Table 4.1 List of Measurement Points and RELAP5 Variable Identifiers (Dependent Data ID Denotes the Identifier of the Data Set from which the Measured Quantity is Extracted) (cont.)

LE31	Hot leg loop seal liquid level	cntrlvar-972
LE45	SG primary liquid level – hot leg	cntrlvar-978
LE46	SG primary liquid level – cold leg	cntrlvar-979
LE51	Cold leg liquid level	cntrlvar-973
LE61	Downcomer liquid level	cntrlvar-977
LE71	Pressurizer liquid level	cntrlvar-976
LE81	SG heater liquid level (secondary)	cntrlvar-980
LE82	SG downcomer liquid level (secondary)	cntrlvar-333
LE91	SIT1 liquid level	cntrlvar-964
LE92	SIT2 liquid level	cntrlvar-965
MA00	Total mass leak from the break	cntrlvar-306
PR00	Atmosphere pressure	p-987010000
PR21	Upper plenum pressure	p-18040000
PR71	Pressurizer pressure	p-84501000
PR81	Secondary circuit pressure	p-912010000
PR91	SIT1 pressure	p-46010000
PR92	SIT2 pressure	p-993010000
PW01	Core power	cntrlvar-969
TE00	Break flow temperature	tempf-983010000
TE11	Heater rod surface temperature	httemp-2800201
TE12	Heater rod surface temperature	httemp-2800801
TE13	Heater rod surface temperature	httemp-2801001
TE14	Heater rod surface temperature	httemp-2801001
TE15	Heater rod surface temperature	httemp-2801001
TE22	Upper plenum coolant temperature	tempf-15010000
TE23	Upper plenum wall temperature	httemp-6100101
TE24	Upper plenum coolant temperature	tempf-18050000
TE41	SG inlet coolant temperature	tempf-854010000
TE42	SG outlet coolant temperature	tempf-802010000
TE43	SG hot leg collector temperature	tempf-599050000
TE44	SG cold leg collector temperature	tempf-606010000
TE45	SG hot leg collector temperature	tempf-599040000
TE46	SG cold leg collector temperature	tempf-606020000
TE47	SG hot leg collector temperature	tempf-599050000
TE48	SG cold leg collector temperature	tempf-606050000
TE61	Downcomer inlet coolant temperature	tempf-1010000
TE62	Downcomer wall temperature	httemp-3500204
TE63	Core inlet coolant temperature	tempf-826010000
TE81	Feedwater temperature	tempf-902011000
TE83	Secondary side temperature	tempf-904040000

Table 4.1 List of Measurement Points and RELAP5 Variable Identifiers (Dependent Data ID Denotes the Identifier of the Data Set from which the Measured Quantity is Extracted) (cont.)

TE85	Secondary side temperature	tempf-904030000
TE87	Secondary side temperature	tempf-904010000

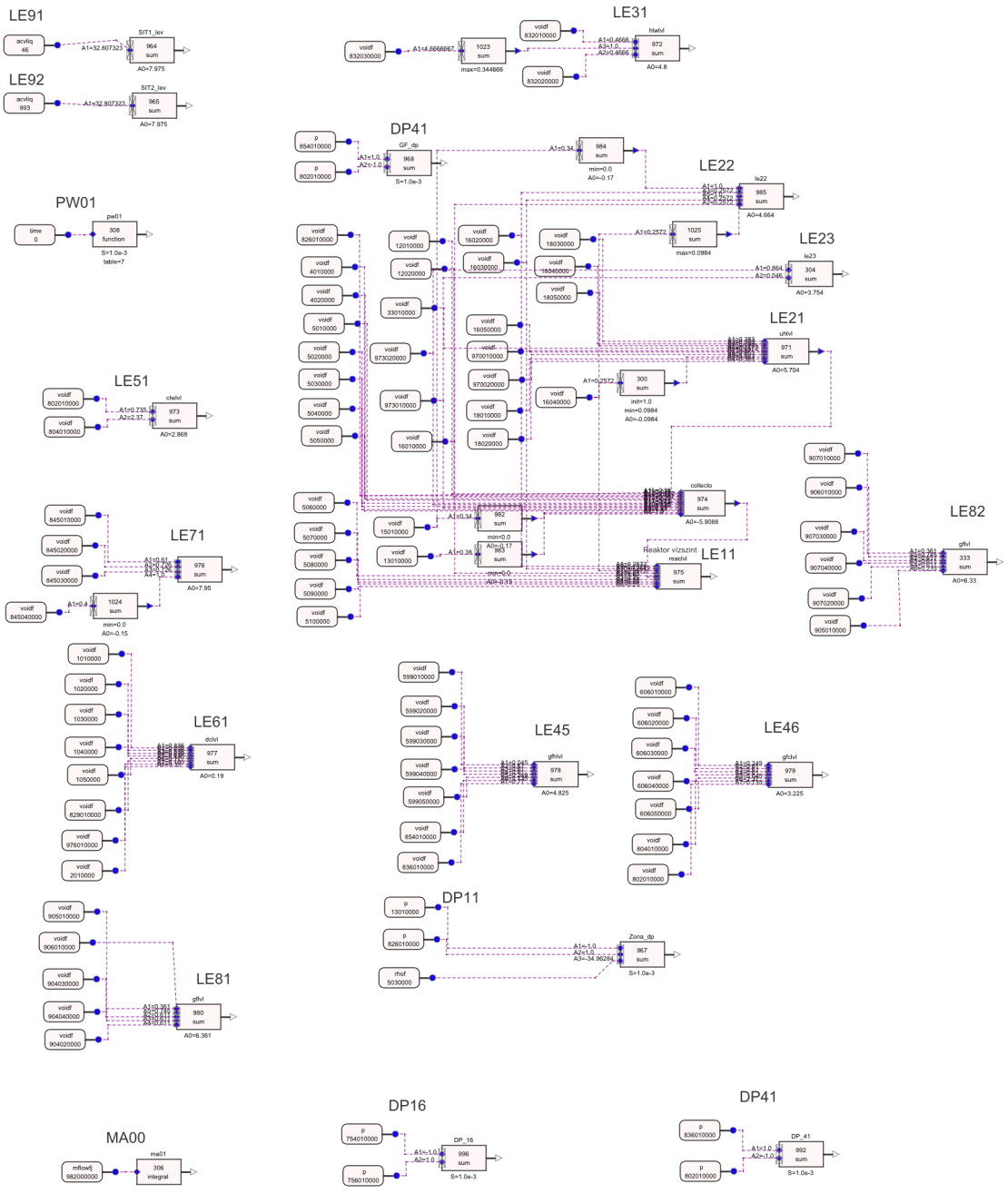

Figure 4.6 Measurement Blocks in the RELAP5 Model

4.4 Steady-State Parameters

The results are summarized in Table 4.2. At the computation of relative errors, the measured values served as reference. Obviously, for the break mass flow parameters, no value was measured in steady state.

Table 4.2 Comparison of Measured and Calculated Steady State Parameters

Parameter	Dimension	Measurement	RELAP5	Absolute error	Relative error [%]
DP11	kPa	5.024E+1	3.394E+01	-1.629E+01	3.24E+01
DP16	kPa	1.490E+3	7.209E+02	-7.691E+02	5.16E+01
DP41	kPa	4.346E+1	3.135E+01	-1.211E+01	2.79E+01
FL00	kg/s	-	-	-	-
FL53	kg/s	4.912E+0	4.911E+0	-1.295E-3	2.64E-2
FL54	kg/s	1.738E+0	4.910E+0	-	-
LE11	m	8.485E+0	8.439E+0	-4.600E-2	5.42E-1
LE21	m	8.485E+0	8.485E+0	-3.000E-7	3.54E-6
LE22	m	5.704E+0	5.704E+0	0.000E+0	0.00E+0
LE23	m	4.664E+0	4.664E+0	0.000E+0	0.00E+0
LE31	m	6.080E+0	6.078E+0	-2.134E-3	3.51E-2
LE45	m	8.445E+0	8.454E+0	9.000E-3	1.07E-1
LE46	m	8.445E+0	8.454E+0	9.000E-3	1.07E-1
LE51	m	5.995E+0	5.973E+0	-2.200E-2	3.67E-1
LE61	m	4.995E+0	4.995E+0	-1.000E-7	2.00E-6
LE71	m	9.124E+0	9.120E+0	-3.993E-3	4.38E-2
LE81	m	8.954E+0	8.536E+0	-4.176E-1	4.66E+0
LE82	m	8.954E+0	8.943E+0	-1.108E-2	1.24E-1
LE91	m	9.440E+0	9.440E+0	-4.000E-7	4.24E-6
LE92	m	9.833E+0	9.830E+0	-3.061E-3	3.11E-2
MA00	kg	-	-	-	-
PR00	MPa	1.000E-1	1.000E-1	0.000E+0	0.00E+0
PR21	MPa	1.233E+1	1.230E+1	-3.391E-2	2.75E-1
PR71	MPa	1.213E+1	1.224E+1	1.026E-1	8.46E-1
PR81	MPa	4.559E+0	4.578E+0	1.871E-2	4.10E-1
PR91	MPa	6.053E+0	6.050E+0	-2.994E-3	4.95E-2
PR92	MPa	6.043E+0	6.040E+0	-2.994E-3	4.96E-2
PW01	kW	6.651E+2	6.650E+2	-1.197E-1	1.80E-2
TE00	K	-	-	-	-
TE11	K	5.762E+2	5.746E+2	-1.568E+0	2.72E-1
TE12	K	6.217E+2	5.899E+2	-3.182E+1	5.12E+0
TE13	K	6.234E+2	5.948E+2	-2.862E+1	4.59E+0
TE14	K	6.252E+2	5.948E+2	-3.042E+1	4.87E+0
TE15	K	6.280E+2	5.948E+2	-3.322E+1	5.29E+0
TE22	K	5.662E+2	5.668E+2	5.662E-1	1.00E-1

Table 4.2 Comparison of Measured and Calculated Steady State Parameters (cont.)

TE23	K	5.629E+2	5.585E+2	-3.582E+0	6.36E-1
TE24	K	5.342E+2	5.499E+2	1.570E+1	2.94E+0
TE41	K	5.667E+2	5.666E+2	-7.219E-2	1.27E-2
TE42	K	5.394E+2	5.394E+2	-4.142E-2	7.68E-3
TE43	K	5.417E+2	5.317E+2	-1.002E+1	1.85E+0
TE44	K	5.362E+2	5.317E+2	-4.528E+0	8.45E-1
TE45	K	5.709E+2	5.654E+2	-5.453E+0	9.55E-1
TE46	K	5.374E+2	5.394E+2	1.961E+0	3.65E-1
TE47	K	5.617E+2	5.666E+2	4.927E+0	8.77E-1
TE48	K	5.316E+2	5.394E+2	7.774E+0	1.46E+0
TE61	K	5.399E+2	5.408E+2	9.440E-1	1.75E-1
TE62	K	5.207E+2	5.300E+2	9.300E+0	1.78E+0
TE63	K	5.401E+2	5.407E+2	6.406E-1	1.19E-1
TE64	K	5.380E+2	5.392E+2	1.173E+0	2.18E-1
TE81	K	4.942E+2	4.941E+2	-8.928E-2	1.81E-2
TE83	K	5.222E+2	5.316E+2	9.359E+0	1.79E+0
TE85	K	5.268E+2	5.313E+2	4.474E+0	8.49E-1
TE87	K	5.287E+2	5.316E+2	2.937E+0	5.56E-1

Since only transient simulation was performed with the break valve being opened at 1500 s, in this subchapter the results that are shown as steady state parameters are extracted from the last time step before the opening of the valve. During this time, control systems functioned in the same manner as it was prescribed for steady-state. In case of reactor heating power, there is a marginal difference between the calculated value and the measured one which stems from an incorrect definition of the data table. In case of pressure values, a good agreement is observed, since these values were set by PI controllers (PR01, PR21 and PR81) or were given as initial conditions in valve-isolated components (PR91, PR92 and PR00). The latter statement holds true for LE91 and LE92 as well. In case of LE61, LE11, LE22 and LE23 the water level is in agreement with the measured data. For pressure drop DP11, DP16 and DP41, a significant deviation is observed which is attributed to an incorrect estimation for the form-loss coefficients by the user. In case of core temperatures, RELAP systematically underestimates which is possibly the result of an incorrect estimation for the heat transfer coefficient in two-phase flow. For the deviation between the measured and calculated values of TE41, the explanation would be similar. It can be seen that in case of the primary side level measurements only negligible difference is observed between the calculated and measured values. This is a result of the one phase flow in the system for which the collapsed level in each cell equals the cell elevation. LE71 also shows good agreement with the measurements which indicate the correct behavior of the level control system. The discrepancy in the initial values of TE62 and TE24 results from incorrectly given initial conditions since the volumes in which they were measured are stagnant. The steam generator primary temperatures (TE41 to TE48) are predicted relatively well. It is observed that the calculated and measured values of FL54 are significantly different. According to [3], the measurements were performed at the same location with different techniques, the one used for FL53 being adequate for higher mass flows which the equipment measuring FL54 could not provide reliably.

By evaluating the parameters in the secondary circuit, it can be seen that there is only an insignificant difference between the measured value of LE81 and the controlled liquid level LE82 while the liquid level in the heater part of the steam generator is much lower in the simulation. It is understandable since the void fraction is significantly higher than in the downcomer which leads to lower collapsed levels in the nodes. The initial feedwater temperature does not differ from the measured because it was set as an input parameter in the time-dependent volume on the suction side of feedwater pump. Concerning the temperatures, the most significant difference is observed in case of TE83 (in the magnitude of percent).

It must be mentioned that in order to maintain the target liquid level in the downcomer, instead of the nominal 0.35 kg/s mass flow, 0.373 kg/s was supplied which indicate differences in the energy balance of the physical system and the model.

4.5 Data Tables

Parameters necessary for the reconstruction of the model are presented in this chapter. The subsystems are identified by a name or its abbreviation as presented in subchapter 4.1 . The parameters which were initialized as RELAP defaults or were not assigned are not listed. The pipe and branch components (Table 4.3) are connected with single junctions. Loss coefficients and area change parameters corresponding to the pipes are set for the subsequent single junction. In all cases, forward and reverse loss coefficients were assumed to be equal. The elevation of connection points from the bottom of each component is referred to as “Cross con. height”. Parameter “Elevation change” stands for the elevation drop from the pipe inlet. Pipes with component names such as “MV11_1” are modeling the flow length of the corresponding valve. Valves are presented separately in Table 4.4, the main components such as accumulators, the pressurizer and pump, time-dependent junctions and volumes and the separator are listed separately (in Table 4.8, Table 4.10, Table 4.5, Table 4.6, Table 4.7 and Table 4.9 respectively). If fluid is entering through a crossflow face, y and z crossflow are set with default flow lengths. In all cases, mass flow refers to liquid mass flow in the following tables. This chapter also presents tabular data required for the parametrization of control systems. In case of pump coast-down, a detailed explanation was given for the control scheme, however, the valve stem vs. time parameters are provided for the sake of simplicity (Table 4.12). Other control schemes relying on tabular data are SCRAM and BREAK. In case of control schemes that require at most two value pairs, necessary information was already given with the definitions of hydraulic components. Furthermore, PI controller parameters are also given in this chapter (Table 4.11). Input dimension determines the dimension of the set-point and “function” refers to the component which is using the output signal (either heat structures or hydraulic components). Material definitions required for the heat structures are also included (Table 4.20 and Table 4.21). Pump velocity table and curves are given in RELAP-specific format in Table 4.22 to Table 4.28.

Table 4.3 Parameters of PIPE and BRANCH Hydraulic Components

Subsystem	COLD LEG				
Name	CLPIP_1	CLPIP_2	CLPIP_3	CLPIP_4	MV11_1
Number	802	804	806	808	17
Component Type	PIPE	PIPE	PIPE	PIPE	PIPE
Flow length [m]	7.35E-1	2.37E+0	2.60E-1	2.45E-1	5.00E-2
Flow area [m^2]	4.185E-3	1.6619E-3	1.6619E-3	1.6619E-3	1.9635E-3
Elevation change [m]	-7.35E-1	-2.37E+0	0.0E+0	1.00E-1	0.0E+0
Number of nodes	1	1	1	1	1
Cross con. height [m]	-	-	-	-	-
Loss coefficient [-]	2.0E+0	0.0E+0	0.0E+0	0.0E+0	0.0E+0
Wall thickness [m]	8.0E-3	5.5E-3	5.5E-3	5.5E-3	5.5E-3
Heat structure	62	42	41	40	56
Subsystem	COLD LEG				
Name	MV11_2	CLPIP_5	CLPIP_6	CLPIP_7	CLPIP_8
Number	29	810	812	814	816
Component Type	PIPE	PIPE	PIPE	PIPE	PIPE
Flow length [m]	5.00E-2	9.30E-1	1.50E+0	5.50E-1	1.125E+0
Flow area [m^2]	1.9635E-3	1.6619E-3	1.6619E-3	1.6619E-3	1.6619E-3
Elevation change [m]	0.0E+0	0.0E+0	1.50E+0	0.0E+0	0.0E+0
Number of nodes	1	1	1	1	1
Cross con. height [m]	-	-	-	-	-
Loss coefficient [-]	0.0E+0	0.0E+0	8.0E-1	0.0E+0	1.0E+0
Wall thickness [m]	5.0E-3	5.5E-3	5.5E-3	5.5E-3	5.5E-3
Heat structure	57	39	38	37	36
Subsystem	DOWNCOMER				LPL
Name	DCTOP_1	DCTOP_2	DC_MID	DC_BOT	LOW_PL
Number	829	976	1	2	826
Component Type	PIPE	PIPE	PIPE	PIPE	PIPE
Flow length [m^2]	1.70E-1	1.05E-1	4.18E+0	1.0015E+0	3.80E-1
Flow area [m]	1.725E-2	1.725E-2	2.595E-3	1.6619E-03	8.171E-3
Elevation change [m]	-1.70E-1	-1.05E-1	-4.18E+0	3.5E-1	3.80E-1
Number of nodes	1	1	5	2	1
Cross con. height [m]	-	5.025E-2	-	-	1.90E-1
Loss coefficient [-]	0.0E+0	0.0E+0	2.0E+0	0.0E+0	0.0E+0
Wall thickness [m]	5.0E-3	5.0E-3	8.0E-3	5.5E-3	1.065E-1
Heat structure	35	36	23	24	22

Table 4.3 Parameters of PIPE and BRANCH Hydraulic Components (cont.)

Subsystem	CORE			RPV	
Name	CORE_IN	CORE	CORE_OUT	UP_BOT	UP_L1
Number	4	5	12	13	971
Component Type	PIPE	PIPE	PIPE	BRANCH	PIPE
Flow length [m]	6.14E-1	2.5E+0	7.00E-2	3.80E-1	4.215E-1
Flow area [m^2]	2.1373E-3	1.4803E-3	8.0324E-3	7.3071E-3	3.3238E-3
Elevation change [m]	6.14E-1	2.5E+0	7.00E-2	3.80E-1	0.0
Number of nodes	2	10	2	1	1
Cross con. height [m]	-	-	-	1.90E-1	-
Loss coefficient	5.0E-1	2.4E-1	5.0E-1	1.0E+0	0.0E+0
Wall thickness [m]	4.0418E-2	3.71E-2	1.065E-01	1.065E-1	4.0418E-2
Heat structure	26	[27, 28]	25	18	26

Subsystem	UPPER PLENUM AND REACTOR PRESSIRE VESSEL					
Name	UP_L2	UP_L3	UP_MID	UP_TOP	UH_BOT	UH_MID
Number	973	975	15	16	970	33
Component Type	PIPE	PIPE	BRANCH	PIPE	PIPE	PIPE
Flow length [m]	9.56E-1	4.215E-1	3.40E-1	1.283E+0	2.75E-1	1.75E-1
Flow area [m^2]	3.3238E-3	3.3238E-3	4.1854E-3	1.6619E-3	1.7404E-2	4.1854E-3
Elevation change [m]	9.56E-1	0.0	3.40E-1	1.283E+0	2.75E-1	1.75E-1
Number of nodes	3	1	1	5	2	1
Cross con. height [m]	2.3E-2 9.1E-1	-	1.70E-1	-	1.05E-1	-
Loss coefficient	0.0E+0	1.0E+0	0.0E+0	7.0E-1	0.0E+0	0.0E+0
Wall thickness [m]	8.00E-3	8.00E-3	8.00E-3	8.00E-3	8.00E-3	8.00E-3
Heat structure	20	19	16	15	61	64

Subsystem	HOT LEG					ENV
Name	HLPIP_1	HLPIP_2	HLPIP_3	HLPIP_4	HLPIP_5	E_PIP
Number	827	832	833	842	836	848
Component Type	PIPE	PIPE	PIPE	BRANCH	PIPE	PIPE
Flow length[m]	7.80E-1	2.86E+0	1.20E-1	3.00E-1	7.70E-1	1.0E+0
Flow area [m^2]	1.6619E-3	1.6619E-3	1.6619E-3	1.6619E-3	1.6619E-3	1.6619E-3

Table 4.3 Parameters of PIPE and BRANCH Hydraulic Components (cont.)

Elevation change [m]	7.80E-1	-1.40E+0	0.0	0.0	7.70E-1	1.0E+0
Number of nodes	1	3	1	1	1	1
Cross con. height [m]	-	-	-	-	-	-
Loss coefficient	0.0E+0	1.0E+0	0.0E+0	7.0E-1	0.0E+0	0.0E+0
Wall thickness [m]	5.50E-3	5.50E-3	5.50E-3	5.50E-3	5.50E-3	-
Heat structure	13	13	13	13	13	-
Name	HOT LEG		PRESSURIZER (PRZ)			
Number	HLPIP_6	UH_TOP	SP_PIP_1	PV12_1		
Component Type	827	18	978	981		
Flow length [m]	PIPE	PIPE	PIPE	PIPE		
Flow area [m^2]	7.35E-1	1.915E+0	5.71E+0	8.00E-1		
Elevation change [m]	4.1854E-3	4.1854E-3	7.8534E-5	1.7671E-4		
Number of nodes [-]	7.35E-1	1.915E+0	5.71E+0	-2.73E-1		
Cross con. height [m]	1	5	2	1		
Loss coefficient [-]	-	-	-	-		
Wall thickness [m]	2.0E+0	1.0E+0	0.0E+0	0.0E+0		
Heat structure	5.50E-3	8.00E-3	-	-		
Subsystem	BREAK	HYDROACCUMULATOR SIT-2				
Name	BREAK_PIP	SIT2_PIP	MV92_1	MV92_2		
Number	983	994	996	30		
Component Type	PIPE	PIPE	PIPE	PIPE		
Flow length [m]	2.05E-1	4.02E+0	3.7365E-1	3.7365E-1		
Flow area [m^2]	4.15476E-4	7.8539E-5	1.7671E-4	1.7671E-4		
Elevation change [m]	0.0E+0	-1.0027E+0	-3.7365E-1	-3.7365E-1		
Number of nodes	1	2	1	1		
Cross con. height [m]	-	-	-	-		
Loss coefficient [-]	1.0E+0	1.2E+1	0.0E+0	0.0E+0		

Table 4.3 Parameters of PIPE and BRANCH Hydraulic Components (cont.)

Subsystem	PRZ	HYDROACCUMULATOR SIT-1			
Name	SURGE_PIP	SIT1_P1	SIT1_P2	MV91_1	MV91_2
Number	36	18	978	998	31
Component Type	PIPE	PIPE	PIPE	PIPE	PIPE
Flow length [m]	2.19028E-1	2.4552E+0	1.9248E+0	3.7365E-1	3.7365E-1
Flow area [m^2]	6.6052E-4	7.85393E-5	7.8534E-5	1.7671E-4	1.7671E-4
Elevation change [m]	-1.575E-1	-2.4552E+0	0.0E+0	-3.7365E-1	-3.7365E-1
Number of nodes	10	1	1	1	1
Loss coefficient	0.0E+0	0.0E+0	1.2E+1	0.0E+0	0.0E+0
Wall thickness [m]	4.5E-3	-	-	-	-
Heat structure	11	-	-	-	-
Subsystem	BYPASS				
Name	BY_BR_1	BY_TA_1	MV12_1	MV12_2	BY_PIP_1
Number	748	18	14	27	752
Component Type	PIPE	PIPE	PIPE	PIPE	PIPE
Flow length [m]	5.19E-1	1.083E+0	2.150E-1	2.150E-1	3.3893E+0
Flow area [m^2]	4.1548E-3	4.1548E-3	7.8536E-3	7.8536E-3	4.1548E-3
Elevation change [m]	-1.60E-1	-1.083E+0	0.0E+0	0.0E+0	-1.700E+0
Number of nodes	1	1	1	1	1
Loss coefficient	1.0E+0	6.0E-1	1.2E+1	0.0E+0	6.0E-1
Wall thickness [m]	8.0E-3	8.0E-3	1.0E-2	1.0E-2	5.5E-3
Heat structure	43	44	58	59	45
Name	BY_PIP_2	BY_PIP_3	BY_PIP_4	CL_HEAT	PV11_1
Number	754	756	756	928	3
Component Type	PIPE	PIPE	PIPE	PIPE	PIPE
Flow length [m]	1.2904E+0	1.083E+0	9.3006E-1	1.75E+0	3.05E-1
Flow area [m^2]	8.024E-3	1.6619E-3	1.6619E-3	4.735E-3	4.1548E-3
Elevation change [m]	-6.45E-1	1.515E+0	7.25E-1	0.0E+0	0.0E+0
Number of nodes	1	1	1	1	1
Loss coefficient	6.0E-1	1.0E+0	1.0E+0	6.0E-1	1.0E+0
Wall thickness [m]	1.6E-2	1.25E-2	5.5E-3	-	1.0E-2
Heat structure	46	48	50	[49,53]	56
Subsystem	BYPASS			SGS	
Name	PV11_2	BY_TA_2	BY_BR_2	SGPIP_11	SGPIP_12
Number	28	762	764	905	912
Component Type	PIPE	PIPE	PIPE	BRANCH	BRANCH
Flow length [m]	3.05E-1	1.068E+0	5.340E-1	3.610E-1	2.330E-1
Flow area [m^2]	4.1548E-3	1.6619E-3	4.185E-3	1.19318E-1	3.05E-2
Elevation change [m]	0.0E+0	1.068E+0	0.0	3.610E-1	2.330E-1
Number of nodes	1	1	1	1	1
Loss coefficient	0.0E+0	1.0E+0	0.0E+0	0.0E+0	0.0E+0
Hydraulic diameter [m]	0.0E+0	0.0E+0	0.0E+0	1.970E-1	1.970E-1
Wall thickness [m]	1.0E-2	4.6E-2	4.6E-2	8.0E-3	-

Table 4.3 Parameters of PIPE and BRANCH Hydraulic Components (cont.)

Wall roughness [m]	0.0E+0	0.0E+0	0.0E+0	3.0E-5	3.0E-5
Heat structure	55	51	52	29,33	-
Subsystem	STEAM GENERATOR SECONDARY SIDE				
Name	SGPIP_6	SGPIP_7	SGPIP_8	SGPIP_9	SGPIP_10
Number	907	904	902	912	914
Component Type	PIPE	PIPE	PIPE	PIPE	PIPE
Flow length [m]	2.256E+0	1.895E+0	8.14E+0	2.910E+0	1.0E-1
Flow area [m^2]	Nodes 1-4: 1.4451E-2 Node 5: 7.2255E-3	Node 1: 7.33E-2 Nodes 2-4: 1.19318E-1	4.909E-4	1.495E-2	4.9088E-4
Elevation change [m]	-2.194E+0	1.833E+0	3.82E+0	2.910E+0	0.0E+0
Number of nodes	5	4	4	5	1
Cross con. height [m]	1.075E+0 1.33E+0 1.99E+0	3.05E-1 9.15E-1 1.525E+0	-	-	-
Loss coefficient	Junc. 1-3: 1.35 Junc. 4: 0.35	0.0	0.0	0.0	0.0
Hydraulic. diameter [m]	0.0E+0	6.0E-3	0.0E+0	1.38E-1	-
Wall thickness [m]	-	1.0E-3	-	-	-
Wall roughness [m]	3.0E-5	1.0E-6	0.0E+0	3.0E-5	-
Heat structure	-	[29, 30, 31, 32]	-	-	-
Subsystem	STEAM GENERATOR PRIMARY SIDE				
Name	SGPIP_1	SGPIP_2	SGPIP_3	SGPIP_4	SGPIP_5
Number	599	611	8	610	606
Component Type	PIPE	PIPE	PIPE	PIPE	PIPE
Flow length [m]	2.114E+0	3.791E+0	3.791E+0	3.791E+0	2.849E+0
Flow area [m^2]	4.185E-3	8.48E-4	8.48E-4	8.48E-4	4.185E-3
Elevation change [m]	2.114E+0	0.0E+0	0.0E+0	0.0E+0	-2.849E+0
Number of nodes	5	3	3	3	5
Cross con. height [m]	1.075E+0 1.33 1.99	-	-	-	1.075E+0 1.33 1.99
Loss coefficient	0.0	0.0	0.0	0.0	0.0
Hydraulic. diameter [m]	7.3E-2	6.0E-3	6.0E-3	6.0E-3	7.3E-2
Wall thickness [m]	8.0E-3	1.0E-3	1.0E-3	1.0E-3	8.0E-3
Wall roughness [m]	1.0E-5	1.0E-6	1.0E-6	1.0E-6	1.0E-5
Heat structure	29	32	31	30	33

Table 4.4 Parameters of VALVE Hydraulic Components

Subsystem	SIT-1	SIT-2	COLD	BYPASS	SGS	SGS
Name	MV_91	MV_92	MV_11	MV_12	PV_22_a	PV_23
Number	823	995	809	926	915	918
Valve Type	MOTOR	MOTOR	MOTOR	MOTOR	MOTOR	MOTOR
Flow area [m^2]	1.767E-4	1.767E-4	1.9635E-3	7.8536E-3	4.9088E-4	4.584E-3
Loss coefficient [-]	0.0	0.0	4.6	3.0	0.0	1.0
Area Change Type	1	1	1	1	1	1
Open Trip	1002	1001	919	861	929	706
Close Trip	907	1	861	919	930	707
Change Rate [1/s]	0.333	0.333	0.25	0.5	0.25	0.25
Initial position [-]	0.0E+0	0.0E+0	0.0E+0	1.0E+0	1.0E+0	1.0E+0
Subsystem	BYPASS	PRZ	SG	BREAK	HPIS	
Name	PV_11	PV12	PV_22	MV_31	MV_77	
Number	925	979	913	982	990	
Valve Type	SERVO	SERVO	SERVO	TRIP	TRIP	
Flow area [m^2]	1.9635E-4	1.767E-4	4.9088E-4	7.068E-6	5.31E-4	
Loss coefficient [-]	2.0E+0	1.0E+0	0.0E+0	2.0E+0	0.0E+0	
Area Change Type	1	1	1	1	1	
Trip	-	-	-	908	924	
Control variable	956	966	705	-	-	
Initial position [-]	1.15E-1	3.00E-4	0.0E+0	0.0E+0	0.0E+0	

Table 4.5 Parameters of ACCUMULATOR Hydraulic Components

Subsystem	SIT-1	SIT-2
Name	SIT-1	SIT-2
Number	46	993
Component Type	ACCUMULATOR	ACCUMULATOR
Area [m^2]	3.0841E-2	3.0841E-2
Height [m]	2.47E+0	2.47E+0
Elevation change [m]	2.47E+0	2.47E+0
Loss coefficient [-]	0.00E+0	0.00E+0
Junction area [m]	7.85393E-5	7.85393E-5
Surge Length [m]	0.00E+0	0.00E+0
Liq. Level [m]	1.465E+0	1.855E+0
Tank Density [kg/m^3]	7.800E+3	7.800E+3
Heat Capacity [J/(kg K)]	5.00E+2	5.00E+2
Pressure (Pa)	5.974E+6	6.02E+6
Temperature (K)	2.93E+2	2.93E+02
Heat structure	-	-

Table 4.6 Parameters of TIME DEPENDENT VOLUME Components

Subsystem	ENV	ENV	HPIS	SGS	SGS	SGS
Name	ENV_HEAT	ENV_SRC	HPIS_TA	FEED_W	ATM	ISO
Number	849	847	991	900	919	916
Component	TMDPVOL	TMDPVOL	TMDPVOL	TMDPVOL	TMDPVOL	TMDPVOL
Flow length [	1.00E+0	1.00E+0	1.00E+1	1.00E+0	1.00E+1	1.00E+1
Elev. change	0.00E+0	0.00E+0	0.00E+0	0.00E+0	0.00E+0	0.00E+0
Area [m^2]	1.00E+0	1.00E+0	1.00E+0	1.00E+0	1.00E+0	1.00E+0
Pressure [	1.00E+5	1.00E+5	1.50E+7	5.07E+6	1.0E+5	4.56E+6
Static quality	-	-	-	-	1.0E+0	1.0E+0
Temperature	2.93E+2	2.93E+2	2.93E+2	4.942E+2	-	-
Heat structures	10:12, 16, 18:27, 34:64	-	-	-	-	-

Subsystem	BREAK	ENV
Name	CNTM	PRZ_VOL
Number	987	41
Component	TMDPVOL	TMDPVOL
Flow length [	1.00E+0	1.00E+0
Elev. change	0.00E+0	0.00E+0
Area [m^2]	1.00E+0	1.00E+0
Pressure [	in Table 13	1.233E+7
Static quality	-	-
Temperature	2.93E+2	5.46E+2
Heat	-	-

Table 4.7 Parameters of TIME DEPENDENT JUNCTION Components

Subsystem	SGS	LPIS	EFS	PRZ
Name	FW_PMP	LPIS_PMP	EFS_PMP	PRZ_PMP
Number	987	35	42	
Component Type	TMDP	TMDP	TMDP JUNC	TMDP JUNC
Control word	1	1	1	1
Flow area [m^2]	4.909E-4	5.310E-4	4.909E-4	4.863E-3
Trip	-	-	-	-
Variable	1004	963	963	989
Table	in Table 15	in Table 16	in Table 17	in Table 18

Table 4.8 Parameters of the Pressurizer

Subsystem	PRESSURIZER
Name	PRZ
Number	907
Component Type	PIPE
Flow length [m]	2.462E+0
Elevation change [m]	2.462E+0
Flow area [m^2]	Nodes 1-3: 8.012E-3 Node 4: 7.521E-3
Elevation change [m]	2.462E+0
Number of nodes [-]	4
Cross con. height [m]	-
Loss coefficient [-]	0.0E+0
Wall thickness [m]	1.60E-2
Heat structure	10, 54
Initial water level [m]	1.1703E+0

Table 4.9 Parameters of the "SEPARATR" Component

Subsystem	SGS
Name	SEPTR
Number	906
Component Type	SEPARATR
Flow length [m]	7.450E-1
Flow area [m^2]	3.050E-2
Elevation change [m]	-7.450E-1
Number of nodes [-]	1
Cross con. height [m]	-
Loss coefficient [-]	Vapor outlet: 0.0E+0 Liquid outlet: 3.5E-1 Two-phase outlet: 3.5E-1
Hydraulic diameter [m]	1.970E-1
Wall roughness [m]	3.0E-5
Wall thickness [m]	-
Heat structure	-
VOVER	1.00E-1
VUNDER	5.50E-1
SEPARATOR MODEL	DEFAULT

Table 4.10 Parameters of the PUMP Component

Subsystem	BYPASS
Name	PMK_PUMP
Number	171
Component Type	PUMP
Flow length [m]	6.350E-1
Flow area [m^2]	Inlet: 7.854E-3 Outlet: 1.662E-3
Elevation change [m]	3.350E-1
Number of nodes [-]	1
Cross con. height [m]	-
Loss coefficient [-]	Inlet 2.0E-1 Outlet: 8.0E-1
Wall thickness [m]	4.60E-2
Heat structure	47
Rated velocity [rad /s]	3.00E+2
Rated Flow [m^3 / s]	5.80E-3
Rated head [m]	1.00E+2
Rated Torque [Nm]	7.473E+2
Inertia [kg·m^2]	1.00E+2
Rated Density [kg/ m^3]	7.800E+2

Table 4.11 Parameters of PI CONTROL BLOCKS

Subsystem	PRZ	SG	SG	PRZ	BYPASS	PRZ
Name	PRZ_CTRL	SG_LEV	SG_PRS	SPRY_MF	FL_CTR	PRZ_LEV
Number	909	702	704	906	932	989
Input parameter	p 973020000	voidf 90401000 90402000 90403000 90404000 90501000 906010000	p 912010000	mflowj 9770000	mflowj 8050000	voidf · DZ 84501000 84502000 84503000 84504000
Input	Pa	m	Pa	kg/s	kg/s	m
Set- point [-]	1.218E+7	8.00E+0	5.07E+6	8.50E-4	4.60E-1	1.32E+0
Coefficient of	1.00E+0	5.00E-1	1.00E+1	1.10E-1	1.10E-1	1.00E-1
Coefficient of	5.00E+0	1.00E-3	5.00E-2	3.40E-1	3.40E-1	1.00E-2
Gain [-]	1.00E-5	1.00E+0	1.00E+0	1.00E+0	1.00E+0	1.00E+0
Minimum	0.00E+0	0.00E+0	0.00E+0	0.00E+0	0.00E+0	-1.00E+0
Maximum	1.00E+0	1.00E+0	1.00E+0	1.00E+0	1.00E+0	1.00E+0
Function	H. struct 54(prz)	FW_PMP	PV22	PV12	PV11	PRZ_PMP

Table 4.12 Valve Stem Position as a Function of Time Elapsed since the Coastdown Initiation (Data is Used for the COASTDOWN Control System)

Time [s]	Valve stem ratio multipliers [-]
0.00E+0	1.00E+0
2.00E+0	1.00E+0
4.00E+0	8.60E-1
8.00E+0	8.50E-1
1.10E+1	7.00E-1
4.00E+1	4.30E-1
4.20E+1	3.30E-1
5.20E+1	3.20E-1
5.60E+1	1.40E-1
1.50E+2	6.00E-2
1.52E+2	0.00E+0

Table 4.13 Power vs. Time Curve Data for Decay Heat Simulation (Table Data is Used in SCRAM Control System)

Time [s]	Power multiplier [-]
0.00E+0	1.00E+0
5.00E-1	9.60E-1
1.00E+0	8.80E-1
2.00E+0	7.50E-1
3.00E+0	6.40E-1
5.00E+0	4.80E-1
7.00E+0	3.50E-1
1.00E+1	2.20E-1
1.50E+1	1.20E-1
2.00E+1	8.20E-2
2.50E+1	6.80E-2
3.00E+1	6.20E-2
4.00E+1	5.90E-2
5.00E+1	5.70E-2
8.00E+1	5.20E-2
1.00E+2	4.80E-2
1.50E+2	4.20E-2
2.00E+2	3.80E-2
3.00E+2	3.50E-2
5.00E+2	3.00E-2
1.00E+3	2.50E-2
6.00E+3	2.50E-2

Table 4.14 Pressure and Temperature vs. Time Curves Defined for the Break Environment (Table Data is used in Parameters Set "Fluid Conditions" of TMDPVOL 987)

Time [s]	Pressure [Pa]	Temperature	Time [s]	Pressure	Temperature
0.000E+0	1.000E+5	2.930E+2	1.720E+3	2.950E+5	2.930E+2
1.500E+3	1.000E+5	2.930E+2	1.755E+3	2.450E+5	2.930E+2
1.504E+3	5.570E+5	2.930E+2	1.760E+3	1.090E+5	2.930E+2
1.523E+3	3.580E+5	2.930E+2	1.780E+3	1.090E+5	2.930E+2
1.554E+3	3.210E+5	2.930E+2	1.790E+3	2.270E+5	2.930E+2
1.577E+3	3.240E+5	2.930E+2	1.810E+3	2.240E+5	2.930E+2
1.583E+3	2.740E+5	2.930E+2	1.815E+3	1.000E+5	2.930E+2
1.593E+3	3.120E+5	2.930E+2	1.825E+3	1.000E+5	2.930E+2
1.645E+3	3.120E+5	2.930E+2	1.835E+3	2.040E+5	2.930E+2
1.657E+3	3.000E+5	2.930E+2	1.840E+3	2.040E+5	2.930E+2
1.658E+3	2.850E+5	2.930E+2	1.850E+3	1.320E+5	2.930E+2
1.660E+3	2.340E+5	2.930E+2	1.865E+3	1.560E+5	2.930E+2
1.665E+3	2.940E+5	2.930E+2	1.880E+3	1.040E+5	2.930E+2
1.670E+3	2.360E+5	2.930E+2	2.190E+3	1.000E+5	2.930E+2
1.675E+3	2.960E+5	2.930E+2	2.200E+3	9.600E+4	2.930E+2
1.685E+3	2.390E+5	2.930E+2	2.500E+3	1.000E+5	2.930E+2

Table 4.15 Mass Flow Data for Component 987 (Search Variable is Interpreted as the Control Variable Given for the Component)

Search variable [-]	Mass flow [kg/s]
-1.00E+0	0.00E+0
0.00E+0	0.00E+0
2.00E+1	2.00E+1

Table 4.16 Mass Flow Data for Component 35 (Search Variable is Interpreted as the Time Elapsed after the LPIS Signal is Initiated)

Search variable [-]	Mass flow [kg/s]
0.000E+0	0.00E+0
1.000E+0	4.20E-2
1.000E+2	4.20E-2
1.000E+6	4.20E-2

Table 4.17 Mass Flow Data for Component 42 (Search Variable is Interpreted as the Time Elapsed after the EFWIS Signal is Initiated)

Search variable [-]	Mass flow [kg/s]
0.000E+0	0.00E+0
1.000E+0	4.20E-2
6.000E+3	4.20E-2

Table 4.18 Power vs Time Data Table for CL_HEAT

Time [s]	Thermal power [W]
0.000E+0	1.854E+4
1.499E+3	1.854E+4
1.500E+3	0.00E+0
1.000E+6	0.00E+0

Table 4.19 Heat Transfer Coefficient vs Time Data for STAGNANT Components

Time [s]	HTC [W/(m^2·K)]
0.000E+0	0.00E+0
1.499E+3	0.00E+0
1.500E+3	7.50E+0
1.000E+6	7.50E+0

Table 4.20 Thermal Properties of Material 1

Temperature [K]	Heat Conduction coefficient [W/(m·K)]	Heat Capacity [J/(m^3·K)]
2.93E+2	1.47E+1	3.900E+6
4.73E+2	1.73E+1	-
7.73E+2	2.10E+1	4.836E+6
2.00E+3	2.10E+1	4.836E+6

Table 4.21 Thermal Properties of Material 2

Temperature [K]	Heat Conduction coefficient [W/(m·K)]	Heat Capacity [J/(m^3·K)]
2.93E+2	2.558E+0	2.147E+6
3.73E+2	2.558E+0	2.484E+6
2.00E+3	2.558E+0	2.484E+6

Table 4.22 Pump Velocity Table

Time [s]	ϖ[rad/s]
0.000E+0	3.00E+2
1.6599E+3	3.00E+2
1.6600E+3	0.00E+0
1.000E+6	0.00E+0

Table 4.23 Pump Head Curves

REGIME HAN		REGIME HVN		REGIME HAD		REGIME HVD	
v/a [-]	h/a^2 [-]	a/v [-]	h/v^2 [-]	v/a [-]	h/a^2 [-]	a/v [-]	h/v^2 [-]
0.0	1.055	0.0	-0.78	-1.0	2.11	-1.0	2.11
0.05	1.064	0.1	-0.6285	-0.9	1.927	-0.9	1.862
0.1	1.079	0.2	-0.478	-0.8	1.759	-0.8	1.65
0.2	1.102	0.3	-0.323	-0.7	1.6105	-0.7	1.474
0.3	1.12	0.31	-0.308	-0.6	1.489	-0.6	1.332
0.4	1.131	0.35	-0.248	-0.5	1.38	-0.5	1.212
0.5	1.131	0.4	-0.169	-0.4	1.282	-0.4	1.105
0.6	1.123	0.45	-0.084	-0.3	1.2	-0.3	1.002
0.7	1.104	0.5015	0.0	-0.2	1.133	-0.2	0.911
0.8	1.0785	0.55	0.082	-0.1	1.0805	-0.1	0.83
0.9	1.043	0.6	0.173	-0.05	1.0615	0.0	0.761
1.0	1.0	0.7	0.365	0.0	1.055		
		0.75	0.461				
		0.8	0.556				
		0.9	0.768				
		0.95	0.881				
		1.0	-0.78				
REGIME HAT		REGIME HVT		REGIME HAR		REGIME HVR	
v/a [-]	h/a^2 [-]	a/v [-]	h/v^2 [-]	v/a [-]	h/a^2 [-]	a/v [-]	h/v^2 [-]
0.0	0.424	0.0	0.761	-1.0	-1.3	-1.0	-1.3
0.1	0.489	0.1	0.71	-0.9	-0.85	-0.8	-1.29
0.2	0.543	0.2	0.664	-0.6	-0.283	-0.5	-1.2
0.3	0.603	0.3	0.644	-0.5	-0.147	-0.2	-1.0
0.4	0.66	0.4	0.653	-0.45	-0.081	0.0	-0.78
0.5	0.7095	0.5	0.6795	-0.384	0.0		
0.6	0.7495	0.6	0.707	-0.35	0.041		
0.7	0.777	0.7	0.746	-0.3	0.106		
0.8	0.804	0.8	0.799	-0.25	0.17		
0.9	0.861	0.9	0.861	-0.2	0.233		
1.0	0.948	1.0	0.948	-0.15	0.29		
				-0.1	0.3395		
				-0.05	0.384		
				0.0	0.424		

Table 4.24 Pump Head Multipliers

X [-]	Y [-]
0.0	0.0
0.2	0.0
0.43	1.0
0.86	1.0

Table 4.25 Pump Torque Curves

REGIME BAN		REGIME BVN		REGIME BAD		REGIME BVD	
v/a [-]	b/a^2 [-]	a/v [-]	b/v^2 [-]	v/a [-]	b/a^2 [-]	a/v [-]	b/v^2 [-]
0.0	0.439	0.0	-0.518	-1.0	1.182	-1.0	1.182
0.05	0.442	0.1	-0.35	-0.9	1.037	-0.9	1.12
0.1	0.46	0.2	-0.184	-0.8	0.911	-0.8	1.093
0.2	0.515	0.3	-0.018	-0.7	0.804	-0.7	1.104
0.3	0.5825	0.31	0.0	-0.6	0.712	-0.6	1.24
0.4	0.647	0.35	0.066	-0.5	0.632	-0.5	1.323
0.5	0.706	0.4	0.151	-0.4	0.567	-0.4	1.34
0.6	0.764	0.45	0.238	-0.3	0.513	-0.3	1.256
0.7	0.823	0.5015	0.32	-0.2	0.473	-0.2	1.122
0.8	0.882	0.55	0.396	-0.1	0.4495	-0.1	1.041
0.9	0.9415	0.6	0.464	-0.05	0.441	0.0	0.948
1.0	1.0	0.7	0.5985	0.0	0.439		
		0.75	0.666				
		0.8	0.731				
		0.9	0.864				
		0.95	0.9305				
		1.0	1.0				
REGIME BAT		REGIME BVT		REGIME BAR		REGIME BVR	
v/a [-]	b/a^2 [-]	a/v [-]	b/v^2 [-]	v/a [-]	b/a^2 [-]	a/v [-]	b/v^2 [-]
0.0	-0.569	0.0	0.984	-1.0	-2.2	-1.0	-2.2
0.1	-0.439	0.1	0.9505	-0.6	-1.59	0.0	-0.518
0.2	-0.318	0.2	0.929	-0.5	-1.39		
0.3	-0.202	0.3	0.905	-0.45	-1.297		
0.4	-0.098	0.4	0.873	-0.384	-1.18		
0.5	0.013	0.5	0.84	-0.35	-1.1205		
0.6	0.121	0.6	0.802	-0.3	-1.04		
0.7	0.229	0.7	0.761	-0.25	-0.956		
0.8	0.345	0.8	0.7205	-0.2	-0.87		
0.9	0.474	0.9	0.678	-0.15	-0.7905		
1.0	0.63	0.95	0.653	-0.1	-0.716		
				-0.05	-0.64		
				0.0	-0.569		

Table 4.26 Pump Torque Multipliers

X [-]	Y [-]
0.0	0.0
1.0	1.0

Table 4.27 Pump Degraded Head Curves

REGIME HAN		REGIME HVN		REGIME HAD		REGIME HVD	
v/a [-]	h/a^2 [-]	a/v [-]	h/v^2 [-]	v/a [-]	h/a^2 [-]	a/v [-]	h/v^2 [-]
0.0	0.165	0.0	0.22	-1.0	-0.82	-1.0	-0.82
0.05	0.774	0.1	0.2285	-0.8	-1.491	-0.9	-0.538
0.1	0.81	0.3	0.248	-0.7	-1.6695	-0.8	-0.33
0.3	0.773	0.5	0.331	-0.5	-1.78	-0.6	-0.098
0.5	0.804	0.7	0.487	-0.3	-1.5	-0.4	-0.045
0.7	0.828	1.0	0.816	-0.2	-1.137	-0.2	-0.039
1.0	0.816			-0.1	-0.5895	0.0	-0.039
				0.0	0.165		
REGIME HAT		REGIME HVT		REGIME HAR		REGIME HVR	
v/a [-]	h/a^2 [-]	a/v [-]	h/v^2 [-]	v/a [-]	h/a^2 [-]	a/v [-]	h/v^2 [-]
0.0	0.165	0.0	0.22	-1.0	-0.82	-1.0	-0.82
0.05	0.774	0.1	0.2285	-0.8	-1.491	-0.9	-0.538
0.1	0.81	0.3	0.248	-0.7	-1.6695	-0.8	-0.33
0.3	0.773	0.5	0.331	-0.5	-1.78	-0.6	-0.098
0.5	0.804	0.7	0.487	-0.3	-1.5	-0.4	-0.045
0.7	0.828	1.0	0.816	-0.2	-1.137	-0.2	-0.039
1.0	0.816			-0.1	-0.5895	0.0	-0.039
				0.0	0.165		

Table 4.28 Pump Degraded Torque Curves

REGIME BAN		REGIME BVN		REGIME BAD		REGIME BVD	
v/a [-]	b/a^2 [-]	a/v [-]	b/v^2 [-]	v/a [-]	b/a^2 [-]	a/v [-]	b/v^2 [-]
0.0	0.0	0.0	0.0	-1.0	0.0	-1.0	0.0
1.0	0.0	1.0	0.0	0.0	0.0	0.0	0.0
REGIME BAT		REGIME BVT		REGIME BAR		REGIME BVR	
v/a [-]	b/a^2 [-]	a/v [-]	b/v^2 [-]	v/a [-]	b/a^2 [-]	a/v [-]	b/v^2 [-]
0.0	0.0	0.0	0.0	-1.0	0.0	-1.0	0.0
1.0	0.0	1.0	0.0	0.0	0.0	0.0	0.0

5 TRACE MODEL

The following model was constructed using version 3.0.2 of the SNAP (Symbolic Nuclear Analysis Package) environment. Calculations were performed using TRACE V5.0 Patch 5 (trace-V50p5-cygwin-ifort13_O1-x64-release.exe). The model's geometry and thermal-hydraulic properties along with the control system implementation are in accordance with subsections 5.1 and 5.2. Throughout the model development, numerous versions were set up of which this document discusses the best fitting model.

5.1 Thermo-Hydraulic Model

The thermo-hydraulic model includes the following parts (component number in the brackets):

- **Downcomer + lower plenum**: downcomer_1 (100), downcomer_2 (110), downcomer_3 (120), downcomer_4 (130), reac_ves_in (140)
- **Reactor core**: reac_ves_core (150)
- **Upper plenum + pressure vessel head**: reac_ves_out (160), reac_ves_mix_chamber_1 (170), reac_ves_mix_chamber_2 (171), reac_ves_up_plenum (180)
- **Hidroaccumulators**: sit_2 (200), sit_2_surge (201), MV92 (202), sit_2_surgeline (203), sit_1 (210), sit_1_surge (211), MV91 (212), sit_1_surgeline (213)
- **Hot leg:** hotleg (220)
- **SG primary side**: HotColl (230), SGPip1 (231), SGPip2 (232), SGPip3 (233), ColdColl (240)
- **Cold leg**: coldleg_1 (250), MV11 (260), coldleg_2 (270)
- **Bypass**: BYPASS1 (280), MV12 (290), BYPASS2 (300), BYPASS3 (310), PMK_PUMP (320), BYPASS4 (330), BYPASS5 (340), BYPASS6 (350), PV11 (360), BYPASS7 (370)
- **Pressurizer**: PRZ (380), PRZ_lvl (381), PRZ_top (390), PRZ_surge (400), PRZ_spray_1 (410), PV12 (420), PRZ_spray_2 (430)
- **Break**: MV31 (440), Break (441)
- **LPIS**: LPIS_surge (460), LPIS (461)
- **SG secondary side**: Downcomer (600), SG_heater (601), SG_cross1 (602), SG_cross2 (603), SG_cross3 (604), SG_cross4 (699)
- **Separator**: Separator_in (605), Separator (606)
- **Secondary side**: Steam_dome (607), Steam_pipe (608), PV22 (609), Steam_boundary (610), SG_feed (611), PV21 (612), Feed_pip (613), Feed_in (614), Steam_relief_pipe_1 (615), Steam_relief_pipe_2 (616), Steam_relief_pipe_3 (617), Steam_relief_pipe_4 (618), Steam_relief_pipe_5 (619), Steam_relief_pipe_6 (620), PV23 (621), Steam_relief_boundary (622)

The components along with the nodalization scheme are illustrated on Figure 5.1.

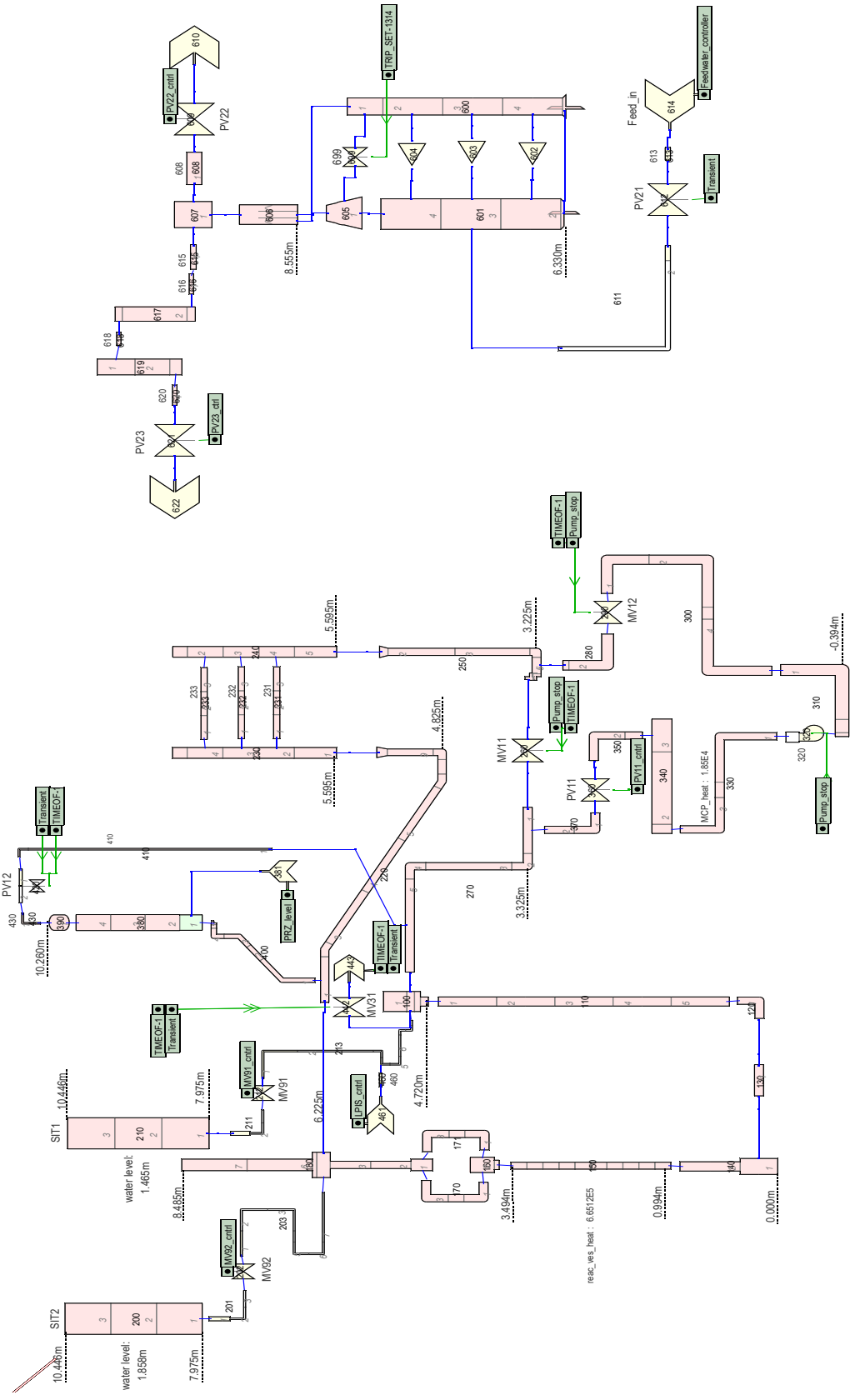

Figure 5.1 Nodalization scheme of the PMK-2 TRACE model

Constructing the TRACE model the following considerations were made:

- Most of the tubes in which the coolant flows are modeled as *[0] No Accumulator* pipes. However, in case of the two safety injection tanks we used the built-in *[1] Accumulator* pipe type.
- There are two particular constituents where we decided to use the built-in components: in the case of the pressurizer (390) and the separator (606).
- The LPIS, the secondary side feedwater intake and the pressurizer level maintainer are modeled through *Fill* components, while *Break* components are used to model the secondary side steam relief boundary, the main steam line boundary and the primary side break itself.
- The pump parameters were taken over from the referred RELAP model [4], however, several changes were made in order to fulfill the model requisites. Moreover, the thermal heat generated by the pump is modeled by introducing 18.5 kW thermal power to the very next pipe (380). The heating power is terminated 150 seconds after the transient initiation.
- The electrically heated core has been divided into 10 control volumes of equal size.
- Similarly to the RELAP5 model, thermal connection between the (primary and secondary loop) piping and the environment is achieved through heat structures, which are attached to the main components. The ambient temperature ('SFT' in TRACE) was 293 K, while different HTC values were set across the components (see in the data tables below) in order to get back the heat loss distribution presented in [1].
- Those (stagnant) control volumes lacking of coolant flow in steady-state, such as the topmost part of the upper plenum (situated above the hot leg) are handled specially. The unwanted heat loss is avoided by setting the HTCs to zero in the connecting heat structures during the steady-state. Omitting the heat transfer in case of the SG uppermost nodes however, would result in a wrong thermal connection between the primary and the secondary side. Hence, these nodes are not considered as stagnant volumes.
- The initial SIT1 and SIT2 water levels are 1.465 m and 1.858 m and their initial pressures are 6.05 MPa and 6.04 MPa, respectively. Liquid temperature inside the hydroaccumulators is 293K, however, because of stability reasons, the initial liquid temperature in the nodes which only contain gas were reduced to 273.15K. For similar reasons, the initial vapor temperature was raised up to 548.5K in the nodes which are full of liquid.
- The downcomer and the heater part of the SG secondary side had been connected at 4 elevations, as seen on Figure 5.1. Throughout the simulations, very high gas temperatures has been observed at low liquid levels in component 605, which often resulted in a crash of the calculation. This unusual behavior led us replace the single junction with a controllable valve. The valve shuts and opens reaching setpoints 0.1 and 0.2 meters in collapsed levels, respectively. By this, the code seems to work properly.
- The initial conditions (e.g. pressure, temperature) in both primary and secondary sides had been set close to the measured steady-state parameters.

Parameters of the Thermo-Hydraulic Model

The data tables below contain the least amount of information from which the model can be reproduced. Remarks considering the data tables are the followings:

- To reduce the extent of this chapter we only listed those parameters which have been modified throughout the modeling meaning that a value or quality of a parameter remained default if it is not stated otherwise.
- Multiple flow areas and hydraulic diameters listed below a component means flow area change through the given pipe.
- The elevation change of a component is negative, when the inlet has a higher elevation than the outlet and zero, when the component is directed horizontally.
- Wall thickness refers to the connecting cylindrical heat structure's thickness. The flat slab heat structures at the steam generator (listed as bold) are always squared, so they can be parameterized with two dimensions: width and thickness.
- An inner tube has been created in the downcomer in accordance with the facility's geometry (see on Figure A.14) by reducing the flow area and adding an inner heat structure.
- The number in the brackets after the friction parameters denotes the edge number(s) on which the given change was made.
- The parameters of the user defined choke flow models are listed in Table 5.28.
- The secondary side reference elevation is at the bottom of the heater/downcomer component, which is placed at 6.33m elevation from the absolute reference (the bottom of component 140).
- In the simulation, Material 52 is used as a component material, unless it is stated otherwise in the tables below.

Table 5.1 Downcomer Parameters

	Downcomer			
Component number	**100**	**110**	**120**	**130**
Number of cells	4	5	1	1
Total length [m]	0.275	4.180	0.700	0.195
Hydraulic diameter [m]	0.160 0.073	0.028	0.046	0.046
Avg. flow area [m^2]	2.010e-2 4.185E-3	2.595E-3	1.662E-3	1.662E-3
Elevation change [m]	-0.275	-4.180	-0.350	0
Lowest elevation of the components axis from reference [m]	4.720	0.540	0.190	0.190
Number of crossflow connections	3	0	0	0
Elevation of crossflow connection points from reference [m]	4.825 4.825 4.825	-	-	-
Wall thickness [mm]	50.0 93.5	8.0	5.5	5.5
Wall roughness [m]	3.0E-5	3.0E-5	3.0E-5	3.0E-5
Inner tube's inner radius [m]	-	0.0175	-	-
Inner tube thickness [mm]	-	5.0	-	-
Friction factor	-1 [4]	-	-	-
Additive loss	0.018 [5]	0.18 [1] 0.025 [2-6]	0.025 [1,2]	0.025 [1] 0.55 [2]
Reverse loss	0.018 [5]	0.18 [1] 0.025 [2-6]	0.025 [1,2]	0.025 [1] 0.55 [2]
Heat structures connected	[105] [106]	[115] [116]	[125]	[135]
Heat transfer coefficient [$W/m^2/K$]	7.5 [1] 6.08 [2-4]	6.08	5.94	5.94

Table 5.2 Lower Plenum, Reactor Core, Upper Plenum and Reactor Vessel Head Parameters

	Lower plenum	Reactor core	Upper plenum, Reactor pressure vessel head			
Component number	**140**	**150**	**160**	**170**	**171**	**180**
Number of cells	2	10	2	3	3	7
Total length [m]	0.994	2.500	0.450	1.575	1.575	3.991
Hydraulic diameter [m]	0.101 0.059	8.032E-3	0.096	0.046	0.046	0.073 0.046 0.160 0.073
Avg. flow area [m^2]	8.012E-3 2.715E-3	1.480E-3	2.715E-3 7.307E-3	1.662E-3	1.662E-3	4.185E-3 1.662E-3 2.010e-2 4.185E-3

Table 5.2 Lower Plenum, Reactor Core, Upper Plenum and Reactor Vessel Head Parameters (cont.)

Elevation change [m]	0.994	2.500	0.450	0.910	0.910	3.991
Lowest elevation of the components axis from reference [m]	0	0.994	3.494	3.754	3.754	4.494
Number of crossflow connections	1	0	2	0	0	4
Elevation of crossflow connection points from reference [m]	0.190	-	3.754 3.754	-	-	4.664 (2) 6.225 (2)
Heater rod inner radius [m]	-	3.55E-3	-	-	-	-
Heater rod thickness [mm]	-	1.0	-	-	-	-
Heater rod surface multiplier	-	19	-	-	-	-
Core isolation thickness [mm]	21.1	21.1	21.1	-	-	-
Core isolation material	51	51	51	-	-	-
Wall thickness [mm]	106.5 [1] 21.1 [2] [M51] 16.0 [2]	21.1 [M51] 16.0 [M52]	21.1 [1] [M51] 16.0 [1] 106.5 [2]	5.5	5.5	90.5 5.5 50.0 8.0
Wall roughness [m]	0	0	3.0E-5	3.0E-5	3.0E-5	3.0E-5
Friction factor	-1 [2,3]	-1 [1,11]	-1 [1,2]	-	-	-1 [2,4,6]
Additive loss	3.5E-3 [2,3]	0.0035 [1,3,5,7,9,11]	0.0035 [1,2]	0.01 [1,4]	0.01 [1,4]	0.01 [2] 0.055 [4]
Reverse loss	3.5E-3 [2,3]	0.0035 [1,3,5,7,9,11]	0.0035 [1,2]	0.01 [1,4]	0.01 [1,4]	0.01 [2] 0.055 [4]
Heat structures connected	[145] [146]	[155]	[165] [166]	[175]	[176]	[185, 186] [187, 188]
Heat transfer coefficient [W/m^2/K]	5.94	5.94	5.94	5.94	5.94	5.94 [1] 21.45 [2-4] 7.5 [5-7]

Table 5.3 Parameters of the Accumulators and their Surge Lines

	Accumulators					
	SIT2	**SIT2 surge line**		**SIT1**	**SIT1 surge line**	
Component number	**200**	**201**	**203**	**210**	**211**	**213**
Number of cells	3	3	7	3	3	9
Total length [m]	2.470	0.956	4.195	2.470	0.911	4.550
Hydraulic diameter [m]	0.197	0.082 0.010	0.010	0.197	0.082 0.010	0.010
Avg. flow area [m^2]	0.030	5.309E-4 7.854E-5	7.854E-5	0.030	5.309E-4 7.854E-5	7.854E-5

Table 5.3 Parameters of the Accumulators and their Surge Lines (cont.)

Elevation change [m]	2.470	-0.480	-1.270	2.470	-0.480	-2.670
Lowest elevation of the components axis from reference [m]	7.975	7.495	6.225	7.975	7.495	4.825
Wall thickness [mm]	11	0	0	11	0	0
Wall roughness [m]	3.0E-5	3.0E-5	3.0E-5	3.0E-5	3.0E-5	3.0E-5
Friction factor	-1 [1]	-1 [1,2,4]	-1 [1,8]	-1 [1]	-1 [1,2,4]	-1 [1,10]
Additive loss	-	5.0 [4]	5.0 [1] 0.5 [2-7]	-	5.0 [4]	5.0 [1] 0.5 [2,4,5,6,8,9] 1.2 [10]
Reverse loss	-	5.0 [4]	5.0 [1] 0.5 [2-7]	-	5.0 [4]	5.0 [1] 0.5 [2,4,5,6,8,9] 1.2 [10]
Heat structures connected	[205]	-	-	[215]	-	-
Heat transfer coefficient [W/m^2/K]	7.50	-	-	7.50	-	-

Table 5.4 Hot Leg and Cold Leg Parameters

	Hot leg	**Cold leg**		
Component number	**220**	**250**	**270**	**280**
Number of cells	10	7	5	2
Total length [m]	4.830	2.975	4.110	2.112
Hydraulic diameter [m]	0.046	0.046	0.046	0.073
Avg. flow area [m^2]	1.662E-3	1.662E-3	1.662E-3	4.185E-3
Elevation change [m]	-0.630	-2.270	1.500	-1.125
Lowest elevation of the components axis from reference [m]	6.225	3.225	3.325	2.077
Number of crossflow connections	1	1	3	0
Elevation of crossflow connection points from reference [m]	6.248	3.202	3.301 4.802 4.848	-
Wall thickness [mm]	5.5	5.5	5.5	8.0
Wall roughness [m]	3.0E-6	0	1.0E-6	3.0E-5
Friction factor	-	-1 [8]	-1 [1]	-1 [3]
Additive loss	0.055 [1]	-	0.040 [5] 0.166 [6]	0.1 [1]
Reverse loss	0.055 [1]	-	0.040 [5] 0.166 [6]	0.1 [1]
Heat structures connected	[225]	[255]	[275]	[285]
Heat transfer coefficient [W/m^2/K]	21.45	6.96 [1-5] 7.5 [6-7]	6.96	6.96

Table 5.5 Bypass Pipes' Parameters

	Bypass					
Component number	**300**	**310**	**330**	**340**	**350**	**370**
Number of cells	4	3	3	3	2	2
Total length [m]	3.654	1.679	3.214	2.090	1.109	1.479
Hydraulic diameter [m]	0.073	0.101	0.046	0.102	0.046	0.046
Avg. flow area [m^2]	4.185E-3	8.012E-3	1.662E-3	8.171E-3	1.662E-3	1.662E-3
Elevation change [m]	-1.750	-0.721	1.464	0	0.674	1.044
Lowest elevation of the components axis from reference [m]	0.327	-0.394	0.017	1.532	1.583	2.257
Number of crossflow connections	0	1	0	2	0	0
Elevation of crossflow connection points from reference [m]	-	-0.343	-	1.481 1.583	-	-
Wall thickness [mm]	8.0	16.0	5.5	12.5	5.5	5.5
Wall roughness [m]	3.0E-5	3.0E-5	3.0E-5	3.0E-5	3.0E-5	3.0E-5
Friction factor	-1 [1,5]	-1 [1]	-1 [1]	-	-1 [3]	-1 [1]
Additive loss	0.06 [5]	0.06 [1]	0.08 [1] 0.10 [4]	-	0.1 [1]	0.1 [3]
Reverse loss	0.06 [5]	0.06 [1]	0.08 [1] 0.10 [4]	-	0.1 [1]	0.1 [3]
Heat structures connected	[305]	[315]	[334] [335]	[345]	[355]	[375]
Heat transfer coefficient [$W/m^2/K$]	6.96	6.96	6.96	6.96	6.96	6.96

Table 5.6 Steam Generator Parameters (Primary Side)

	Steam generator				
Component number	**230**	**231**	**232**	**233**	**240**
Number of cells	5	3	3	3	5
Total length [m]	2.849	3.791	3.791	3.791	2.849
Hydraulic diameter [m]	0.073	6.000E-3	6.000E-3	6.000E-3	0.073
Avg. flow area [m^2]	4.185E-3	7.728E-4	7.728E-4	7.728E-4	4.185E-3
Elevation change [m]	2.849	0	0	0	-2.849
Lowest elevation of the components axis from reference [m]	5.595	6.641	7.263	7.884	5.595
Number of crossflow connections	5	0	0	0	5

Table 5.6 Steam Generator Parameters (Primary Side) (cont.)

Elevation of crossflow connection points from reference [m]	6.641 7.263 7.884 7.884 8.320	-	-	-	6.641 7.263 7.884 7.884 8.320
Wall thickness [mm]	8.0	1.0	1.0	1.0	8.0
Wall roughness [m]	1.0E-5	1.0E-6	1.0E-6	1.0E-6	1.0E-6
Surface multiplier	1.0	27.333	27.333	27.333	1.0
Wall roughness [m]	1.0E-5	1.0E-6	1.0E-6	1.0E-6	1.0E-5
Friction factor	-	-	-	-	-
Additive loss	-	0.008 [1,4]	0.008 [1,4]	0.008 [1,4]	-
Reverse loss	-	0.008 [1,4]	0.008 [1,4]	0.008 [1,4]	-
Heat structures connected	[712] [730] [731]	[700]	[701]	[702]	[713] [732] [733]
Heat transfer coefficient [W/m^2/K]	21.45	-	-	-	6.96

Table 5.7 Pressurizer Parameters

	Pressurizer				
Component number	**380**	**390**	**400**	**410**	**430**
Number of cells	4	1	6	2	2
Total length [m]	2.260	0.200	2.190	5.887	0.475
Hydraulic diameter [m]	0.076 0.101	0.101	0.029	0.010	0.010
Avg. flow area [m^2]	7.521E-3 8.012E-3	8.012E-3	6.605E-4	7.854E-5	7.854E-5
Elevation change [m]	2.260	-0.200	1.552	5.687	0.275
Lowest elevation of the components axis from reference [m]	7.800	10.06	6.248	4.848	10.26
Number of crossflow connections	1	0	0	0	0
Elevation of crossflow connection points from reference [m]	8.000	-	-	-	-
Wall thickness [mm]	16.0	16.0	4.5	2.0	2.0
Wall roughness [m]	3.0E-5	3.0E-5	3.0E-5	3.0E-5	3.0E-5
Friction factor	-1 [1]	-1 [1]	-1 [7]	-1 [3]	-1 [1,3]
Heat structures connected	[705] [706]	[706]	[707]	[708]	[709]
Heat transfer coefficient [W/m^2/K]	7.56	7.56	21.45	6.96	6.96

Table 5.8 Secondary Side Parameters Part 1

	Secondary side					
Component number	**600**	**601**	**602**	**603**	**604**	**605**
Number of cells	5	4	-	-	-	1
Total length [m]	2.256	1.895	-	-	-	0.361
Hydraulic diameter [m]	0.197 8.0E-3	8.0E-3	8.0E-3	8.0E-3	8.0E-3	8.0E-3 0.197
Avg. flow area [m^2]	3.0481E-3 0.014 7.226E-3	0.073 0.119	0.864	0.864	0.864	0.155
Elevation change [m]	-2.225	1.864	-	-	-	0.361
Lowest elevation of the components axis from reference [m]	0	0	0.337	0.948	1.559	1.864
Number of crossflow connections	4	3	0	0	0	1
Elevation of crossflow connection points from reference [m]	0.337 0.948 1.559 2.0445	0.337 0.948 1.559	-	-	-	2.0445
Wall thickness [mm]	3.0 [M52] 16 [M50]	-	-	-	-	8.0
Wall roughness [m]	3.0E-5	3.0E-5	3.0E-5	3.0E-5	3.0E-5	3.0E-5
Wall material	[52,50]	52	-	-	-	52
Friction factor	-	-	-	-	-	-1 [2]
Additive loss	0.35 [1] 1.35 [6]	0.135 [1] 0.04 [2-5]	10.0	10.0	10.0	0.40 [1] 0.35 [2]
Reverse loss	0.35 [1] 1.35 [6]	1.35 [1] 0.4 [2-5]	10.0	10.0	10.0	0.04 [1] 0.035 [2]
Heat structures connected	[714] [**726**]	[700,701] [702] [**725**] [730] [732]	-	-	-	[**723**] [731] [733]
Flat slab HS width [m]	0.1202	0.3822	-	-	-	0.36855
Flat slab HS thickness [mm]	95.0	95.0	-	-	-	95.0
Heat transfer coefficient [$W/m^2/K$]	7.5	-	-	-	-	7.5

Table 5.9 Secondary Side Parameters Part 2

	Secondary side					
Component number	**606**	**607**	**608**	**611**	**613**	**615**
Number of cells	1	1	1	2	1	1
Total length [m]	0.598	0.380	0.340	8.319	0.1	0.24
Hydraulic diameter [m]	0.197	0.197	0.076 0.025	0.015 0.026 5.0e-3	0.026 0.015	0.029
Avg. flow area [m^2]	0.030	0.030	4.537E-3	5.309E-4	5.309E-4	6.605E-4
Elevation change [m]	0.598	0.380	0	3.835	0	0
Lowest elevation of the components axis from reference [m]	2.225	2.823	3.013	-2.892	-2.892	3.013
Number of crossflow connection	0	2	0	0	0	0
Elevation of crossflow connection points from reference [m]	-	3.013 3.013	-	-	-	-
Wall thickness [mm]	11.0	11.0	6.3	-	-	4.5
Wall roughness [m]	3.0E-5	3.0E-5	3.0E-5	3.0E-5	3.0E-5	3.0E-5
Wall material	50	50	52	-	-	52
Friction factor	-1 [1]	-	-1 [2]	-1 [1,3]	-1 [2]	-
Additive loss	0.35 [1-3]	0.35 [1]	-	-	-	-
Reverse loss	0.35 [1-3]	0.35 [1]	-	-	-	-
Heat structures connected	[715]	[715] [724]	[716]	-	-	[717]
Flat slab HS width [m]	-	0.17459	-	-	-	-
Flat slab HS thickness [mm]	-	50.0	-	-	-	-
Heat transfer coefficient [$W/m^2/K$]	7.5	7.5	7.5	-	-	7.5

Table 5.10 Secondary Side Parameters Part 3

	Secondary side				
Component number	**616**	**617**	**618**	**619**	**620**
Number of cells	1	3	1	3	1
Total length [m]	0.131	1.705	0.112	1.205	0.131
Hydraulic diameter [m]	0.022	0.138	0.022	0.138	0.022
Avg. flow area [m^2]	3.801E-4	0.0150	3.801E-4	0.0150	3.801E-4
Elevation change [m]	0	1.705	0	-1.205	0

Table 5.10 Secondary Side Parameters Part 3 (cont.)

Lowest elevation of the components axis from reference [m]	3.013	2.928	4.563	3.628	3.713
Number of crossflow connection	0	2	0	2	0
Elevation of crossflow connection points from reference [m]	-	3.013 4.563	-	3.713 4.563	-
Wall thickness [mm]	4.0	6.0	4.0	6.0	4.0
Wall roughness [m]	3.0E-5	3.0E-5	3.0E-5	3.0E-5	3.0E-5
Choke flow model	-	-	-	-	3
Heat structures connected	[718]	[719]	[720]	[721]	[722]
Heat transfer coefficient [W/m^2/K]	7.5	7.5	7.5	7.5	7.5

Table 5.11 Separator Specific Parameters

Separator properties	
Component number	**606**
Separator type	0
Side tube junction cosine	-1.0
Offtake model option	Off
Separator count	1
Dryer count	0
Carryover	0.0
Carryunder	0.0
Minimum barrel void	1.0E-4
Maximum barrel void	0.9999

Table 5.12 Pressurizer Specific Parameters

Pressurizer properties	
Component number	**320**
Heater power [W]	0.0
Pressure setpoint [Pa]	1.214E7
Pressure differential [Pa]	5.0E-5
Heater cutoff level [m]	0.0

Table 5.13 Pump Basic Properties

PMK_PUMP			
Component number	**320**	Efficiency [%]	85
Pump type	2	Effective MOI [kg*m^2]	100
Number of cells	2	Pump curve option	0
Total length [m]	0.36	Rated head [m^2/s^2]	981.0
Hydraulic diameter [m]	0.050 0.065	Rated torque [N*m]	100.0

Table 5.13 Pump Basic Properties (cont.)

Avg. flow area [m^2]	1.963E-3 3.318E-3	Rated volumetric flow [m^3/s]	5.8E-3
Elevation change [m]	0.36	Rated density [kg/m^3]	780.0
Lowest elevation of the components axis from reference [m]	-0.343	Rated speed [rad/s]	155.0
Wall roughness [m]	3.0E-5	Initial speed [rad/s]	208.85
Friction factor	-1 [3]	Off speed [rad/s]	0
Additive loss	0.02 [1] 0.08 [3]	Maximum speed change [rad/s]	50.00
Reverse loss	0.02 [1] 0.08 [3]	Speed scale factor	1.0
Reverse rotation	0	Initial motor torque [N*m]	0
Degradation option	2	Off motor torque	0

Table 5.14 Pump Homologous Head Curves Part 1

PMK_PUMP - Single-phase homologous head curve tables							
Region 1		**Region 2**		**Region 3**		**Region 4**	
q/ω	**h/ω^2**	**ω/q**	**h/q^2**	**ω/q**	**h/q^2**	**q/ω**	**h/ω^2**
-1.0	2.11	-1.0	-1.3	-1.0	2.11	-1.0	-1.3
-0.9	1.927	-0.8	-1.29	-0.9	1.862	-0.9	-0.85
-0.8	1.759	-0.5	-1.2	-0.8	1.65	-0.6	-0.283
-0.7	1.6105	-0.2	-1.0	-0.7	1.474	-0.5	-0.147
-0.6	1.489	0.0	-0.78	-0.6	1.332	-0.45	-0.081
-0.5	1.38	0.1	-0.6285	-0.5	1.212	-0.384	0.0
-0.4	1.282	0.2	-0.478	-0.4	1.105	-0.35	0.041
-0.3	1.2	0.3	-0.323	-0.3	1.002	-0.3	0.106
-0.2	1.133	0.31	-0.308	-0.2	0.911	-0.25	0.17
-0.1	1.0805	0.35	-0.248	-0.1	0.83	-0.2	0.233
-0.05	1.0615	0.4	-0.169	0.0	0.761	-0.15	0.29
0.0	1.055	0.45	-0.084	0.1	0.71	-0.1	0.3395
0.05	1.064	0.5015	0.0	0.2	0.664	-0.05	0.384
0.1	1.079	0.55	0.082	0.3	0.644	0.0	0.424
0.2	1.102	0.6	0.173	0.4	0.653	0.1	0.489
0.3	1.12	0.7	0.365	0.5	0.6795	0.2	0.543
0.4	1.131	0.75	0.461	0.6	0.707	0.3	0.603
0.5	1.131	0.8	0.556	0.7	0.746	0.4	0.66
0.6	1.123	0.9	0.768	0.8	0.799	0.5	0.7095
0.7	1.104	0.95	0.881	0.9	0.861	0.6	0.7495
0.8	1.0785	1.0	1.0	1.0	0.948	0.7	0.777
0.9	1.043					0.8	0.804
1.0	1.0					0.9	0.861
						1.0	0.948

Table 5.15 Pump Homologous Head Curves Part 2

PMK_PUMP - Fully-degraded homologous head curve tables							
Region 1		Region 2		Region 3		Region 4	
q/ω	h/ω^2	ω/q	h/q^2	ω/q	h/q^2	q/ω	h/ω^2
-1.0	-0.82	-1.0	0.8	-1.0	-0.82	-1.0	0.8
-0.8	-1.491	-0.5	0.45	-0.9	-0.538	-0.6	0.797
-0.7	-1.6695	-0.2	0.29	-0.8	-0.33	-0.4	0.51
-0.5	-1.78	0.0	0.22	-0.6	-0.098	-0.2	0.233
-0.3	-1.5	0.1	0.2285	-0.4	-0.045	0.0	-0.046
-0.2	-1.137	0.3	0.248	-0.2	-0.039	0.2	-0.366
-0.1	-0.5895	0.5	0.331	0.0	-0.039	0.4	-0.58
0.0	0.165	0.7	0.487	0.2	-0.066	0.6	-0.6805
0.05	0.774	1.0	0.816	0.4	-0.097	0.8	-0.676
0.1	0.81			0.6	-0.173	1.0	-0.482
0.3	0.773			0.8	-0.331		
0.5	0.804			1.0	-0.482		
0.7	0.828						
1.0	0.816						

Table 5.16 Pump Homologous Head Curves Part 3

PMK_PUMP - Single phase homologous torque curve tables							
Region 1		Region 2		Region 3		Region 4	
q/ω	β/ω^2	ω/q	β/q^2	ω/q	β/q^2	q/ω	β/ω^2
-1.0	1.182	-1.0	-2.2	-1.0	1.182	-1.0	-2.2
-0.9	1.037	0.0	-0.518	-0.9	1.12	-0.6	-1.59
-0.8	0.911	0.1	-0.35	-0.8	1.093	-0.5	-1.39
-0.7	0.804	0.2	-0.184	-0.7	1.104	-0.45	-1.297
-0.6	0.712	0.3	-0.018	-0.6	1.24	-0.384	-1.18
-0.5	0.632	0.31	0.0	-0.5	1.323	-0.35	-1.1205
-0.4	0.567	0.35	0.066	-0.4	1.34	-0.3	-1.04
-0.3	0.513	0.4	0.151	-0.3	1.256	-0.25	-0.956
-0.2	0.473	0.45	0.238	-0.2	1.122	-0.2	-0.87
-0.1	0.4495	0.5015	0.32	-0.1	1.041	-0.15	-0.7905
-0.05	0.441	0.55	0.396	0.0	0.984	-0.1	-0.716
0.0	0.439	0.6	0.464	0.1	0.9505	-0.05	-0.64
0.05	0.442	0.7	0.5985	0.2	0.929	0.0	-0.569
0.1	0.46	0.75	0.666	0.3	0.905	0.1	-0.439
0.2	0.515	0.8	0.731	0.4	0.873	0.2	-0.318
0.3	0.5825	0.9	0.864	0.5	0.84	0.3	-0.202
0.4	0.647	0.95	0.9305	0.6	0.802	0.4	-0.098
0.5	0.706	1.0	1.0	0.7	0.761	0.5	0.013
0.6	0.764			0.8	0.7205	0.6	0.121
0.7	0.823			0.9	0.678	0.7	0.229
0.8	0.882			0.95	0.653	0.8	0.345
0.9	0.9415			1.0	0.63	0.9	0.474
1.0	1.0					1.0	0.63

Table 5.17 Pump Homologous Head Curves Part 4

PMK_PUMP - Fully-degraded homologous torque curve tables							
Region 1		**Region 2**		**Region 3**		**Region 4**	
q/ω	**β/ω^2**	**ω/q**	**β/q^2**	**ω/q**	**β/q^2**	**q/ω**	**β/ω^2**
-1.0	0.0	-1.0	0.0	-1.0	0.0	-1.0	0.0
0.0	0.0	0.0	0.0	0.0	0.0	0.0	0.0
1.0	0.0	1.0	0.0	1.0	0.0	1.0	0.0

Table 5.18 Pump Head-Degradation and Torque Degradation Multiplier Curves

PMK_PUMP			
Head-degradation multiplier curve		**Torque degradation multiplier curve**	
0.0	0.0	0.0	0.0
0.2	0.0	1.0	0.0
0.43	1.0		
0.86	1.0		
1.0	0.0		

Table 5.19 Valve Properties Part 1

	Valve properties				
Component name	**MV11**	**MV12**	**MV31**	**MV91**	**MV92**
Number of cells	0	0	0	0	0
Total length [m]	-	-	-	-	-
Hydraulic diameter [m]	0.050	0.100	3.2E-3	0.015	0.015
Flow area [m^2]	1.963E-3	7.854E-3	8.042E-6	1.767E-4	1.767E-4
Elevation change [m]	-	-	-	-	-
Elevation from reference level [m]	3.325	2.077	4.825	7.495	7.495
Wall roughness [m]	0	3.0E-5	0	0	0
Internal loss model	0	0	1	0	0
Friction factor	-1	-1	-	-1	-1
Additive loss	-	-	-	5.0	5.0
Reverse loss	-	-	-	5.0	5.0
Choke flow model	0	0	2	0	0
Maximum valve rate [1/s]	0.5	0.333	10	0.333	0.333
Off adjustment rate [1/s]	0.5	0.333	10	0.333	0.333
Initial flow area fraction	0.0	1.0	0.0	0.0	0.0
Valve stem position	0.0	1.0	0.0	0.0	0.0

Table 5.20 Valve Properties Part 2

	Valve properties				
Component name	**PV11**	**PV12**	**PV21**	**PV22**	**PV23**
Number of cells	0	2	0	0	0
Total length [m]	-	0.4	-	-	-
Hydraulic diameter [m]	0.050	0.015	0.015	0.025	0.006
Flow area [m^2]	1.963E-3	1.767E-4	1.767E-4	4.909E-4	2.827E-5
Elevation change [m]	-	0	-	-	-
Elevation from reference level [m]	2.257	10.535	-2.892	3.013	3.713
Wall roughness [m]	3.0E-5	3.0E-5	3.0E-5	3.0E-5	3.0E-5
Friction factor	-1	-1 [1,3]	-1	-1	-1
Choke flow model	-	-	-	-	3
Maximum valve rate [1/s]	0.5	1.0E5	0.25	0.25	0.476
Off adjustment rate [1/s]	0.5	1.0E5	0.25	0.25	0.476
Initial flow area fraction	0.2	3.3E-4	1.0	1.0	0.0
Valve stem position	0.2	3.3E-4	1.0	1.0	0.0

Table 5.21 BREAK Components' Parameters

	Break components		
Component name	**Break**	**Steam_boundary**	**Steam_relief_boundary**
Component number	**443**	**610**	**622**
Break type	1	0	0
Temperature table option	3	0	3
Length [m]	0.12	1.0	1.0
Volume [m^3]	1.0E5	4.909E-4	1.0E5
Initial gas volume fraction	1.0	1.0	1.0
Initial mixture temperature [K]	380.0	531.395	380
Initial pressure [Pa]	1.0E5	4.5E6	1.0E5

Table 5.22 Fill Components' Parameters

	Fill components		
Component name	**PRZ_lvl**	**LPIS**	**Feed_in**
Component number	**381**	**461**	**614**
Fill type	5	5	5
Length [m]	1.0	1.0	1.0
Volume [m^3]	5.309E-4	500	5.309E-4
Initial liquid temperature [K]	598.2	293.0	494.2
Initial vapor temperature [K]	598.2	293.0	494.2
Initial pressure [Pa]	1.211E7	1.15E7	4.56E6
Initial coolant mass flow [kg/s]	0	0	0.35
Liquid velocity [m/s]	0	0	1.0

Table 5.23 Fill Tables

Fill tables	
PRZ_lvl (381)	
Independent variable: Gate -91 (PRZ_level)	Mixture mass flow [kg/s]
-1.0	-1.0
0.0	0.0
1.0	1.0
LPIS (461)	
Independent variable: Gate -6 (Scram_timer)	Mixture mass flow [kg/s]
0.0	0.0
0.05	0.042
1.0	0.042
Feed_in (614)	
Independent variable: Multiply -89 (PV21_cntrl)	Mixture mass flow [kg/s]
0.0	0.0
1.0	1.0

Table 5.24 Pump Coastdown Table

Pump coastdown table			
Time [s]	Flow area fraction [-]	Time [s]	Flow area fraction [-]
0.0	1.0	42.0	0.33
2.0	1.0	52.0	0.32
4.0	0.86	56.0	0.14
8.0	0.85	97.0	0.09
11.0	0.7	135.0	0.07
15.0	0.63	150.0	0.06
22.0	0.55	151.0	0.01
30.0	0.5	152.0	0.0
40.0	0.43	1.0E6	0.0

Table 5.25 Decay Power vs. Time (Part 1)

Decay heat simulator							
Time [s]	Power [W]	Time [s]	Power [W]	Time [s]	Power [W]	Time [s]	Power [W]
0.0	6.6512E5	40.0	3.84E4	80.0	3.44E4	120.0	3.0E4
1.0	6.31E5	41.0	3.84E4	81.0	3.44E4	121.0	3.0E4
2.0	5.58E5	42.0	3.8E4	82.0	3.4E4	122.0	3.0E4
3.0	4.79E5	43.0	3.8E4	83.0	3.4E4	123.0	3.0E4
4.0	4.12E5	44.0	3.8E4	84.0	3.4E4	124.0	3.0E4
5.0	3.55E5	45.0	3.8E4	85.0	3.36E4	125.0	3.0E4
6.0	3.056E5	46.0	3.8E4	86.0	3.36E4	126.0	3.0E4
7.0	2.604E5	47.0	3.8E4	87.0	3.36E4	127.0	3.0E4
8.0	2.236E5	48.0	3.76E4	88.0	3.36E4	128.0	2.96E4
9.0	1.92E5	49.0	3.76E4	89.0	3.36E4	129.0	2.96E4
10.0	1.64E5	50.0	3.76E4	90.0	3.36E4	130.0	2.96E4
11.0	1.424E5	51.0	3.76E4	91.0	3.3E4	131.0	2.96E4
12.0	1.264E5	52.0	3.7E4	92.0	3.3E4	132.0	2.96E4
13.0	1.204E5	53.0	3.7E4	93.0	3.24E4	133.0	2.96E4
14.0	9.96E4	54.0	3.7E4	94.0	3.24E4	134.0	2.9E4
15.0	8.76E4	55.0	3.7E4	95.0	3.24E4	135.0	2.9E4
16.0	7.9E4	56.0	3.64E4	96.0	3.24E4	136.0	2.96E4
17.0	7.24E4	57.0	3.64E4	97.0	3.2E4	137.0	2.96E4
18.0	6.7E4	58.0	3.64E4	98.0	3.2E4	138.0	2.96E4
19.0	6.2E4	59.0	3.64E4	99.0	3.2E4	139.0	2.9E4
20.0	5.7E4	60.0	3.64E4	100.0	3.16E4	140.0	2.9E4
21.0	5.36E4	61.0	3.6E4	101.0	3.16E4	141.0	2.96E4
22.0	5.16E4	62.0	3.6E4	102.0	3.16E4	142.0	2.96E4
23.0	4.96E4	63.0	3.6E4	103.0	3.16E4	143.0	2.96E4
24.0	4.8E4	64.0	3.6E4	104.0	3.16E4	144.0	2.96E4
25.0	4.6E4	65.0	3.6E4	105.0	3.16E4	145.0	2.9E4
26.0	4.44E4	66.0	3.56E4	106.0	3.1E4	146.0	2.9E4
27.0	4.4E4	67.0	3.56E4	107.0	3.1E4	147.0	2.84E4
28.0	4.3E4	68.0	3.56E4	108.0	3.1E4	148.0	2.84E4
29.0	4.2E4	69.0	3.56E4	109.0	3.16E4	149.0	2.84E4
30.0	4.1E4	70.0	3.56E4	110.0	3.1E4	150.0	2.84E4
31.0	4.04E4	71.0	3.56E4	111.0	3.1E4	151.0	2.84E4
32.0	4.04E4	72.0	3.56E4	112.0	3.1E4	152.0	2.84E4
33.0	4.0E4	73.0	3.5E4	113.0	3.04E4	153.0	2.8E4
34.0	3.96E4	74.0	3.5E4	114.0	3.04E4	154.0	2.84E4
35.0	3.96E4	75.0	3.5E4	115.0	3.04E4	155.0	2.84E4
36.0	3.96E4	76.0	3.5E4	116.0	3.04E4	156.0	2.84E4
37.0	3.9E4	77.0	3.44E4	117.0	3.04E4	161.0	2.8E4
38.0	3.84E4	78.0	3.44E4	118.0	3.0E4	166.0	2.76E4
39.0	3.84E4	79.0	3.44E4	119.0	3.0E4	171.0	2.64E4

Table 5.26 Decay Power vs. Time (Part 2)

Time [s]	Power [W]	Time [s]	Power [W]	Time [s]	Power [W]	Time [s]	Power [W]
176.0	2.64E4	376.0	2.2E4	756.0	1.8E4	1316.0	1.7E4
181.0	2.6E4	381.0	2.2E4	766.0	1.8E4	1336.0	1.7E4
186.0	2.6E4	386.0	2.2E4	776.0	1.8E4	1356.0	1.7E4
191.0	2.56E4	391.0	2.16E4	786.0	1.8E4	1376.0	1.7E4
196.0	2.56E4	396.0	2.16E4	796.0	1.76E4	1396.0	1.64E4
201.0	2.56E4	406.0	2.16E4	806.0	1.76E4	1416.0	1.64E4
206.0	2.5E4	416.0	2.1E4	816.0	1.76E4	1436.0	1.64E4
211.0	2.5E4	426.0	2.1E4	826.0	1.76E4	1456.0	1.64E4
216.0	2.5E4	436.0	2.04E4	836.0	1.76E4	1476.0	1.64E4
221.0	2.5E4	446.0	2.04E4	846.0	1.76E4	1496.0	1.64E4
226.0	2.44E4	456.0	2.04E4	856.0	1.7E4	1516.0	1.64E4
231.0	2.44E4	466.0	2.04E4	866.0	1.76E4	1536.0	1.64E4
236.0	2.44E4	476.0	2.04E4	876.0	1.7E4	1556.0	1.64E4
241.0	2.44E4	486.0	2.0E4	886.0	1.7E4	1576.0	1.64E4
246.0	2.44E4	496.0	2.0E4	896.0	1.7E4	1596.0	1.6E4
251.0	2.4E4	506.0	2.0E4	906.0	1.7E4	1616.0	1.64E4
256.0	2.4E4	516.0	1.96E4	916.0	1.7E4	1636.0	1.6E4
261.0	2.4E4	526.0	1.96E4	926.0	1.7E4	1656.0	1.64E4
266.0	2.4E4	536.0	1.96E4	936.0	1.64E4	1676.0	1.6E4
271.0	2.36E4	546.0	1.96E4	946.0	1.64E4	1696.0	1.64E4
276.0	2.36E4	556.0	1.96E4	956.0	1.7E4	1716.0	1.64E4
281.0	2.36E4	566.0	1.96E4	966.0	1.64E4	1736.0	1.64E4
286.0	2.36E4	576.0	1.9E4	976.0	1.64E4	1756.0	1.6E4
291.0	2.36E4	586.0	1.9E4	986.0	1.64E4	1776.0	1.6E4
296.0	2.36E4	596.0	1.9E4	996.0	1.64E4	1796.0	1.6E4
301.0	2.3E4	606.0	1.9E4	1016.0	1.64E4		
306.0	2.36E4	616.0	1.9E4	1036.0	1.64E4		
311.0	2.3E4	626.0	1.84E4	1056.0	1.64E4		
316.0	2.24E4	636.0	1.84E4	1076.0	1.64E4		
321.0	2.3E4	646.0	1.9E4	1096.0	1.64E4		
326.0	2.24E4	656.0	1.84E4	1116.0	1.64E4		
331.0	2.24E4	666.0	1.84E4	1136.0	1.64E4		
336.0	2.24E4	676.0	1.9E4	1156.0	1.64E4		
341.0	2.24E4	686.0	1.84E4	1176.0	1.64E4		
346.0	2.24E4	696.0	1.8E4	1196.0	1.64E4		
351.0	2.2E4	706.0	1.8E4	1216.0	1.64E4		
356.0	2.24E4	716.0	1.84E4	1236.0	1.64E4		
361.0	2.2E4	726.0	1.84E4	1256.0	1.64E4		
366.0	2.2E4	736.0	1.8E4	1276.0	1.64E4		
371.0	2.2E4	746.0	1.8E4	1296.0	1.64E4		

Table 5.27 Pressure of the Component which Simulates the Blowdown Tank

Break environment pressure simulator					
Time [s]	Pressure [Pa]	Time [s]	Pressure [Pa]	Time [s]	Pressure [Pa]
0	100000	165	294000	325	100000
4	557000	170	236000	335	204000
23	358000	175	296000	340	204000
54	321000	185	239000	350	132000
77	324000	220	295000	365	156000
83	274000	255	245000	380	104000
93	312000	260	109000	690	100000
145	312000	280	109000	700	96000
157	300000	290	227000	1000	100000
158	285000	310	224000	1.0E+06	100000
160	234000	315	100000		

Table 5.28 User Defined Choke Flow Models

User defined choke flow models		
	Choke flow model 2	Choke flow model 3
Subcooled multiplier	1.2	0.4
Two-phase multiplier	1.0	0.4

Table 5.29 User Defined Materials' Properties

Material 50 (SG_steel)				
Temperature [K]	Density [kg/m^3]	Specific Heat [W*s/kg/K]	Therm. Cond. W/m/K	Emissivity -
373.0	7800.0	500.0	51.1	0.84
473.0	7800.0	530.0	47.7	0.84
573.0	7800.0	560.0	44.2	0.84
773.0	7800.0	620.0	44.2	0.84
Material 51 (CORE_isolation)				
Temperature [K]	Density [kg/m^3]	Specific Heat [W*s/kg/K]	Therm. Cond. W/m/K	Emissivity -
273.0	2700.0	795.0	2.558	0.9
2000.0	2700.0	795.0	2.558	0.9
Material 52 (standard)				
Temperature [K]	Density [kg/m^3]	Specific Heat [W*s/kg/K]	Therm. Cond. W/m/K	Emissivity -
273.0	7800.0	500.0	14.7	0.84
293.0	7800.0	500.0	14.7	0.84
473.0	7800.0	530.0	17.3	0.84
773.0	7800.0	620.0	21.0	0.84
2000.0	7800.0	620.0	21.0	0.84

5.2 Control Systems

The implemented control systems are in charge both to secure the steady-state parameters and implement the required actions triggered by the transient. The short description of the control systems is listed below in the relevant paragraphs.

- **BREAK**: Opening the valve (MV31) that models the break. The valve opens when the transient signal is set to 1, in our case after a 2000 s long steady state run.
- **SCRAM**: In steady-state conditions the total heating power deposited into the reactor core is 665.12 kW. When the pressure in the upper plenum drops below the setpoint (PR21 < 11.15MPa), the modeling of decay heat (see in Table 5.25 and Table 5.26) is being initiated.
- **SIT_1, SIT2**: The valves (MV91 and MV92) isolating accumulators SIT1 and SIT2 open if the pressure reaches their setpoints (5.90MPa for both). The valves are shut when the liquid level in the accumulators decreases below 0.245 and 1.035 meters respectively.
- **FLOW**: The constant steady-state mass flow rate of 4.91kg/s was set by controlling the valve stem area of the valve PV11 by the PI controller PV11_cntrl.
- **COAST-DOWN**: The pump coastdown starts, when the pressure decreases under the coastdown setpoint (PR21 < 9.21MPa). This is modeled by closing valve PV11 as seen in Table 5.24. 150 seconds after the transient signal, valve MV11 starts to open, valve MV12 starts to close and the pump shuts down. By these actions, a natural circulation takes place in the primary loop.
- **PRIMARY PRESSURE**: In steady-state conditions, a constant mass flow of around 8.0E-04kg/s is maintained in the pressurizer spray pipe (PRZ_spray1). The nominal pressure in the upper plenum (12.33MPa) is achieved by a PI controller (PRZ_cntrl) by heating the coolant present in the lowermost node of the PRZ component (pipe 380). In order to minimize the time required to reach the steady-state condition we raised the maximum heating power from the nominal 3200 W to 5000 W. Starting the transient disables the heating and closes valve PV12, which terminates the spray injection into the pressurizer.
- **PRESSURIZER LEVEL**: The desired pressurizer level (1.32m) for the transient start is achieved by the PRZ_level PI controller, which regulates the mass flow coming from the relevant fill component (381). The operation of this controller is terminated by the transient signal.
- **SG PRESSURE**: The steady-state SG secondary pressure (4.56MPa) is set by a PI controller (PV22_cntrl), which is responsible to adjust the valve stem position of valve PV22. The transient signal automatically shuts the valve, which takes 6 seconds.
- **SG PRESSURE LIMITATION & BLEED**: The pressure limitation of the SG is achieved by controlling the PV23 valve: it opens and closes when reaching the pressure setpoints (5.3MPa and 4.9MPa respectively). The secondary side bleed is being initiated 150 seconds after reaching the pressure setpoint (PR21 < 9.21MPa) by fully opening valve PV23.
- **SG LEVEL**: The secondary side feedwater flow provided by the fill component (Feed_in) is controlled by the PI controller PV21_cntrl in order to maintain 8.95 m liquid level in the steam generator. In our case, a significant amount of steam is present in the heater part of the SG. To avoid liquid outflow at the top of the SG the control system has been set to

measure the collapsed water level from the downcomer side (see in Figure 5.2). Initiating the transient terminates the PI controller and starts the stoppage of the feedwater flow. The run-out takes 6 seconds where the decrease is linear.

- **LPIS***:* supplies a mass flow of 4.2E-02 kg/s once the pressure in the upper plenum drops below 1.04 MPa.
- **EMERGENCY FEEDWATER***:* intake starts off when the secondary side pressure decreases under 0.93 MPa. EFW system introduces the same mass flow as the LPIS.
- **VALVE 699:** during the transient, the module 605 and the first cell of module 600 is completely emptied due to the decreasing secondary water level. At this moment, the temperature of these cells jumped to thousands of degrees in the test calculations and thus it crashed. To avoid this problem, the artificial valve 699 was built in (connecting these two cells) which closes when the water level drops below 1 cm, and reopens when it rises above 2 cm.

The above-mentioned control systems are presented on Figure 5.2.

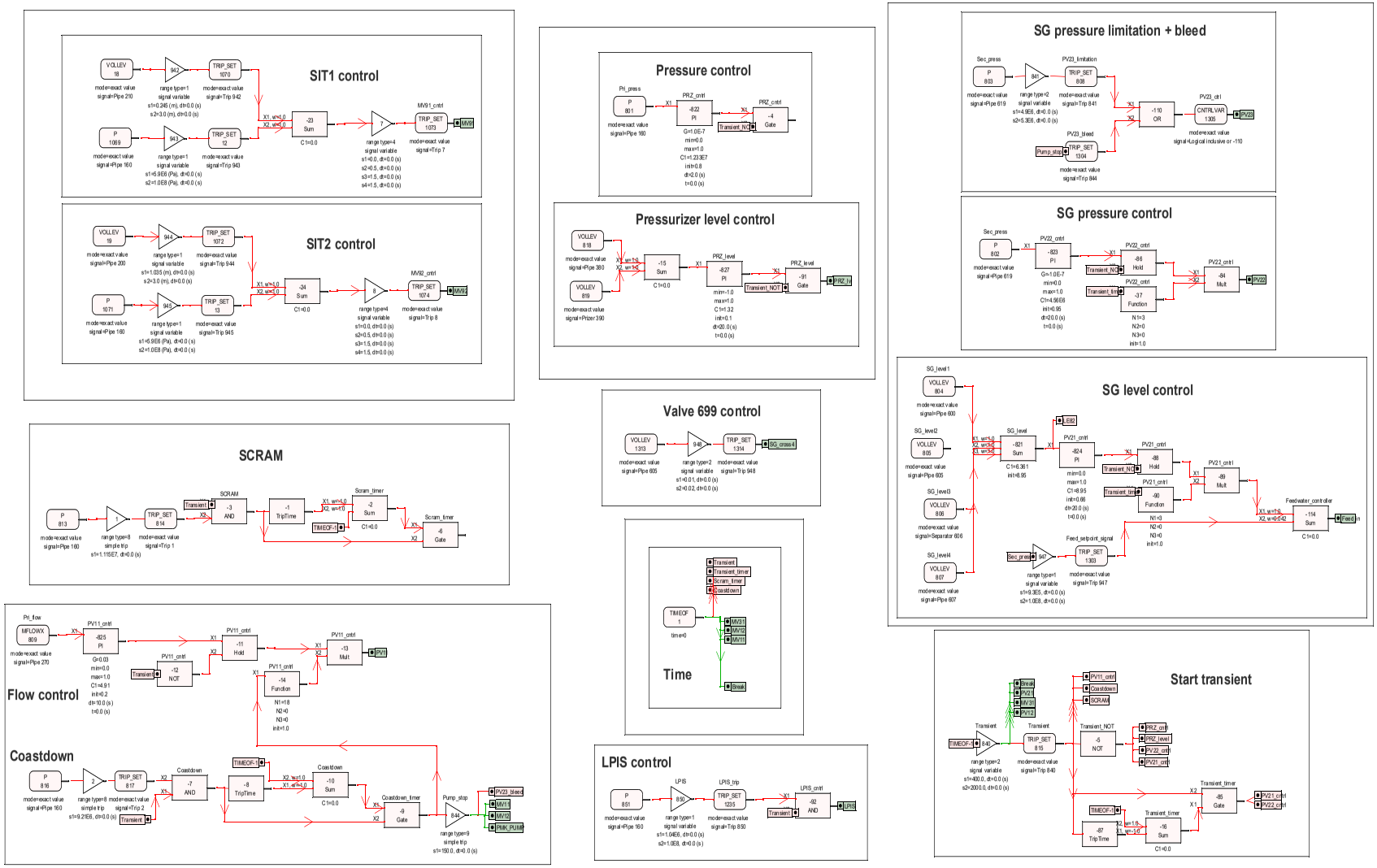

Figure 5.2 Control Systems of the PMK-2 TRACE Model

5.3 Measurements

In order to compare the simulation results with the measured quantities, we created the signals listed in Table 5.30, which are in accordance with the measurements specified in [3].

Table 5.30 List of the Measurements and the TRACE Signal-Variable ID Numbers (from which the Relevant Data was Extracted)

Identification	Measured quantity	Signal-variable ID
DP11	Core pressure drop	1215
DP16	Pump pressure drop	1251
DP41	SG primary pressure drop	1216
FL00	Break mass flow	1228
FL53	Cold leg mass flow 1	1227
FL54	Cold leg mass flow 2	1253
LE11	Reactor liquid level	1217
LE21	Upper plenum liquid level part 1 (5.504/9.220 m)	1232
LE22	Upper plenum liquid level part 2 (4.664/5.504 m)	1218
LE23	Upper plenum liquid level part 3 (3.754/4.664 m)	1252
LE31	Hot leg loop seal liquid level	1221
LE45	SG primary liquid level – hot leg	1222
LE46	SG primary liquid level – cold leg	1220
LE51	Cold leg liquid level	1230
LE61	Downcomer liquid level	1223
LE71	Pressurizer liquid level	1219
LE81	SG liquid level (secondary side, heater)	1226
LE82	SG liquid level (secondary side, downcomer)	1310
LE91	SIT1 liquid level	1224
LE92	SIT2 liquid level	1225
MA00	Total mass leaked through break	1254
PR00	External pressure	1229
PR21	Upper plenum pressure	1211
PR71	Pressurizer pressure	1250
PR81	Secondary circuit pressure	1212
PR91	SIT1 pressure	1213
PR92	SIT2 pressure	1214
PW01	Core power	1233
TE00	Break flow temperature	1246
TE11	Heater rod surface temperature (at 1.494 m)	1199
TE12	Heater rod surface temperature (at 3.464 m)	1200
TE13	Heater rod surface temperature (at 3.464 m)	1201
TE14	Heater rod surface temperature (at 3.464 m)	1202
TE15	Heater rod surface temperature (at 3.464 m)	1203
TE22	Upper plenum coolant temperature (at 4.644 m)	1204
TE23	Upper plenum wall temperature	1205
TE24	Upper plenum coolant temperature (at 8.375 m)	1247
TE41	SG inlet coolant temperature (primary side)	1206
TE42	SG outlet coolant temperature (primary side)	1207

Table 5.30 List of the Measurements and the TRACE Signal-Variable ID Numbers (from which the Relevant Data was Extracted) (cont.)

TE43	Heat exchanger inlet coolant temp. (at 8.163 m)	1237
TE44	Heat exchanger outlet coolant temp. (at 8.163 m)	1240
TE45	Heat exchanger inlet coolant temp. (at 7.591 m)	1238
TE46	Heat exchanger outlet coolant temp. (at 7.591 m)	1241
TE47	Heat exchanger inlet coolant temp. (at 6.385 m)	1239
TE48	Heat exchanger outlet coolant temp. (at 6.385 m)	1242
TE61	Downcomer inlet coolant temperature	1208
TE62	Downcomer wall temperature	1209
TE63	Core inlet coolant temperature	1210
TE64	Pump inlet temperature	1249
TE81	SG feedwater temperature	1248
TE83	SG secondary side temperature (at 8.163 m)	1243
TE85	SG secondary side temperature (at 7.591 m)	1244
TE87	SG secondary side temperature (at 6.385 m)	1245

Remarks regarding the measurement signals in the TRACE code

- Two cold leg mass flows (FL53 and FL54) are listed. In terms of the measurement locations there is no difference between them, however the [3] draws attention on different measurement techniques used. It is stated that FL53 describes the higher mass flows better, while FL54 should be used at lower mass flow rates.
- The upper plenum liquid levels (LE21 and LE22) are measured from 5.457 and 6.225 meters respectively.
- The external pressure (PR00) refers to the tanks pressure onto which the break mass flow drains off. This measured quantity has been passed to our code in a form of a break component table (Table 5.27) and initiates when the transient starts.
- The total core power (PW01) applied has also been given to the code as an input according to the measured quantities. The decay heat run-off initiated by the transient can be seen in Table 5.25 and Table 5.26.
- Retrieving the heater rod surface temperatures happens at various elevations from the innermost node of the relevant heat structure as shown in Table 5.30, however in the TRACE model it is not possible to gather temperature data from an exact point. Therefore, these temperatures are approximated in the way that is shown in Figure 5.3.
- The wall temperatures presented, such as TE23 and TE62, are measured in the outermost node of the pipes.
- When creating liquid level signals, we had to take into consideration that the built-in collapsed water level signal variable cannot distinguish between horizontal and vertical dimensions of a pipe component; therefore, we had to manually subtract the horizontal length of the relevant component.
- In case of the secondary side SG liquid level there were two signals generated. Whilst LE81 measures the water level from the heater part, the LE82 does so from the downcomer component.

- Certain measured and simulated data, such as DP16, PR00, TE00 and TE64 were not taken into consideration when evaluating the results for different reasons (e.g. incorrect measured values, triviality or irrelevant).

The aforementioned signals along with their supplemental control blocks are shown in Figure 5.3.

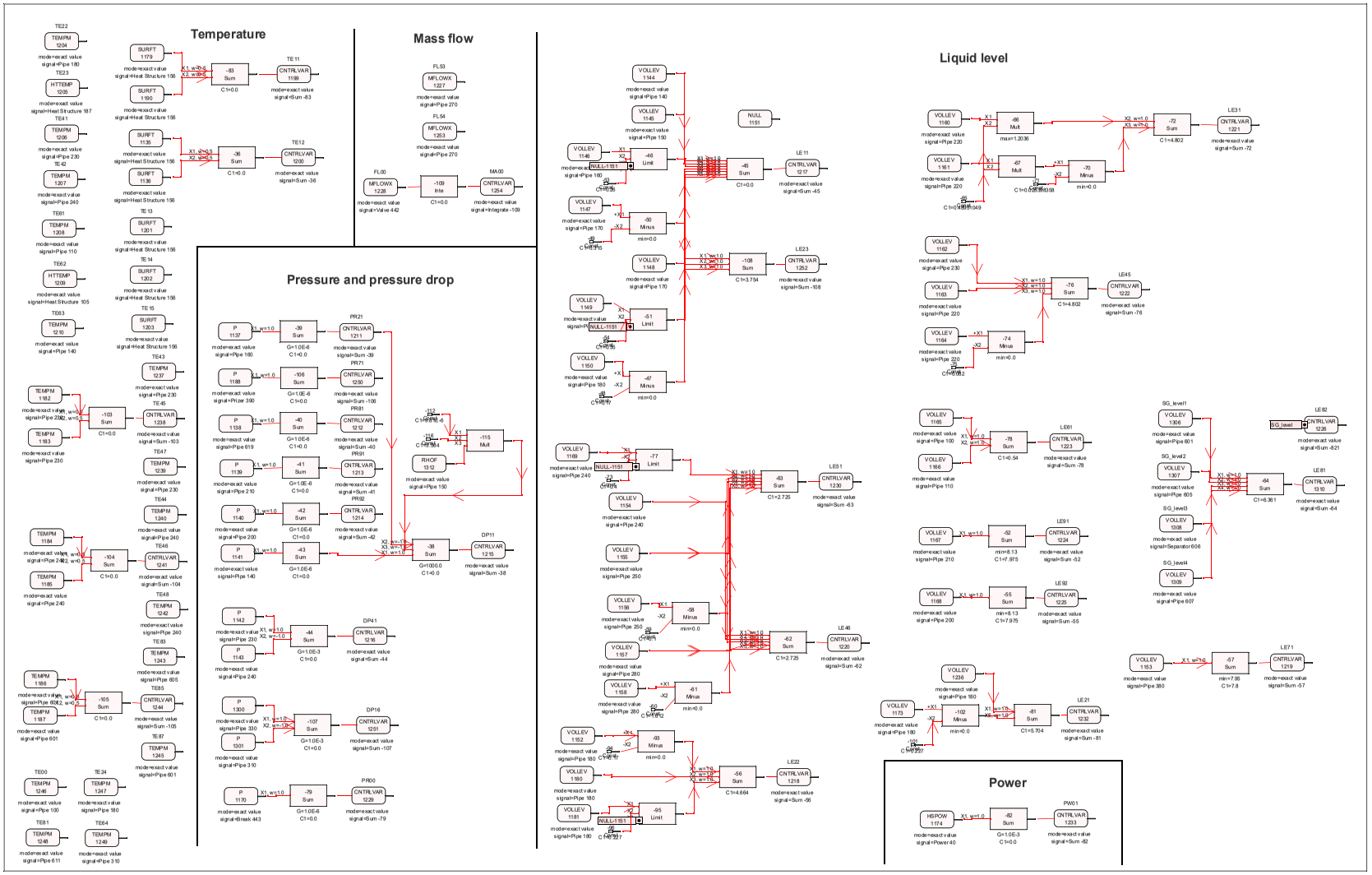

Figure 5.3 Measurement Signals of the TRACE Model

5.4 Steady-State Parameters

In order to achieve the proper steady-state conditions, the transient is being initiated after 2000 seconds from the calculation begin. Throughout the first 1700 seconds of the steady-state the minimum and maximum time step sizes were 1.0E-7 and 0.1 s respectively, while the graphics interval was set to 1.0s. The remaining time interval of the steady-state and the transient (except from the first 200 seconds in the transient) runs with a 0.01 s maximum time step and a 0.1 s graphic interval. Mainly to reduce the cold leg mass flow fluctuations caused by the steam the maximum time step has been reduced to 0.005 seconds for the first 200 seconds after the transient initiation.

The following table summarizes the calculated steady-state parameters and their deviation from the measured values.

Table 5.31 Steady-State Measurement and TRACE Calculation Comparison

Parameter	Dimension	Measurement	TRACE	Absolute error	Relative error [%]
DP11	kPa	50.24	52.01	1.776	3.54
DP16	kPa	1490	1483	-6.92	0.46
DP41	kPa	43.46	45.37	1.911	4.40
FL00	kg/s	-	-	-	-
FL53	kg/s	4.912	4.909	-0.0028	0.058
FL54	kg/s	1.738	4.909	-	-
LE11	m	8.485	8.485	0	0
LE21	m	8.485	8.485	0	0
LE22	m	5.704	5.704	0	0
LE23	m	4.664	4.664	0	0
LE31	m	6.080	6.08	0	0
LE45	m	8.445	8.444	-0.001	0.012
LE46	m	8.445	8.444	-0.001	0.012
LE51	m	5.995	5.995	0	0
LE61	m	4.995	4.995	0	0
LE71	m	9.124	9.120	-0.0044	0.049
LE81	m	8.954	8.422	-0.532	5.94
LE82	m	8.954	8.950	-0.0037	0.041
LE91	m	9.440	9.441	0.0005	0.006
LE92	m	9.833	9.833	0	0
MA00	kg	-	-	-	-
PR00	MPa	0.1	0.1	0	0
PR21	MPa	12.329	12.361	0.0323	0.26
PR71	MPa	12.133	12.294	0.1611	1.33
PR81	MPa	4.559	4.547	-0.0120	0.26
PR91	MPa	6.053	6.050	-0.0033	0.054
PR92	MPa	6.043	6.041	-0.0017	0.028
PW01	kW	665.12	665.12	0	0
TE00	K	-	-	-	-
TE11	K	576.2	574.3	-1.94	0.34
TE12	K	621.7	589.6	-32.1	5.17

Table 5.31 Steady-State Measurement and TRACE Calculation Comparison (cont.)

TE13	K	623.4	593.3	-30.1	4.83
TE14	K	625.2	593.3	-31.9	5.11
TE15	K	628.0	593.3	-34.7	5.53
TE22	K	566.2	565.5	-0.69	0.12
TE23	K	562.9	542.0	-20.9	3.71
TE24	K	534.2	535.8	1.57	0.29
TE41	K	566.7	565.2	-1.52	0.27
TE42	K	539.4	539.0	-0.39	0.07
TE43	K	541.7	531.9	-9.76	1.80
TE44	K	536.2	531.7	-4.53	0.85
TE45	K	570.9	564.1	-6.76	1.18
TE46	K	537.4	538.9	1.53	0.28
TE47	K	561.7	564.9	3.16	0.56
TE48	K	531.6	539.0	7.42	1.40
TE61	K	539.9	539.4	-0.48	0.09
TE62	K	520.7	537.4	16.7	3.22
TE63	K	540.1	539.3	-0.77	0.14
TE64	K	538.0	538.8	0.82	0.15
TE81	K	494.2	494.2	0.01	0.002
TE83	K	522.2	531.3	9.09	1.74
TE85	K	526.8	531.3	4.52	0.86
TE87	K	528.7	531.4	2.74	0.52

- DP11 and DP41 pressure drops in the TRACE model were set to be higher than those in the measurement. The reason behind systematic overestimation is the sudden rise of these parameters at the very beginning of the measurements.
- The primary side mass flow rate (FL53), the SIT pressures (PR91, PR92), the reactor power (PW01), the liquid levels (LExx) and the feedwater temperature (TE81) are in accordance with the measured quantities, because these parameters are either given the code as input tables, set by control systems or in a strong correlation with the controlled parameters.
- The primary PR21 and secondary PR81 pressures are controlled parameters and thus they show good agreement with the measurements. A small difference can be observed due to the small fluctuations caused by the PI controllers. However, the pressurizer pressure shows a more significant error, which indicates that the flow frictions are not perfectly set, since the water level is adequate.
- The heater rod surface temperatures (TE11-15) are systematically underestimated by the code. The heat transfer coefficient between the rods and the coolant in the experiment is probably lower than that calculated by TRACE.
- The calculated coolant temperatures (TE22, TE24, TE41, TE42, TE61, TE63 and TE64) are close to the measured quantities, which means, that the heat losses are modeled properly.
- Both TE43 and TE44 are being measured in stagnant nodes, which are difficult to simulate with one-dimensional hydraulic codes. Therefore, the margin can be acceptable.

- The experimentally measured values of the primary side temperatures of the steam generator (TE41, TE47, TE45 and TE46, TE44, TE42) behave strangely. Going up in the hot collector, the temperatures are 566.7 °C, 561.7 °C and 570.9 °C respectively. Therefore, the lower part temperature is the lowest, and the middle part is warmer than the inlet (top part is the stagnant volume). Going down in the cold collector, the temperatures are 537.4 °C, 531.6 °C and 539.4 °C. Therefore, the lower part temperature is the lowest and the outlet is even warmer than the middle part. Based on the available information, this behavior cannot be explained and thus the comparison with the TRACE results is also difficult. The collector temperatures of TRACE show an expected trend.
- A considerable discrepancy can be observed between the measurements and the simulation in case of wall temperatures, such as TE23 and TE62. These could be approximated more precisely if we knew more detailed information about the location of the measuring point and the thermal insulation used, but this information is not available in the description of the experimental facility.
- The secondary side temperatures (TE83, TE85 and TE87) are significantly different. In case of TRACE, all three of these show saturation temperatures, while the measured values are lower and increase downwards. This suggests that the TRACE model cannot properly calculate the heat transfer and overestimates the internal mixing. Using a more detailed nodalization could be a solution to this problem and thus it could be a field for further development.

6 APROS MODEL

Since 2000, our institute has gained a lot of experience in application of APROS (Advanced PROcess Simulator) thermo-hydraulic system code developed in Finland. It has been serving both teaching and research purposes, one of which was the model development for a similar experiment (SPE-2) conducted also on the PMK-2 facility [2]. Although the APROS version in which this thermo-hydraulic model had been built (5.11) is outdated by now, it provided a solid basis for the current project. The model was reconstructed in one of the latest versions of APROS (6.08) and modified according to the SPE-4 experiment. Due to the differences between code versions and the experiments investigated, the model also required some fine tuning (e.g. discharge coefficients, nodalization).

6.1 Thermo-Hydraulic Model

The six-equation thermal hydraulic model of APROS was used with WS fluid (non-equilibrium mixture of water and steam calculated with the IAPWS-IF97 steam tables, without boric acid). All of the primary and secondary components have been placed on the N1 scheme (shown on Figure 6.1).

The main components and their names are the following:

- **External downcomer** (*DC_TOP, DC_MIDDLE, DC_BOTTOM_1, DC_BOTTOM_2, DC_MID_IN1 – DC_MID_IN5*)
- **Lower plenum** (*LOWER_PLENUM*)
- **Reactor core** (*CORE_INLET, CORE, FUEL, CORE_OUTLET, CORE_WALL1 – CORE_WALL10*)
- **Upper plenum** (*UP_BOTTOM, UP_L1, UP_L2, UP_L3, UP_MIDDLE, UP_TOP, UH_BOTTOM*)
- **Upper head** (*UH_MIDDLE, UH_TOP*)
- **Hot leg** (*HL_PIP1, HL_PO1, HL_PIP2, HL_PO2, HL_PIP3, HL_PO3, HL_PIP4, HL_PO4, HL_PIP5, HL_PO5, HL_PIP6*)
- **Cold leg** (*CL_PIP1, CL_PO1, CL_PIP2, CL_PO2, CL_PIP3, CL_PO3, CL_PIP4, CL_PO4, MV11, CL_PO5, CL_PIP5, CL_PO6, CL_PIP6, CL_PO7, CL_PIP7, CL_PO8, CL_PIP8*)
- **Cold leg bypass** (*BYPASS_BR1, BYPASS_TA1, MV12, BYPASS_PO1, BYPASS_PIP1, BYPASS_PO2, BYPASS_PIP2, BYPASS_PO3, PMK_PUMP, BYPASS_PO4, BYPASS_PIP3, BYPASS_PO5, PREHEATER, BYPASS_PO6, BYPASS_PIP4, BYPASS_PO7, PV11, BYPASS_TA2, BYPASS_BR2*)
- **Steam generator and feedwater line** (*FW_PO1, PV21, SG, SD_PIP1, SD_TA1, SD_BR1, SG_HS1 – SG_HS17)*
- **Steam lines** (*SL_PIP2, SL_PO2, PV22, SL_PO4, SL_PIP1, SL_PO1, SL_PIP3, SL_TA1, SL_PIP4, SL_TA2, SL_PIP5, SL_PO3, PV23, SL_PO5*)

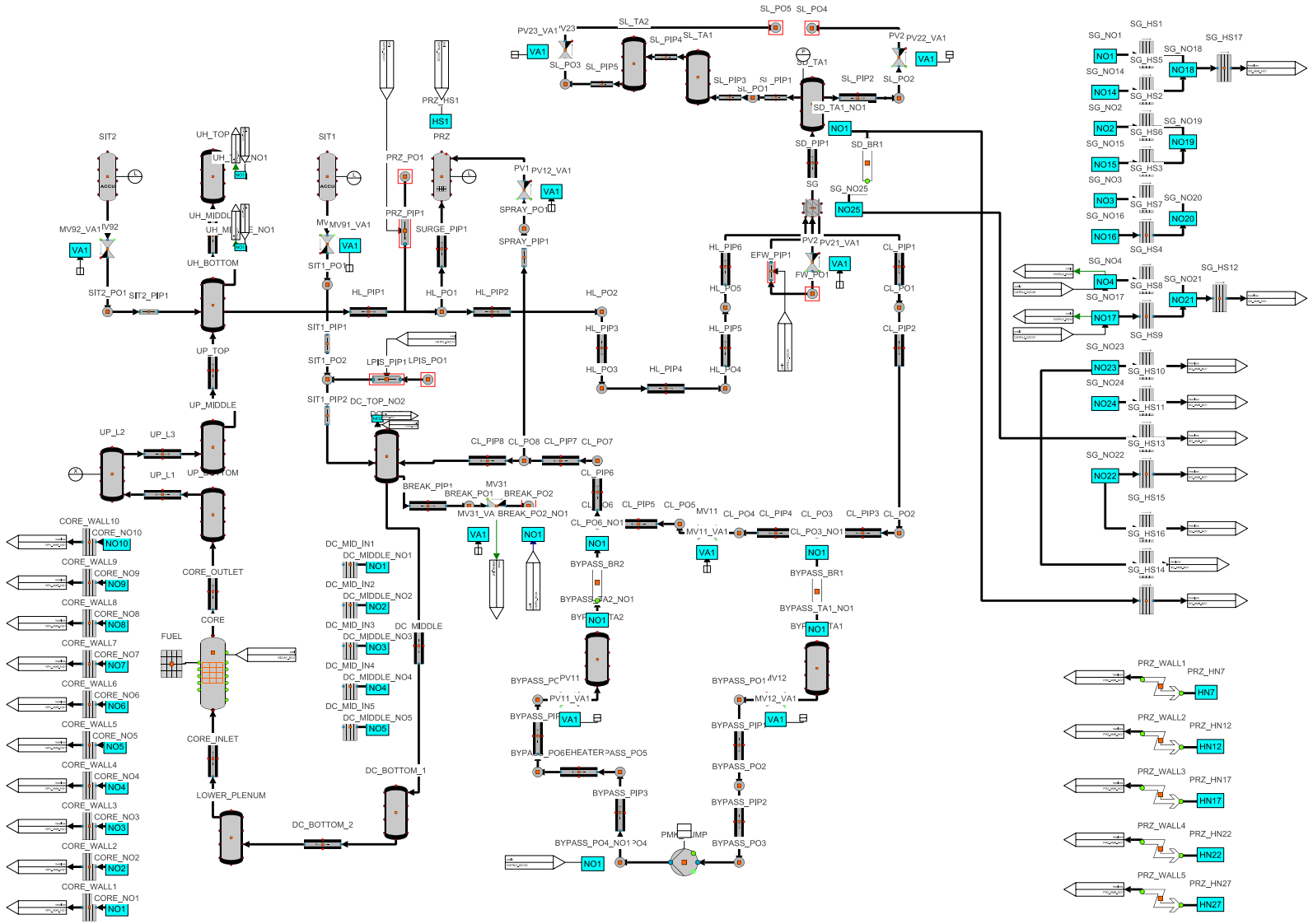

Figure 6.1 'N1' Scheme of the APROS Model (Primary and Secondary Circuit)

- **Emergency feedwater injection** (*EFW_PIP1*)
- **Pressurizer with spray and surge lines** (*SURGE_PIP1, PRZ, SPRAY_PIP1, SPRAY_PO1, PV12, PRZ_WALL1 – PRZ_WALL5*)
- **Simplified pressurizer level control system** (*PRZ_PO1, PRZ_PIP1*)
- **Accumulators with surge lines** (*SIT1, MV91, SIT1_PO1, SIT1_PIP1, SIT1_PO2, SIT1_PIP2, SIT2, MV92, SIT2_PO1, SIT2_PIP1*)
- **Low pressure injection system** (*LPIS_PO01, LPIS_PIP1*)
- **Break model** (*BREAK_PIP1, BREAK_PO1, MV31, BREAK_PO2*)

Some notes for modeling considerations:

- There is no intentional geometric modification; real values from the sources were used.
- Similarly to RELAP5 and TRACE models, the reactor core consists of 10 thermo-hydraulic nodes.
- HEAT_TANK and HEAT_PIPE modules have a single node in most cases. Precise modeling of processes taking place in the bypass loop turned out to be less important, therefore the number of nodes in these pipes is set to 0. In case of the longer tubes, such as the hot and cold leg pipelines and the downcomer the division was refined by increasing the number of nodes. The downcomer top region (*DC_TOP*) consists of 2 nodes.
- Steam generator model was constructed by combining multiple modules, such as HEAT_TANK, HEAT_PIPE and the built in SG component. Moreover, an additional branch (*SD_BR1*) was needed to allow coolant circulation in the upper part of the SG vessel. The pipe component operates with 4 computation-level nodes, while in case of the nodalization of the built-in steam generator, recommendations of the APROS user manual was followed.
- The HEAT_PIPE and HEAT_TANK modules of the steam generator contain heat structures to model the cylindrical wall. However, the built-in steam generator model of APROS does not create heat structures between the primary collectors and the secondary circuit, and for the outer wall, so additional heat structures were added for this purpose. *SG_HS1 – SG_HS8* modules model the heat transfer between the primary collectors and the secondary side, while *SG_HS9 – SG_HS17* modules represent the outer wall and calculate the heat loss.
- The middle part of the downcomer consists of six modules: a HEAT_PIPE models the hydraulic volume and the outer wall (*DC_MIDDLE*), and there are five additional heat structures (*DC_MID_IN1 – DC_MID_IN5*) for the inner metal structure.
- Since there is no measurement information about the nominal pressure drops across the valves, BASIC_VALVE modules with separate controlling circles were used instead of the CONTROL_VALVE-s.

- Critical flow model has been applied for both the break and the steam dump valves (MV31 and PV23, respectively). The available information about the boundary conditions of the secondary side bleeding is scarce, therefore a constant pressure was applied in this case. The gradient change of the measured secondary pressure during the secondary bleeding could not be observed in the first test runs. It made the long-term characteristics of the secondary pressure hard to replicate; therefore, we decided to lower the relevant discharge parameter once the pressure reaches the point of the gradient change. Based on the measurement data, values of 0.74 (PR81 > 2.7 MPa) and 0.43 (PR81 < 2.7 MPa) were used in case of valve PV23, while MV31 operated with a constant discharge coefficient of 0.9 throughout the whole transient.

- The 'Phase separation option' and the 'Calculation mode of node velocity' are set to 0 in the primary HEAT_TANK modules. The volume of the TANK modules is small compared to the flow area of the connected pipes, so there is no need for artificial separation of the steam and water phases. Furthermore, the steam and water velocities taken into account in the node are well approximated by the mass flow-weighted averages of the velocities calculated in the associated calculation-level thermos-hydraulic branches (only those branches that also transfer momentum are taken into account).

- In APROS the heat transfer in nodes between phases are modelled using an additional interface. The heat transfer between the gas-interface and the liquid-interface can be modified by a heat transfer efficiency factor. In the accumulator nodes these efficiency factors had to be increased for stability reasons. NO6_GAS_INT_HT_EFFI and NO6_LIQ_INT_HT_EFFI are 5.0 instead of 1.0. (This setting is only available in the calculation level node.) The gas phase temperature would cool down too much (below 1 °C) during injection without this modification, causing very low injection rates and accidental running stops.

- Due to the scaling of such facilities like the PMK-2, special emphasis should be placed on the modeling of heat capacities and heat losses. Accordingly, the model is primarily composed of HEAT_PIPE and HEAT_TANK modules. Special components, such as the core and the steam generator required additional heat structures (*CORE_WALL1 – CORE_WALL10, SG_HS9 – SG_HS17*) when modeling their walls. The downcomer of the facility contains an internal metal structure that represents the inner wall of the downcomer of the real plant. In the APROS model, this internal structure is taken into account by additional heat structure modules (*DC_MID_IN1 – DC_MID_IN5*). In the case of the pressurizer, extra heat transfer modules (*PRZ_WALL1 – PRZ_WALL5*) were added to connect the outer surface of the wall (heat structure) to the environment. The heat structures responsible for the heat loss modeling were connected to so-called "Not in simulation" points (see "Name of eternal point" rows of the data tables and Figure 6.2) with ambient parameters (293 K, 0.1 MPa). In order to approximate the measured distribution of heat losses [1] precisely, the efficiencies were adjusted through multiplication factors accordingly.

- The form loss coefficient settings are based on the measured pressure drops of the facility.

- The stagnant volumes (like the upper head and the top of the SG collectors) are treated in a special way during the steady state calculation as described in chapter 6.2. The pipe and tank modules positioned between the PV23 steam dump valve and the steam generator also form a stagnant volume until the beginning of secondary bleeding. If the heat loss is taken into account here, then the temperature drops to the ambient level and thus a significant amount of water condenses and stucks in the tanks. To prevent this process, the heat loss is neglected in these modules.

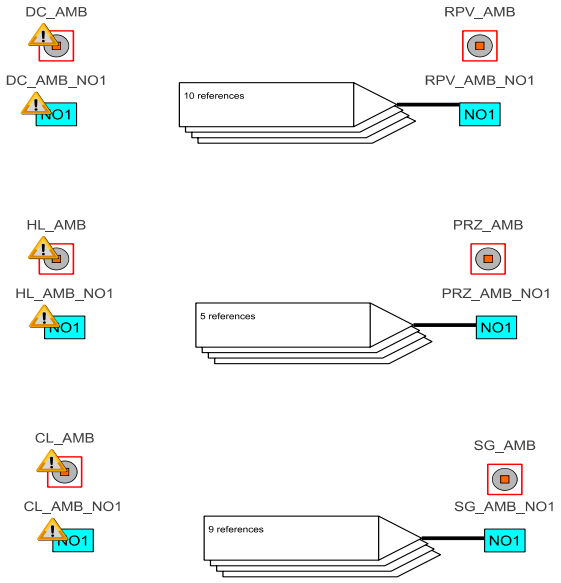

Figure 6.2 APROS 'Heatloss' Scheme

Parameters of the thermo-hydraulic model

The most important parameters of the modules are presented in the following tables.

Table 6.1 Reactor Core Parameters

	CORE
Module type	DESIGN_REACTOR
Relative power	1
Elevation of reactor bottom from ref. level [m]	0.994
Angle between flow direction and horizontal	90
Total length of the heated part [m]	2.5
Number of calculation nodes in heated part	10
Flow area [m^2]	0.0014803
Hydraulic diameter [m]	0.0080324
Form loss coefficient	1.05
Number of interfacial friction correlation	1
Is process component controlled	True

Table 6.2 Parameters of the Reactor Core Heat Structure

	FUEL
Module type	DESIGN_REACTOR_HS
Coordinate system	2
Inside radius [mm]	8.1
Thickness of first layer [mm]	1
Number of parallel heat structures	19
Material number of first layer	5
Number of nodes in the first layer	2
Is axial heat conduction solved	1
Is heat transfer calculated on inner surface	0
Is heat transfer calculated on outer surface	1
Nominal heating power [MW]	0.66512

Table 6.3 Steam Generator Parameters

	SG
Module type	STEAM_GENERATOR_HORI
Flow area of collector [m^2]	0.0041854
Height of collector [m]	2.115
Is collector divided into several nodes	T
Inside radius of one steam generator tube [mm]	3
Outside radius of one steam generator tube [mm]	4
Average length of steam generator tubes [m]	3.791
Number of parallel steam generator tubes	82
Number of tube rows	82
Material number of steam generator tubes	5
Form loss coefficient of tubes	0.85
Hydraulic diameter of steam generator tubes [m]	0.006
Number of calculation nodes inside the tube	3
Bottom elevation from reference level [m]	6.33
Flow area of downcomer [m^2]	0.014451
Number of generated downcomer lines	1
Free volume of heater [m^3]	0.24948
Height of heater [m]	1.865
Number of calculation nodes in the heater	3
Is heater divided horizontally	F
Volume of steam dome [m^3]	0.061089
Height of steam dome [m]	0.36
Number of calculation nodes in the steam dome	2
Elevation of feedwater injection from bottom [m]	1.105
Form loss coefficient of second circuit	1
Hydraulic diameter of second circuit [m]	0.008
Cross flow area [m^2]	2
Form loss coefficient of cross flow	1
Efficiency of heat transfer inside the tubes [%]	100
Efficiency of heat transfer in the 2. circuit [%]	100

Table 6.4 Pressurizer Parameters

	PRZ
Module type	PRESSURIZER
Height of pressurizer [m]	2.46
Cross-sectional free area of pressurizer [m^2]	0.0080118
Bottom elevation from reference level [m]	7.8
Elevation of connection point from bottom[5]	2.46
Outside radius of heater [mm]	12.5
Length of heater [m]	0.4
Number of heaters	1
Nominal heating power [MW]	0.0032
Thickness of wall [mm]	16
Number of radial heat structure nodes on wall	5
Number of calculation nodes	5
Calculation mode of node velocity	1

Table 6.5 Pump Parameters

	PMK_PUMP	
Module type	BASIC_PUMP	
Flow length of pump [m]	0.635	
Flow area [m^2]	0.0080118	
Nominal volumetric flow [m^3/s]	0.0057692	
Nominal density [kg/m^3]	780	
Type of characteristic head curve	2	
Point of head curve[1]	0.000000	210.99
Point of head curve[2]	1.2820500E-03	207.48
Point of head curve[3]	2.5641001E-03	204.1
Point of head curve[4]	3.8461499E-03	200.72
Point of head curve[5]	5.1282002E-03	197.21
Point of head curve[6]	6.4102998E-03	193.83
Exponent for head dependency on speed	2	
Time constant of coasting down [s]	1	
Is heat generation of pump calculated	F	

Table 6.6 Point Parameters Part 1

	HL_ PO1	HL_ PO2	HL_ PO3	HL_ PO4	HL_ PO5	CL_ PO1	CL_ PO2	CL_ PO3	CL_ PO4	CL_ PO5
Elevation from reference level [m]	6.225	6.225	4.825	4.825	5.595	5.595	3.225	3.225	3.225	3.325

Table 6.7 Point Parameters Part 2

	CL_ PO6	CL_ PO7	CL_ PO8	BYPASS_ PO1	BYPASS_ PO2	BYPASS_ PO3	BYPASS_ PO4
Elevation from reference level [m]	3.325	4.825	4.825	2.027	0.327	-0.318	0.017

Table 6.8 Point Parameters Part 3

	BYPASS_ PO5	BYPASS_ PO6	BYPASS_ PO7	SIT1_ PO1	SIT1_ PO2	SIT2_ PO1	FW_ PO1	SL_ PO1
Elevation from reference level [m]	1.532	1.532	2.257	7.495	5.35	7.495	5.85	9.343

Table 6.9 Point Parameters Part 4

	SL_ PO2	SL_ PO3	SL_ PO4	SL_ PO5	SPRAY_ PO1	PRZ_ PO1	BREAK_ PO1	BREAK_ PO2	LPIS_ PO01
Elevation from reference level [m]	9.343	10.043	9.343	10.043	10.535	6.225	4.825	4.825	5.35

Table 6.10 Tank Parameters Part 1

	DC_TOP	DC_ BOTTOM_1	LOWER_ PLENUM	UP_ BOTTOM	UP_L2
Height of tank [m]	0.275	0.35	0.38	0.38	0.956
Cross-sectional free area of tank [m^2]	0.017404	0.0016619	0.008012	0.0073071	0.0033238
Elevation of tank bottom from reference level [m]	4.72	0.19	0	3.564	3.731
Elevation of connection point from bottom [m]	[3, 7, 8] 0.105	[5] 0.35	[1] 0.38 [7] 0.19	[1] 0.19	[5] 0.933 [8] 0.023
Hydraulic diameter [m]	0	0	0	0	0.046
Thickness of first layer in the wall [mm]	90	5.5	135	135	5.5
Number of nodes in first layer of the wall	5	2	2	2	2
Name of external point	DC_AMB	DC_AMB	RPV_AMB	RPV_AMB	RPV_AMB

Table 6.11 Tank Parameters Part 2

	UP_ MIDDLE	UH_ BOTTOM	UH_TOP	BYPASS_ TA1	BYPASS_ TA2
Height of tank [m]	0.34	0.275	1.915	1.038	1.068
Cross-sectional free area of tank [m^2]	0.0041854	0.017404	0.0041845	0.0041854	0.0016619
Elevation of tank bottom from reference level [m]	4.494	6.12	6.57	2.187	2.257
Elevation of connection point from bottom [m]	[3] 0.17 [5] 0.34	[3] 0.105 [5] 0.275 [7] 0.105	-	-	-
Hydraulic diameter [m]	0	0	0	0	0
Thickness of first layer in the wall [mm]	90.5	90	8	8	5.5
Number of nodes in first layer of the wall	2	5	5	2	2
Name of external point	RPV_AMB	RPV_AMB	RPV_AMB	CL_AMB	CL_AMB

Table 6.12 Tank Parameters Part 3

	SD_TA1	SL_TA1	SL_TA2
Height of tank [m]	0.38	1.705	1.205
Cross-sectional free area of tank [m^2]	0.0304805	0.0149571	0.0149571
Elevation of tank bottom from reference level [m]	9.153	9.258	9.958
Elevation of connection point from bottom [m]	[2] 0.19 [6] 0.19	[1] 1.635 [8] 0.085	[4] 0.085 [6] 0.935
Hydraulic diameter [m]	0	0	0
Number of calculation nodes	1	2	2
Thickness of first layer in the wall [mm]	11	6	6
Material number of first layer in the wall	17	5	5
Number of nodes in first layer of the wall	5	2	2
Name of external point	SG_AMB	-	-

Table 6.13 Pipe Parameters Part 1

	DC_MIDDLE	DC_BOTTOM_2	CORE_INLET	CORE_OUTLET
Flow length of pipe [m]	4.18	0.6515	0.614	0.07
Inside radius [mm]	36.5	23	29.402	29.402
Thickness of first layer in the wall [mm]	8	5.5	20.598	20.598
Thickness of second layer in the wall [mm]	-	-	16.5	16.5
Flow area [m^2]	0.002595	0	0.0021372	0.002715
Hydraulic diameter [m]	0.028	0	0.030612	0.0080324
Number of parallel pipes	1	1	1	1
Material number of first layer in the wall	5	5	14	14
Material number of second layer in the wall	-	-	5	5
Form loss coefficient	2	1.4	0.2	0.2
Is momentum transferred in beginning of pipe	T	T	T	T
Is momentum transferred in the end of pipe	T	T	T	T
Number of calculation nodes inside the pipe	5	1	1	1
Number of nodes in first layer of the wall	5	2	2	2
Number of nodes in second layer of the wall	-	-	1	1
Is heat transferred to connection points	F	T	F	F
Number of interfacial friction correlation	-	-	-	1
Name of external point	DC_AMB	DC_AMB	RPV_AMB	RPV_AMB

Table 6.14 Pipe Parameters Part 2

	UP_L1	UP_L3	UP_TOP	UH_MIDDLE	HL_PIP1
Flow length of pipe [m]	0.4215	0.4405	1.286	0.175	0.28
Inside radius [mm]	23	23	23	36.5	23
Thickness of first layer in the wall [mm]	5.5	5.5	5.5	8	5.5
Flow area [m^2]	0.0033238	0.0033238	0	0	0
Hydraulic diameter [m]	0.046	0.046	0	0	0
Number of parallel pipes	2	2	1	1	1
Material number of first layer in the wall	5	5	5	5	5

Table 6.14 Pipe Parameters Part 2 (cont.)

Form loss coefficient	1	1	0.7	0	0
Is momentum transferred in beginning of pipe	T	T	T	F	T
Is momentum transferred in the end of pipe	T	T	T	T	T
Number of calculation nodes inside the pipe	1	1	1	1	1
Number of nodes in first layer of the wall	2	2	2	5	5
Is heat transferred to connection points	T	T	T	T	T
Number of interfacial friction correlation	6	6	6	-	-
Name of external point	RPV_AMB	RPV_AMB	RPV_AMB	RPV_AMB	HL_AMB

Table 6.15 Pipe Parameters Part 3

	HL_PIP2	HL_PIP3	HL_PIP4	HL_PIP5	HL_PIP6
Flow length of pipe [m]	0.5	2.86	0.42	0.77	0.735
Inside radius [mm]	23	23	23	23	36.5
Thickness of first layer in the wall [mm]	5.5	5.5	5.5	5.5	8
Flow area [m^2]	0	0	0	0	0
Hydraulic diameter [m]	0	0	0	0	0
Number of parallel pipes	1	1	1	1	1
Material number of first layer in the wall	5	5	5	5	5
Form loss coefficient	0	0	0	0	0.5
Is momentum transferred in beginning of pipe	T	T	T	T	T
Is momentum transferred in the end of pipe	T	T	T	T	F
Number of calculation nodes inside the pipe	1	2	1	1	1
Number of nodes in first layer of the wall	5	2	2	2	2
Is heat transferred to connection points	T	T	T	T	T
Name of external point	HL_AMB	HL_AMB	HL_AMB	HL_AMB	HL_AMB

Table 6.16 Pipe Parameters Part 4

	CL_PIP1	CL_PIP2	CL_PIP3	CL_PIP4	CL_PIP5
Flow length of pipe [m]	0.735	2.37	0.26	0.245	0.93
Inside radius [mm]	36.5	23	23	23	23
Thickness of first layer in the wall [mm]	8	5.5	5.5	5.5	5.5
Flow area [m^2]	0	0	0	0	0
Hydraulic diameter [m]	0	0	0	0	0
Number of parallel pipes	1	1	1	1	1
Material number of first layer in the wall	5	5	5	5	5
Form loss coefficient	0.5	0	0	0	0
Is momentum transferred in beginning of pipe	F	T	T	T	T
Is momentum transferred in the end of pipe	T	T	T	T	T
Number of calculation nodes inside the pipe	1	2	1	1	1
Number of nodes in first layer of the wall	2	2	2	2	2
Is heat transferred to connection points	T	T	T	T	T
Name of external point	CL_AMB	CL_AMB	CL_AMB	CL_AMB	CL_AMB

Table 6.17 Pipe Parameters Part 5

	CL_PIP6	CL_PIP7	CL_PIP8	SURGE_PIP1
Flow length of pipe [m]	1.5	0.555	1.125	2.213
Inside radius [mm]	23	23	23	14.5
Thickness of first layer in the wall [mm]	5.5	5.5	5.5	4.5
Flow area [m^2]	0	0	0	0
Hydraulic diameter [m]	0	0	0	0
Number of parallel pipes	1	1	1	1
Material number of first layer in the wall	5	5	5	5
Form loss coefficient	0.8	0	1	0
Is momentum transferred in beginning of pipe	T	T	T	F
Is momentum transferred in the end of pipe	T	T	T	T
Number of calculation nodes inside the pipe	1	1	1	2
Number of nodes in first layer of the wall	2	2	2	2

Table 6.17 Pipe Parameters Part 5 (cont.)

Is heat transferred to connection points	T	T	T	T
Name of external point	CL_AMB	CL_AMB	CL_AMB	PRZ_AMB

Table 6.18 Pipe Parameters Part 6

	BYPASS_PIP1	BYPASS_PIP2	BYPASS_PIP3	BYPASS_PIP4
Flow length of pipe [m]	3.3893	1.2904	3.265	0.93006
Inside radius [mm]	36.5	50.5	23	23
Thickness of first layer in the wall [mm]	8	16	5.5	5.5
Flow area [m^2]	0	0	0	0
Hydraulic diameter [m]	0	0	0	0
Number of parallel pipes	1	1	1	1
Material number of first layer in the wall	5	5	5	5
Form loss coefficient	0.6	0.2	0.8	1
Is momentum transferred in beginning of pipe	T	T	T	T
Is momentum transferred in the end of pipe	T	T	T	T
Number of calculation nodes inside the pipe	0	0	0	0
Number of nodes in first layer of the wall	2	2	2	2
Is heat transferred to connection points	T	T	T	T
Name of external point	CL_AMB	CL_AMB	CL_AMB	CL_AMB

Table 6.19 Pipe Parameters Part 7

	PREHEATER	SD_PIP1	SL_PIP1	SL_PIP2	SL_PIP3
Flow length of pipe [m]	1.71	0.598	0.24	0.24	0.131
Inside radius [mm]	51	98.5	14.5	38.2	11
Thickness of first layer in the wall [mm]	12.5	11	4.5	6.3	4
Flow area [m^2]	0	0	0	0	0
Hydraulic diameter [m]	0	0	0	0	0
Number of parallel pipes	1	1	1	1	1
Material number of first layer in the wall	5	17	5	5	5
Form loss coefficient	1	1	1	1	0
Is momentum transferred in beginning of pipe	T	T	F	F	F

Table 6.19 Pipe Parameters Part 7 (cont.)

Is momentum transferred in the end of pipe	T	F	F	F	F
Number of calculation nodes inside the pipe	0	4	0	0	0
Number of nodes in first layer of the wall	2	5	2	2	2
Is heat transferred to connection points	T	T	T	T	T
Name of external point	CL_AMB	SG_AMB	-	SG_AMB	-

Table 6.20 Pipe Parameters Part 8

	SL_PIP4	SL_PIP5	BREAK_PIP1
Flow length of pipe [m]	0.112	0.131	0.190
Inside radius [mm]	11	11	11.5
Thickness of first layer in the wall [mm]	4	4	6
Flow area [m^2]	0	0	0
Hydraulic diameter [m]	0	0	0
Number of parallel pipes	1	1	1
Material number of first layer in the wall	5	5	5
Form loss coefficient	0	0	0
Is momentum transferred in beginning of pipe	F	F	F
Is momentum transferred in the end of pipe	F	F	T
Number of calculation nodes inside the pipe	1	0	1
Number of nodes in first layer of the wall	2	2	2
Is heat transferred to connection points	T	T	T
Name of external point	-	-	-

Table 6.21 Pipe Parameters Part 9

	LPIS_PIP1	SIT1_PIP1	SIT1_PIP2	SIT2_PIP1
Flow length of pipe [m]	0.1	2.695	1.685	4.025
Flow area [m^2]	1.13097E-4	7.85398E-5	7.85398E-5	7.85398E-5
Form loss coefficient	1	6	6	12
Is momentum transferred in beginning of pipe	F	T	T	T
Is momentum transferred in the end of pipe	F	T	F	F
Number of calculation nodes inside the pipe	0	1	1	1

Table 6.22 Pipe Parameters Part 10

	SPRAY_PIP1	PRZ_PIP1	EFW_PIP1
Flow length of pipe [m]	5.71	0.1	1.48
Flow area [m^2]	7.85398E-5	1.0E-3	1.0E-3
Form loss coefficient	0	1	1
Is momentum transferred in beginning of pipe	F	F	F
Is momentum transferred in the end of pipe	F	F	F
Number of calculation nodes inside the pipe	0	0	0

Table 6.23 Valve Parameters Part 1

	MV11	MV12	MV31	MV91	MV92
Flow length of valve [m]	0.1	0.43	0.015	0.7473	0.7473
Flow area [m^2]	1.9635E-03	7.8536E-03	8.04248E-6	1.767E-04	1.767E-04
Driving time of valve [s]	2	3	0.1	0	0
Loss coefficient of fully open valve	4.6	3	0	0	0
Discharge coefficient	0.75	0.75	0.9	0.75	0.75
Is momentum transferred over the valve	T	T	T	T	T
Thickness of first layer in the wall [mm]	10	10	0	0	0
Material number of first layer in the wall	5	5	-	-	-
Number of nodes in first layer of the wall	2	2	-	-	-

Table 6.24 Valve Parameters Part 2

	PV11	PV12	PV21	PV22	PV23
Flow length of valve [m]	0.61	0.8	1.48	0.1	0.1
Flow area [m^2]	1.9635E-03	1.7671E-04	5.3093E-04	4.9087E-04	2.8274E-05
Driving time of valve [s]	2	0	6	6	2.1
Loss coefficient of fully open valve	5	1	4100	300	5
Discharge coefficient	0.75	0.75	0.75	0.75	0.74 (0.43)
Is momentum transferred over the valve	T	F	F	F	F
Thickness of first layer in the wall [mm]	10	0	0	0	0
Material number of first layer in the wall	5	-	-	-	-
Number of nodes in first layer of the wall	2	-	-	-	-

Table 6.25 Branch Parameters

	BYPASS_BR1	BYPASS_BR2	SD_BR1
Flow length of branch [m]	0.519	0.534	0.958
Flow area [m^2]	0.004185	0.0016619025	3.0E-3
Is branch situated between node centers	F	F	F
Input elevation from reference level	3.225	2.791	9.153
Output elevation from reference level	2.706	3.325	8.195
Elevation from reference level	3.225	3.325	8.195
Form loss coefficient	1	1	100
Is momentum transferred over the branch	F	F	F

Table 6.26 Accumulator Parameters

	SIT1	SIT2
Height of accumulator [m]	2.47	2.47
Cross-sectional free area of accumulator [m^2]	0.03048	0.03048
Bottom elevation from reference level [m]	7.975	7.975

Table 6.27 Parameters of the Additional Core and Downcomer Heat Structures

	CORE_WALL1 – CORE_WALL10	DC_MID_IN1 – DC_MID_IN5
Name of connection point on the inner surface	CORE_NO1 – CORE_NO10	-
Name of connection point on the outer surface	RPV_AMB_NO1	DC_MIDDLE_NO1 – DC_MIDDLE_NO5
Coordinate system	2	2
Inside radius [mm]	29.402	17.5
Thickness of first layer [mm]	20.598	5
Thickness of second layer [mm]	16.5	-
Length [m]	0.25	0.836
Bottom elevation from reference level [m]	0.994, 1.244, …, 3.244	3.884, 3.048, … , 0.54
Angle between heat structure and horizontal	90	90
Hydraulic diameter of inner surface [m]	0.05881	0.035
Hydraulic diameter of outer surface [m]	0.133	0.045
Number of equal heat structures	1	1
Material number of first layer	14	5
Material number of second layer	5	-
Number of nodes in the first layer	3	3
Number of nodes in the second layer	3	-
Efficiency of heat transfer (outer surface) [%]	20.7	100

Table 6.28 Parameters of the Additional SG Heat Structures 1 (Hot Collector)

	SG_HS1	SG_HS2	SG_HS3	SG_HS4
Name of connection point on the inner surface	SG_NO1	SG_NO2	SG_NO3	SG_NO4
Name of connection point on the outer surface	SG_NO18	SG_NO19	SG_NO20	SG_NO21
Coordinate system	2			
Inside radius [mm]	36.5			
Thickness of first layer [mm]	8			
Height [m]	0.621667			0.25
Angle between heat structure and horizontal	90			
Hydraulic diameter of inner surface [m]	0.073			
Hydraulic diameter of outer surface [m]	0.089			
Number of equal heat structures	1			
Material number of first layer	5			
Number of nodes in the first layer	2			

Table 6.29 Parameters of the Additional SG Heat Structures 2 (Cold Collector)

	SG_HS5	SG_HS6	SG_HS7	SG_HS8
Name of connection point on the inner surface	SG_NO14	SG_NO15	SG_NO16	SG_NO17
Name of connection point on the outer surface	SG_NO18	SG_NO19	SG_NO20	SG_NO21
Coordinate system	2			
Inside radius [mm]	36.5			
Thickness of first layer [mm]	8			
Height [m]	0.621667			0.25
Angle between heat structure and horizontal	90			
Hydraulic diameter of inner surface [m]	0.073			
Hydraulic diameter of outer surface [m]	0.089			
Number of equal heat structures	1			
Material number of first layer	5			
Number of nodes in the first layer	2			

Table 6.30 Parameters of the Additional SG Heat Structures 3 (Cylindrical Wall)

	SG_HS9	SG_HS10	SG_HS11	SG_HS12	SG_HS13
Name of connection point on the inner surface	SG_NO23	SG_NO24	SG_NO25	SG_NO21	SG_NO22
Name of connection point on the outer surface	SG_AMB_NO1				
Coordinate system	2				
Inside radius [mm]	235				
Thickness of first layer [mm]	3				
Thickness of second layer [mm]	16				
Height [m]	0.621667			0.18	
Angle between heat structure and horizontal	90				
Hydraulic diameter of inner surf. [m]	0.47				
Hydraulic diameter of outer surf. [m]	0.508				
Number of equal heat structures	1				
Material number of first layer	5				
Material number of second layer	17				
Number of nodes in the first layer	2				
Number of nodes in the second layer	1				
Efficiency of heat transfer on the outer surface [%]	15				

Table 6.31 Parameters of the Additional SG Heat Structures 4 (Other Walls)

	SG_HS14	SG_HS15	SG_HS16	SG_HS17
Conn. point on the inner surface	SD_TA1_NO1	SG_NO22	SG_NO23	SG_NO18
Conn. point on the outer surface	SG_AMB_NO1			
Coordinate system	1 (Cartesian)			
Thickness of first layer [mm]	50	95		
Length [m]	0.17459	0.36855	0.1202	0.3822
Breadth [m]	0.17459	0.36855	0.1202	0.3822
Bottom elevation from reference level [m]	9.533	8.555	6.235	
Angle between heat structure and horizontal	0			
Number of equal heat structures	1			
Material number of first layer	17			
Number of nodes in the first layer	3	4		
Efficiency of heat transfer on the outer surface [%]	15			

Table 6.32 Parameters of the Additional Pressurizer Heat Transfer Modules

	PRZ_ WALL1	PRZ_ WALL2	PRZ_ WALL3	PRZ_ WALL4	PRZ_ WALL5
Name of HS node	PRZ_HN7	PRZ_HN12	PRZ_HN17	PRZ_HN22	PRZ_HN27
Name of thermo-hydraulic node	PRZ_AMB_NO1				
Hydraulic diameter [m]	0.133				
Efficiency of heat transfer 1.	0.3				

Table 6.33 Efficiency of Heat Transfer on the Walls to Model the Heat Loss Distribution

Main parts of the facility	Efficiency of heat transfer on the walls [%]
Downcomer	22.8
Core	20.7
Hot leg	152.3
Pressurizer	30
Cold leg + bypass	41.6
SG pipes	80
Secondary side	15

Table 6.34 Break Pressure Boundary, Decay Heat and Pump Coast-Down Tables

Time [s]	Pressure [Pa]
-1e6	100000
0	100000
4	557000
23	358000
54	321000
77	324000
83	274000
93	312000
145	312000
157	300000
158	285000
160	234000
165	294000
170	236000
175	296000
185	239000
220	295000
255	245000
260	109000
280	109000
290	227000
310	224000
315	100000
325	100000
335	204000
340	204000
350	132000
365	156000
380	104000
690	100000
700	96000
1000	100000
1e6	100000

Time [s]	Power [kW]
0	665.12
1	631
2	558
3	479
4	412
5	355
6	305.6
7	260.4
9	192
11	142.4
14	99.6
17	72.4
21	53.6
25	46
30	41
40	38.4
60	36.4
80	34.4
100	31.6
150	28.4
200	25.6
400	21.6
700	18
996	16.4
1e6	16.4

Time [s]	Coast-down multiplier
0	1
2	1
4	0.86
8	0.85
11	0.7
15	0.63
22	0.55
30	0.5
40	0.43
42	0.33
52	0.32
56	0.14
97	0.09
135	0.07
150	0.06
151	0.01
152	0
1e6	0

Table 6.35 Thermal Properties of Redefined Materials

	Material 5 (stainless steel)	Material 14 (ceramic for core)	Material 17 (Mn steel for SG)
Unit of the temperature	2 (Kelvin)		
Density [kg/m^3]	7800	2700	7800
Starting point of temperature range for (C_p × ρ)	0	0	0
	293	293	293
	773	373	773
Coefficient of (heat capacity × density), 1. range	3900000.0	2146500.0	3900000.0
	0.0	0.0	0.0
Coefficient of (heat capacity × density), 2. range	3328650.0	910406.25	3328650.0
	1950.0	4218.75	1950.0
Coefficient of (heat capacity × density), 3. range	4836000.0	2484000.0	4836000.0
	0.0	0.0	0.0
Starting point of temperature range for λ	0	0	0
	293		373
	473		473
	773		573
Coefficient of heat conductivity, 1. range	14.7	2.558	51.1
	0.0	0.0	0.0
Coefficient of heat conductivity, 2. range	10.46777778	-	63.782
	1.4444444 E-2		-3.4 E-2
Coefficient of heat conductivity, 3. range	11.46633333	-	64.255
	1.2333333 E-2		-3.5 E-2
Coefficient of heat conductivity, 4. range	21.0	-	44.2
	0.0		0.0

6.2 Control Systems

Based on the literature [1] and [3], the subsystems on the control schemes implement the following functions:

- *Break:* opens the valve modeling the break. The outlet pressure boundary is controlled by a table during the transient, which is started by setting the BINARY_SETPOINT module named TRANSIENT0 to True. This signal is also used in other parts of the model.
- *SCRAM:* the reactor shutdown is initiated by the low primary pressure (PR21 < 11.15 MPa). The heating power is then calculated with the given remnant heat table (decay heat).
- *SIT isolation:* the valves between the accumulators and the primary circuit (MV91, MV92) open at the primary pressure of 5.9 MPa and close at the water levels of 0.245 m (SIT1) and 1.035 m (SIT2), respectively.
- *Flow control:* the nominal mass flow is set by a circuit using a PI controller. At low primary pressure (PR21 < 9.21 MPa), the COASTDOWN signal changes to 'True' and starts the coastdown program of the main circulating pump: the PV11 valve closes in 152 s, then the MV11 opens, the MV12 closes and the pump stops.
- *Pressure control:* in the real facility, the pressurizer spray operates intermittently. In the model, a constant spray injection of 8.5×10^{-4} kg/s is set before the transient so that the pressurizer is not a stagnant volume. This mass flow was determined to result in a stable steady state at about 70 % heater power. The PR21 pressure is set to the desired value by controlling the heater power with a circuit using a PI controller. The PV12 spray valve closes and the heater shuts down at the TRANSIENT0 signal.
- *Pressurizer level control:* the LE71 level is set to the desired value by supplying or extracting water from the primary system through the PRZ_PIP1 pipe. The mass flow rate of this pipe is controlled by a circuit using a PI controller, and it is set to zero at the TRANSIENT0 signal.
- *LPIS control:* the low pressure injection system is initiated by the low primary pressure (PR21 < 1.04 MPa). This system provides a continuous 0.042 kg/s mass flow rate.
- *SG level control:* the LE81 (LE82) level is set to the desired value with the PV21 feed water valve controlled by a circuit using a PI controller. The PV21 closes at the TRANSIENT0 signal.
- *SG pressure control:* the secondary pressure is set to the desired value with the PV22 steam valve controlled by a circuit using a PI controller. The PV22 closes at the TRANSIENT0 signal.
- *SG pressure limitation + secondary bleed:* the PV23 steam dump valve provides both the steam generator pressure limitation and the secondary side bleed functions. It opens at 5.3 MPa and closes at 4.9 MPa to limit the pressure, but this operation did not occur, because the pressure did not reach the opening value during the transient. The secondary bleed starts 150 s after the initiation of the pump coastdown (PR21 < 9.21 MPa) and remains ongoing throughout the transient.
- *EFW control:* the emergency feedwater injection system is initiated by the low secondary pressure (PR81 < 0.93 MPa). This system provides a continuous 0.042 kg/s mass flow rate.

- *RPV head initial temperature:* the issue of dead-ends (stagnant volumes), such as the uppermost part of the reactor vessel and the downcomer (see UH_TOP and UH_MIDDLE on Figure 6.1), is treated differently during the steady-state of APROS compared to the other two models. It is managed by inserting an amount of heat equal to the loss into the affected nodes. In the control circuit, the input of the GENERAL_SUM modules is the NO6_HT_HEAT_FLOW parameter of the nodes (which is the total heat flow from the connected heat structures to the node), while the output is (-1) times the input. The DC_CONTROLLER sets the NO6_GIVEN_HEAT_FLOW parameter of the nodes (which is the amount of extra heating power inserted to the thermal hydraulic node) to be equal to the output of the GENERAL_SUM module. This extra heating power is set to zero at the TRANSIENT0 signal.
- *SG collector head initial temperature:* the uppermost nodes of the primary collectors of the steam generator form similar stagnant volumes as the described reactor vessel nodes. The lost heat is transferred to the secondary side and is compensated in a manner analogous to that described in the previous section.
- *Heat added by the pump:* in line with the technical document [1], thermal power of 18.5 kW is deposited to the node downstream of the MCP. The modeling of the pump heat generation is disabled by the pump stop signal.

The control schemes are shown on Figure 6.3 and Figure 6.4.

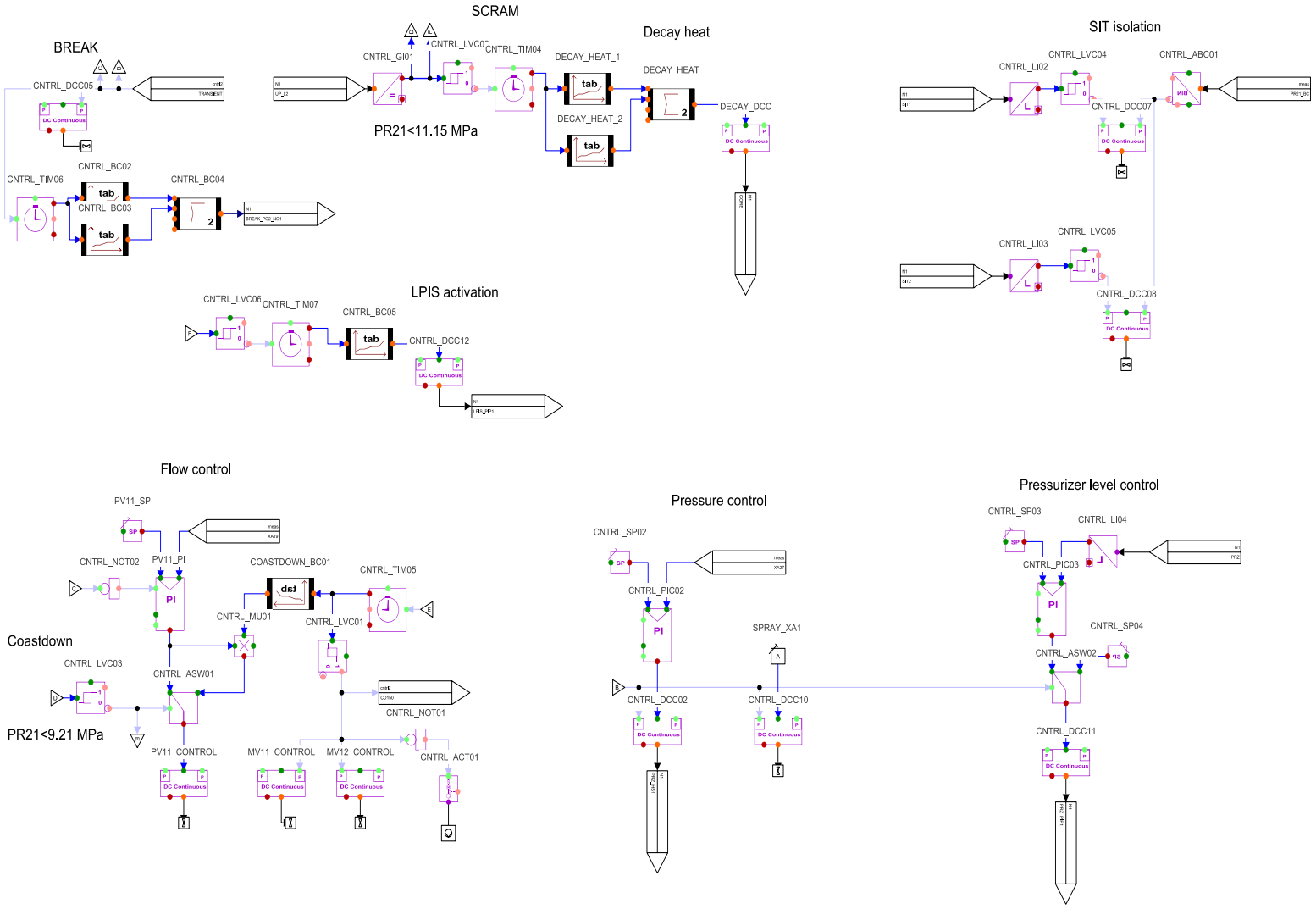

Figure 6.3 ‘CNTRL’ Control Scheme of the APROS Model

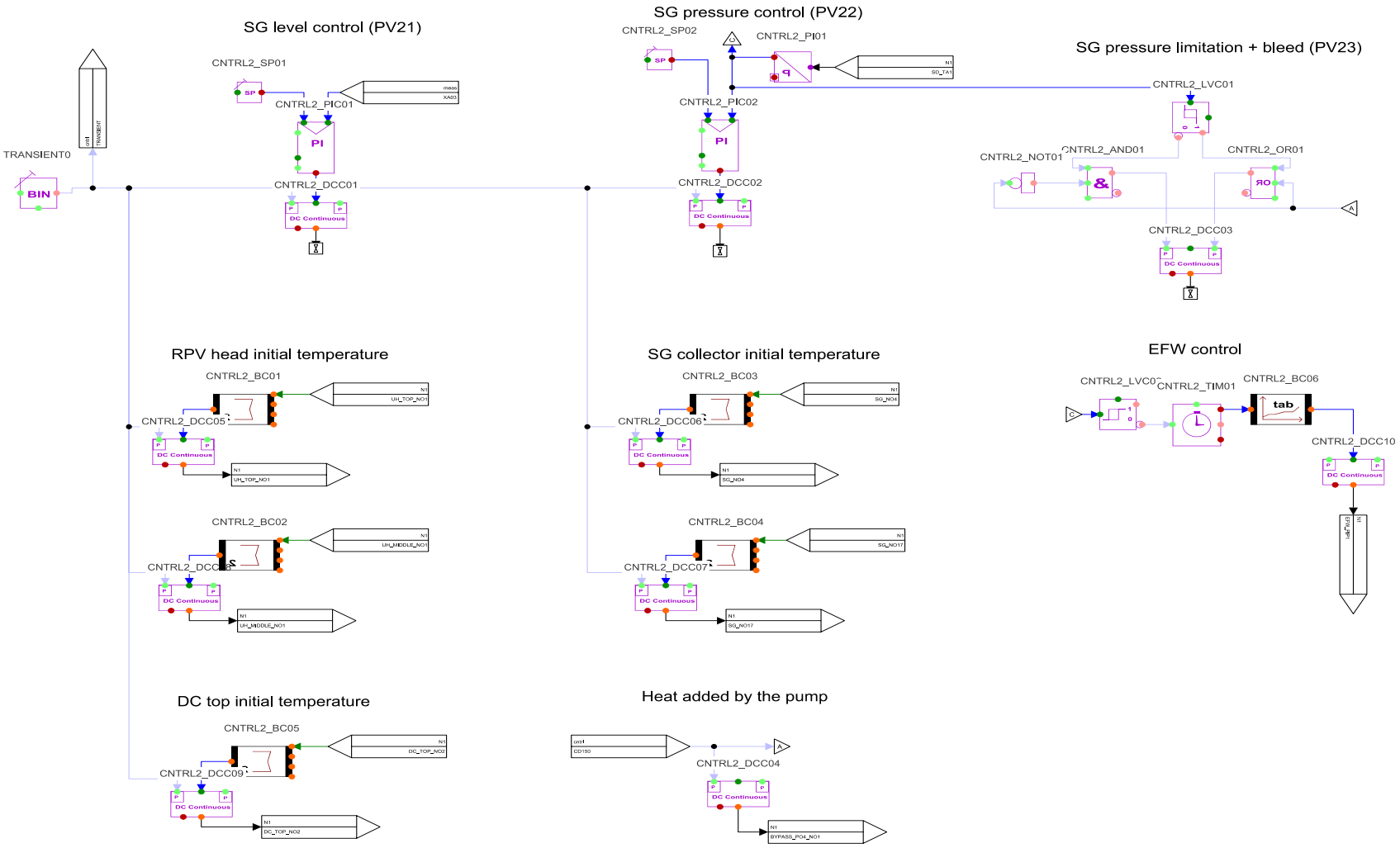

Figure 6.4 ‘CNTRL2’ Control Scheme of the APROS Model

6.3 Measurements

The measurements implemented in the model are presented in Table 6.36. All of the required calculations were performed by an SCL script included in the MEAS_UC user component (see Figure 6.5). This provides the measurement signals also for the *Flow control*, *SG level control, Pressure control* and *SIT isolation*. The wall temperatures TE23 and TE62 are measured in the outermost heat structure layer (furthest from the fluid). The heater temperatures TE11, TE12, TE13, TE14 and TE15 are measured in the innermost heat structure layer.

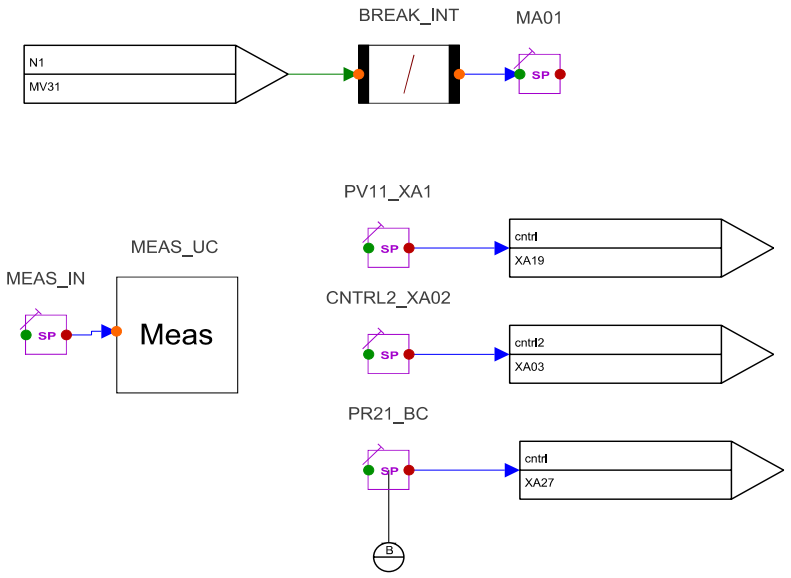

Figure 6.5 'Meas' Measurement Scheme of the APROS Model

Table 6.36 Measurement Signals in the APROS Model

ID	Measured quantity	APROS parameters
DP11	Core pressure drop	(LOWER_PLENUM_07 PO11_PRESSURE - UP_BOTTOM_02 PO11_PRESSURE) * 1000 - 0.001 * 9.81 * 3.564 * CORE_NO1 NO6_LIQ_DENS
DP16	Main circulation pump dP	(BYPASS_PO4 PO11_PRESSURE - BYPASS_PO3 PO11_PRESSURE) * 1000
DP41	SG primary pressure drop	(HL_PO5 PO11_PRESSURE - CL_PO1 PO11_PRESSURE) * 1000
FL01	Break mass flow	MV31 VA11_MIX_MASS_FLOW
FL53	Cold leg mass flow (normal)	CL_PIP8 PI13_MIX_MASS_FLOW
FL54	Cold leg mass flow (low flow)	CL_PIP8 PI13_MIX_MASS_FLOW

Table 6.36 Measurement Signals in the APROS Model (cont.)

LE11	Reactor liquid level	LOWER_PLENUM_NO1 NO6_LIQ_LEVEL + CORE_INLET_NO1 NO6_LIQ_LEVEL + CORE_NO1 NO6_LIQ_LEVEL + CORE_NO2 NO6_LIQ_LEVEL + CORE_NO3 NO6_LIQ_LEVEL + CORE_NO4 NO6_LIQ_LEVEL + CORE_NO5 NO6_LIQ_LEVEL + CORE_NO6 NO6_LIQ_LEVEL + CORE_NO7 NO6_LIQ_LEVEL + CORE_NO8 NO6_LIQ_LEVEL + CORE_NO9 NO6_LIQ_LEVEL + CORE_NO10 NO6_LIQ_LEVEL + CORE_OUTLET_NO1 NO6_LIQ_LEVEL + UP_BOTTOM_NO1 NO6_LIQ_LEVEL (max. 0.167) + UP_L2_NO1 NO6_LIQ_LEVEL (max. 0.91) + (UP_MIDDLE_NO1 NO6_LIQ_LEVEL – 0.147) (min 0.0) + UP_TOP_NO1 NO6_LIQ_LEVEL + UH_BOTTOM_NO1 NO6_LIQ_LEVEL + UH_MIDDLE_NO1 NO6_LIQ_LEVEL + UH_TOP_NO1 NO6_LIQ_LEVEL
LE21	Upper plenum liquid level 1	UH_TOP_NO1 NO6_LIQ_LEVEL + UH_MIDDLE_NO1 NO6_LIQ_LEVEL + UH_BOTTOM_NO1 NO6_LIQ_LEVEL + (UP_TOP_NO1 NO6_LIQ_LEVEL – 0.87) (min 0.0) + 5.704
LE22	Upper plenum liquid level 2	UP_TOP_NO1 NO6_LIQ_LEVEL (max 0.87) + (UP_MIDDLE_NO1 NO6_LIQ_LEVEL – 0.17) (min 0.0) + 4.664
LE23	Upper plenum liquid level 3	(UP_L2_NO1 NO6_LIQ_LEVEL – 0.023) (min 0.0, max 0.91) + 3.754
LE31	Hot leg loop seal liquid level	HL_PO2_NO1 NO6_LIQ_LEVEL + HL_PIP3_NO1 NO6_LIQ_LEVEL + HL_PIP3_NO2 NO6_LIQ_LEVEL + HL_PO3_NO1 NO6_LIQ_LEVEL + 4.742 (min 4.802, max 6.08)
LE45	SG primary liquid level – hot leg	HL_PO4_NO1 NO6_LIQ_LEVEL + HL_PIP5_NO1 NO6_LIQ_LEVEL + HL_PO5_NO1 NO6_LIQ_LEVEL + HL_PIP6_NO1 NO6_LIQ_LEVEL + SG_NO1 NO6_LIQ_LEVEL + SG_NO2 NO6_LIQ_LEVEL + SG_NO3 NO6_LIQ_LEVEL + SG_NO4 NO6_LIQ_LEVEL + 4.802

Table 6.36 Measurement Signals in the APROS Model (cont.)

LE46	SG primary liquid level – cold leg	CL_PO1_NO1 NO6_LIQ_LEVEL + CL_PIP1_NO1 NO6_LIQ_LEVEL + CL_PO2_NO1 NO6_LIQ_LEVEL + CL_PIP2_NO1 NO6_LIQ_LEVEL + CL_PIP2_NO2 NO6_LIQ_LEVEL + SG_NO14 NO6_LIQ_LEVEL + SG_NO15 NO6_LIQ_LEVEL + SG_NO16 NO6_LIQ_LEVEL + SG_NO17 NO6_LIQ_LEVEL + 3.202
LE51	Cold leg liquid level	CL_PO1_NO1 NO6_LIQ_LEVEL + CL_PIP1_NO1 NO6_LIQ_LEVEL (max 0.195) + CL_PIP2_NO1 NO6_LIQ_LEVEL + CL_PIP2_NO2 NO6_LIQ_LEVEL + CL_PO2_NO1 NO6_LIQ_LEVEL + 3.202
LE61	Downcomer liquid level	DC_BOTTOM_1_NO1 NO6_LIQ_LEVEL + DC_MIDDLE_NO1 NO6_LIQ_LEVEL + DC_MIDDLE_NO2 NO6_LIQ_LEVEL + DC_MIDDLE_NO3 NO6_LIQ_LEVEL + DC_MIDDLE_NO4 NO6_LIQ_LEVEL + DC_MIDDLE_NO5 NO6_LIQ_LEVEL + DC_TOP_NO1 NO6_LIQ_LEVEL + DC_TOP_NO2 NO6_LIQ_LEVEL + 0.19
LE71	Pressurizer liquid level	PRZ PR11_LIQ_LEVEL + 7.8 (min 7.95)
LE81	SG secondary liquid level (calculated in the riser section)	SG_NO18 NO6_LIQ_LEVEL + SG_NO19 NO6_LIQ_LEVEL + SG_NO20 NO6_LIQ_LEVEL + SG_NO21 NO6_LIQ_LEVEL + SG_NO22 NO6_LIQ_LEVEL + SD_PIP1_NO1 NO6_LIQ_LEVEL + SD_PIP1_NO2 NO6_LIQ_LEVEL + SD_PIP1_NO3 NO6_LIQ_LEVEL + SD_PIP1_NO4 NO6_LIQ_LEVEL + SD_TA1_NO1 NO6_LIQ_LEVEL + 6.33

Table 6.36 Measurement Signals in the APROS Model (cont.)

(LE82)	*SG secondary liquid level (calculated in the downcomer section)*	*SG_NO23 NO6_LIQ_LEVEL* *+ SG_NO24 NO6_LIQ_LEVEL* *+ SG_NO25 NO6_LIQ_LEVEL* *+ SG_NO21 NO6_LIQ_LEVEL* *+ SG_NO22 NO6_LIQ_LEVEL* *+ SD_PIP1_NO1 NO6_LIQ_LEVEL* *+ SD_PIP1_NO2 NO6_LIQ_LEVEL* *+ SD_PIP1_NO3 NO6_LIQ_LEVEL* *+ SD_PIP1_NO4 NO6_LIQ_LEVEL* *+ SD_TA1_NO1 NO6_LIQ_LEVEL* *+ 6.33*
LE91	SIT1 liquid level	SIT1_NO1 NO6_LIQ_LEVEL + 7.975
LE92	SIT2 liquid level	SIT2_NO1 NO6_LIQ_LEVEL + 7.975
MA01	Total mass leaked	Calculated by the *BREAK_INT* integral module
PR01	Back pressure behind the break	BREAK_PO2 PO11_PRESSURE
PR21	Upper plenum pressure	UP_BOTTOM_01 PO11_PRESSURE
PR71	Pressurizer pressure	PRZ_02 PO11_PRESSURE
PR81	Secondary circuit pressure	SL_TA2 TA13_PRESSURE
PR91	SIT1 pressure	SIT1_09 PO11_PRESSURE
PR92	SIT2 pressure	SIT2_09 PO11_PRESSURE
PW01	Core power	CORE RE14_POWER * 665.12
TE01	Break flow coolant temperature	BREAK_PO1_NO1 NO6_TEMPERATURE
TE11	Heater rod surface temperature (at 1.494m height)	0.5 * CORE_HN3 HSN_TEMPERATURE + 0.5 * CORE_HN5 HSN_TEMPERATURE + 273.15
TE12	Heater rod surface temperature (at 2.954m height)	0.5 * CORE_HN15 HSN_TEMPERATURE + 0.5 * CORE_HN17 HSN_TEMPERATURE + 273.15
TE13	Heater rod surface temperature (at 3.464m height)	CORE_HN19 HSN_TEMPERATURE + 273.15
TE14	Heater rod surface temperature (at 3.464m height)	CORE_HN19 HSN_TEMPERATURE + 273.15
TE15	Heater rod surface temperature (at 3.464m height)	CORE_HN19 HSN_TEMPERATURE + 273.15
TE22	Upper plenum coolant temperature	UP_MIDDLE_NO1 NO6_TEMPERATURE + 273.15
TE23	Upper plenum wall temperature	UH_BOTTOM_HN5 HSN_TEMPERATURE + 273.15
TE24	Upper head coolant temperature	UH_TOP_NO1 NO6_TEMPERATURE + 273.15

Table 6.36 Measurement Signals in the APROS Model (cont.)

TE41	SG inlet coolant temperature (primary circuit)	HL_PO5 PO11_TEMPERATURE + 273.15
TE42	SG outlet coolant temperature (primary circuit)	CL_PO1 PO11_TEMPERATURE + 273.15
TE43	SG hot collector coolant temperature (8.163 m)	SG_NO4 NO6_TEMPERATURE + 273.15
TE44	SG cold collector coolant temperature (8.163 m)	SG_NO17 NO6_TEMPERATURE + 273.15
TE45	SG hot collector coolant temperature (7.591 m)	0.5 * SG_NO2 NO6_TEMPERATURE + 0.5 * SG_NO3 NO6_TEMPERATURE + 273.15
TE46	SG cold collector coolant temperature (7.591 m)	0.5 * SG_NO15 NO6_TEMPERATURE + 0.5 * SG_NO16 NO6_TEMPERATURE + 273.15
TE47	SG hot collector coolant temperature (6.385 m)	SG_NO1 NO6_TEMPERATURE + 273.15
TE48	SG cold collector coolant temperature (6.385 m)	SG_NO14.NO6_TEMPERATURE + 273.15
TE61	Downcomer inlet coolant temperature	DC_MIDDLE_NO1 NO6_TEMPERATURE + 273.15
TE62	Downcomer wall temperature	DC_TOP_HN5 HSN_TEMPERATURE + 273.15
TE63	Core inlet coolant temperature	LOWER_PLENUM_NO1 NO6_TEMPERATURE + 273.15
TE64	Main circulation pump inlet coolant temperature	BYPASS_PO3_NO1 NO6_TEMPERATURE + 273.15
TE81	Feed water temperature	SG_NO19 NO6_TEMPERATURE + 273.15
TE83	SG secondary coolant temperature in the middle section (8.163 m)	SG_NO21 NO6_TEMPERATURE + 273.15
TE85	SG secondary coolant temperature in the middle section (7.591 m)	0.5 * SG_NO20 NO6_TEMPERATURE + 0.5 * SG_NO19 NO6_TEMPERATURE + 273.15
TE87	SG secondary coolant temperature in the middle section (6.385 m)	SG_NO18 NO6_TEMPERATURE + 273.15

6.4 Modifications

As mentioned before, an earlier APROS model (constructed by the Institute in 2013) of the SPE-2 experiment [2] served a useful basis for the model development of the SPE-4. From the model structure and model component point of view these models share mostly common

features except for some modifications required due to the different experiments under investigation (SPE-2 / SPE-4) and the APROS version differences. A few model corrections were also needed. Most important of these differences are the following:

- Most of the setpoints of the control systems are different in the SPE-2 and SPE-4 experiments, like the initial mass flow rate of the primary circuit, liquid level of the pressurizer and steam generator, primary and secondary pressures, initiation pressure of SCRAM and MCP coastdown, opening pressure and closing liquid levels of the accumulator injection.
- In the real facility, there have been two configuration of the pressurizer surge line over time. In one configuration, the surge line was longer and it was connected to the lowest point of the hot leg. In the other, the surge line was connected to the top point of the hot leg. The old model implemented the first configuration, while the second was built and in use at the time of the SPE-4 experiment. The surge line and the nodalization of the hot leg was modified accordingly.
- The old model does not have a pressurizer level control system, but it has been added to the new model to ensure the required, initial level. This system is immediately switched off at the start of the transient.
- The pressurizer module of the old model contains a heat structure modeling its wall, but the outer surface is not connected. It means that the heat capacity is taken into account, but the heat loss is not. In the new model, we made up for this and connected the outer surface to the ambient point with heat transfer modules. The effect of the unknown thermal insulation was taken into account by constant multiplication factors to obtain the published heat loss like in the case of other wall heat structures.
- The initial steam generator water levels were significantly different in the two experiments (SPE2 – 8 m, SPE4 – 8.95 m from the reference level), so the modification of the upper part of the SG model was necessary.
- In the SPE-4 (contrary to the SPE-2), a secondary side bleeding was performed, therefore a more detailed steam line (and a specific control system) was required both in the real facility and in the model. The *SL_PIP1, SL_PIP3-5* pipes and the *SL_TA1-2* tanks represent the steam lines and the main steam collector of the real plant.
- In the SPE-4 experiment, the emergency feedwater system was also available, so it has been added together with its control system.
- The high pressure emergency core cooling system was available during the transient in the SPE-2 experiment. However, it was not used in SPE-4, so this system was deleted. On the other hand, modeling of the low pressure ECC system was required in the case of SPE-4 (contrary to SPE-2). This system supplies coolant to the surge line of the *SIT1* accumulator, so the modification of the surge line was also necessary. The control of ECC injection changed accordingly.
- The time required for the secondary side isolation is slightly different in the SPE-2 (4.0 s) and SPE-4 (6.0 s) experiments according to related IAEA tecdocs [3], [5].
- The tables describing the break pressure boundary, the decay heat of the core and the coastdown of the main circulation pump has also been modified to follow the measured properties.
- The break diameter is slightly different in the SPE-2 (3.0 mm) and SPE-4 (3.2 mm) experiments according to related IAEA tecdocs [3], [5].

- The extra heat structures of the steam generator were created in a hidden way in the old model. It means that these modules did not appear on the schemes as they existed only at the calculation level of APROS. This method can no longer be used in APROS 6 versions, because one of the main new principles is that all modules and connections have to be visible. Consequently, the N1 scheme of the new model contains these modules as well, and their parameters are the same. However, the old model contained only the cylindrical heat structures, while the new takes into account the bottom and roof walls as well.
- The inner side of the wall of the core channel is covered with a ceramic material with poor thermal conductivity, so it was neglected in the old model. However, it still has a small effect on the processes according to our investigation, and thus the new model includes this as well.
- Due to the above described modifications concerning the heat structures, the outer heat transfer efficiencies of the walls, with which the heat losses and their distribution can be adjusted, had to be redefined.
- Modification of the pump curve was needed to properly adjust the DP16 pressure change of the pump in the steady state.
- A small adjustment of the discharge coefficient of the break and the steam dump valve was also required.
- In the old model, the connections between the schemes were provided by the so-called ‘slave copies’ of the modules involved. This method has been replaced in the new APROS versions by flag connections due to the visibility principle mentioned above.
- The measurement signals were previously generated using the standard APROS modules. The new version now has the built-in SCL scripting language, which provides a much faster and easier way to calculate the signals. Some of these had to be modified and a few new were added because the measurements did not exactly match in the two experiments (SPE-2/SPE-4).

6.5 Steady-State Parameters

The steady state was reached by a long transient run of the model without opening the break valve, since APROS is not able to directly calculate the steady state. A maximum time step of 0.1 s was used for the steady state calculation and 0.01 s for the real transient. The minimum number of iterations was 5 and the maximum was 30. To calculate the water-steam parameters, parallel calculation was enabled (*ECCO WS_PARALLELIZED 1*), and the iteration of the control model was also enabled (*ECCO AUTOMATION_ITERATED TRUE*). The parameters describing the steady state are presented in Table 6.37. The measured data were taken from the CD appendix of [1].

Table 6.37 Steady State Parameters of the APROS Model

Parameter	Dimension	Measurement	APROS	Absolute error	Relative error [%]
DP11	kPa	50.24	50.28	0.038	0.08
DP16	kPa	1490	1491	1.4	0.10
DP41	kPa	43.46	43.48	0.016	0.04
FL00	kg/s	-	-	-	-
FL53	kg/s	4.912	4.91	-0.002	0.04
FL54	kg/s	1.738	4.91	-	-
LE11	m	8.485	8.485	0.0	0.0
LE21	m	8.485	8.485	0.0	0.0
LE22	m	5.704	5.704	0.0	0.0
LE23	m	4.664	4.664	0.0	0.0
LE31	m	6.080	6.08	0.0	0.0
LE45	m	8.445	8.445	0.0	0.0
LE46	m	8.445	8.445	0.0	0.0
LE51	m	5.995	5.974	-0.021	0.35
LE61	m	4.995	4.995	0.0	0.0
LE71	m	9.124	9.119	-0.005	0.05
LE81	m	8.954	8.528	-0.426	4.76
LE82	m	8.954	8.95	-0.004	0.04
LE91	m	9.440	9.44	0.0	0.0
LE92	m	9.833	9.833	0.0	0.0
MA00	kg	-	-	-	-
PR00	MPa	0.1	0.1	-	-
PR21	MPa	12.329	12.33	0.001	0.01
PR71	MPa	12.133	12.274	0.141	1.16
PR81	MPa	4.559	4.560	0.001	0.02
PR91	MPa	6.053	6.037	-0.016	0.26
PR92	MPa	6.043	6.029	-0.014	0.24
PW01	kW	665.12	665.12	0.0	0.0
TE00	K	-	-	-	-
TE11	K	576.2	557.4	-18.75	3.25
TE12	K	621.7	572.2	-49.51	7.96
TE13	K	623.4	578.1	-45.31	7.27
TE14	K	625.2	578.1	-47.11	7.54
TE15	K	628.0	578.1	-49.91	7.95
TE22	K	566.2	564.5	-1.70	0.30
TE23	K	562.9	555.7	-7.18	1.28
TE24	K	534.2	535.4	1.21	0.23
TE41	K	566.7	564.1	-2.56	0.45
TE42	K	539.4	538.5	-0.91	0.17
TE43	K	541.7	564.1	22.43	4.14
TE44	K	536.2	538.9	2.67	0.50
TE45	K	570.9	563.0	-7.94	1.39
TE46	K	537.4	538.4	1.00	0.19
TE47	K	561.7	563.8	2.08	0.37
TE48	K	531.6	538.5	6.92	1.30

Table 6.37 Steady State Parameters of the APROS Model (cont.)

TE61	K	539.9	538.8	-1.06	0.20
TE62	K	520.7	530.6	9.90	1.90
TE63	K	540.1	538.8	-1.33	0.25
TE64	K	538.0	538.3	0.30	0.06
TE81	K	-	-	-	-
TE83	K	522.2	531.4	9.18	1.76
TE85	K	526.8	531.4	4.60	0.87
TE87	K	528.7	531.5	2.80	0.53

Some notes on the initial values:

- The pressure drop of the primary side of the steam generator (DP41) and the core (DP11) were adjusted with realistic form loss coefficients and show good agreement with the measurements. The pump has also been successfully initiated, as shown by DP16.
- The pressures (PR00, PR21, PR81, PR91, PR92), primary mass flow rate (FL53), water levels (LE71, LE91, LE92) and the power of the core (PW01) are close to the measured values as most of these are controlled, while the accumulators are separated by valves.
- There are two measurements for the primary mass flow rate, one of which is accurate for higher rates (FL53) and the other for lower (FL54). As a consequence, FL54 is not relevant in the steady state and shows a significant difference.
- The steam generator water level is a controlled parameter; however, it is not obvious where to measure it in the model. The secondary side of the real steam generator is one continuous volume, while it is modelled with the combination of a downcomer and a riser. Therefore, two measurements are implemented in APROS: LE81 – riser, LE82 – downcomer. The water level control system uses the LE82 and thus it is quite close to the real measured value. The void fraction of the riser is much higher, so the collapsed level is lower.
- Most of the water levels (LE11, LE21, LE22, LE23, LE31, LE45, LE46, LE51 and LE61) show perfect match as the primary system is filled with water and purely single-phase flow is achieved.
- The fuel temperatures (TE11, TE12, TE13, TE14 and TE15) are systematically underestimated by the code. The heat transfer coefficient in the real facility was probably not as high as that calculated by APROS with the Dittus-Boelter correlation.
- The calculated cold- and hot leg fluid temperatures (TE22, TE24, TE41, TE42, TE61, TE63 and TE64) are close to the measured values, which indicates that the heat transfer towards the environment and the secondary circuit was properly modeled in the steady state.
- Both TE43 and TE44 are being measured in stagnant nodes, which are difficult to simulate with one-dimensional hydraulic codes. Therefore, the margin can be acceptable.
- The experimentally measured values of the primary side temperatures of the steam generator (TE41, TE47, TE45 and TE46, TE44 and TE42) behave strangely. Going up in the hot collector, the temperatures are 566.7 °C, 561.7 °C and 570.9 °C respectively. Therefore, the lower part temperature is the lowest, and the middle part is warmer than the inlet (top part is the stagnant volume). Going down in the cold collector, the

temperatures are 537.4 °C, 531.6 °C and 539.4 °C. Therefore, the lower part temperature is the lowest and the outlet is even warmer than the middle part. Based on the available information, this behavior cannot be explained and thus the comparison with the APROS results is also difficult. The collector temperatures of APROS show an expected trend.

- In order to reduce the error of the wall temperature (TE23, TE62) calculations, more accurate information about the exact location of the measurements and the thermal insulation of the facility should be available.
- The secondary side temperatures (TE83, TE85 and TE87) are significantly different. In case of APROS, all three of these show saturation temperatures, while the measured values are lower than the saturation temperature and they increase downwards. This suggests that the APROS model cannot properly calculate the heat transfer and overestimates the internal mixing. Using a more detailed nodalization could be a solution to this problem and thus it could be a field for further development.

7 SPE-4 TRANSIENT CALCULATION

The transient can be divided into 3 main stages:

0 – ~160 s:

The transient is initiated by opening valve MV31 located at the downcomer top region. A significant drop of the primary pressure can be observed as the discharge of the coolant (water) begins through the break. The reactor is stopped, while the pump coastdown program and the hydroaccumulator injection is initiated. The evaporation that starts at the highest points of the primary circuit and behind the pump (probably caused by the pressure drop of valve PV11) breaks the rate of this rapid pressure drop. Initially a single-phase water followed by a low-vapor two-phase mixture break flow is observed. The primary pressure decreases near the secondary, so the direction of heat transfer in the steam generator is reversed and the primary pressure stagnates. An early clearance of the hot leg loop-seal is observed at the moment which corresponds with the end of the coast-down procedure.

~160 - 350 s:

Subsequently, the steam was partially condensed in the hot leg pipelines by the entering emergency core cooling water and partially in the SG. Due to this, the drop of the primary pressure and the injection rate of the SITs was intensified and the delivered subcooled water refilled the hot leg loop-seal. Within a short time, the primary pressure fell under to that of the secondary and the cold leg loop-seal emptied suddenly. Following the termination of the accumulator injection, the second and final clearing of the hot leg loop-seal took place. The water discharged from the hot leg was partially pressed through the steam generator into the cold leg, temporarily increasing its water level.

350 – 1800 s:

After the opening of the hot leg loop-seal, in both the hot and cold sides of the circuit a two-phase flow with a high void fraction was established. Later, the continuous decrease of water level in the reactor vessel leads to the dryout of the heating rods. Meanwhile, the primary pressure reaches the initiating pressure of the low pressure injection system. Due to this injection, rewetting of the rods could be observed in time and thus their cooling was ensured. At the end of the experiment, the loop-seals were not yet refilled, but the remnant heat is successfully removed by the LPIS injection and the secondary feed and bleed.

A comparison of the measured and calculated parameters is shown in Figure 7.1 - Figure 7.49. Our comments on the figures are summarized below. In the Figures the legend “Measurement” denotes the data published in [1], while “TRACE”, “APROS” and “RELAP” curves show the calculation results from the BME NTI’s model simulations.

The sequence of main events during the transient is presented in Table 7.1.

Table 7.1 Sequence of Events

Sequence of Events	Measurement (SPE-4) [1]	Measurement (SPE-4) [3]	Calculation (RELAP5)	Calculation (TRACE)	Calculation (APROS)
Break valve (MV31) opening	0 s	0 s	0 s	0 s	0 s
SCRAM initiation	4 s	-	3.3 s	2.7 s	2.0 s
Secondary side isolation	0.0 - 6.0 s	-	0.0 - 6.0 s	0.0 - 6.0 s	0.0 - 6.0 s
Pump coast-down interval	10.0 - 158.0 s	-	9.1 - 159.1 s	7.7 - 157.7 s	7.5 – 157.5 s
Pressurizer empties	16.0 s	23 s	11.0 s	7.1 s	14.7 s
Hydroaccumulator injection starts	26.0 s	26 s	23 s	20 s	27 s
Start of two-phase break flow	-	44 s	34 s	43 s	44 s
Reactor vessel collapsed level reaches the elevation of the hot leg	78.0 s	78 s	65 s	63 s	89 s
Reactor vessel collapsed level reaches the top of the core	-	125 s	185 s	161 s	233 s
Dry-out begins	(138), 1127 s	138 s	1055 s	(483), (934), 1019 s	(240), (336), 692 s
Secondary bleed initiation	160 s	-	160 s	158 s	158 s
Hot leg loop-seal clearing	165, 345 s	165 s	157, 430 s	108, 196, 460 s	130, 356 s
Cold leg loop-seal clearing	226 s	250 s	191 s	189 s	256 s
Primary pressure equals secondary pressure	248 s	-	(54), 214s	(61), 184 s	(38), 260 s
Termination of SIT1 injection	308 s	310 s	370 s	429 s	323 s
Termination of SIT2 injection	310 s	310 s	380 s	412 s	324 s
LPIS initiation	1380 s	1380 s	1192 s	1274 s	1120 s
Maximum cladding temperature	1385 s 731 K	-	1202 s 724 K	1297 s 801 K	1235 s 871 K
Cladding temperature exceeds 873 K	-	No	No	No	No
Secondary side pressure drops below 0.8 MPa	-	1720 s	1505 s	No	1770 s
Transient termination	1800 s	1800 s	1800 s	1800 s	1800 s

UPPER PLENUM and PRESSURIZER PRESSURES (PR21, PR71)

On Figure 7.1 (PR21) a good agreement can be observed between the curves. Between roughly 200 and 300 seconds TRACE calculates a steeper, but shorter drop of the pressure. The explanation of this phenomenon is that the first clearance of the hot leg loop seal is sharper and the depleted state is maintained for a longer period of time. As a result, the re-formation and final clearance of the hot leg loop seal are shifted in time. After 300 seconds, TRACE results follow the measured values as the two curves almost overlap.

In case of RELAP, the gradient of the pressure drop is predicted well between 150 and 300 seconds except for the plateau between 70 and 150 seconds. As consequence of this plateau, RELAP overestimates the measured values between 150 and 300 seconds. During the refilling of the hot leg loop seal the expected temporary rise in pressure is not observed on the pressure curve. Similarly to TRACE, the results of RELAP approximate the measured values accurately after 350 seconds.

In a similar way to RELAP, APROS also simulates a plateau between 70 and 150 seconds although at a lower pressure. Until 300 seconds, the pressures estimated by APROS are between the values from RELAP and TRACE and approximate the measurement very well. The local pressure valley present at 300 seconds is predicted but with a slight delay and a slightly lower value. In the following stage of the transient APROS also approximates the measured values accurately but due to the longer and more severe dry-out the pressure decreases to a slightly lower level in the next 900 seconds. The extra heat transferred to the fluid during re-wetting causes the pressure to augment in the simulation. From this point on, APROS shows the best agreement with the measured values.

By the end of the transient, the pressures calculated by the codes are close to the measured values although all three underestimate it slightly. The low-pressure injection is actuated when pressure PR21 reaches 1.04 MPa. During the later stage of the transient, the pressure curves are rather flat and as a consequence, small differences between the pressures lead to a time shift in the initiation of the low-pressure injection system. Similar phenomena are observed on Figure 7.2 (PR71) for which similar explanations hold true.

STEAM GENERATOR SECONDARY SIDE PRESSURE (PR81)

The secondary side becomes completely isolated by the 6th second of the transient, therefore an initial rise can be observed in pressure PR81 (Figure 7.3). It is, however, stopped before reaching the setpoint of the relief valve both in the simulations and the measurement due to the reversed heat transfer in the steam generator (from secondary to primary side). The secondary-side bleed operation through valve PV23 is started 150 seconds after the initiation of the pump coast-down which accelerates the drop of the secondary pressure.

It can be observed that TRACE follows the measurement well throughout the transient. The initial peak of pressure is predicted well, however in the time period before the initiation of the bleed a less significant decrement in pressure is observed. During the first part of the blowdown, TRACE and the measured curves are quasi parallel which means a slight overestimation. Later on, this discrepancy decreases and eventually disappears.

In the RELAP simulation, a higher initial elevation of pressure was calculated. RELAP underestimates the drop of pressure under the time of the coast-down which combined with the more significant initial rise of pressure leads to a more apparent discrepancy between the measured and simulated results. Until 400 seconds, the gradient of the pressure is predicted

well, the pressures run quasi parallel to the measured values although overestimating them. The change of gradient in the pressure curve around 450 s is not that significant than in case of the corresponding earlier (around 350s) change in the measured values, which results in underestimating the measured pressures by the end of the transient. In a similar manner to PR21, the flat pressure gradients lead to a shifted actuation of the emergency feedwater system.

APROS overestimates the initial pressure peak (in a similar way to RELAP) and then the pressure starts to decrease following the slope of the TRACE calculation until the actuation of the bleed signal. During the bleed APROS approximates the secondary pressure better than the other two codes although in this case a unique modelling modification was applied. In the other two codes, the discharge coefficient(s) of valve PV23 were assumed to be constant contrarily to the APROS model where it is switched to a lower value at the time the secondary pressure reaches 2.7 MPa as described in chapter 6.1. The short plateau observed in the measured values around 1300-1400 s is simulated the best with the APROS model.

ACCUMULATOR PRESSURE AND LIQUID LEVEL (PR91, PR92, LE91, LE92)

As seen on Figure 7.4, Figure 7.5 and Figure 7.18, Figure 7.19, the characteristic of the pressure and water level curves are similar which is expected as the two quantities are closely related.
The injection is modeled qualitatively well by all three models as the gradient of level and pressure drop is similar to that observed on the measured curves. As it was seen on Figure 7.1 (PR21), between around 70 and 150 s, the primary pressure of RELAP and APROS stagnates due to the evaporation in the system, which impedes the injections from the accumulator. The same stagnation is observed in TRACE results, although its duration is shorter and the process starts slightly later (at a lower pressure). During this period, the injection was continuous with a decreased intensity in the measurement. This different behavior caused a greater calculation discrepancy. In the APROS simulation the injection following the plateau is commenced slightly earlier and the by the termination of the injection the supplied mass flow rate is higher thus giving a more accurate estimation for the time of depletion. The injection of RELAP and TRACE slows down at the end resulting in a more delayed termination.

PRESSURE VESSEL LIQUID LEVELS (LE11, LE21, LE22, LE23 and LE61)

Concerning liquid level LE21 (Figure 7.7), in the simulations, at the beginning of the transient a significant lowering of the liquid level is observed, which follows the measurement qualitatively well, however, this drop occurs later in the APROS model and earlier in the other models than in the measurement. In the simulations, the level is decreased approximately until it has reached the elevation of the hot leg nozzle. Until the termination of the accumulator injection, the water levels slightly rise in all three simulations. Following the injection period, due to the continuous boiling, a slow decrease is observed in the measurement while in case of the simulations, this process is more intense and in approximately 100 seconds the water column reaches the level of the lower measurement gauge. By the end of the transient, due to the initiation of the injection from the LPIS the water levels start to increase (at around 1300 seconds in RELAP, 1400 seconds in TRACE and APROS and 1500 seconds in the measurement).

In case of LE22 and LE23 (Figure 7.8, Figure 7.9) an initial lowering of the levels can be observed as in LE21. In the first stage of the transient, the clearing and re-formation of the loop seals which is related to the injection from the accumulators has a dominant contribution to the

evolution of the water levels. Both for the measurement and the simulations, periods of depletion and refill are observed but these processes occur at different times (at 500 s in RELAP and TRACE and 550 s in APROS). The trend line shows a decreasing tendency in the simulations and in the measurement after the hot leg loop seal clearing, which leads to the water level reaching the measurement gauge. This indicates that the top of the core is exposed around 1200 seconds in RELAP and TRACE and even earlier in APROS. In this stage of the transient, RELAP shows better agreement with the measured values of LE23. It is worth to mention that the position of the transducer in the measurement of LE22 according to [3] was located at the elevation of 4.664 m. It was found rather contradictory that around the time of the core dry-out measurement LE23 shows complete depletion while in case of LE22 the liquid level stays approximately 30 cm above the location of the transducer. This would indicate an erroneous definition of the measurement point location in [3]. By the end of the transient, due to the injection from the LPIS, a rise of water level is observed which was also apparent in LE21.

For all simulations, in accordance with the previously evaluated water levels, LE11 (Figure 7.6) shows a fast initial drop of the liquid level which then starts to rise due to the injection from the hydro-accumulators. During the accumulator injection, the abrupt peaks and valleys present in the measurement are only observed with much smaller amplitudes in the RELAP and APROS simulations and are shifted in time in the TRACE simulation. At the end of this process, all three codes underestimate the liquid level and this discrepancy is maintained throughout the following period of slow lowering. At the final stage of the transient, the liquid levels rise in the simulations as well as in the measurement for which the reason is the LPIS injection, which results in a successful re-flood of the core.

In case of the downcomer liquid level LE61 (Figure 7.14), TRACE and RELAP predict the occurrence and magnitude of the initial drop while APROS estimates accurately only the latter. After the depletion of the accumulators, a continuous slow lowering of the liquid level is observed in the measured values in accordance with LE11, indicating the boiling of the coolant. The starting time and characteristic of this process are predicted very well by RELAP. In the TRACE simulation, between roughly 300 and 550 seconds, the liquid level in the downcomer is quasi constant. After 550 seconds, TRACE also predicts a continuous drop of water level for both LE61 and LE11. The trend of the APROS simulation is steeper but starts roughly at the same time as in RELAP. In a similar manner to the previously evaluated water levels, both LE11 and LE61 increase at the end of the transient due to the injection from the LPIS, in agreement with the measurement. As consequence of the earlier actuation of the injection, the simulated water levels start to rise earlier.

LOOP SEAL AND SG COLLECTOR LIQUID LEVELS (LE31, LE51, LE45, LE46)

Liquid levels LE31 (Figure 7.10) and LE45 (Figure 7.11) show the evolution of the hot leg loop seal during the transient. The reactor-side loop seal LE31 is cleared at around 100 seconds both in the simulations and the measurement which is apparent in the decrease of the water level observed in LE45. During the first clearing, a temporary rise is present in the measurement which was not simulated by either code, although in case of RELAP, the lowering of the level briefly stops. The loop seal remains cleared for a longer period of time in the TRACE simulation and re-formation only occurs at roughly 250 seconds while in the RELAP simulation, the refill is completed earlier, around 189 s. APROS simulation shows that the re-formation occurs around halfway between the two other codes (around at 200 s) and thus is closest to the measurement. The final clearance of the loop seal is delayed by approximately 100, 80 seconds compared to the measurement in TRACE and RELAP, respectively. APROS on the other hand estimates the

time of final clearance accurately. The heavy fluctuations observed in the RELAP and the smaller ones present in APROS results are presumed to be a consequence of water passing from the RPV to the hot leg, which leads to a two-phase flow.

As seen on Figure 7.11 (LE45), the rapid drop of measured liquid level around 187 s occur approximately 60 seconds earlier in RELAP and TRACE which is in agreement with a similar phenomenon observed in LE31. Following a more elongated accumulator injection, the late decrease of the level occurs with a delay of 100 s in RELAP and TRACE with respect to the measurement and by the end of this process, the codes overestimate the measured values by roughly one meter. Although by the end of the transient, APROS also overestimates the measured values it can be said that both the initial phase and the period of accumulator injection are modelled relatively well, providing the best agreement with the measured values. This systematic overestimation of the final liquid levels indicates that a significant amount of coolant is trapped in the steam generator side loop seal. It can be noted however that the passing of the steam to the steam generator through the loop seal is ensured in the second stage of the transient. The water amount trapped here explains the lower levels observed in the core (LE11).

Liquid levels LE46 (Figure 7.12) and LE51 (Figure 7.13) show the evolution of the cold leg loop seal during the transient. Following the termination of the coast-down process, the cold leg loop seal is cleared in both the measurement and the simulations, although in TRACE and RELAP this occurs slightly earlier which is closely related to the earlier clearing of the hot leg loop seal. At the time of the final clearance of the hot leg loop seal, a rise in the cold leg liquid level is observed leading to a local maximum, the magnitude of which is underestimated by TRACE and estimated well by RELAP along with its characteristic. In case of both RELAP and TRACE, the appearance of this peak is delayed by approximately 100 seconds with respect to the measurement. APROS estimates both the occurrence and the magnitude of the peak accurately.

On the long term, a practically constant water level was measured which coincides with the lowest elevation point in the main circulation branch (3.202 m from the reference level). RELAP and TRACE results show that this water level has decreased to a lower value, which indicates that during natural circulation, in the connecting volumes of the bypass branch (which are stagnant during the transient i.e. there is no flow through the volumes) a significant boiling is present resulting in an additional drop in the liquid level which was not shown by the measurement and neither by APROS. Following the initiation of LPIS, by the end of the transient, the water levels increase slightly in APROS and TRACE simulation. Contrary to these two, this increment is only marginal in RELAP. In case of LE46, the measured values show a slow increasing liquid level after 500 s which was not simulated by either code.

PRESSURIZER LEVEL (LE71)

In the models, a level-control system was implemented in order to set the initial level correctly (Figure 7.15). The depletion process is simulated accurately by the three codes. In order to interpret the differences between the quasi-stationary levels at the later stage of the transient, the following should be noted: the elevation of the bottom of the pressurizer is 7.80 m from the reference level. The measurement point orifice is located at an elevation of 7.95 meters. Contrary to that, water levels below this height are measured. This deviation is in the magnitude of measurement error. In the simulations, a limit of 7.95 m was set in order to keep the measured level above the presumed location of the measurement point.

SECONDARY SIDE LIQUID LEVELS (LE81, LE82)

It has to be considered that in the measurement, only one liquid level was registered (identified as LE81) however, in the simulations two datasets were extracted (Figure 7.16 and Figure 7.17) for the reasons mentioned in the model documentation chapters. On Figure 7.16, there is a substantial, initial difference between the simulated and measured values of LE81 which becomes less apparent after the collapse of the steam blanket in the heater. Furthermore, as presented in [3], between 165 and 340 seconds, the measured values are incorrect.

At the beginning of the transient during the isolation of the secondary side, a sudden drop is observed following which the level first increases with the increasing pressure then stagnates until the initiation of the secondary bleed. During the bleed period, the levels decrease continuously until the initiation of the emergency feedwater injection which leads to a rise of water levels. The characteristic of the processes is predicted well until the EFW injection, but the curve gradients are somewhat different. After the initiation of the emergency feedwater system, the three codes show a slowly increasing liquid level while in the measurement only the lowering of the level is observed.

PRESSURE DROP (DP11, DP41)

In the simulations, pressure drop DP11 (Figure 7.20) was calculated by taking into account the hydrostatic pressure difference which was calculated from the geometrical elevation between the measurement points. Such correction was not required for DP41 (Figure 7.21) as the measurement points are located at the same elevations. For both quantities, during the pump coast-down, TRACE shows good agreement with the measured data, although heavy fluctuations are observed around 50 s which is presumed to be a consequence of steam appearing behind PV11, resulting in fluctuating mass flows. Following the termination of the coast-down, the smaller fluctuations are also caused by the fluctuation of the mass flows as seen on Figure 7.23 (FL54). After approximately 500 seconds when pure steam exits through the break and thus the fluctuations of the mass flow rate cease, the differential pressure curve becomes a bit smoother and follows a similar characteristic to that of measured values. After the time of the initiation of the LPIS injection (1250 s in TRACE, 1400 s in the measurement), the pressure drop decreases in absolute value.

In case of RELAP, the steady-state pressure drops underestimate the measured ones, which originate from not being able to adjust the form loss coefficients properly. For both quantities, RELAP predicts the characteristics well and the observed fluctuations are smaller in magnitude compared to TRACE. The effects of the injection from the LPIS are apparent on the simulated pressure drops just as in the measurement.

APROS shows a similar trend in the change of the differential pressures however following the coast-down fluctuations are present constantly which are greater in magnitude compared to the other codes. The effects of the LPIS are analogous to the other cases. For DP11 and DP41 it is noted that following the depletion of the hot leg loop seal, all three codes overestimate the measurement in absolute value.

MASS FLOW RATES (FL53, FL54)

Regarding the flow rate measurements, it has to be noted that FL53 (Figure 7.22) and FL54 (Figure 7.23) were measured at the same location but with different techniques one being more adequate for small mass flows and the other being more suitable for higher mass flows. It was

stated in [3] that the measured values FL53 are accepted at the first 61 seconds of the transient while at its later stage, FL54 is representative. During the time of the pump coast-down, RELAP and APROS show a good agreement with the measured flow rates. TRACE also predicts a correct characteristic during the majority of the coast-down period, however as it was discussed at DP11, heavy fluctuations are present starting from 50 s. Following the coast-down period in the first stage of natural circulation, the magnitude of the fluctuations becomes smaller in the TRACE simulation and also appear in the measurement and the other two simulations, although less significantly. The fluctuations also suggest that the simulation of the two phase natural circulation proved to be difficult for the codes. In the simulations after 500 seconds, pure steam exits through the break which results in an insignificant flow rate. Surprisingly, a rather significant flow rate was measured for which an explanation is yet to be found. Following the initiation of the LPIS, both the measured and calculated mass flows augment.

TOTAL MASS LEAKED (MA00) and BREAK FLOW RATE (FL00)

In the simulations, critical flow model was applied. In the FL00 measurement until approximately 44 seconds (shown on Figure 7.24), one-phase break flow is observed, followed by a low vapor fraction two-phase flow until 250 s. After that two-phase flow with low liquid fraction is present, while after 400 seconds, only steam exits through the break. In case of APROS, TRACE and RELAP steam is present from the beginning of the transient (starting from approximately 44, 43 and 35 seconds, respectively) albeit only in a small fraction. In RELAP and TRACE, until 200 seconds there is a small fluctuating void fraction which can be observed in the series of subsequent valleys and peaks on the curves. Between 200 and 300 seconds, a steady outflow is experienced in both simulations with a high steam ratio. From 300 to 500 seconds, a heavily unsteady two-phase outflow is observed with a significant liquid fraction. After 500 seconds, pure steam is exhausted from the system. In APROS the outflow shows a different behavior. Until around 380 s an outflow with minimal gas void fraction is experienced following which the gas fraction increases. From 450 s pure steam exits through the break. Following the initiation of the LPIS, a small fraction of liquid appears again at the break in all three simulations.

The total leaked mass MA00 is presented on Fig. 7.25. Before the one-phase steam outflow (until around 500 s) each curve shows a different characteristic which can be traced back to the differences in the break mass flow rates and the break void fraction. From 500 seconds, RELAP and TRACE simulations yield nearly identical values which follow the characteristic of the measured values although underestimating them by approximately 6 kg. This discrepancy can partly be explained by the higher amount of coolant being trapped in the hot leg loop seal. Furthermore, no information was found about the quantity of coolant trapped in the detached bypass loop. This uncertainty serves as a possible explanation for the difference in the total leaked mass since the mass of the coolant in the bypass branch can be different in the measurement and in the simulations. As a result of the LPIS injection at the end of the transient a more rapidly increasing break mass is observed in APROS.

CORE POWER (PW01)

As expected, since decay heat power was given as a power vs time data table after the SCRAM initiation, the curves follow the measured values well (Figure 7.26). It can be seen on the curves corresponding to the simulations that the SCRAM signal is actuated earlier than in the measurement which can be explained by the faster drop in primary pressure.

HEATER ROD SURFACE TEMPERATURES (TE11 TO TE15)

As it can be observed on Figure 7.27, Figure 7.28, Figure 7.29, Figure 7.30 and Figure 7.31 (TE11 to TE15), the measured and calculated initial temperatures differ significantly, the simulated values systematically underestimating those of the measurement while TRACE and RELAP are almost identical. Following the simulated shutdown of the reactor, the differences lower gradually because the temperatures are in the range of the saturation temperatures and because of the decreasing decay heat. In the measurement, the surface of the heater rod was exposed briefly in the first stage of the transient (around 140 seconds) and is uncovered for a longer period of time at the later stage of the transient (from 1100 to 1400 seconds). In the TRACE simulation, a brief earlier and a late dry-out can be observed with a slightly different timing (480 and 1020 seconds). The late dry-out in the TRACE simulation starts approximately around 930 seconds but the surface is re-wetted temporarily and it is only after 1020 seconds that the surface remains dry for a longer period of time. The late temperature peaks are quite similar in characteristic in the TRACE simulation and the measurement. In TRACE, this process starts earlier and the drought is present for a longer period of time which leads to higher maximum.

The core surface temperatures obtained from RELAP also show good agreement with the measurement however, only the greater, second peak is observed in the RELAP calculation. The apparent dry-out has occurred a bit earlier compared to the measurement, the increase of temperature being slightly steeper and the duration of the peak being shorter. The value of the temperature peak was approximated very well by RELAP.

In case of APROS both the initial and later dry-out are greater in magnitude and longer in duration. The major dry-out starts around 700 s and the peak temperature reaches 871 K which is significantly higher than in the other simulations and the measurement. The characteristic of the curve is similar to the measured which suggests that the thermal coupling was modelled adequately and it is the early dry-out that leads to the higher maximum value.

Following the re-wetting, the measured and simulated temperatures show good agreement. Concerning TE11, contrary to the measurement, the corresponding section of the core was not uncovered and thus, no temperature peak is seen in the RELAP and TRACE simulations. In APROS, this peak is present but earlier compared to the measurement and with a lower peak. Finally, the cooling of the heating rods was ensured in both the simulations and the measurement.

UPPER PLENUM and DOWNCOMER WALL TEMPERATURES (TE23, TE62)

For TE62 (Figure 7.44) it can be noted that RELAP and TRACE qualitatively predict the evolution of the temperature. However, the effect of the injection from the accumulators is not observed, and thus at the second part of the transient the difference between the measured and calculated temperatures is higher. Both simulations tend to overestimate the measured values of TE62 throughout the transient.

Until the high flow-rate injection from the accumulators, APROS shows quasi constant temperatures, while an elongated cooling period is observed after the termination of the injection. It is probably an effect of the cold liquid from the accumulators being in thermal contact with the wall. At around 1200 s, APROS shows a more intense cooling which results

from the LPIS injection. This effect is not observed in the other simulations and is present only with a smaller change of gradient in the measurement around 1400 s.
It has to be mentioned that the measurement was performed in the lid of the downcomer while in case of RELAP and TRACE, the temperatures were extracted from the heat structure corresponding to the uppermost, cylindrical node of the downcomer. It has to be considered that no sufficient information was found about the radial location of temperature measurement points and the quality and quantity of local insulation used in the experiment and thus the evaluation of this problem requires further investigation.

Concerning TE23 (Figure 7.33), the RELAP and TRACE simulations systematically underestimate the measured temperatures but follow the characteristic qualitatively well. In case of RELAP, a better agreement is observed between the measured and calculated initial values. It can be seen that the initial temperature calculated by APROS slightly differ from the measured value but during the transient it shows a really good agreement.

UPPER PLENUM FLUID TEMPREATURES (TE22, TE24)

As observed on Figure 7.32 (TE22), all three codes give qualitatively good results. For TE22, TRACE and RELAP differ significantly from the measurement only at the time of the core dry-out. APROS predicted this change of temperature although with a higher peak and a less elongated shape. This difference is assumed to stem from the re-wetting following the longer and more significant dry-out in the APROS code. As a consequence of the dry-out, a lower temperature liquid and a higher temperature vapor phase is present in the upper plenum. Presumably, the reason for the temperature peak observed on the measurement data is due to the gauge being in contact with the high temperature steam while in the simulations, the presented temperature is a mixture-averaged quantity.

In RELAP, the initial temperature of the stagnant component where TE24 (Figure 7.34) was measured was erroneously set to a higher value. For TE24, it can be stated that TRACE shows good agreement with the measurement. In the major part of the transient, similarly to the measurement, TRACE calculates higher temperatures for TE24 than for TE22, which possibly indicates the presence of superheated steam in the upper head region. In the RELAP simulations, no such phenomenon is expected since the behavior of TE24 and TE22 is very similar. In APROS the effects of the accumulator injection are more apparent. After the injection has terminated, a slower decrease of temperature is observed (compared to the other codes and the measurement) which suggests that a higher quantity of superheated steam is accumulated in the upper head.

STEAM GENERATOR INLET AND OUTLET TEMPREATURES (TE41, TE42)

As it can be seen on Figure 7.35 and Figure 7.36, the three codes show good agreement with the measurements in case of both quantities. One significant difference can be noted, namely that in TRACE and RELAP, the more elongated accumulator injection and later clearance of the hot leg loop seal leads to a delayed rise of the inlet temperature TE41 (around 450-500 seconds). Contrarily to that, in case of TE41, APROS follows the measured occurrences better but during the same period, the temperature of the coolant in the cold leg collector (TE42) decreases to a lower level than in the measurement and the other simulations. As it was discussed previously for TE22 (see Figure 7.32) the re-wetting at higher fuel bundle temperatures results in the local maxima seen around 1300 s in both TE41 and TE42. The

same peaks appear in the collector temperatures discussed in the next section and in core inlet temperature TE63 (see below).

STEAM GENERATOR COLLECTOR TEMPERATURES (TE43 TO TE48)

The exact measurement locations could not be realized in the models which can lead to differences in the temperatures. In case of temperatures TE45 (Figure 7.39), TE46 (Figure 7.40), TE47 (Figure 7.41) and TE48 (Figure 7.42), a good agreement is observed between the calculated and measured values. In the simulations, TE47 (hot collector, lower part) displays a local minimum after the termination of the accumulator injection, while this minimum is not present in measurement data. Interestingly, in the measured values of TE45 (hot collector, middle part), this local minimum is present even though the measurement location is above that of TE47. This and the discrepancies between the calculated and measured initial values suggest that it is probable that the measured data sets of TE45 and TE47 were interchanged.

Concerning TE43 (Figure 7.37) and TE44 (Figure 7.38), the measurement took place in the uppermost stagnant volume which proves to be a difficulty for each code due to the limitation of one-dimensional flow modeling. Despite that, RELAP and APROS results show good agreement with the measured values while TRACE tends to overestimate these temperatures starting from 250s which indicates the presence of superheated steam in the simulation.

DOWNCOMER and CORE INLET TEMPERATURES (TE61, TE63)

For both TE61 (Figure 7.43) and TE63 (Figure 7.45), it can be stated that results of the simulations show good agreement with the measured values. Significant differences are observed in two periods of time, the first being the stage following the termination of accumulator injection. At this time, according to the TRACE simulation, the downcomer remains entirely filled with liquid for a longer period of time than in the measurement (LE61 - Figure 7.14) which results in lower mixture-averaged temperatures. This is also partly true for RELAP while results from APROS are closer to the measured data. By the end of the transient, due to the earlier actuation of the LPIS, a more significant temperature drop is observed in the RELAP calculations. The same phenomenon causes the oscillation of temperatures from 1200 s in the APROS simulation and similar effects are observed in TRACE although on a smaller scale.

FEEDWATER TEMPERATURE (TE81)

Concerning the TRACE and RELAP models, at the beginning of the transient, the secondary side of the steam generator is isolated and the inlet pipe becomes stagnant, which results in a constant TE81 (Figure 7.46) temperature until the saturation temperature corresponding to the secondary pressure reaches approximately 494 K. At the later stage of the blowdown the pressure is decreasing continuously followed by a decreasing saturation temperature. After the start of the temperature drop, both TRACE and RELAP predicts a characteristic similar to that of the measured values, although a time delay is present in the simulations with respect to the measurement due to the different gradient of the pressure drop. In the APROS model, a simplified feedwater and emergency feedwater circuit is implemented which does not contain a thermo-hydraulic node and thus does not permit the accurate extraction of TE81. The visualized curve shows the temperature of the connecting node of the steam generator in which the feedwater and emergency feedwater enter. As consequence, until the saturation temperature is reached the calculated values cannot be compared directly with the measurement or the other

two codes. Following that, the characteristic of the curve is similar to the other three curves. In RELAP and TRACE simulations, the effect of the initiation of emergency feedwater injection is much less significant compared to the measurement and APROS.

SECONDARY SIDE FLUID TEMPERATURES (TE83, TE85, TE87)

It has to be noted that the TE83 (Figure 7.47), TE85 (Figure 7.48) and TE87 (Figure 7.49) temperatures are measured at the vertical center plane of the secondary side while in the codes the mixture temperatures of the heater were extracted. Similarly to the temperature measurements in the primary side collectors, the exact locations of the measurements could not be reproduced in the simulations. All three simulations predict the characteristic of the temperature curves qualitatively well however tends to slightly overestimate the secondary coolant temperature values in the steam generator which is related to the over-estimation of the secondary pressures. In case of the measured temperatures, at the beginning of the emergency feedwater injection a temporary rise can be observed. In the simulations, this phenomenon is only apparent in APROS.

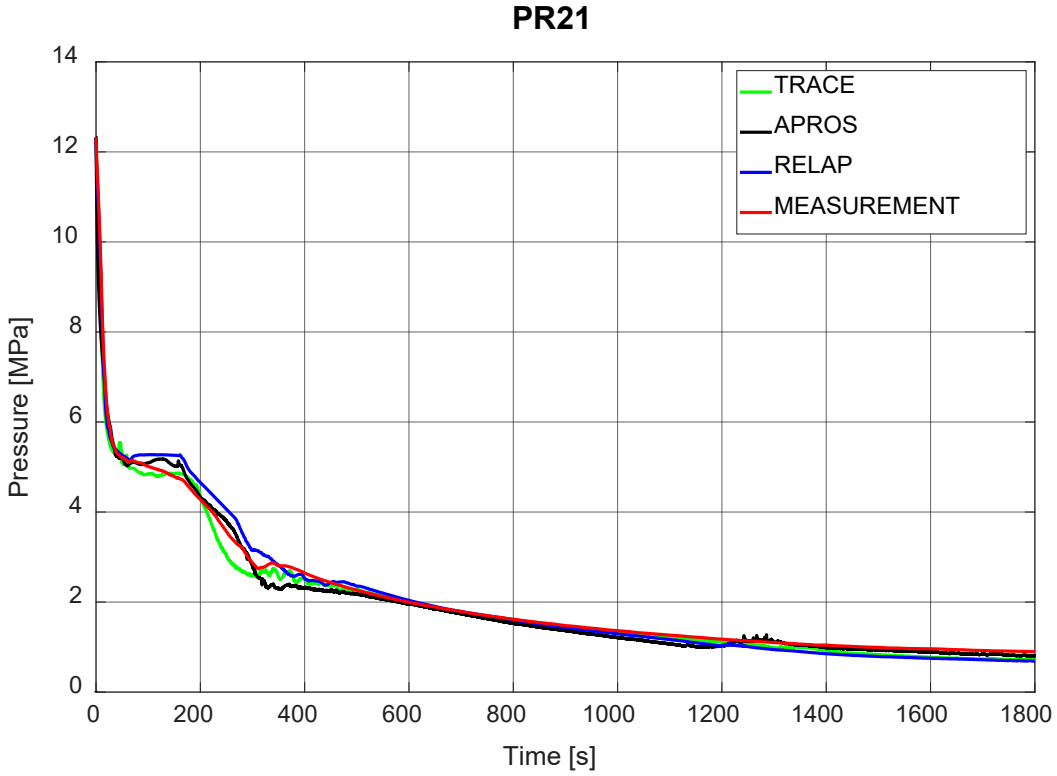

Figure 7.1 Upper Plenum Pressure

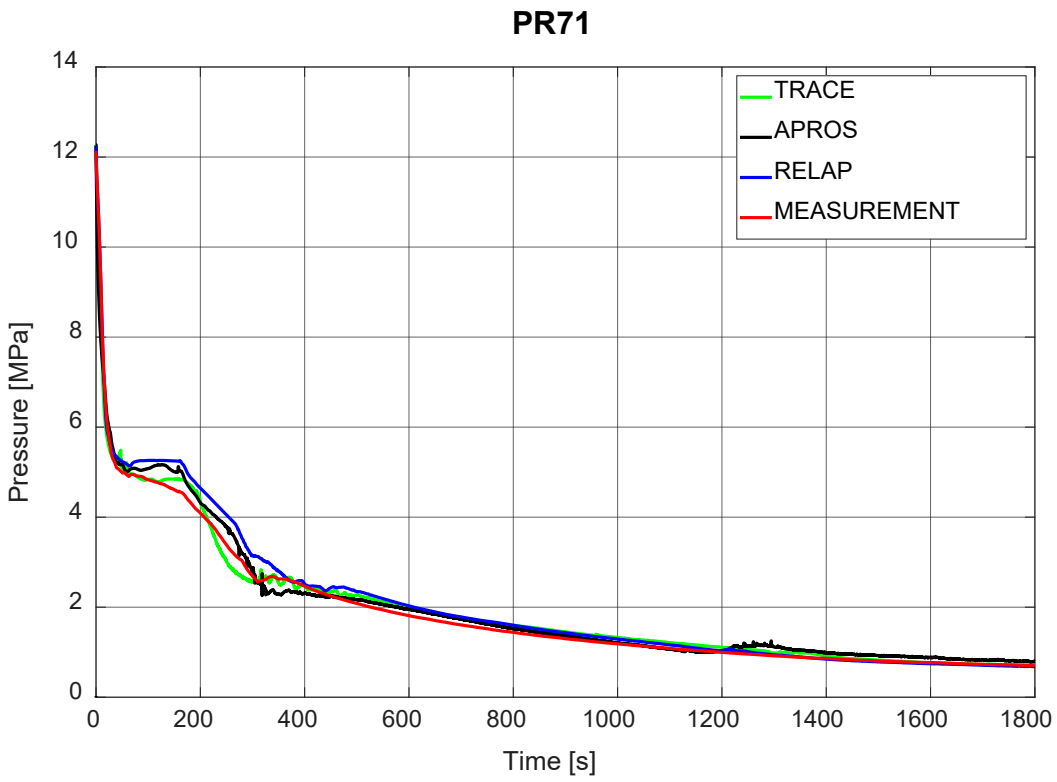

Figure 7.2 Pressurizer Pressure

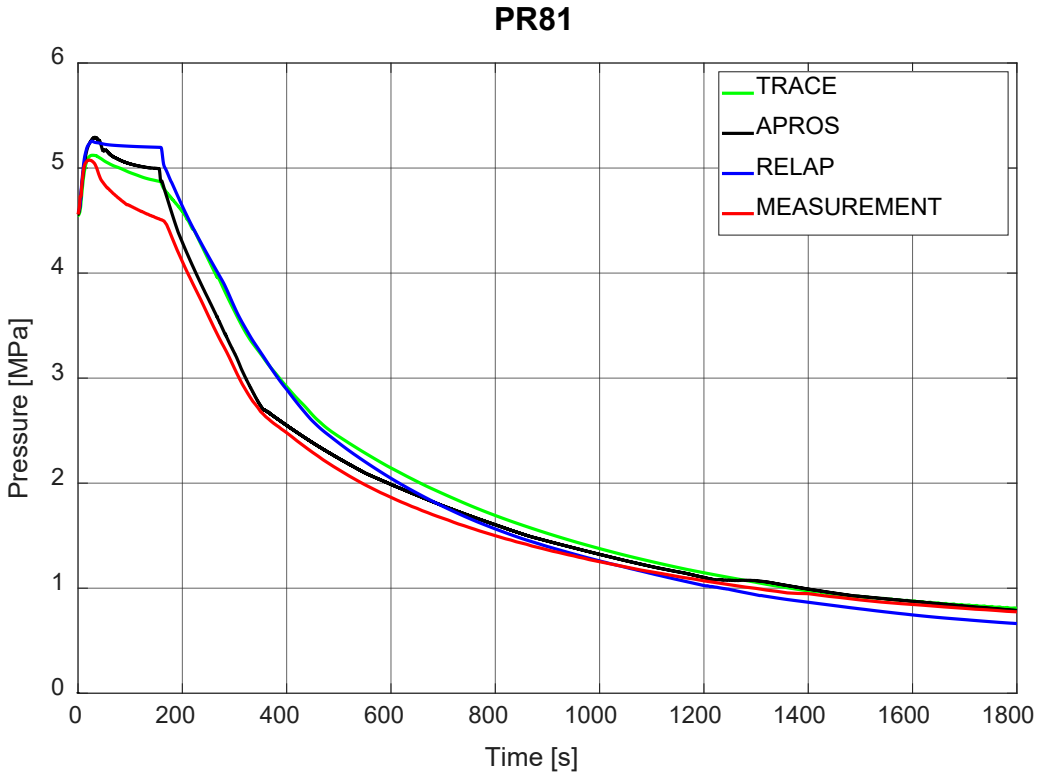

Figure 7.3 Secondary Circuit Pressure

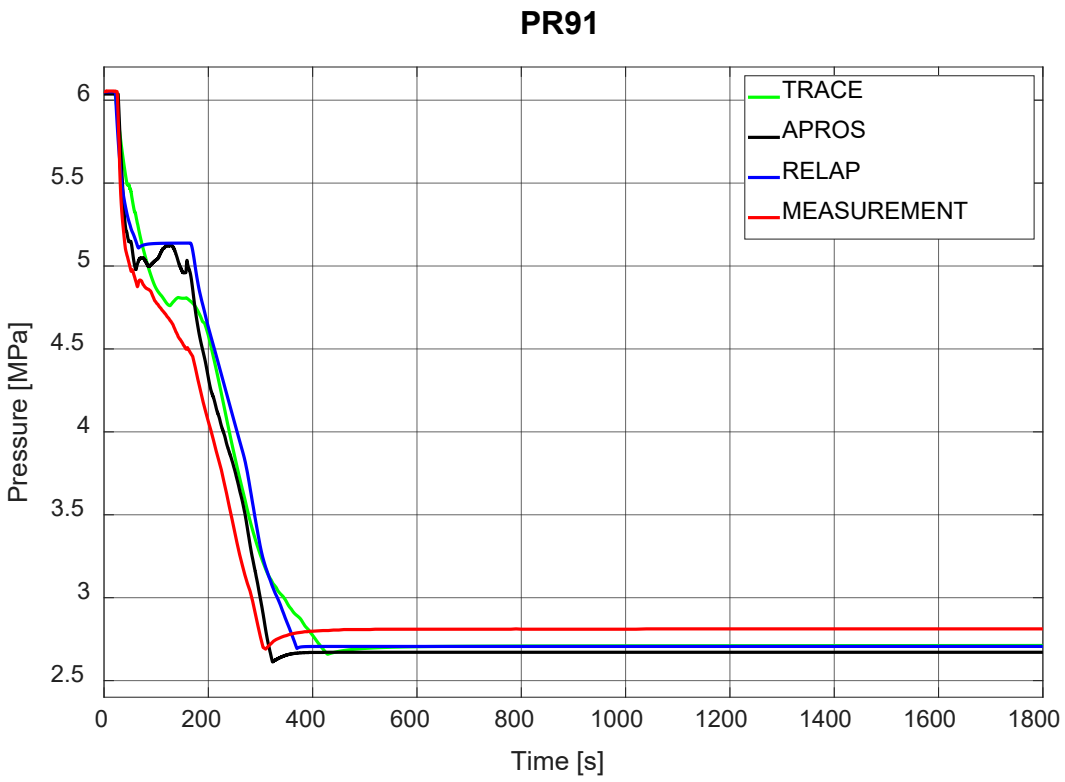

Figure 7.4 SIT1 Pressure

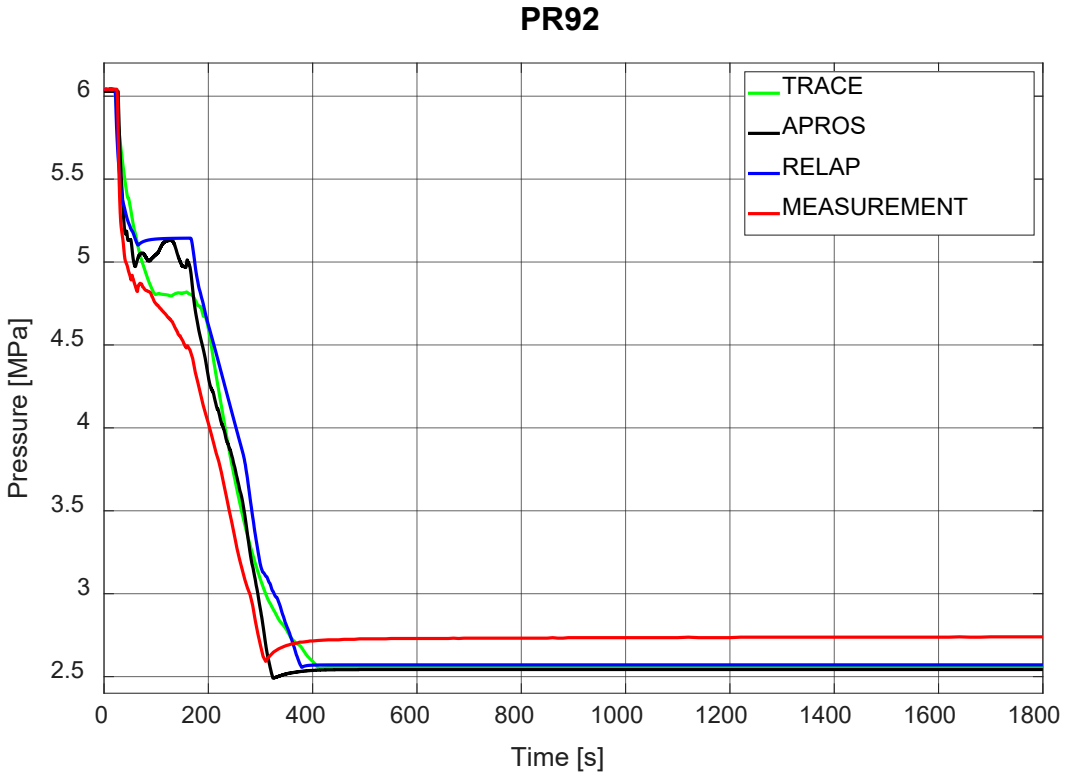

Figure 7.5 SIT2 Pressure

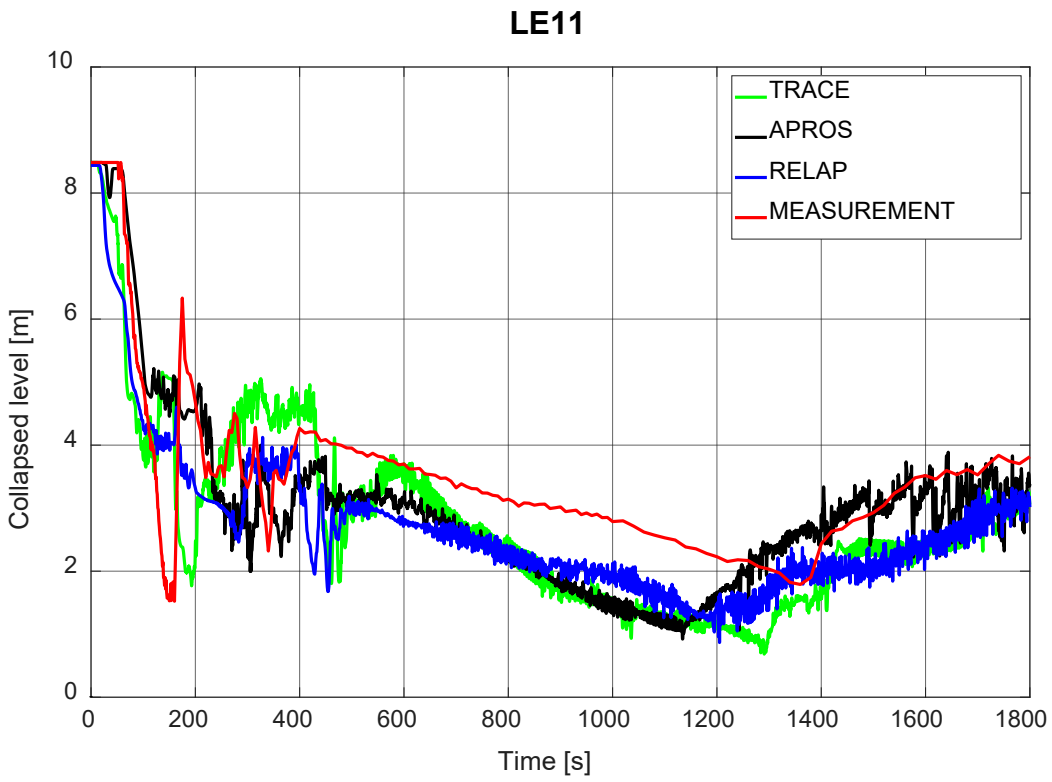

Figure 7.6 Reactor Vessel Liquid Level

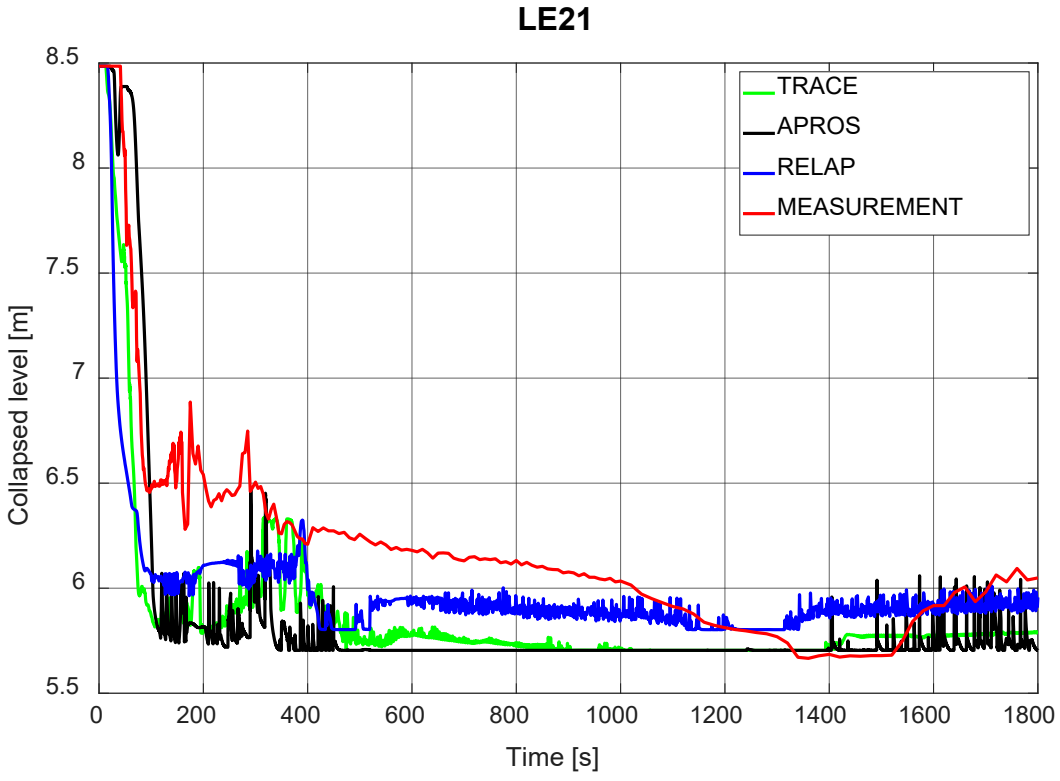

Figure 7.7 Upper Plenum Liquid Level 1

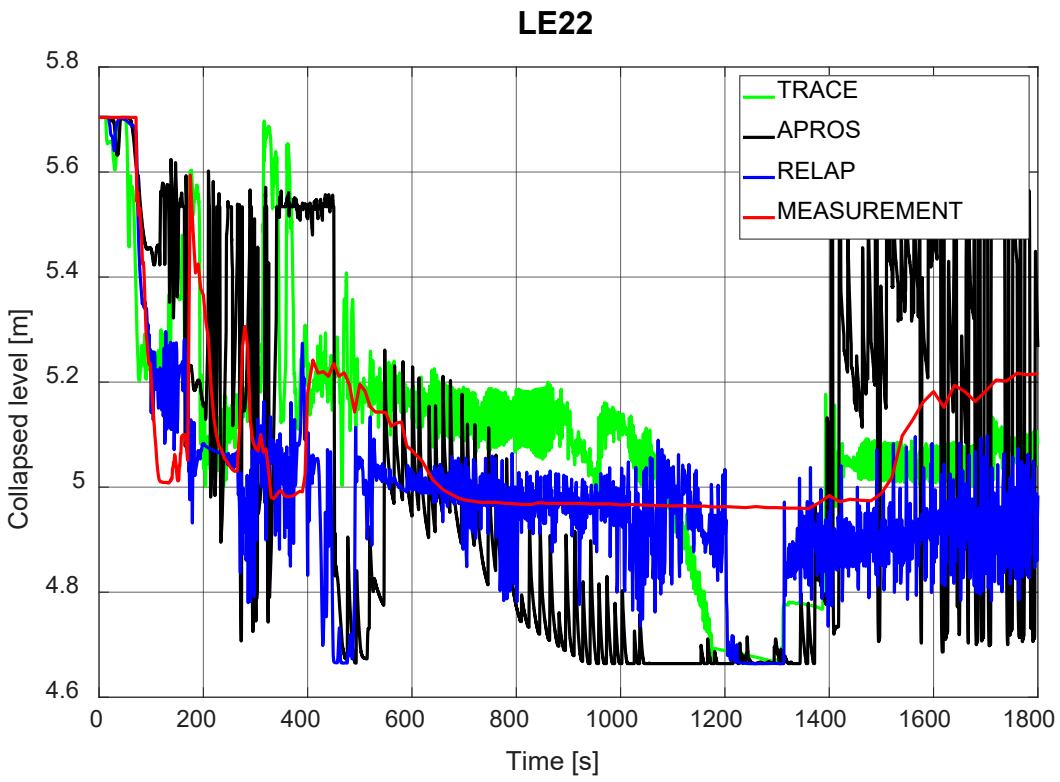

Figure 7.8 Upper Plenum Liquid Level 2

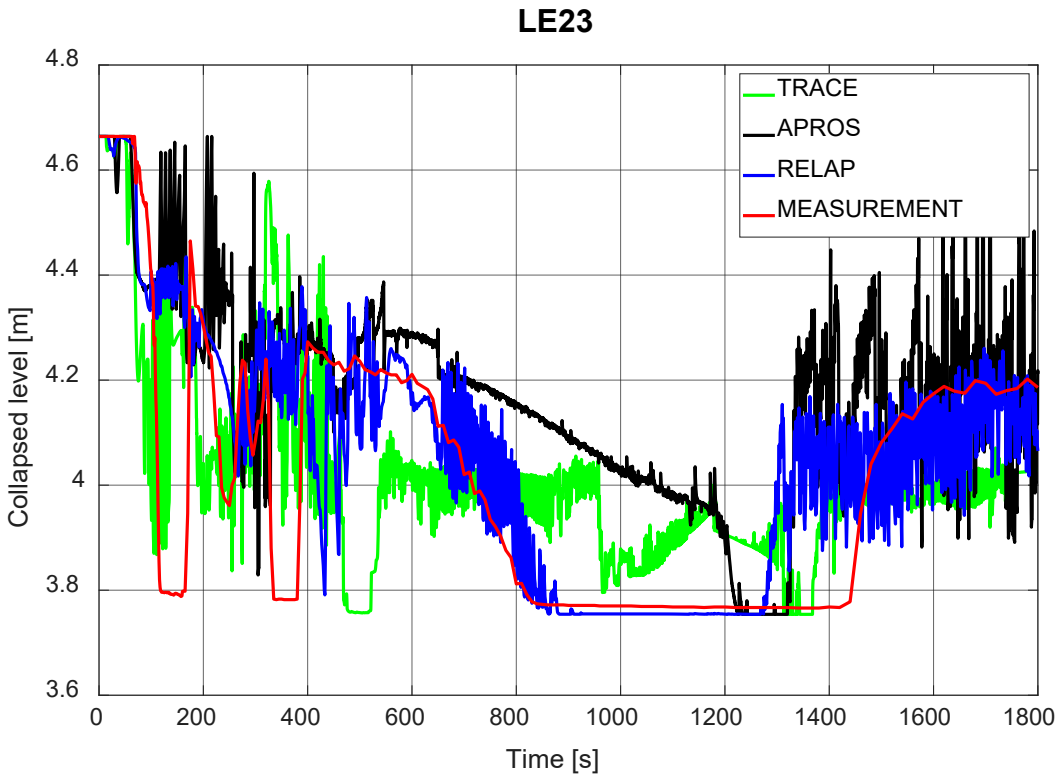

Figure 7.9 Upper Plenum Liquid Level 3

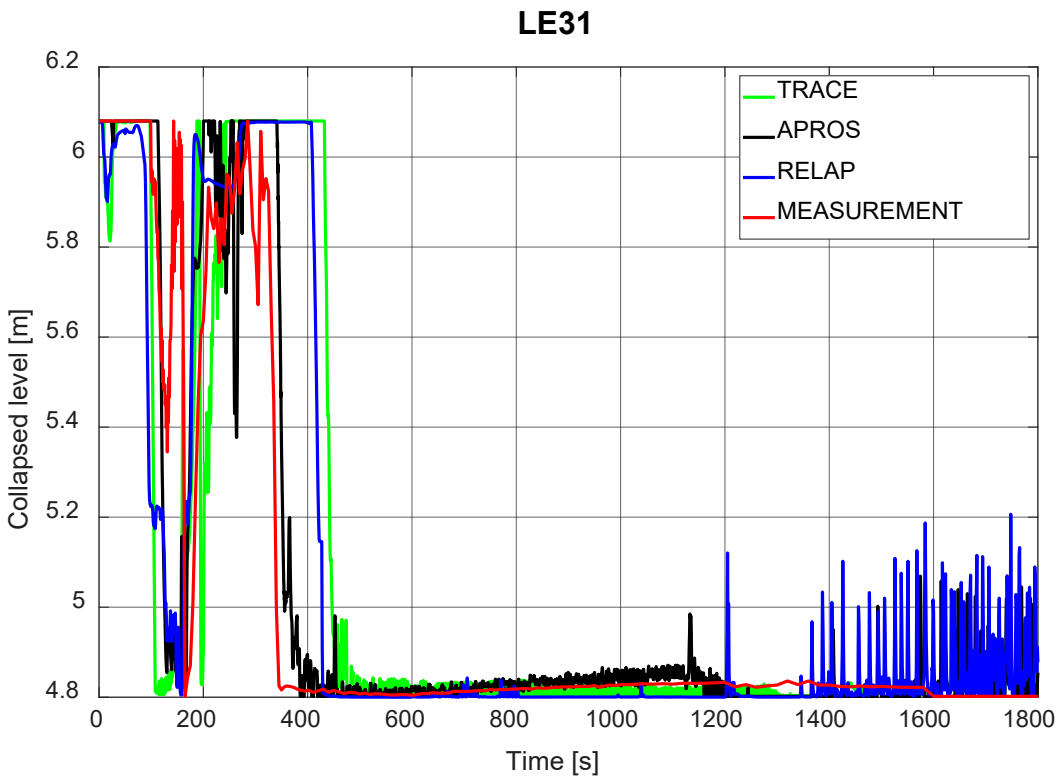

Figure 7.10 Hot Leg Loop Seal Liquid Level

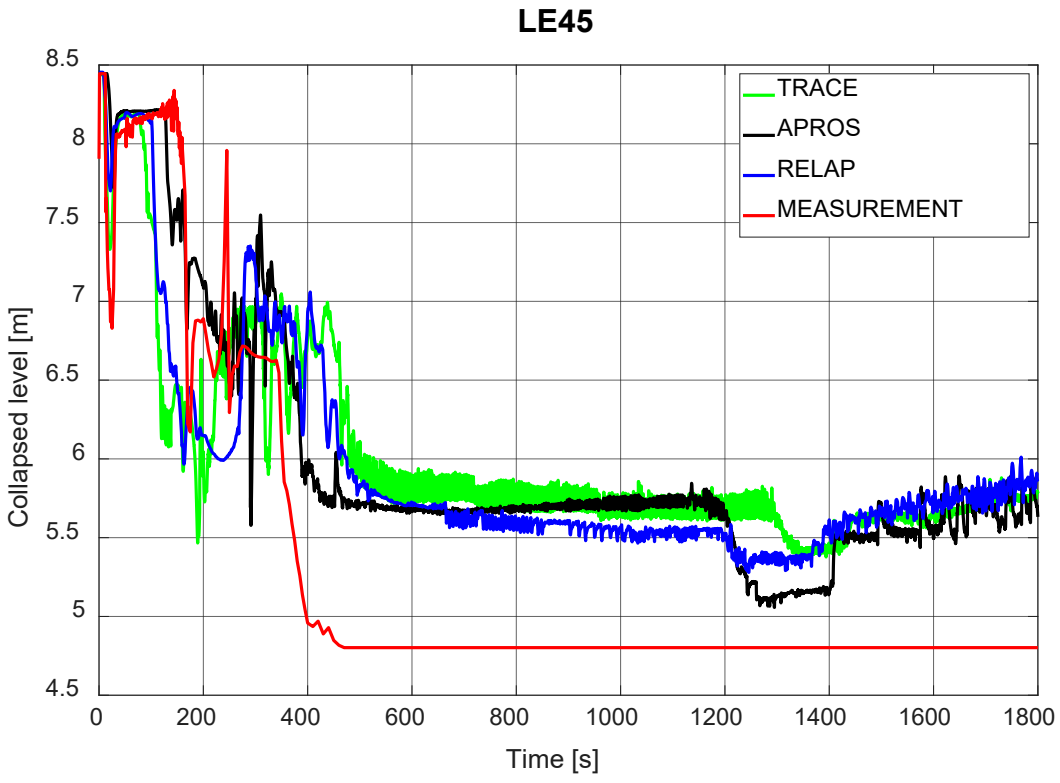

Figure 7.11 SG Primary Liquid Level (Hot Leg)

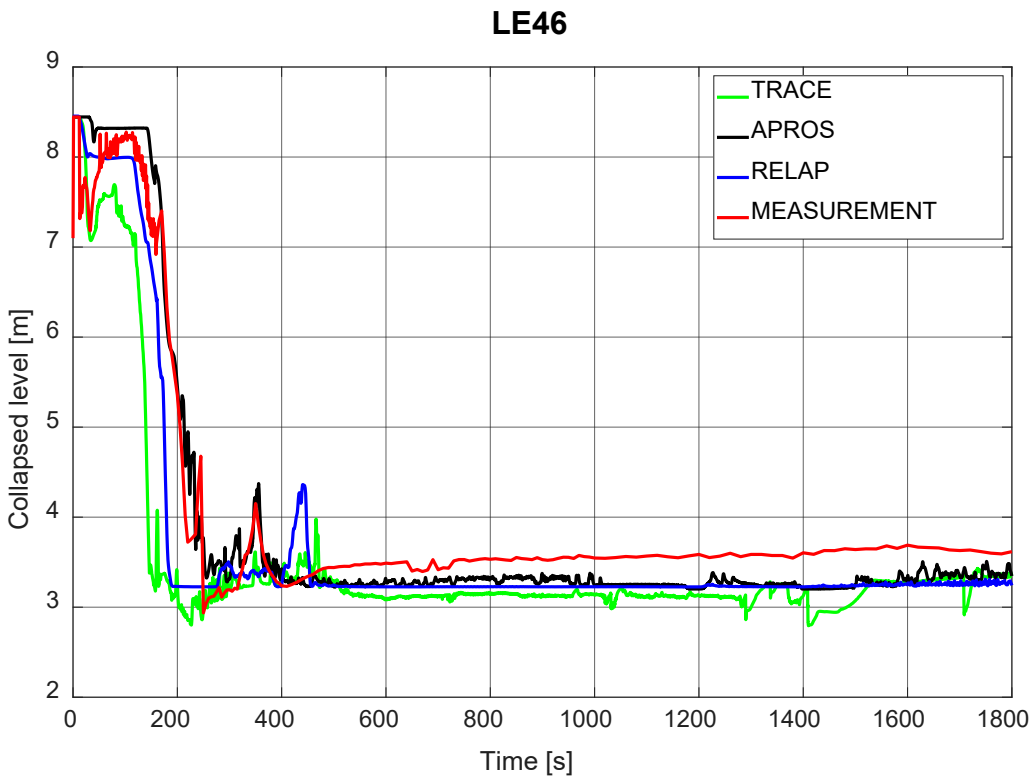

Figure 7.12 SG Primary Liquid Level (Cold Leg)

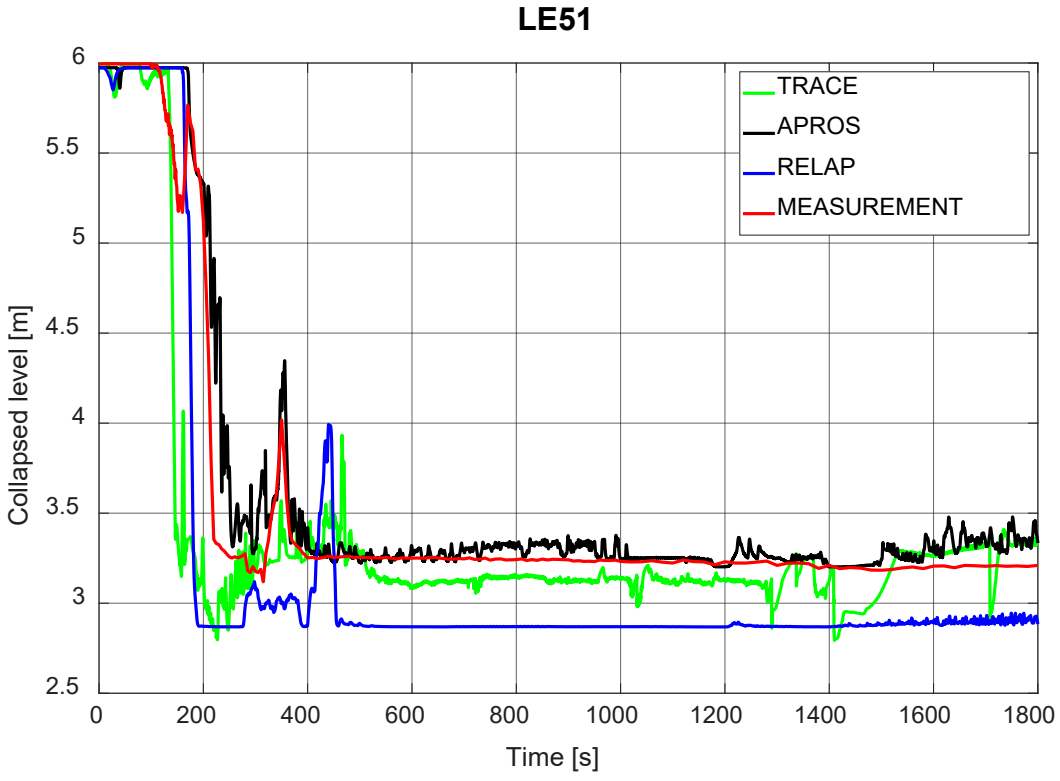

Figure 7.13 Cold Leg Liquid Level

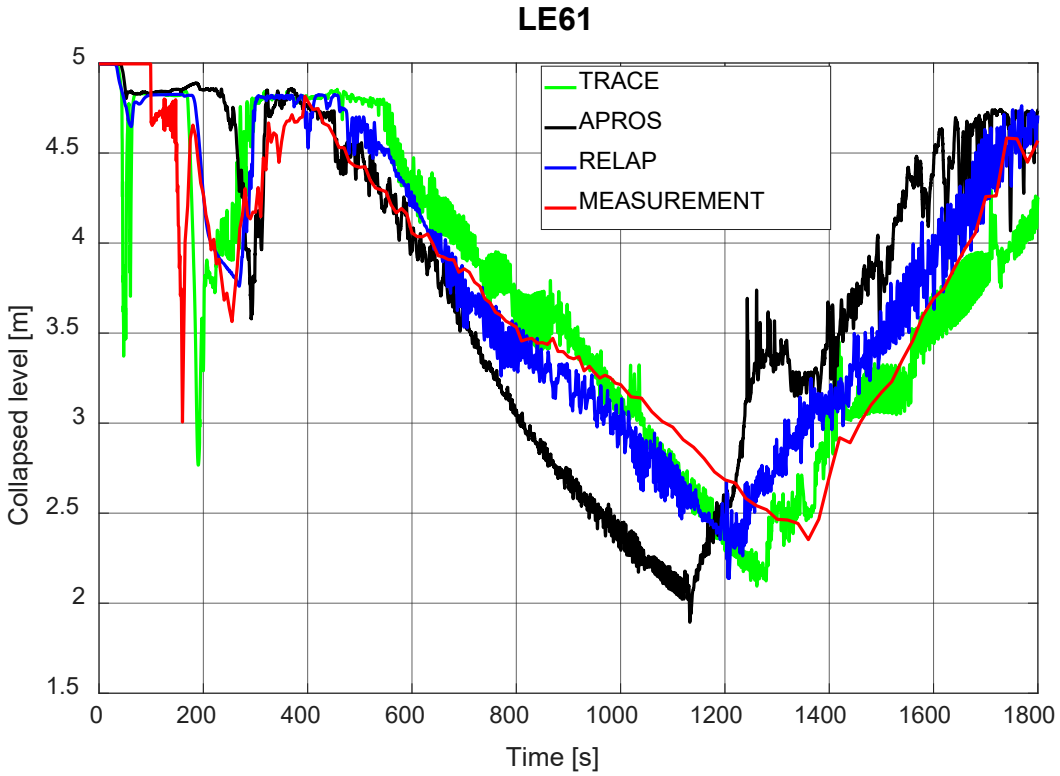

Figure 7.14 Downcomer Liquid Level

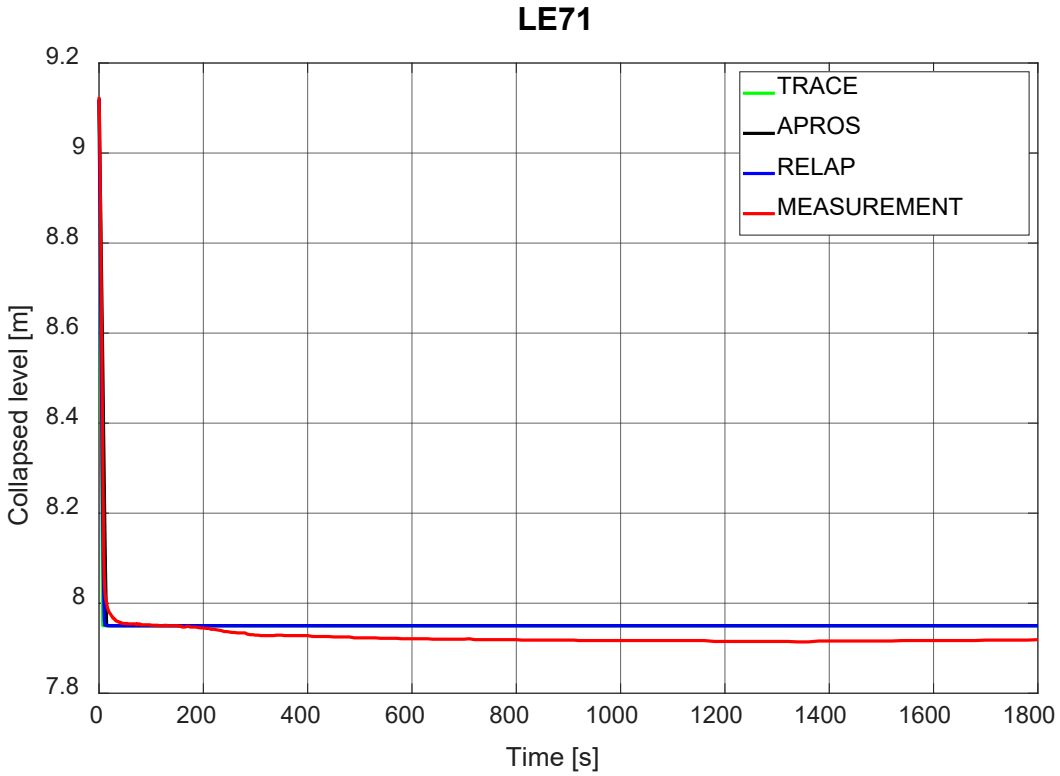

Figure 7.15 Pressurizer Liquid Level

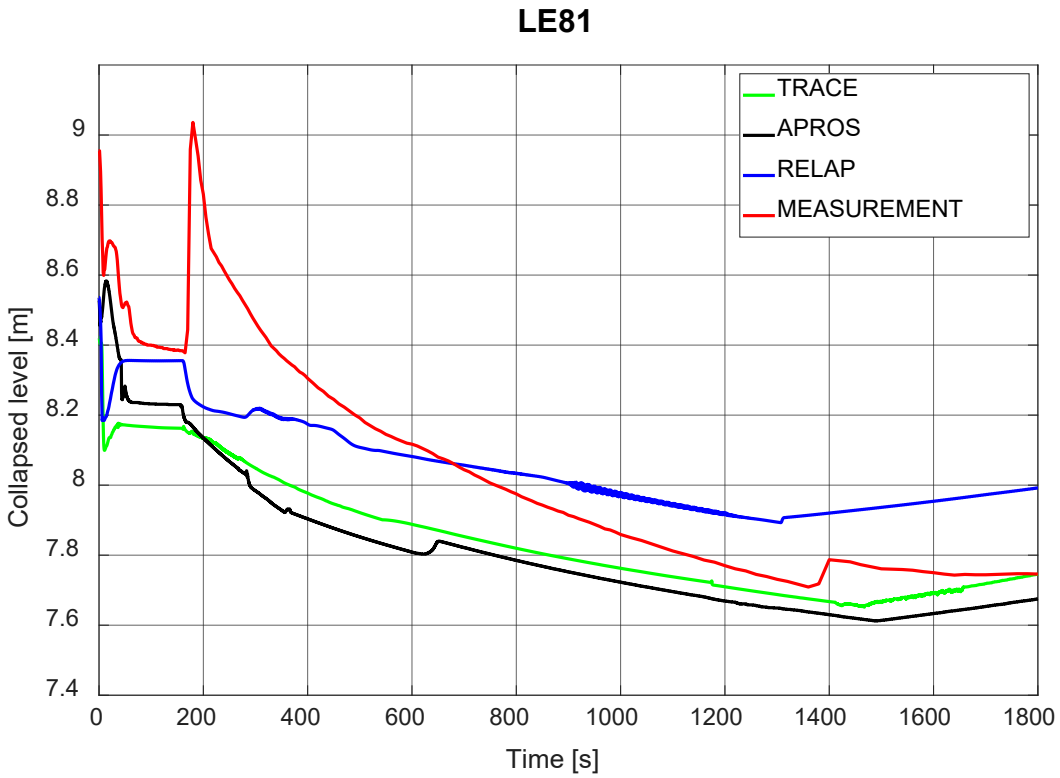

Figure 7.16 SG Secondary Liquid Level (Heater)

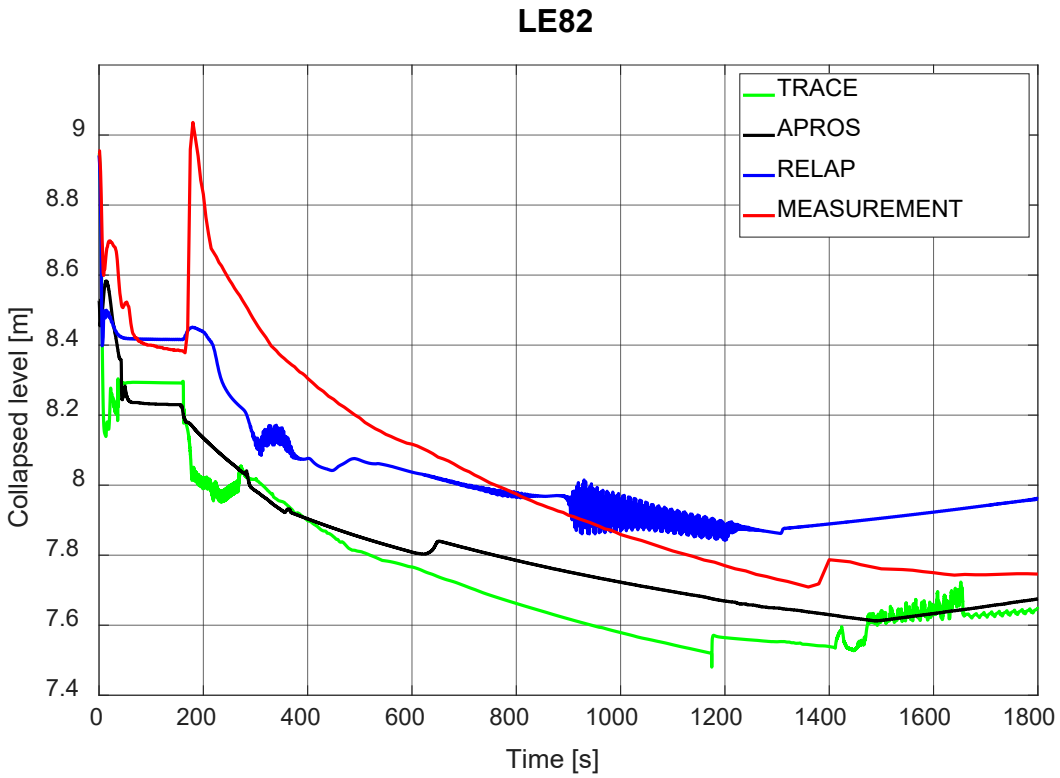

Figure 7.17 SG Secondary Liquid Level (Downcomer)

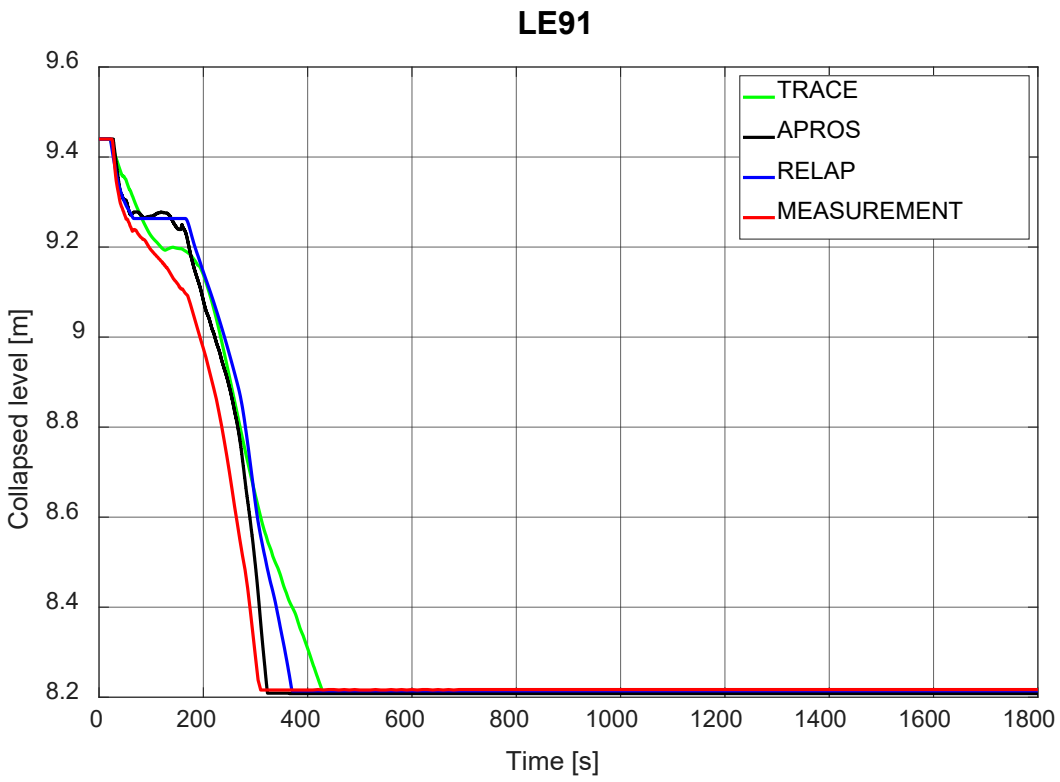

Figure 7.18 SIT1 Liquid Level

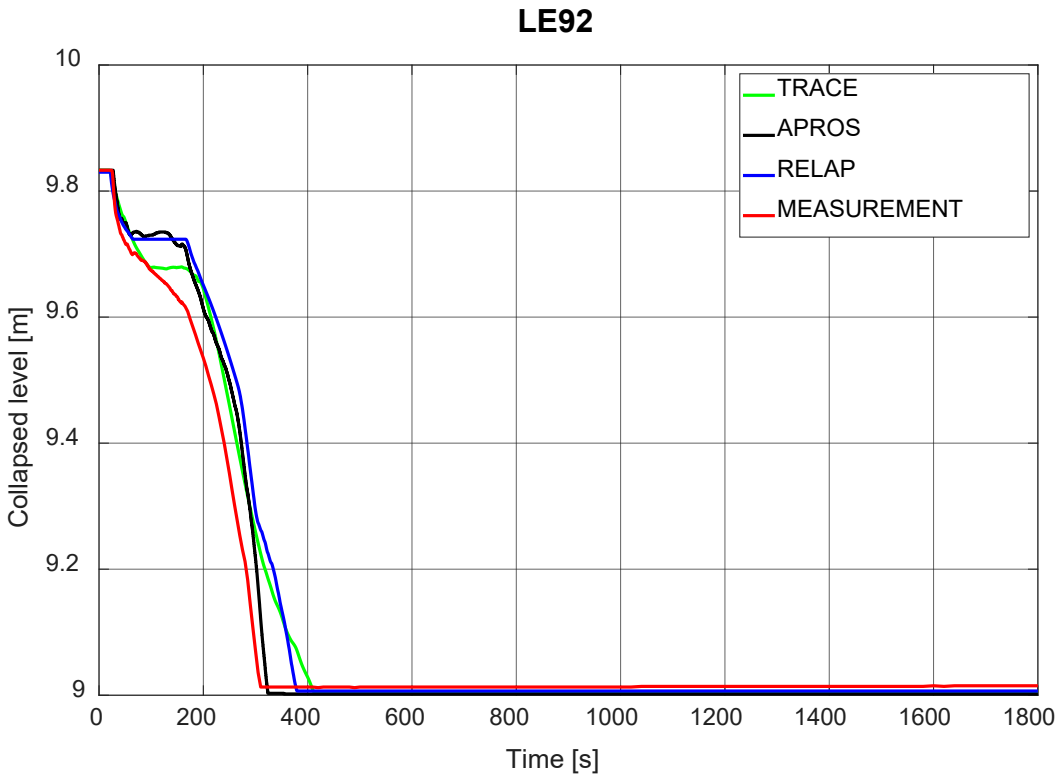

Figure 7.19 SIT2 Liquid Level

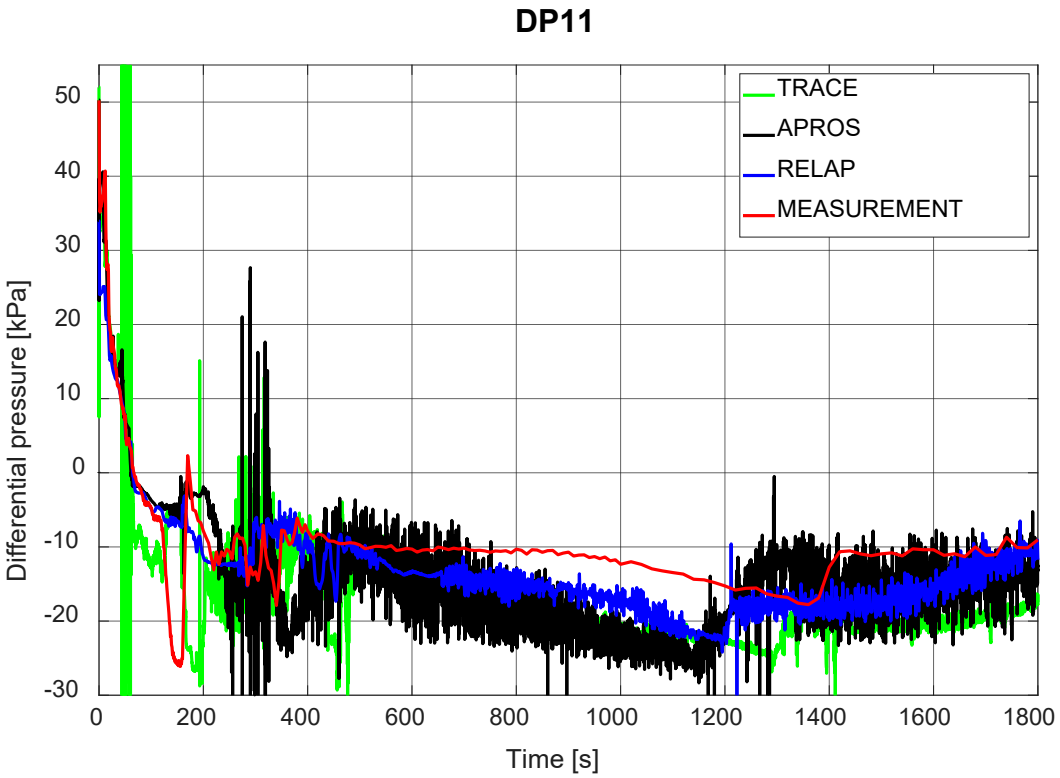

Figure 7.20 Reactor Core Pressure Drop

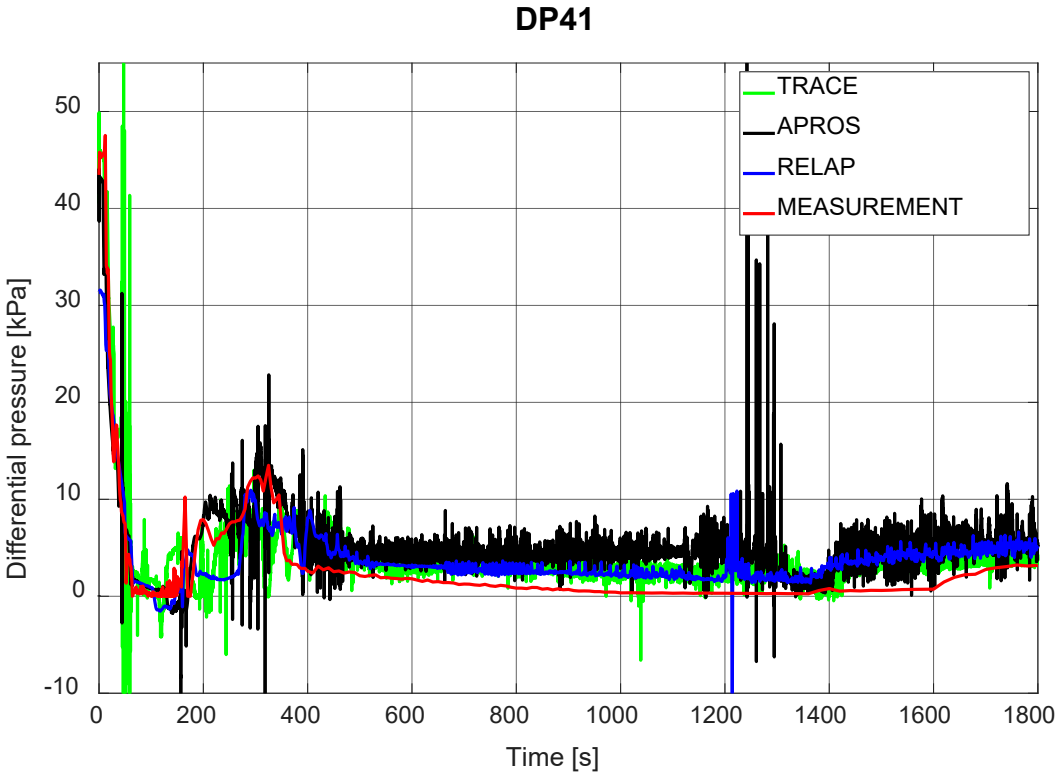

Figure 7.21 SG Primary Pressure Drop

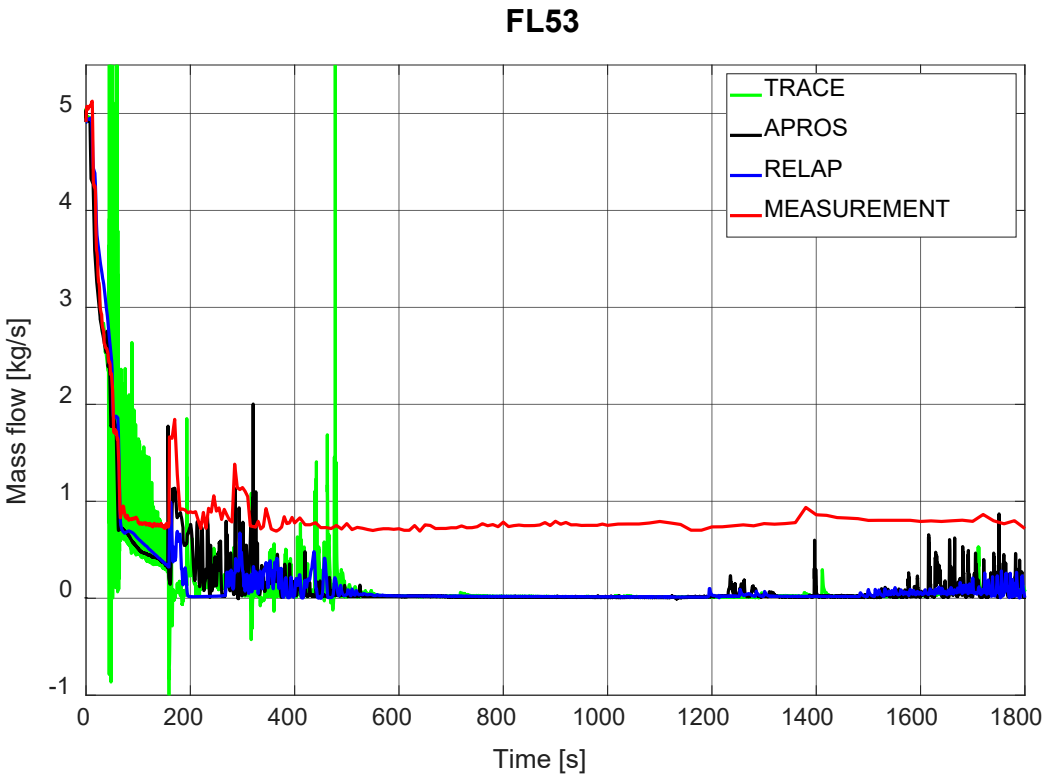

Figure 7.22 Cold Leg Mass Flow (Normal)

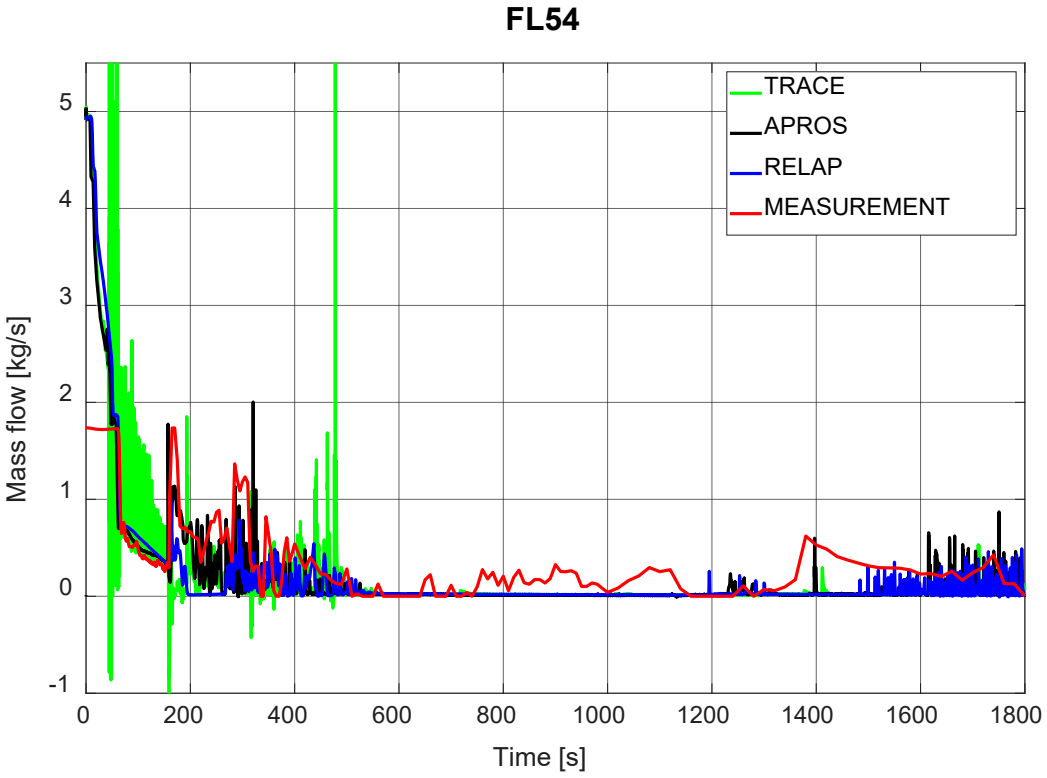

Figure 7.23 Cold Leg Mass Flow (Low Flow)

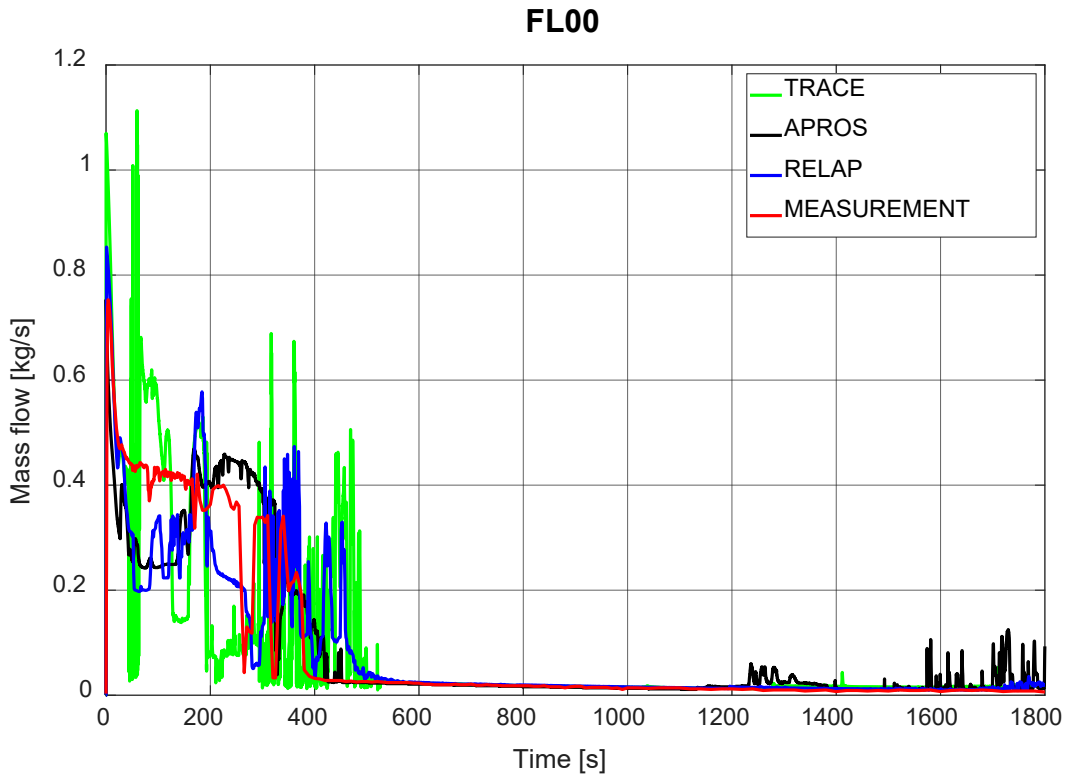

Figure 7.24 Break Mass Flow

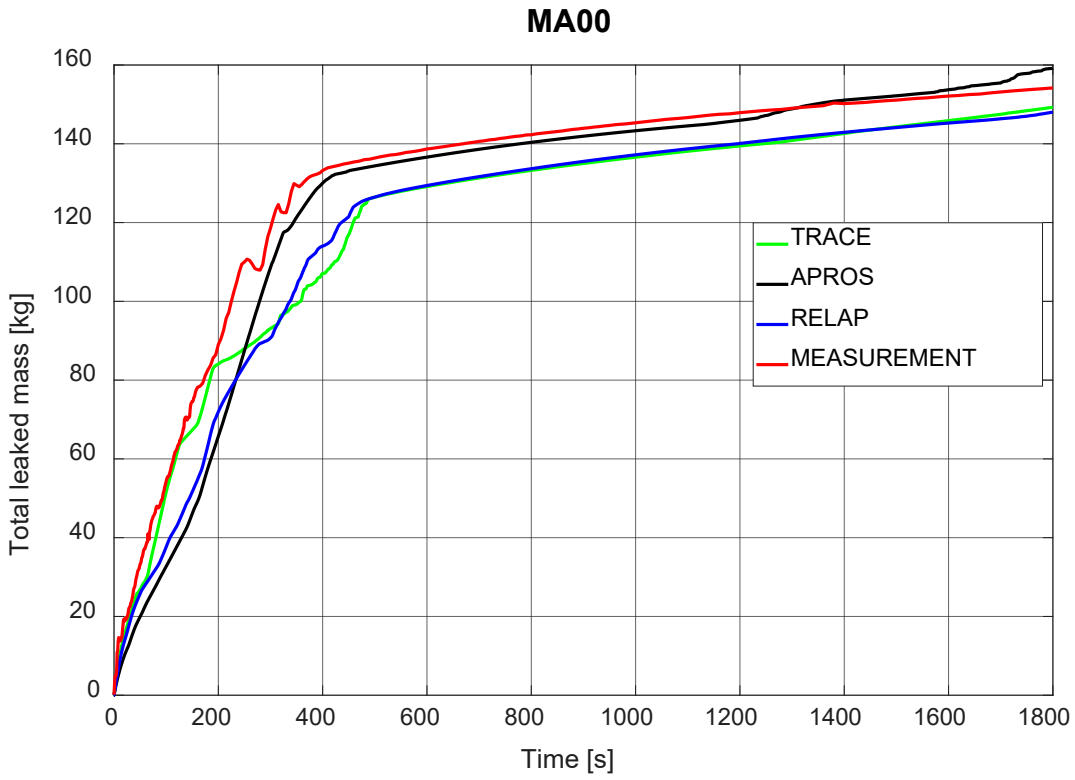

Figure 7.25 Total Mass Leaked through Break

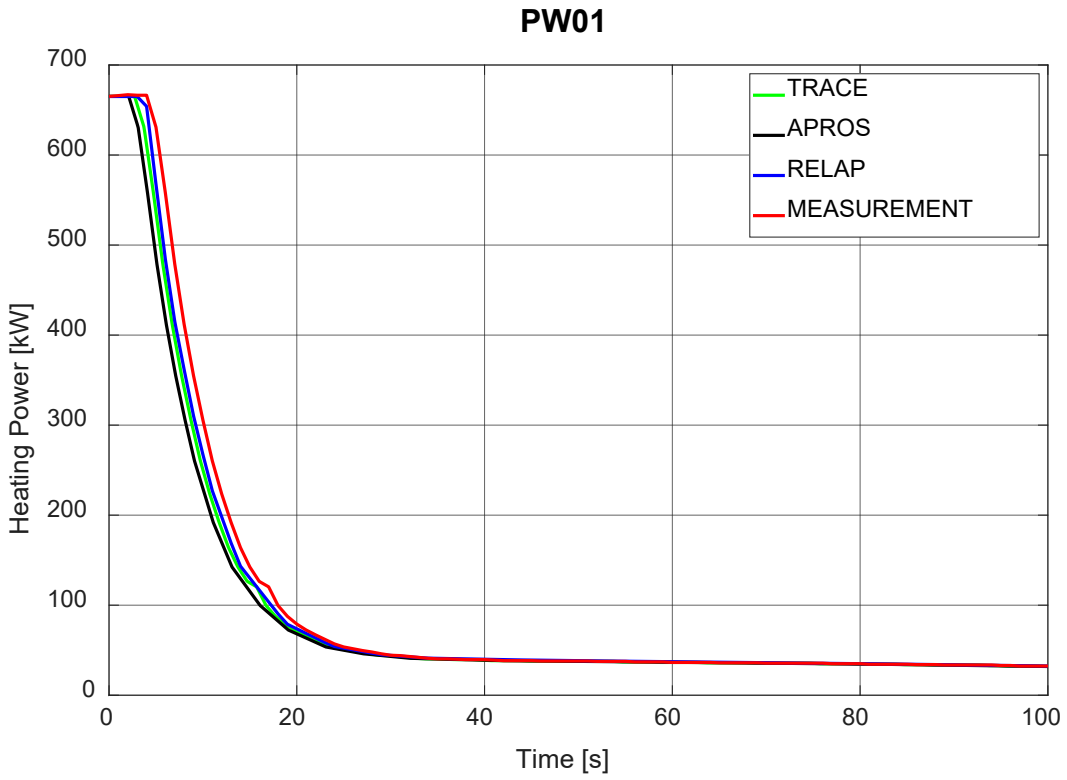

Figure 7.26 Reactor Core Power (Electric)

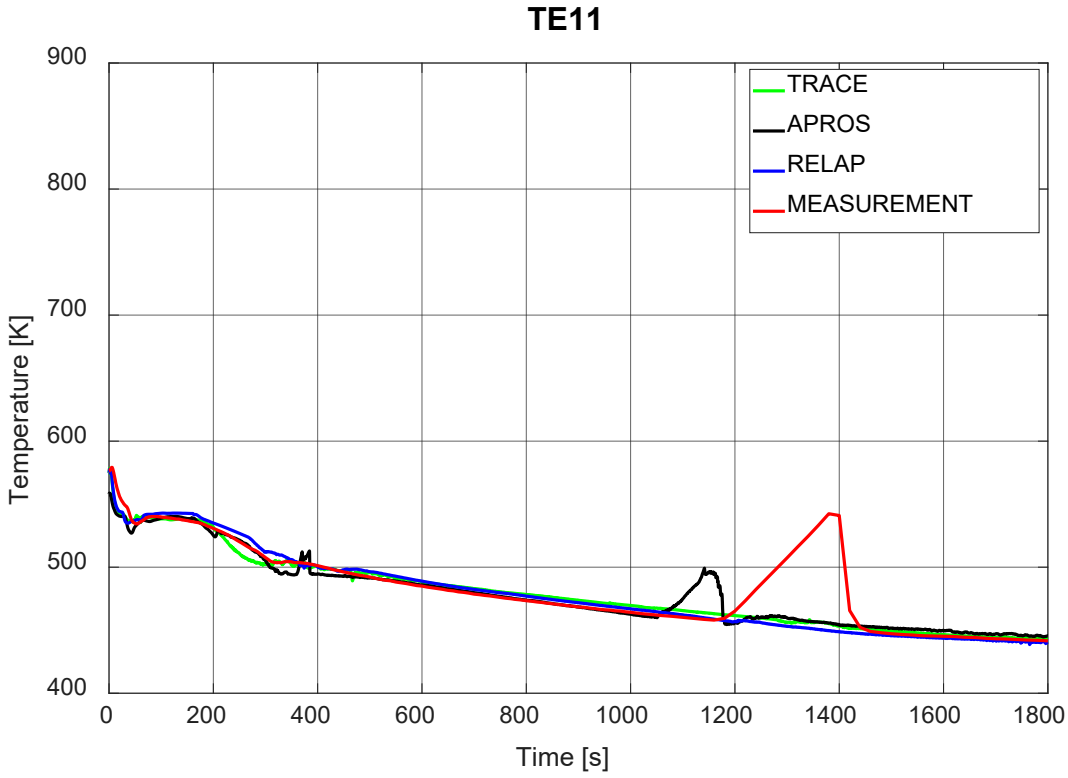

Figure 7.27 Heater Rod Surface Temperature (at 1.494 m Height)

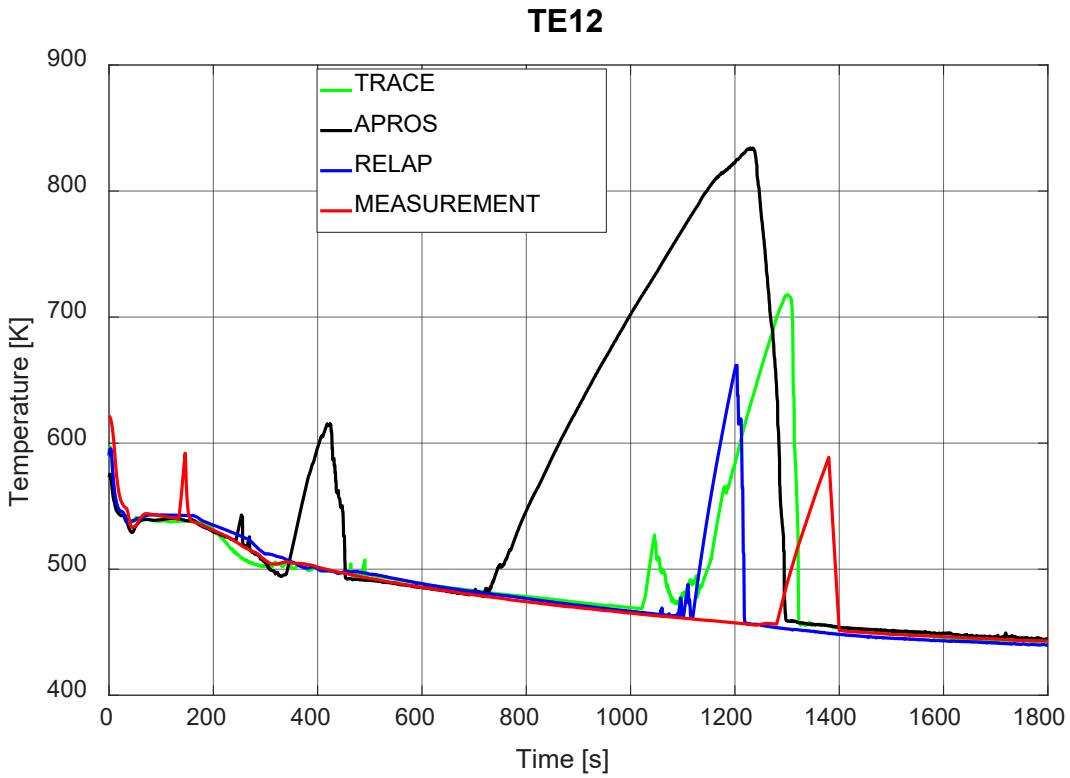

Figure 7.28 Heater Rod Surface Temperature (at 3.464 m Height)

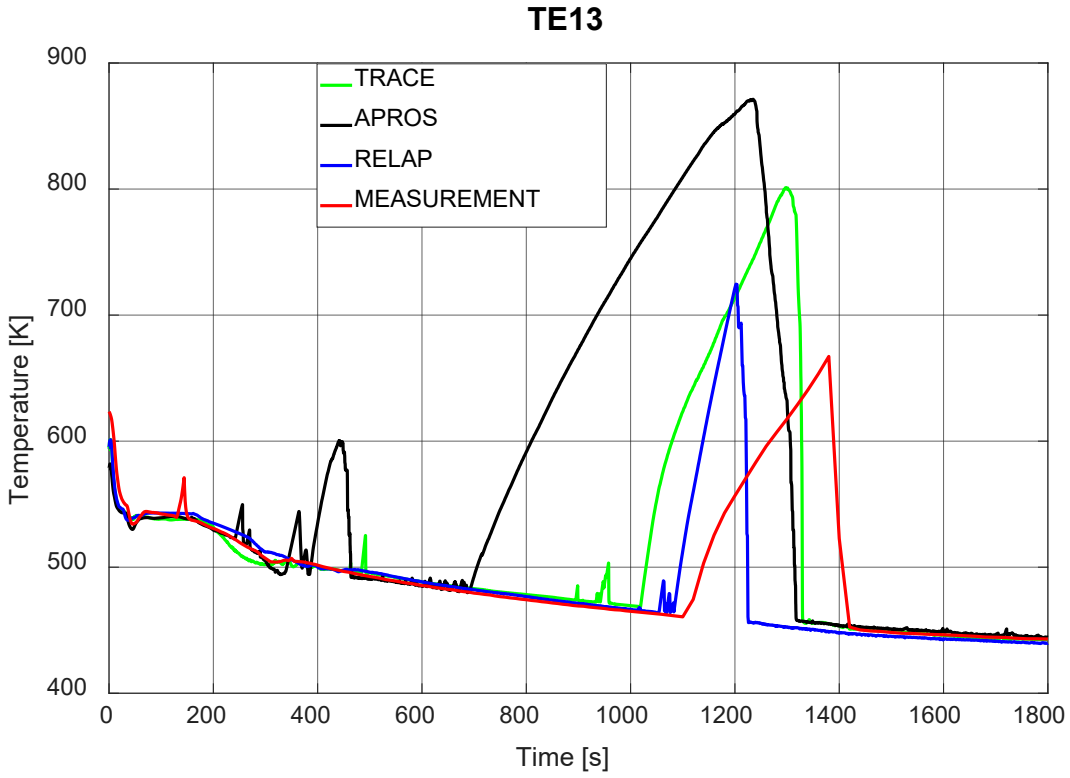

Figure 7.29 Heater Rod Surface Temperature (at 3.464 m Height)

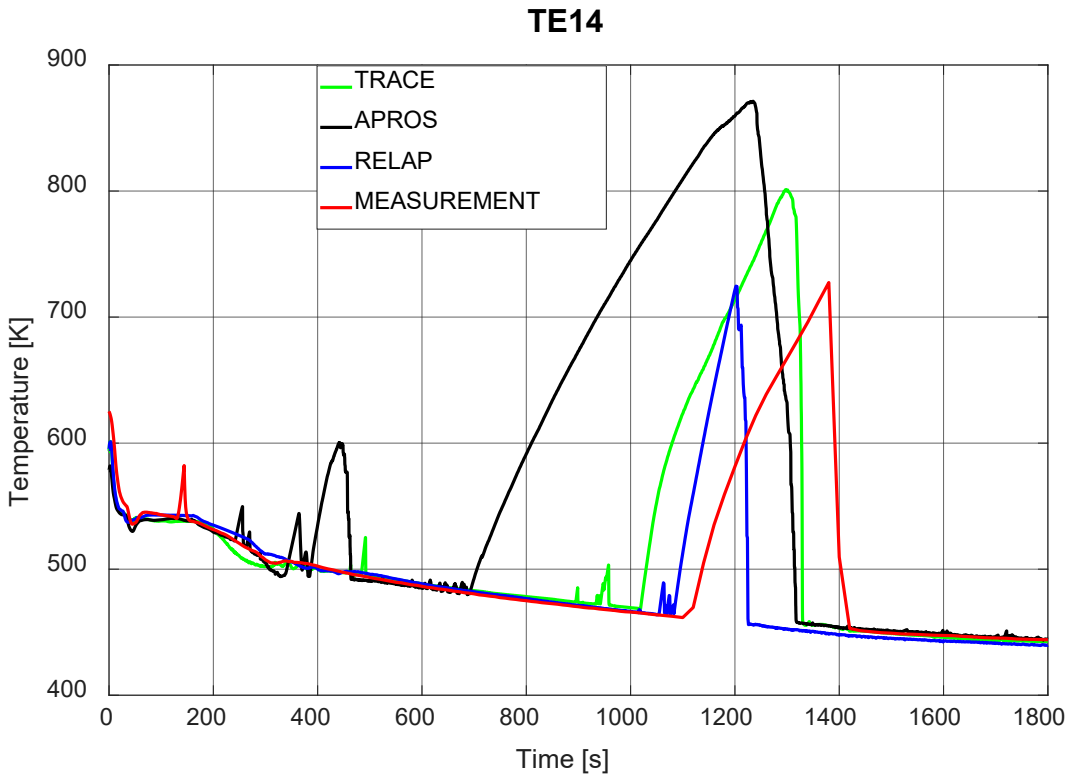

Figure 7.30 Heater Rod Surface Temperature (at 3.464 m Height)

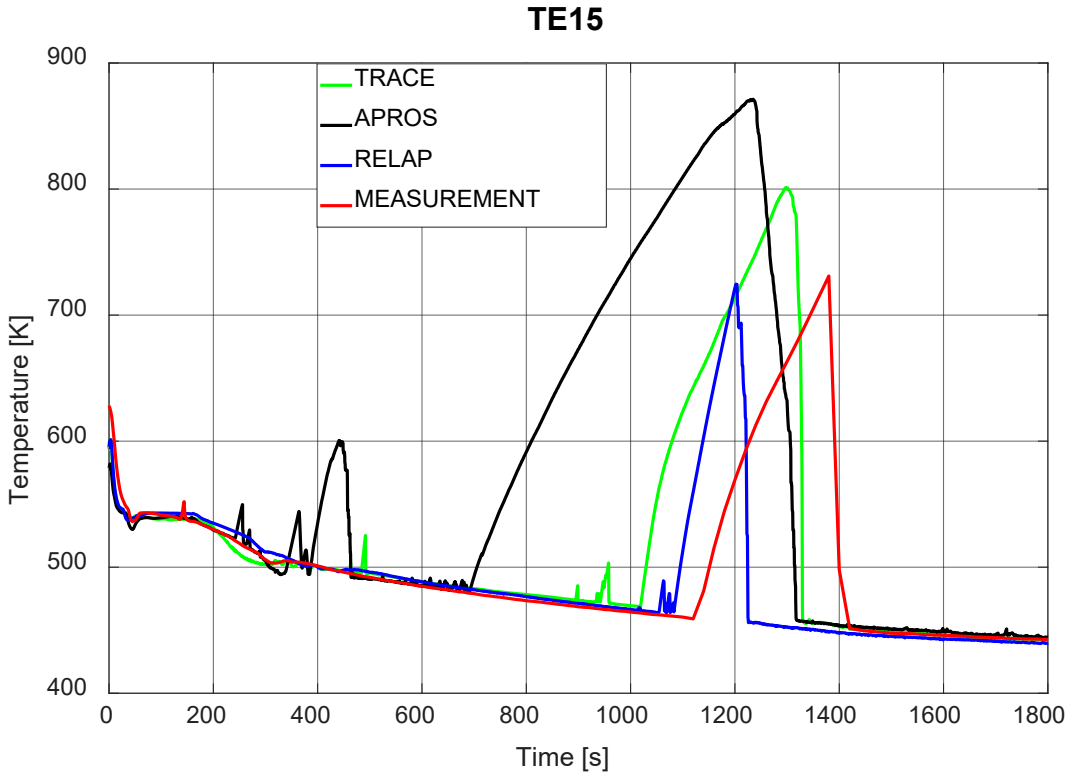

Figure 7.31 Heater Rod Surface Temperature (at 3.464 m Height)

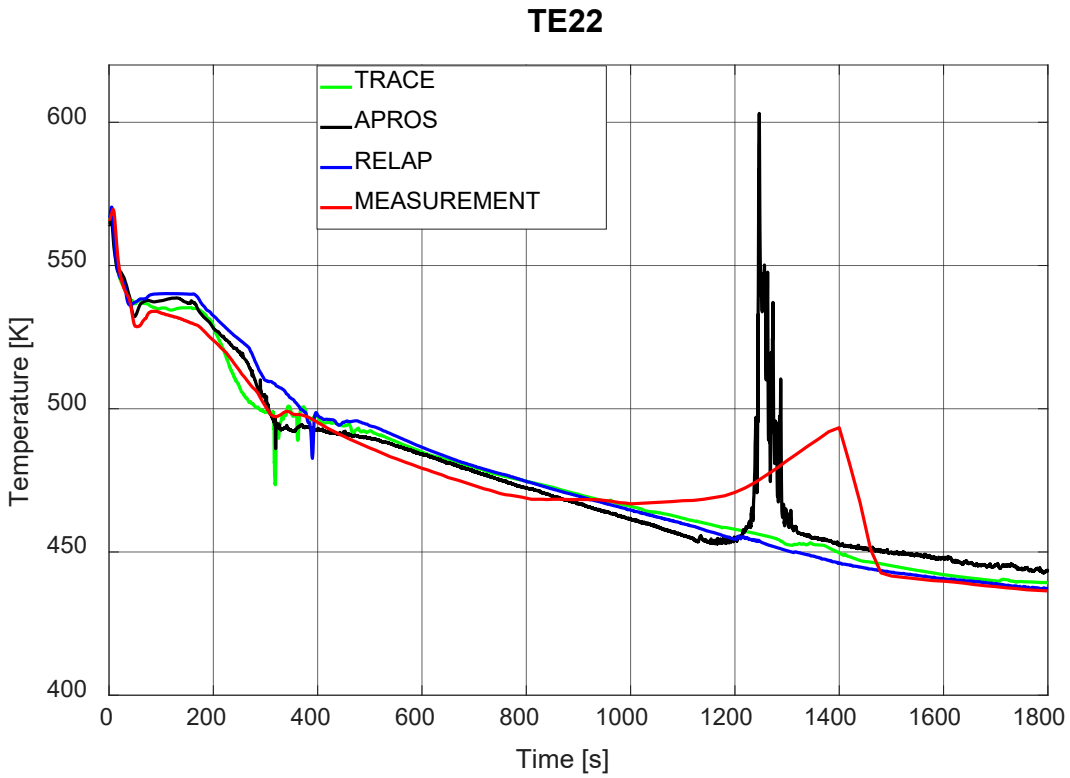

Figure 7.32 Upper Plenum Coolant Temperature (at 4.644 m Height)

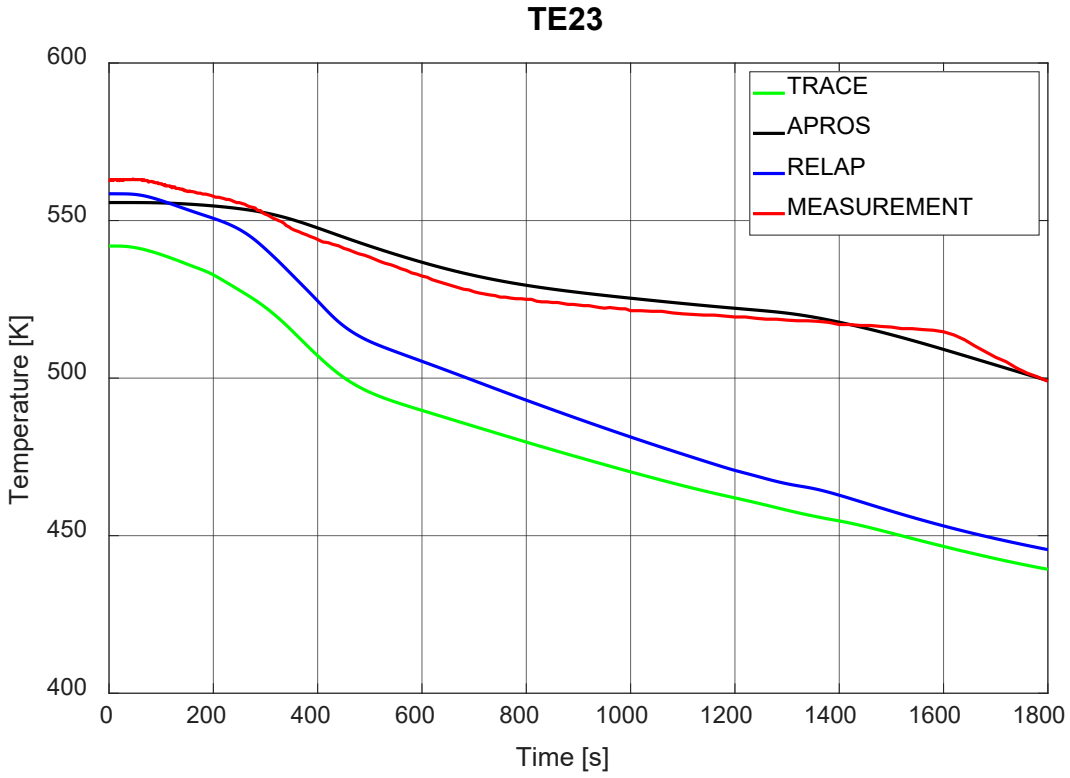

Figure 7.33 Upper Plenum Wall Temperature

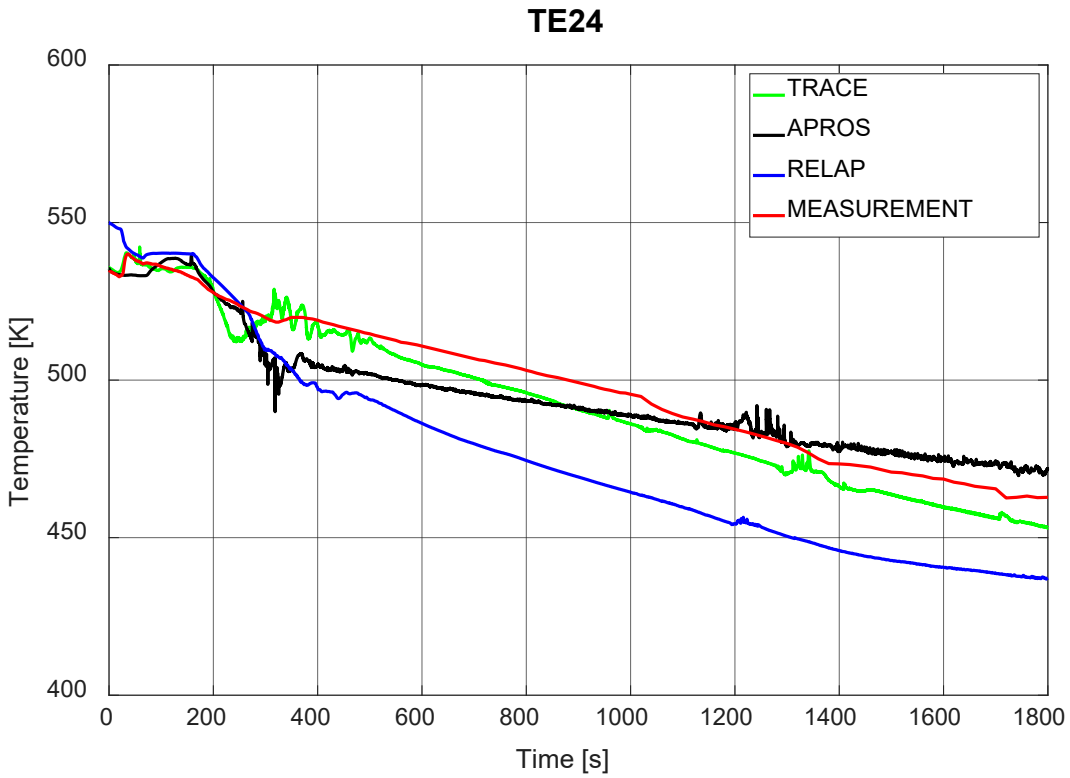

Figure 7.34 Upper Plenum Coolant Temperature (at 8.375 m Height)

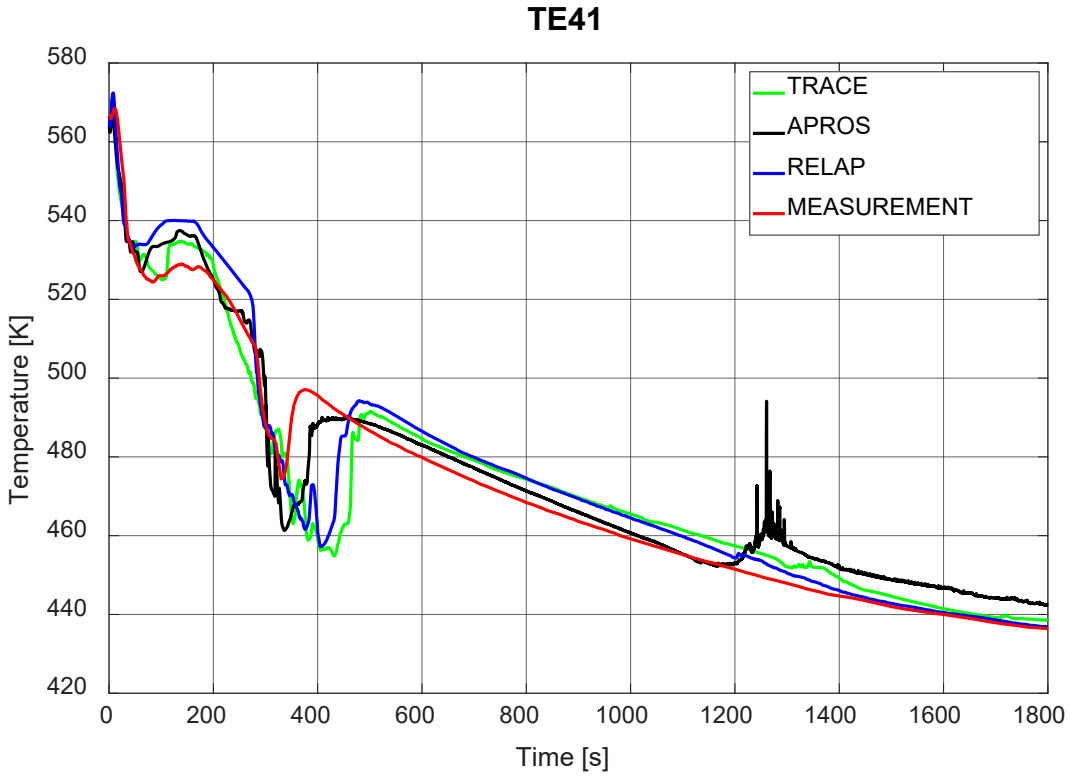

Figure 7.35 SG Inlet Coolant Temperature (Primary Side)

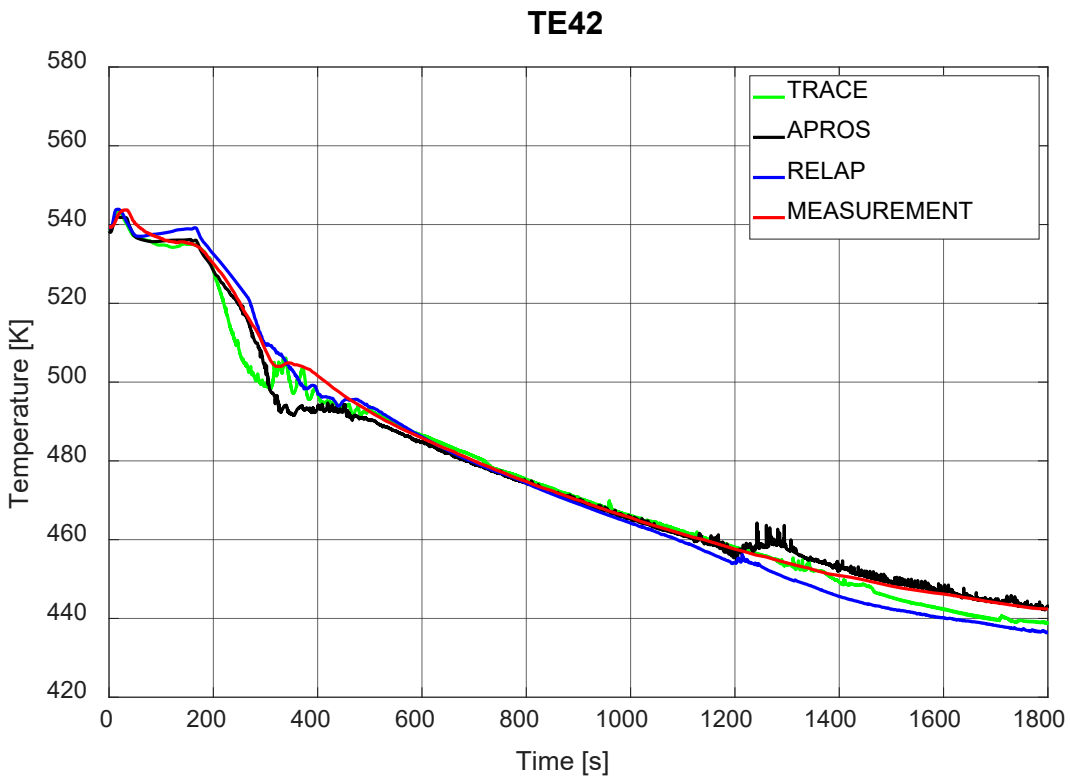

Figure 7.36 SG Outlet Coolant Temperature (Primary Side)

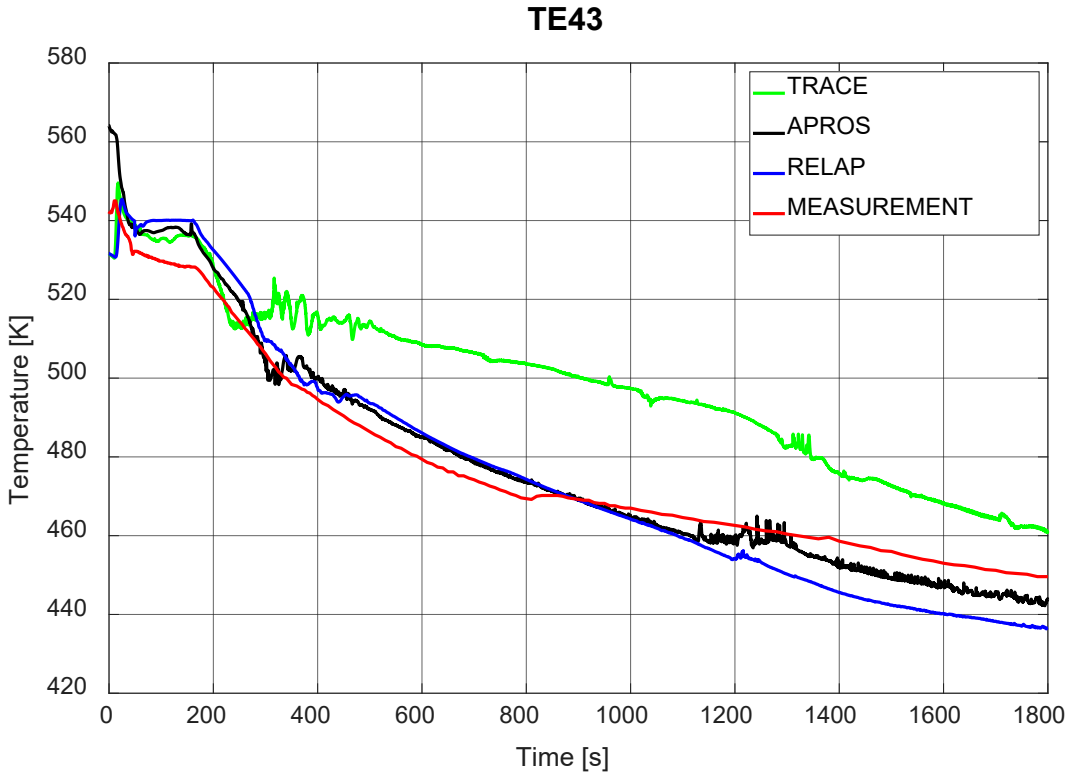

Figure 7.37 SG Hot Collector Coolant Temperature (at 8.163 m Height)

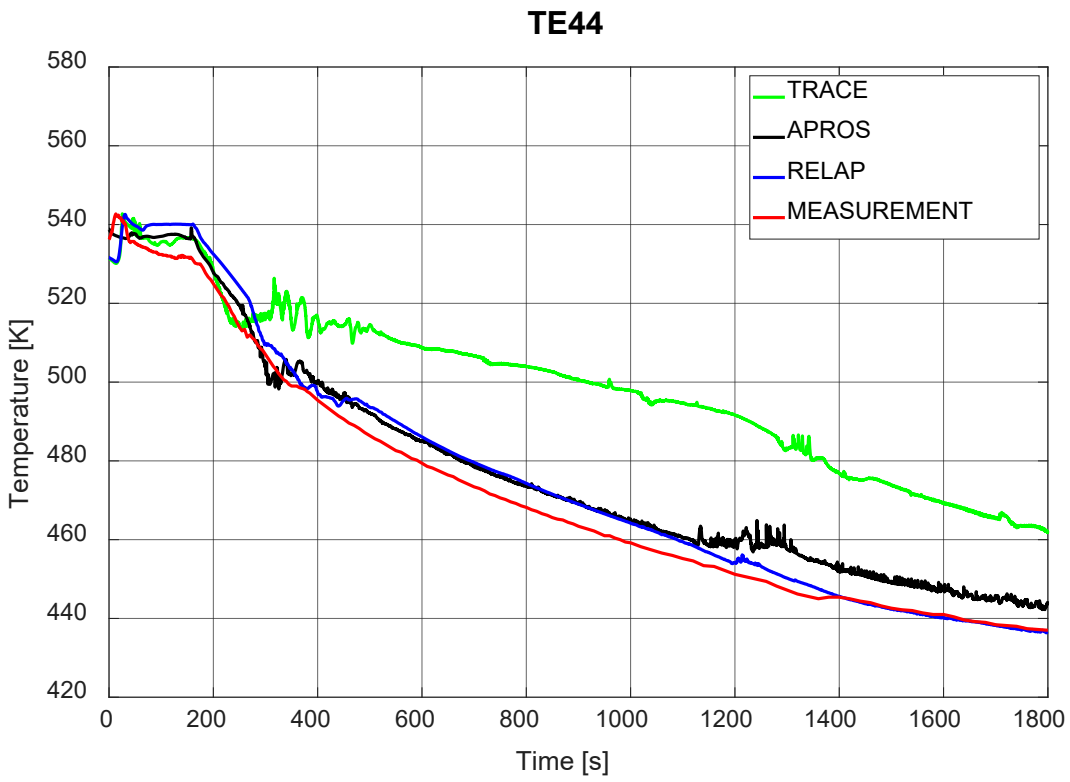

Figure 7.38 SG Cold Collector Coolant Temperature (at 8.163 m Height)

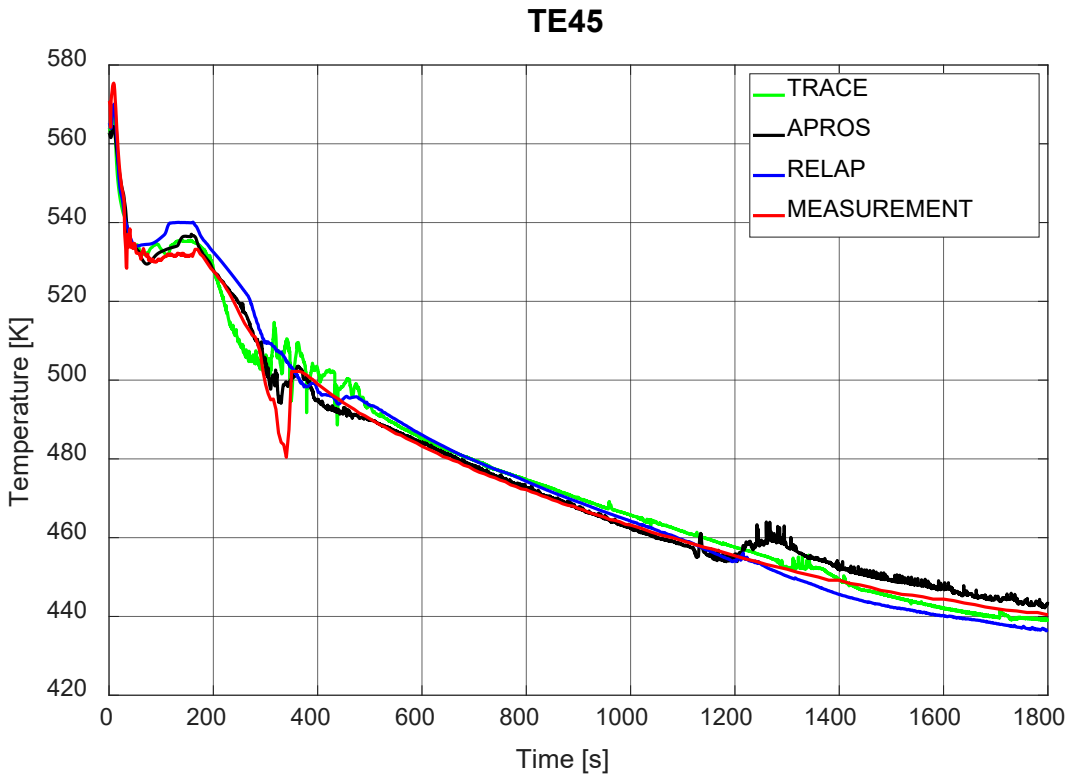

Figure 7.39 SG Hot Collector Coolant Temperature (at 7.591 m Height)

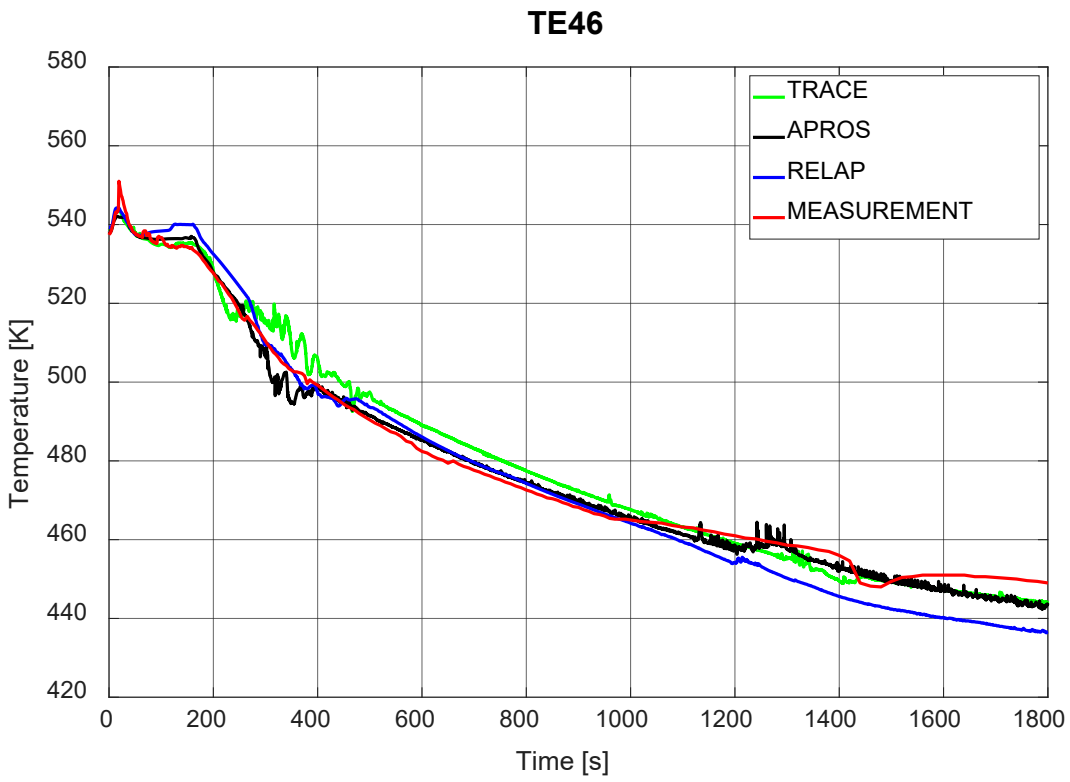

Figure 7.40 SG Cold Collector Coolant Temperature (at 7.591 m Height)

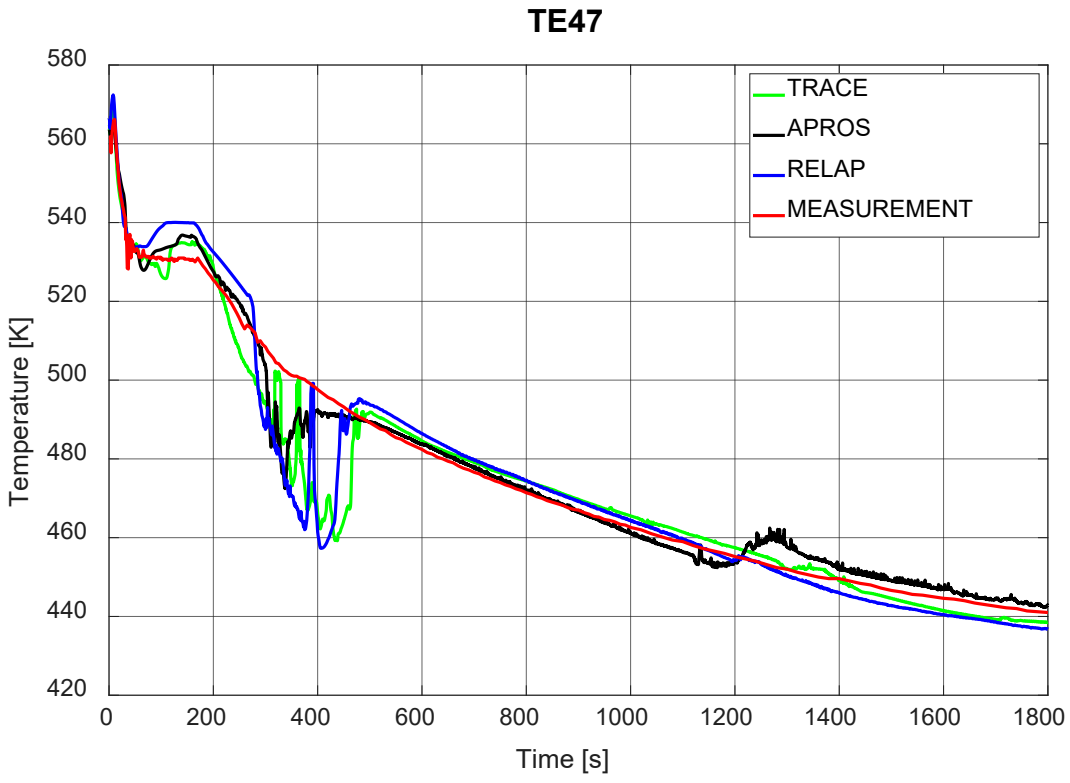

Figure 7.41 SG Hot Collector Coolant Temperature (at 6.385 m Height)

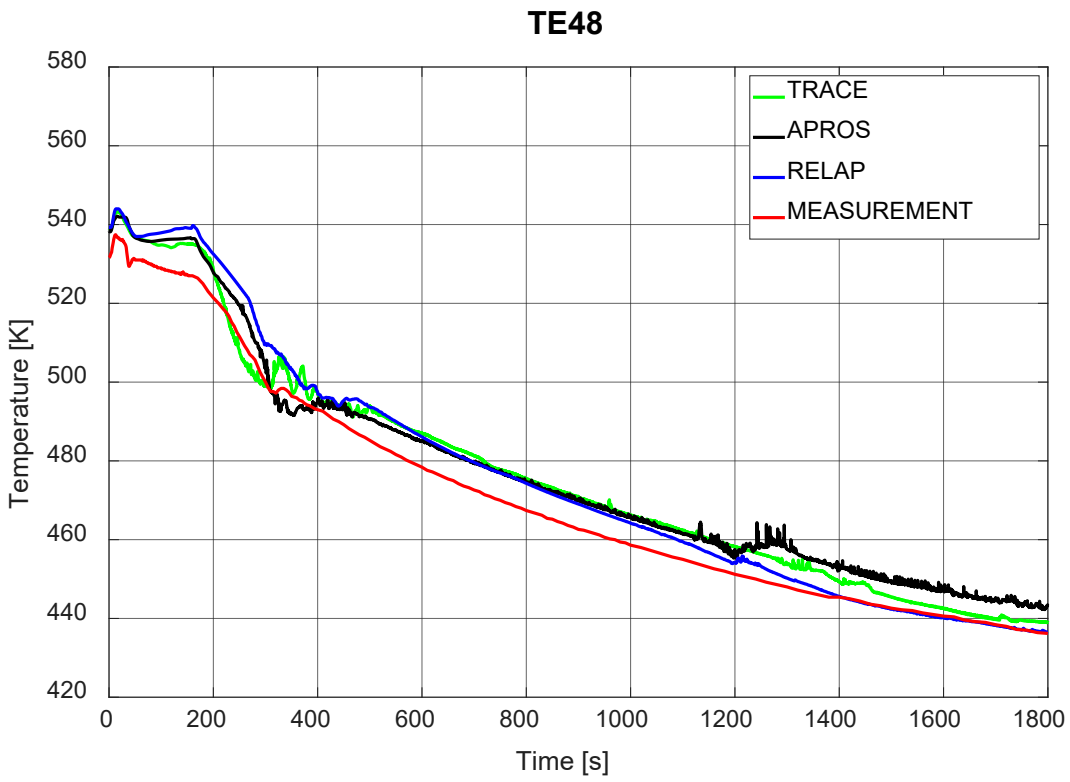

Figure 7.42 SG Cold Collector Coolant Temperature (at 6.385 m Height)

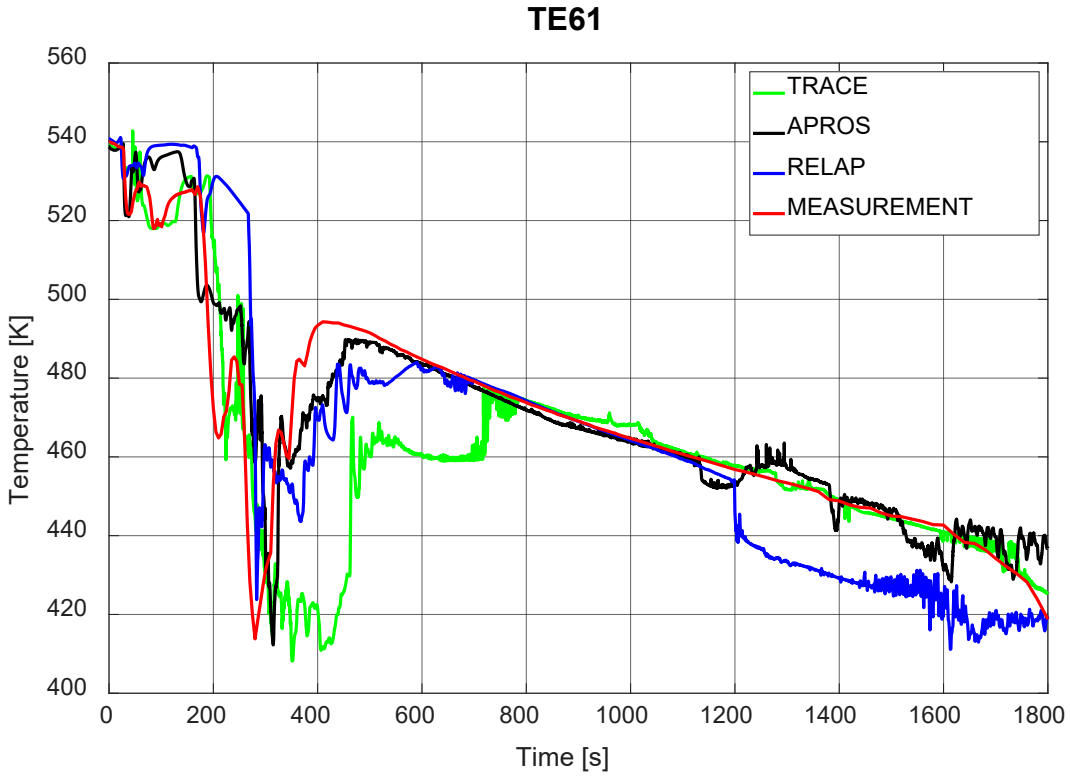

Figure 7.43 Downcomer Inlet Coolant Temperature

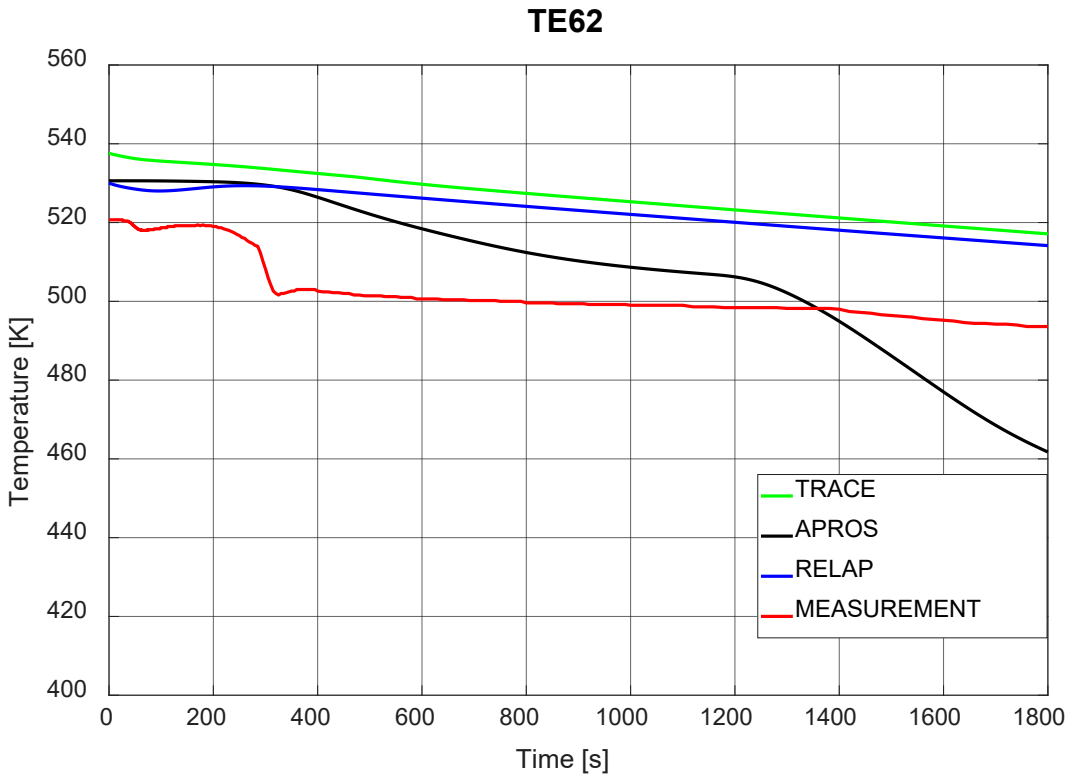

Figure 7.44 Downcomer Wall Temperature

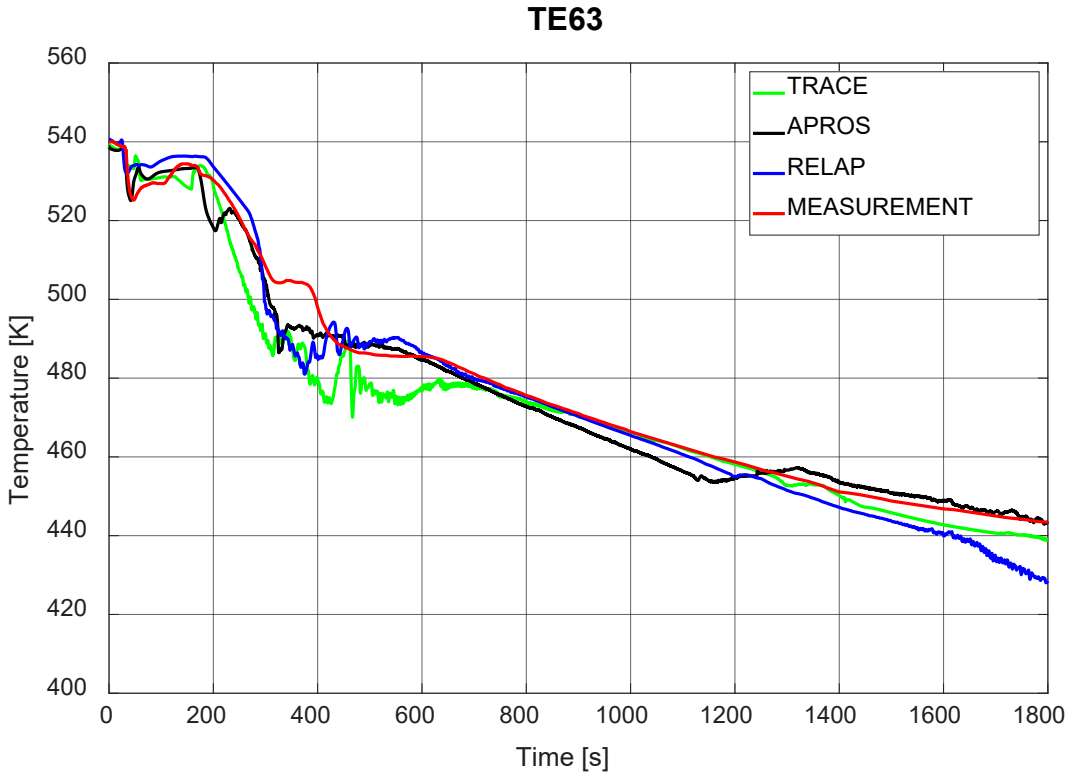

Figure 7.45 Core Inlet Coolant Temperature

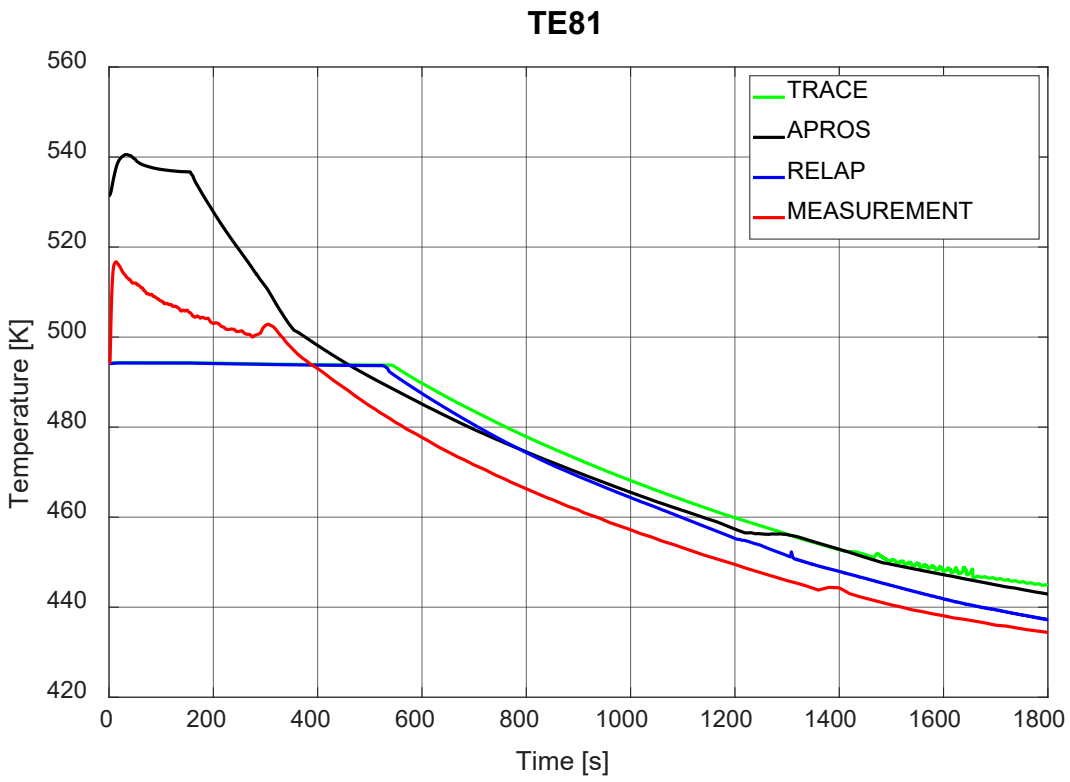

Figure 7.46 Feedwater Temperature

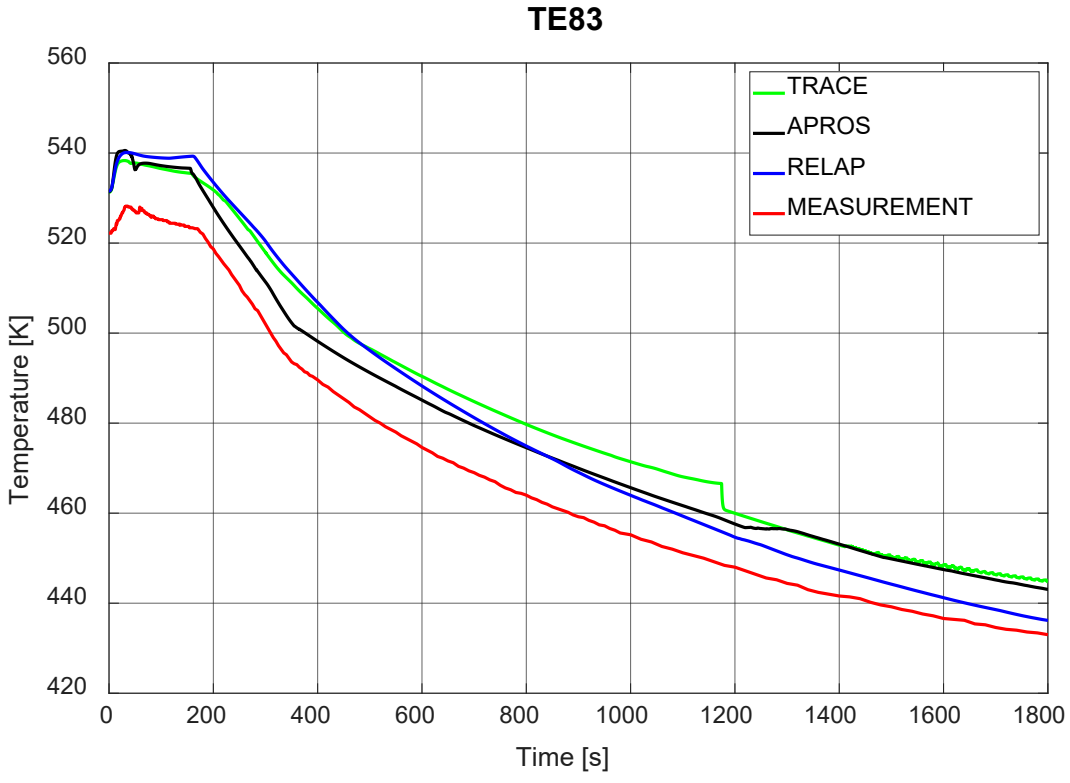

Figure 7.47 SG Secondary Coolant Temperature (Middle Part at 8.163 m Height)

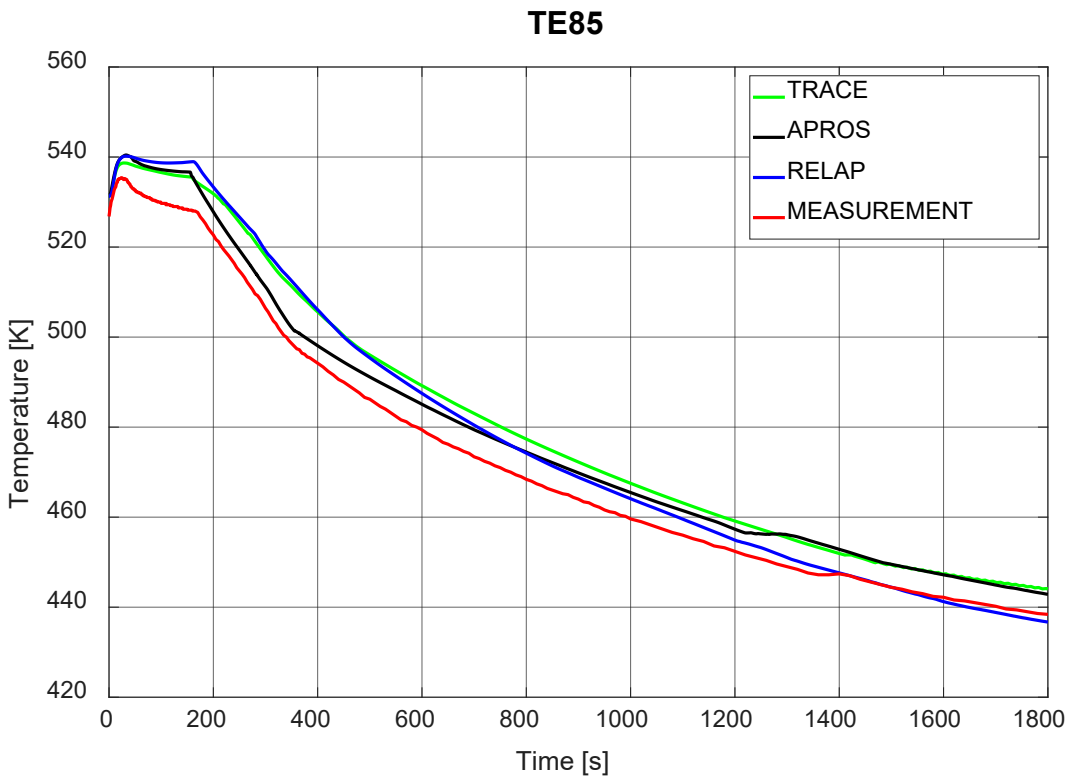

Figure 7.48 SG Secondary Coolant Temperature (Middle Part at 7.591 m Height)

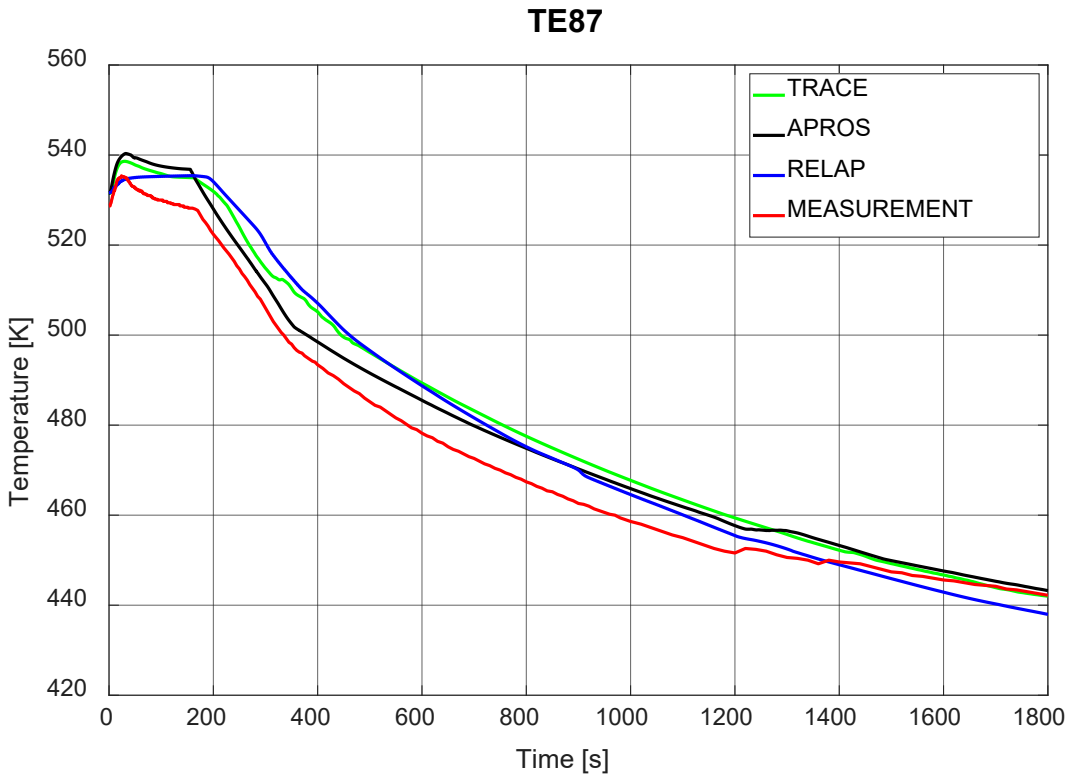

Figure 7.49 SG Secondary Coolant Temperature (Middle Part at 6.385 m Height)

8 QUANTITATIVE ASSESSMENT OF THE SIMULATION RESULTS

Throughout the years the researchers developed numerous quantification methods in order to measure the accuracy achieved by the different thermal-hydraulic models. The most widely used ones are the Fast Fourier Transform Method (FFTBM) [6], [7], [8] and the Stochastic Approximation Ratio Based Method (SARBM) [9]. Both of these methods have been previously applied for IAEA SPE-4 models, the results of which could be compared with our calculations.

8.1 The Original Quantitative Methods

In the first applications of the FFTBM two parameters, namely the Average Amplitude (AA) and the Weighted Frequency (WF), served as accuracy measures. The dimensionless AA represents relative differences, while WF emphasises the relevant frequency range. SARBMs output can be represented with one main accuracy measure, called SAR, however, the usage of the Accuracy Factor (AF) derived from SAR (AF = 1 - SAR) is much more common. In general, it can be stated, that the lower the AA and AF measures, the higher the overall simulations accuracy. High frequency errors are less important in thermal-hydraulic simulations, thus higher WF values are more favourable. In order to obtain a global accuracy measure the single parameters (primary pressure, core liquid level, fuel rod temperature, etc.) have to be multiplied by weighting factors (w_f), the values of which should be set carefully, taking into consideration three main aspects: measurement accuracy, safety relevance and relevance with respect to the primary pressure. The total accuracies AA_{tot} and AF_{tot} are calculated necessarily as the weighted sum of the chosen single parameters, for which certain quality categories (Table 8.1) had been defined by the professionals. It should be mentioned, that the categories listed below are also applicable for single parameter evaluations, however, in case of the primary pressure, the acceptability limit of K = 0.1 had been defined.

Table 8.1 Acceptability Limits for Calculation Accuracy [10]

Quality	FFTBM	SARBM
acceptable	$AA_{tot} \le K = 0.4$	$AF_{tot} \le K = 0.2$
very good	$AA_{tot} \le 0.3$	$AF_{tot} \le 0.1$
good	$0.3 < AA_{tot} \le 0.5$	$0.1 < AF_{tot} \le 0.25$
poor	$0.5< AA_{tot} \le 0.7$	$0.25< AF_{tot} \le 0.45$
very poor	$0.7 < AA_{tot}$	$0.45 < AF_{tot}$

8.2 Applications of the Original Quantitative Methods

The earliest FFTBM analysis (1995) [11] of the SPE-4 experiment was performed on the calculations of the Jožef Stefan Institute, Slovenia. It can be stated, that the models constructed in different RELAP versions proved to be qualified (AA_{tot} values ranging between 0.1 and 0.22), according to the above-mentioned acceptability limits. It has to be mentioned, however, that only one of the simulations was capable of modelling the permanent core dry-out, which surprisingly had the worst AA_{tot} value out of the total 9 runs. This result shows that those calculations which are not accurate enough regarding the timing of a certain process (e.g. core dry-out) could produce worse overall results than those without dry-out occurrence. This finding warns us to interpret the results of a quantitative assessment carefully and remind us the importance of combining it with a qualitative evaluation.

The pre- and post-test FFTBM analyses, considering the primary pressures, of all four SPEs were performed in 1996 [12] with specific RELAP and CATHARE models. The overall results were rather good, however, only the post-test analysis could predict the core dry-out in case of the SPE-4. Later articles suggest that single-parameter evaluations should be handled carefully, even though the overall importance of the given parameter and its influence on the system. These kinds of analyses are quite useful to get a first impression of the accuracy, but a multi-parameter analysis is required to make a full judgement.

Article [3] contains a detailed FFT based method analysis of the calculations performed by the participants of the IAEA SPE-4 benchmark test [3]. It includes the analysis of both the pre- and post-test simulations for altogether 12 parameters. The strict primary pressure criterion ($K < 0.1$) has been met only by less than half of the calculations. The previously described anomaly of the core dry-out timing and occurrence is also studied here as the most accurate pre- and post-test calculations (with the lowest AA_{tot} values) did not predict the dry-out at all. The overall accuracies show good general agreement, the post-test calculations being more precise.

In order to improve the FFT based method and extend its functionality, two new measures were introduced later, as discussed in [10]. The minimal Variable Accuracy (VA_{min}) gives the maximum of the variable accuracies (VA_i), while the Number of Discrepancies (ND) stands for the number of parameters, which have VA_i-s exceeding the limit (K). A study of the SPE-4 analysis [10] has proved that the new measures of FFTBM are beneficial as they were able to provide a more accurate overview and highlight the weaknesses of the models. Furthermore, the results achieved by the stochastic approximation ratio based method are in a good agreement with those obtained from the FFTBM calculation, although DP11 is highlighted as the least accurate parameter instead of TE15. The difference could be due to the underlying fundamentals of the methods used.

Our institute was given with a Microsoft Excel Add-in containing the FFTB and SARB methods which has been tested and validated with qualitative assessments of the SPE-4 benchmark test. All of the necessary information about the usage of the software and the previous evaluations of SPE-4 can be found in [13] and in the user manual, giving opportunity for comparison. Thanks to Mr. Andrej Prošek, we got access to the Excel Add-in and the data of three post-test calculations (named as UKRP, SIEP, and PZ1P in [13]) selected from the list of [10]. All three reference models predicted the dry-out occurrence qualitatively well and their overall AA values were among the bests, so it could be beneficial to do a comparison between our three new models and the referred ones. Table 8.2 and Table 8.3 show the original accuracy measures for the first 25 minutes of the transient and the new FFTBM measures (VA_{min}, ND), respectively. Although the UKRP and APROS results are slightly over the strict primary pressure limit, all 6 codes fell under the ‘very good’ quality range. As the qualitative evaluation (Figure 7.1) did not show such primary pressure discrepancy in case of APROS, we are going to investigate this further later in this chapter. Table 8.2 shows, that some of parameters have systematically higher AA values than the typical. These parameters are the reactor pressure drop (DP11), the mass flow rate of the break (FL01), the core liquid level (LE11) and the heater rod surface temperature (TE15). In case of TRACE, the reactor pressure drop and the break mass flow predictions are unacceptable; these will be further investigated later in this chapter. The single AA-s of the cladding temperatures demonstrate well the sensitivity of the method to the timing of the peak issue discussed earlier. A disagreement was found comparing the qualitative and the quantitative evaluations of the upper plenum temperature (TE22): in Figure 7.32 APROS was the only one predicting the temperature peak, however, the FFTBM method considers it as the poorest out of the three new calculations. The stem of this issue is presumably similar to that in case of the core dry-out discussed in earlier applications [11].

Table 8.2 Summary of the Original FFTBM Results for the Selected Variables (UKRP, SIEP and PZ1P were taken from [13])

		Window 0 – 1500 s					
ID	**Variables**	***AA* (UKRP)**	***AA* (SIEP)**	***AA* (PZ1P)**	***AA* (APROS)**	***AA* (RELAP5)**	***AA* (TRACE)**
1	DP11	0.777	0.803	0.704	0.569	0.471	1.380
2	FL01	0.815	0.763	1.024	0.674	0.817	1.222
3	LE11	0.786	0.473	0.483	0.460	0.446	0.584
4	LE31	0.337	0.328	0.827	0.276	0.366	0.404
5	LE46	0.296	0.286	0.714	0.274	0.341	0.447
6	LE91	0.027	1.000	0.724	0.030	0.039	0.039
7	MA01	0.108	0.080	0.067	0.098	0.103	0.107
8	PR21	0.112	0.092	0.094	0.126	0.054	0.078
9	PR81	0.093	0.002	0.075	0.064	0.097	0.077
10	TE15	0.356	0.410	0.211	0.721	0.448	0.504
11	TE22	0.154	0.175	0.104	0.117	0.098	0.095
12	TE63	0.062	0.106	0.070	0.048	0.056	0.063
	AA_{tot}	**0.224**	**0.263**	**0.260**	**0.230**	**0.197**	**0.255**

Table 8.3 Summary of the Original FFTBM Results for the IAEA-SPE-4 Calculations (UKRP, SIEP and PZ1P were taken from [13])

Calculation	AA_{tot}	VA_{min}	VA_{min} **variable**	***ND***
	Window 0 – 350 s			
UKRP	0.189	0.459	LE11	1
SIEP	0.229	0.600	LE91	1
PZ1P	0.247	0.505	LE31	3
APROS	0.145	0.241	LE11	0
RELAP5	0.156	0.231	LE11	0
TRACE	0.212	0.502	DP11	1
	Window 0 – 1120 s			
UKRP	0.179	0.446	LE11	1
SIEP	0.220	0.600	LE91	1
PZ1P	0.235	0.498	LE31	3
APROS	0.277	1.788	TE15	1
RELAP5	0.164	0.371	TE15	0
TRACE	0.251	0.779	TE15	2
	Window 0 – 1500 s			
UKRP	0.224	0.534	TE15	2
SIEP	0.263	0.615	TE15	2
PZ1P	0.260	0.497	LE31	3
APROS	0.230	1.082	TE15	1
RELAP5	0.197	0.673	TE15	1
TRACE	0.255	0.756	TE15	2

In most cases, ND shows 1-3 parameter failures out of the investigated ones, which are generally in accordance with those indicated by the original FFTBM measures (e.g. heater rod temperature, pressure drop). The core dry-out issue could also be observed, especially in case of the APROS simulation, which is considered the most accurate before the predicted cladding temperature rise, but shows serious discrepancies by the relevant measures afterwards. According to the applied quantitative methods all of our new models are qualified as RELAP5 is considered to predict the processes the most accurately, while APROS and TRACE is giving somewhat similar results to the old simulations evaluated by JSI. It has to be mentioned, however, that the measurement of accumulator water level (LE91) in SIEP and hot leg water level (LE31) in PZ1P had some known failures [13], [3], the effect of which can be seen in both tables. These errors could not be taken into consideration when performing the quantitative evaluation [13] and their contribution on the accuracy measures remained unknown.

8.3 Improvement of the Quantitative Methods and their Application

Despite being widely used, the original FFTBM was often criticized for its inconsistent behavior, especially when faced triangular-shaped graphs. Such characteristics could be seen in case of the permanent dry-out of the core followed by a reflooding. In order to fix these problems, development suggestions have been given in [14] and [15], the first of which is the use of a much finer subdivision of the transient period. During the time-dependent evaluations performed as a result, one of the most important observation was the so called ‘edge effect’. The calculation of FFT would require infinite signals, while in case of real (finite) data sets one has to extend the signal periodically. Such process can easily magnify the discrepancies occurring at the time window edges by making artefacts in the frequency domain. This could give an explanation on the strange behavior experienced beforehand and is a key finding regarding the accuracy of the quantitative method. As suggested in articles [14] and [15], the benefits of the FFTBM could be preserved while the artefacts are being eliminated, by using the so called signal mirroring before applying the Fast Fourier Transformation. In order to demonstrate the abilities of the ‘improved FFTBM by signal mirroring’, evaluation of the LOFT L2-5 test series had been carried out [16], of which the major findings are summarized below:

- By the nature of the original method, edge effect was positively and artificially influencing the accuracy measures especially in those cases, where the characteristic of the parameter was monotonically increasing or decreasing in time.
- The low primary pressure limit was originally set by analyzing small break LOCA transients, which have great pressure difference. However, in those cases characterized by a moderate primary pressure decrease (such as the SPE-3), the requirement systematically wasn’t met by the calculations. Moreover, according to [17] the criterion might be too strict for the improved FFT based method, as LOFT L2-5 test results were rather inconsistent when comparing FFTBM and ACAP measures.
- The contribution of the edge effect to the accuracy measures is less significant in those time windows characterized by a rather plain change compared to the sharp drops.
- In case of the original FFT based method an unusual behavior has been observed when dealing with signals consisting of a triangular-shaped period (e.g. a core dry-out followed by quenching). Despite giving consistent results for the timeframe of the whole transient, the time-dependent accuracy evolution was often misleading in such cases. It was found, that these errors were partly due to the so-called artificial edges developed through the dry-out process.

Based on the tests it can be stated, that the improvements suggested by the authors of [14] and [15] successfully eliminated the source of the formerly experienced inconsistent behavior and the applicability of the improved FFTBM has been proved. It has to be mentioned, however, that the old FFT based model can also be used in some cases, but the results obtained should be interpreted carefully by the user. Fortunately, the Excel add-in previously used gives a possibility of calculating with the improved FFTBM, so it would be practical to repeat the evaluation and perform a similar comparison as in the previous section. However, no previous article was found regarding the quantitative evaluation of the SPE-4 experiment with the improved method. Therefore, Table 8.4 and Table 8.5 summarize only the results of our own calculations without comparing them to other applications.

A general trend of average amplitude (AA_m, AF_m and the total values) increments could be observed by comparing Table 8.4 and Table 8.2. The minimal (1.18, FL01, TRACE) and maximal (2.38, PR81, TRACE) ratios are quite distant, which is consistent with the expectations based on the above referred articles. The parameters with the most serious discrepancies remained the same (DP11, FL01, LE11 and TE15), but heater rod temperature is still the only one failing in case of APROS and RELAP as shown by the ND values in Table 8.5. Besides the cladding temperature, the reactor pressure drop and water level predicted by TRACE could not fulfill the requirements either. It is worth to mention, however, that TRACE was the only model predicting the sudden drop of LE11 (Figure 7.6) at around 150 s, but with a slight delay resulting in a worse accuracy measure. Based on the $AA_{m,tot}$ values all of our calculations are within the acceptability limit and RELAP5 remained the most accurate. However, the primary pressure (PR21) criterion could not be fulfilled by either of the codes, therefore, we would like to add some remarks regarding this limit. Since the accuracies of the calculations in general are quite good and the pressure (PR21, PR81) accuracy measures are also satisfactory, the criterion of K < 0.1 for PR21 may be rather strict than justified. Based on the current study and the statements of [16], the revision of this standard could be worth to reconsider if used for the improved version of FFTBM. We would like to suggest the usage of a value around 0.2 as in our calculations the average amplitudes of PR21 increased by about a factor of 2 when using the improved FFT based method.

Table 8.4 Summary of the Improved FFTBM and SARBM Results (for the Selected Variables)

		Window 0 – 1800 s					
		APROS		**RELAP5**		**TRACE**	
ID	**Variables**	***AF_m***	***AA_m***	***AF_m***	***AA_m***	***AF_m***	***AA_m***
1	DP11	0.401	0.867	0.335	0.676	0.481	2.082
2	FL01	0.372	0.846	0.396	1.026	0.517	1.439
3	LE11	0.239	0.655	0.266	0.623	0.304	0.840
4	LE31	0.035	0.359	0.061	0.484	0.068	0.521
5	LE46	0.077	0.358	0.119	0.474	0.191	0.630
6	LE91	0.006	0.044	0.010	0.057	0.010	0.058
7	MA01	0.063	0.200	0.090	0.197	0.086	0.209
8	PR21	0.077	0.279	0.074	0.121	0.069	0.168
9	PR81	0.059	0.152	0.112	0.224	0.105	0.183
10	TE15	0.255	0.941	0.140	0.589	0.136	0.659
11	TE22	0.024	0.170	0.028	0.152	0.025	0.141
12	TE63	0.009	0.076	0.013	0.097	0.014	0.099
	total	**0.094**	**0.335**	**0.090**	**0.289**	**0.101**	**0.369**

Table 8.5 Summary of the Improved FFTBM Results for the IAEA-SPE-4 Calculations

Calculation	$AA_{m,tot}$	VA_{min}	VA_{min} variable	ND
	Window 0 – 350 s			
APROS	0.202	0.362	PR21	0
RELAP5	0.195	0.331	LE11	0
TRACE	0.270	0.747	DP11	2
	Window 0 – 1100 s			
APROS	0.294	1.176	TE15	1
RELAP5	0.213	0.364	LE11	0
TRACE	0.320	0.736	DP11	3
	Window 0 – 1500 s			
APROS	0.337	1.450	TE15	1
RELAP5	0.288	0.910	TE15	1
TRACE	0.376	1.055	TE15	3
	Window 0 – 1800 s			
APROS	0.335	1.412	TE15	1
RELAP5	0.289	0.884	TE15	1
TRACE	0.369	0.989	TE15	3

In our calculations with the improved FFTBM, the transient has been divided to 36 time intervals (0-50 s, 0-100 s, 0-150 s, etc.) which enables a detailed, time dependent investigation of the most important measures. Figure 8.1 to Figure 8.4 show the evolution of the AA (PR21, TE15), AA_{tot} and AF_{tot} values throughout the transient, respectively. Figure 8.1 indicates that the major discrepancy concerning the primary pressure is gained in the very first stage of the transient, between 0 and 50 seconds. This time interval is characterized by the major blowdown, resulting in a sudden pressure drop. Although APROS seemed to predict this phase relatively well based on the qualitative evaluation, the quantitative analysis pointed out the opposite with the AA value of 0.254. Even though APROS simulation fails the primary pressure criterion because of this first 50 s long period, we would still consider it acceptable, as the pressure at the end of the great blowdown and the following trend throughout the transient are both impressive (see in Figure 7.1). It is also confirmed by the observation that APROS has the smallest further AA increment among the three models.

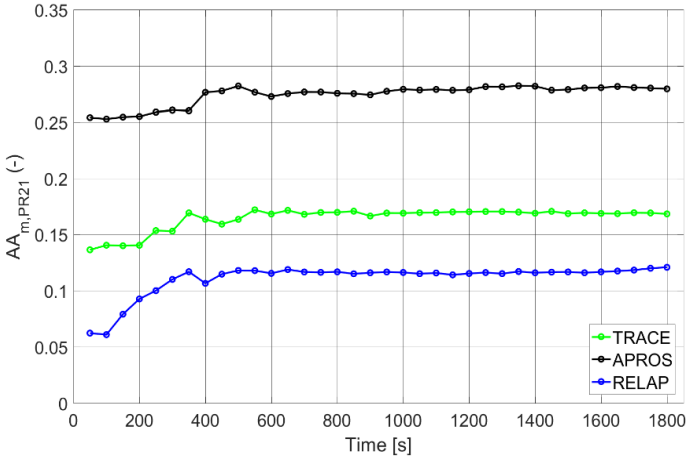

Figure 8.1 AA_m Accuracy Measure of PR21

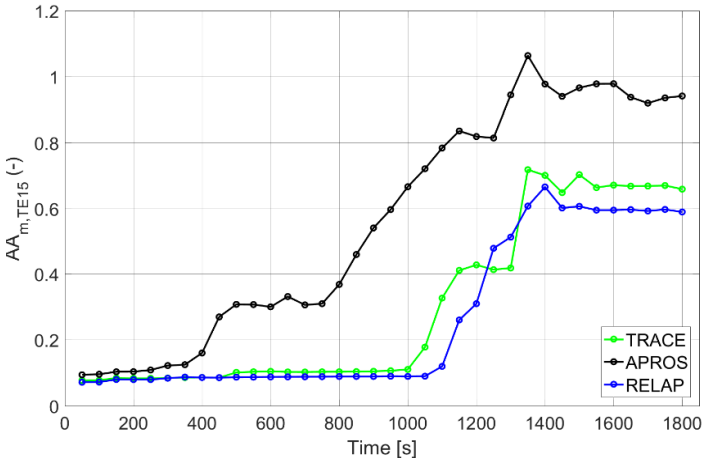

Figure 8.2 AA_m Accuracy Measure of TE15

Fuel rod temperatures (Figure 8.2) are calculated quite well ($AA_m < 0.15$) in the earlier stage (0-400 s) by all three codes. The timing of the core dry-out and the following rewetting is however poorly simulated (Figure 7.31), which resulted in large discrepancies. The worst accuracy measure achieved by APROS, is partially due to the small amplitude series of early dry-outs and the incorrect timing of the great dry-out. The evolution of $AA_{m,TE15}$ values in case of RELAP5 and TRACE are somewhat similar.

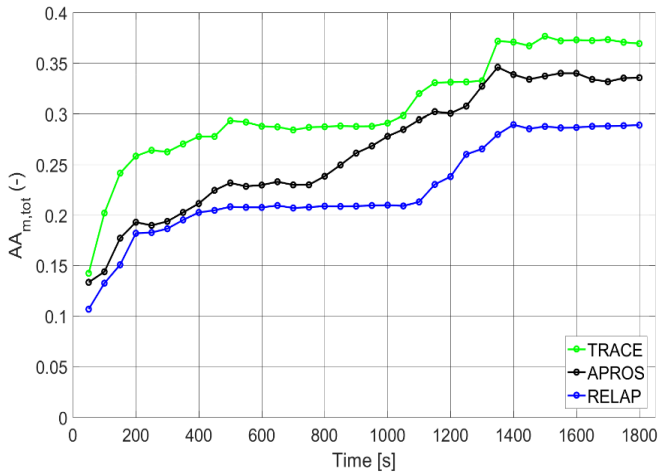

Figure 8.3 Total Accuracy Evolution ($AA_{m,\,tot}$)

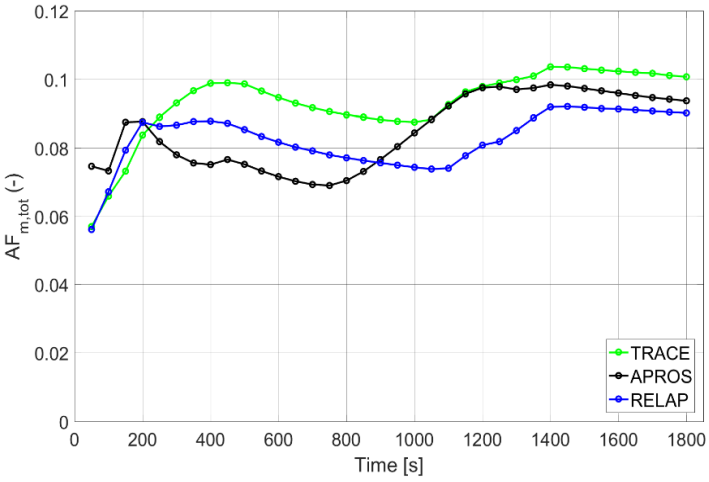

Figure 8.4 Total Accuracy Evolution ($AF_{m,tot}$)

Both the evolution of FFTBMs $AA_{m,tot}$ (Figure 8.3) and SARBMs $AF_{m,tot}$ (Figure 8.4) indicate, that the aforementioned dry-out and the complex processes, taking place until the hot and cold leg loop seal clearings, give the major contribution to the total inaccuracy. During the rest of the transient, a stagnation of $AA_{m,tot}$ and a decrease of $AF_{m,tot}$ is observed. Both measures are showing consistent behavior to the previous findings and mostly to each other as well.

However, APROS is assessed a bit differently, especially in the first period of great pressure drop. It suggests that the global measures are affected by the accuracies of the relevant parameters differently. Nevertheless, it can be stated, that both measures are capable of providing an overview of the overall simulation accuracies.

As already noted before (and also indicated by Table 8.4), TRACE produced unacceptable results in terms of the reactor pressure drop (DP11) and the break mass flow (FL01). These inaccuracies could partly stem from the heavy fluctuations between 43 and 63 s (seen in Figure 7.20 and Figure 7.24, respectively) presumably caused by the steam appeared at valve PV11. Unfortunately, no attempt was successful in order to get rid of this issue during the model development phase. Finally, we would like to approximate the effect of these fluctuations on the relevant accuracy measures. In order to do so, the data of the above-mentioned time interval has been substituted with its linear interpolation in case of DP11 and FL01, while other parameters remained unchanged. This newly constructed, hypothetical data set has also undergone the quantitative analysis of which the improved accuracy measures are compared to those of the real date set in Table 8.6 and Table 8.7.

Table 8.6 Effect of the DP11 and FL01 Fluctuations on the Improved FFTBM Results (*Fluctuations Eliminated by Interpolation)

		Window 0 – 1800 s					
		TRACE		**TRACE***		**Relative differences**	
ID	**Variables**	AF_m	AA_m	AF_m	AA_m	ΔAF_m [%]	ΔAA_m [%]
1	DP11	0.481	2.082	0.451	0.918	6.24	55.91
2	FL01	0.517	1.439	0.497	1.257	3.87	12.65
	total	**0.101**	**0.369**	**0.099**	**0.332**	**1.98**	**10.03**

Table 8.7 Effect of the DP11 and FL01 Fluctuations on the Improved FFTBM Results 2 (*Fluctuations Eliminated by Interpolation)

Calculation	$AA_{m,tot}$	VA_{min}	VA_{min} **variable**	**ND**
	Window 0 – 350 s			
TRACE	0.270	0.747	DP11	2
TRACE*	0.227	0.437	LE11	1
	Window 0 – 1100 s			
TRACE	0.320	0.736	DP11	3
TRACE*	0.280	0.504	LE11	2
	Window 0 – 1500 s			
TRACE	0.376	1.055	TE15	3
TRACE*	0.338	1.055	TE15	2
	Window 0 – 1800 s			
TRACE	0.369	0.989	TE15	3
TRACE*	0.332	0.989	TE15	2

Based on the results it can be stated, that reducing the fluctuations influenced the accuracy measures positively, however, FFTBM seems to be much more sensitive compared to SARBM (Table 8.6). Furthermore, fluctuations of DP11 have much higher contribution in both methods. Although each of the reactor pressure drop and the break mass flow rate are still considered very poor according to Table 8.1, this time they both fulfill the VA_{min} criterion, hence the ND

values are reduced in each time window (Table 8.7). As seen in Table 8.6, the fluctuations also had a significant contribution to the $AA_{m,tot}$ value, which is now close to the global accuracy of APROS listed in Table 8.4.

9 CONCLUSION

We successfully developed an APROS, RELAP5 and TRACE model suitable for the simulation of the IAEA SPE-4 code validation benchmark experiment, which are described in detail in chapter 4, 5 and 6. Then we performed simulations of the SPE-4 experiment with our models, the results of which were compared to the measurement data sets. All of our experiences based on the qualitative evaluation are explained in detail in chapter 7. It is important to mention that several test calculations were required during the development of the models, partly for debugging and partly for finding the most suitable code settings. The fidelity of the model results appears to be especially sensitive for the value of the discharge coefficients applied on the break and steam dump valves.

The qualitative analysis has been supplemented with a quantitative assessment in chapter 8, which gave us a deeper insight into the discrepancies experienced between the simulations and the measurements performed on the PMK-2 facility. It was found, that the most challenging parameters to simulate were similar across the codes and consistent to the findings in chapter 7. The least accurate parameters were (according to FFTB and SARB methods) the fuel rod temperature, the break mass flow rate and the reactor water level along with its differential pressure.

All in all, we can state that our new models are suitable for the given task and the calculation results show a good agreement with the measurements, RELAP5 being the most accurate. However, in order to reduce the deviations, we would recommend further investigation of the nodalization in the downcomer top and upper plenum regions especially in case of the APROS and TRACE models (e.g. 3D reactor vessel of TRACE). In addition to that, the effect of an assumed, unintended early phase secondary circuit leakage could also be beneficial to analyze.

Moreover, we would like to add a remark regarding the primary pressure limit (K = 0.1) currently used in the improved FFTBM calculations. Based on our results, the primary pressure criterion that has been primarily determined for the original FFT based method may be too strict, as it does not take into consideration the contribution of eliminating the so called edge effect. As discussed in chapter 8, our calculations would suggest the usage of a higher acceptability limit somewhere around K = 0.2 in case of the improved FFTBM.

10 REFERENCES

[1] L. Szabados, Gy. Ézsöl L. Perneczky, I Tóth: Results of the Experiments Performed in the PMK-2 Facility for VVER safety studies, Budapest, 2007.

[2] A. Csige, A. Szabó, A. Aszódi: Az IAEA SPE-2 benchmark modellezése az APROS kóddal (Modeling of the IAEA SPE-2 benchmark with the APROS code, in Hungarian), BME-NTI-630/2013, Budapest, 2013

[3] IAEA-TECDOC-848: Simulation of a loss of coolant accident without high pressure injection but with secondary side bleed and feed, Vienna, 1995.

[4] J. Bánáti, 1995. Assessment of RELAP5/MOD3.1 code for the IAEA SPE-4 experiment, ASME/JSME Fluids Engineering and Laser Anemometry Conference and Exhibition, August 13-18, 1995, Hilton Head Island, South Carolina. Vol. 223.

[5] IAEA-TECDOC-477: Simulation of a loss of coolant accident with hydroaccumulator injection, Vienna, 1988.

[6] Ambrosini, W., Bovalini, R., D'Auria, F., 1990. Evaluation of accuracy of thermalhydraulic code calculations. Energia Nucleare, vol. 7, pp. 5-16.

[7] Leonardi, M., D'Auria, F., Pochard, R., 1994. Methodology for the evaluation of thermalhydraulic codes accuracy. Proceedings of "New trends in Nuclear System Thermohydraulics" Conference, Pisa May 30-June 2, 1994.

[8] Bovalini, R., D'Auria, F., Leonardi, M., 1992. Qualification of the Fast Fourier Transform based methodology for the quantification of thermalhydraulic code accuracy. DCMN Report, NT 194 (92), Pisa, July 1992.

[9] Islamov, R., Ustinov, V., 2000. Uncertainty analysis and stochastic approximation. Proc. Int. Mtg. Best-Estimate Methods in Nuclear Installation Safety Analysis (BE-2000), Washington, DC, November, 2000.

[10] Prošek, A., 2002. Lessons learned from accuracy assessment of IAEA-SPE-4 experiment predictions. Nuclear Energy for New Europe 2002 (International Conference), Kranjska Gora, Slovenia, September 9-12, 2002.

[11] Frogheri, M., D'Auria, F., Leonardi, M., Prošek, A., Mavko, B., Parzer, I., 1995. Application of the FFT method to an IAEA-SPE-4 experiment simulation. Jahrestagung Kerntechnik '95, Annual Meeting on Nuclear Technology, ISSN 0720-9207.

[12] D'Auria, F., Eramo, A., Frogheri, M., Galassi, G.M., 1996. Accuracy quantification in SPE-1 to SPE-4 organised by IAEA. International Conference on Nuclear Engineering, Volume 3, ASME 1996.

[13] Prošek, A., Mavko, B., 2003. A tool for quantitative assessment of code calculations with an improved fast Fourier transform based method. Elektrotehniski Vestnik/ Electrotechnical Review. 70. 291-296.

[14] Prošek, A., Mavko, B., 2009. Quantitative Code Assessment with Fast Fourier Transform Based Method Improved by Signal Mirroring. International agreement report, NUREG/IA-0220, Washington: U. S. NRC.

[15] Prošek, A., Leskovar, M., 2011. Application of Fast Fourier Transform for Accuracy Evaluation of Thermal-Hydraulic Code Calculations. Fourier Transforms – Approach to Scientific Principles, ISBN 978-953-307-231-9, Pages 447 – 468

[16] OECD/NEA, 2006. BEMUSE Phase 2 Report: Re-Analysis of the ISP-13 Exercise, Post Test Analysis of the LOFT L2-5 Test Calculation. OECD/NEA Report, Committee on the Safety of Nuclear Installations (CSNI), NEA/CSNI/R(2006)2.

[17] Kunz, R.F., Kasamala, G.F., Mahaffy, J.H., Murray, C.J., 2002. On the automated assessment of nuclear reactor system code accuracy. Nuclear Engineering and Design, 211, 2-3 (February 2002), 245-272, ISSN 0029-5493.

[18] Mavko, B., Prošek, A., D'Auria, F., 1997. Determination of code accuracy in predicting small-break LOCA experiment. Nucl. Technol. 120, 1-19.

[19] Varju, T., Aranyosy, Á., Orosz, R., Holl, V., Hajas, T., Aszódi, A., 2021. Analysis of the IAEA SPE-4 small-break LOCA experiment with RELAP5, TRACE and APROS system codes, Nuclear Engineering and Design, Volume 377, 111109, June 2021. (https://doi.org/10.1016/j.nucengdes.2021.111109)

APPENDIX A

Subsystems of the PMK-2 facility are shown on the following figures [1], [2], [5].

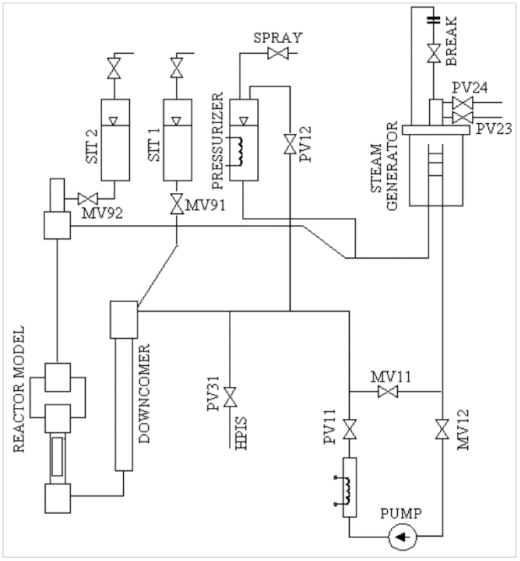

Figure A.1 Flow Diagram of the PMK-2 Facility [1], [2]

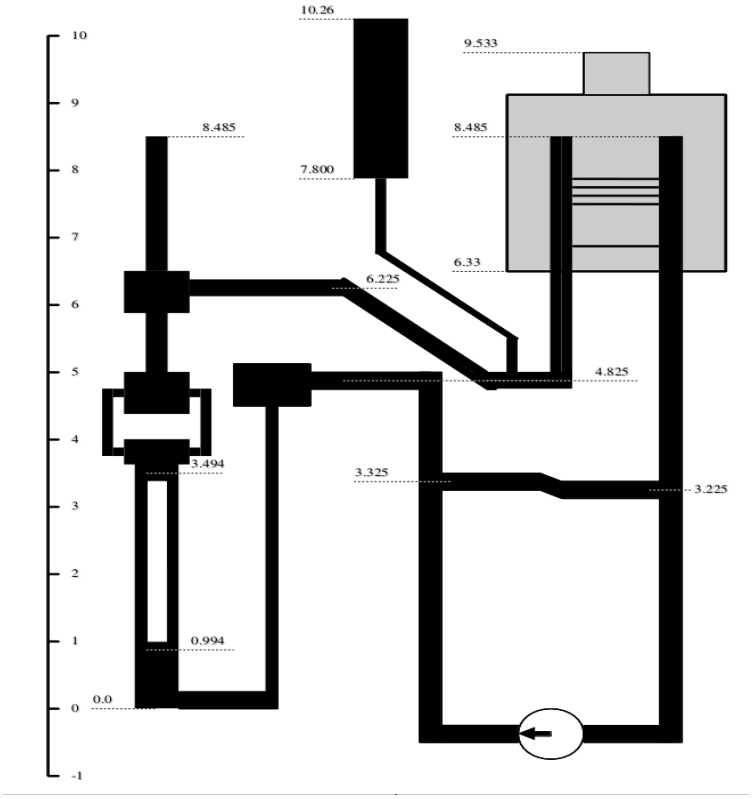

Figure A.2 Elevation Diagram [1], [2]

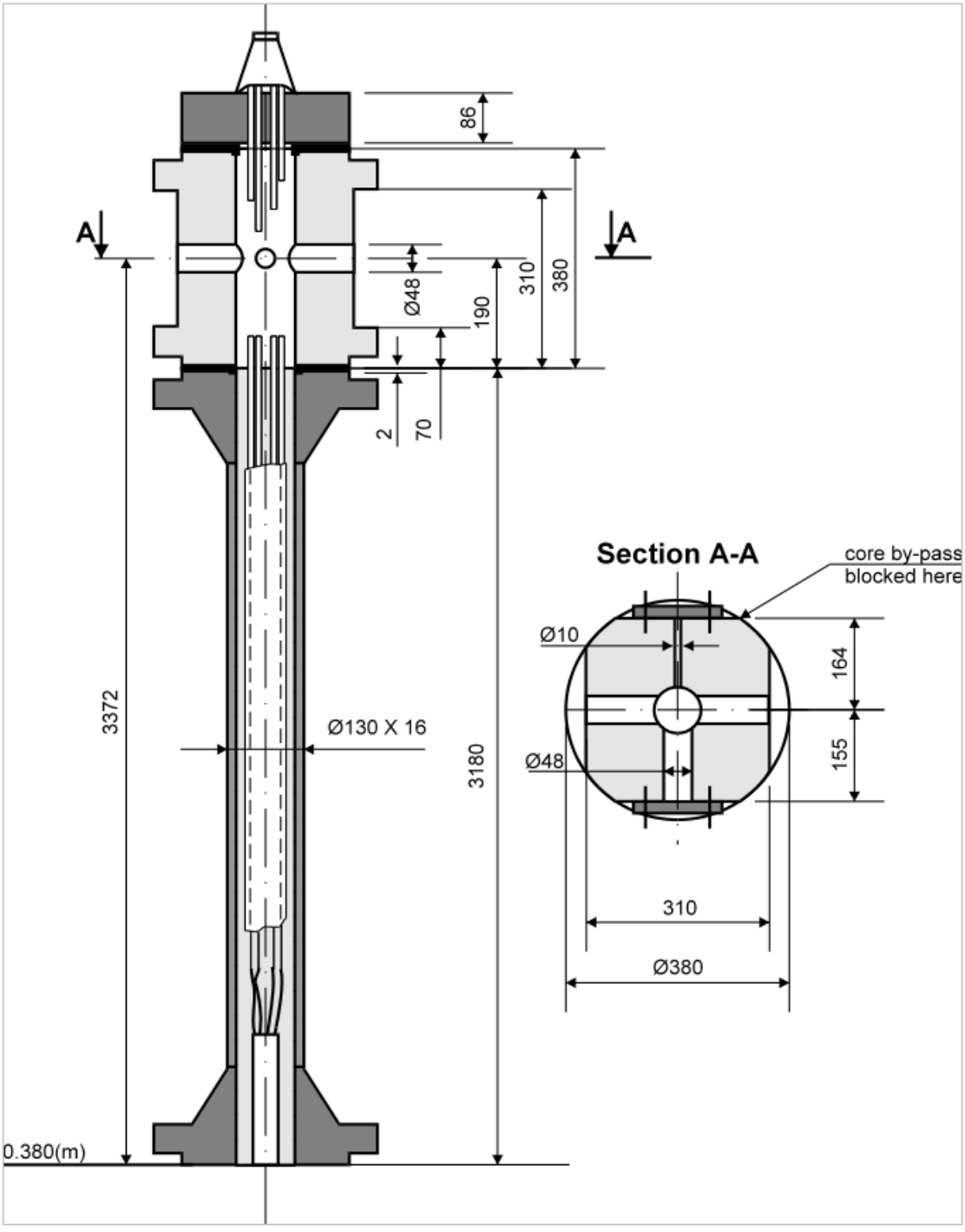

Figure A.3 Core Model [1], [2]

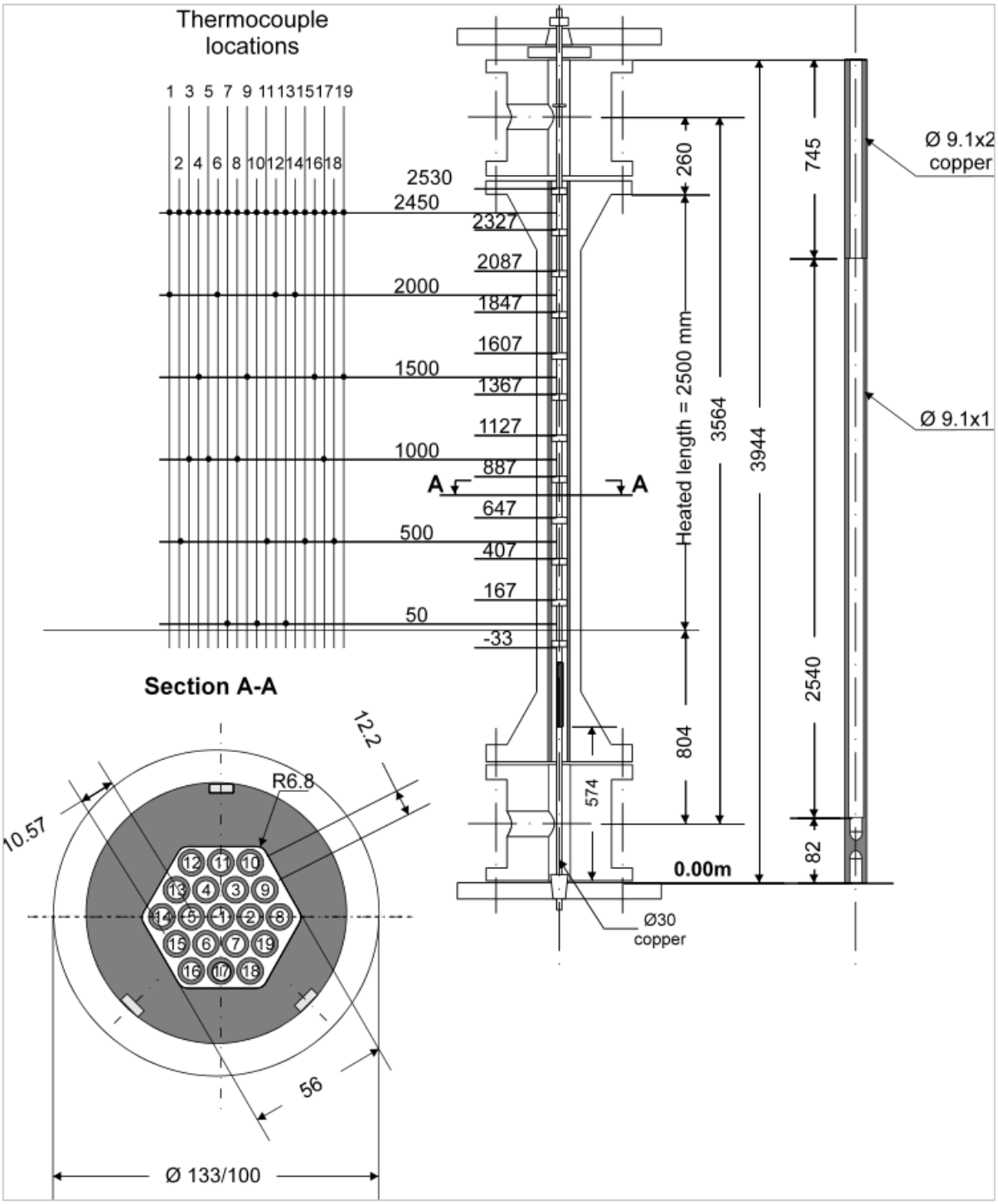

Figure A.4 19-Rod Heater Bundle [1], [2]

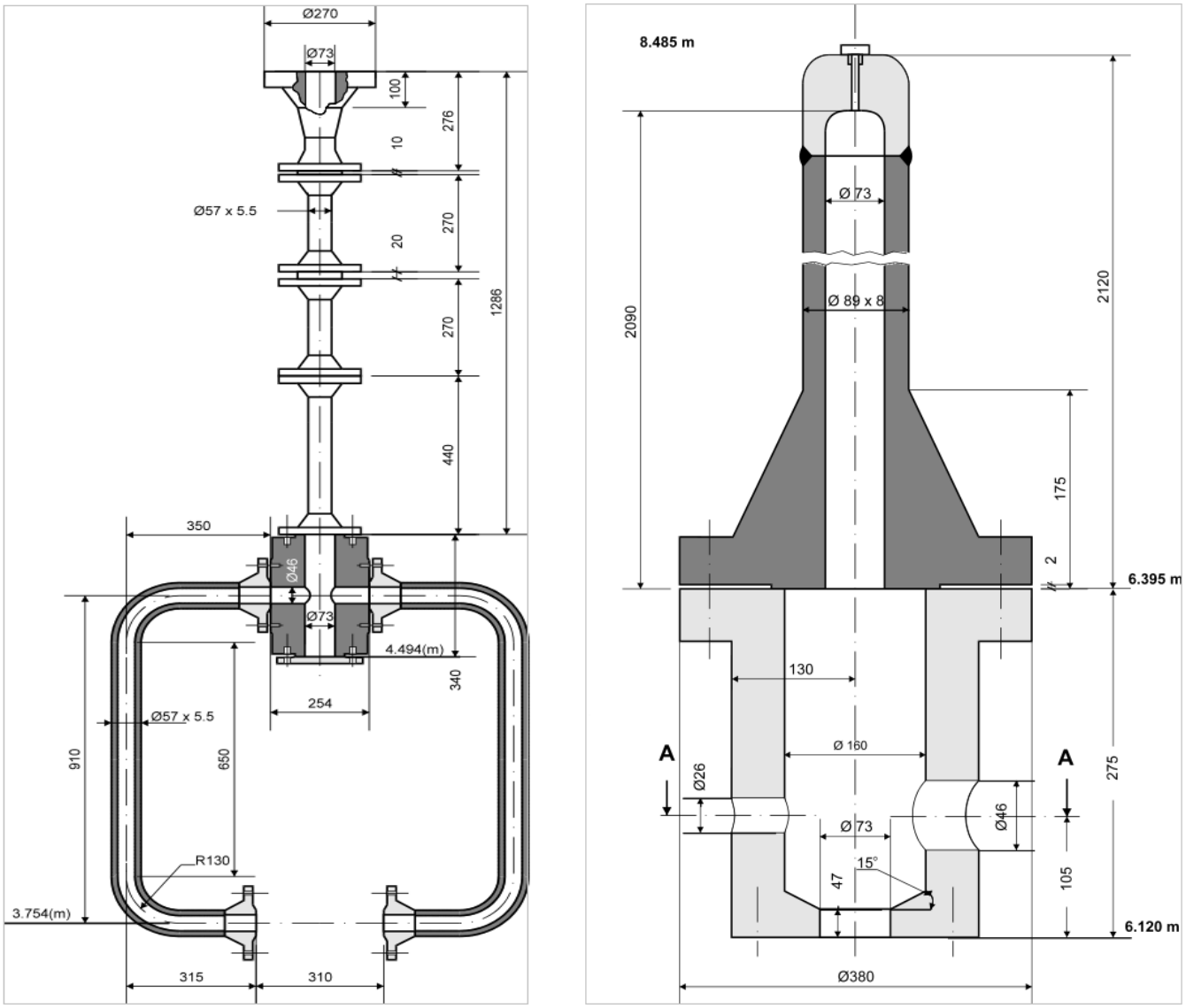

Figure A.5 Upper Plenum and Upper Head [1], [2]

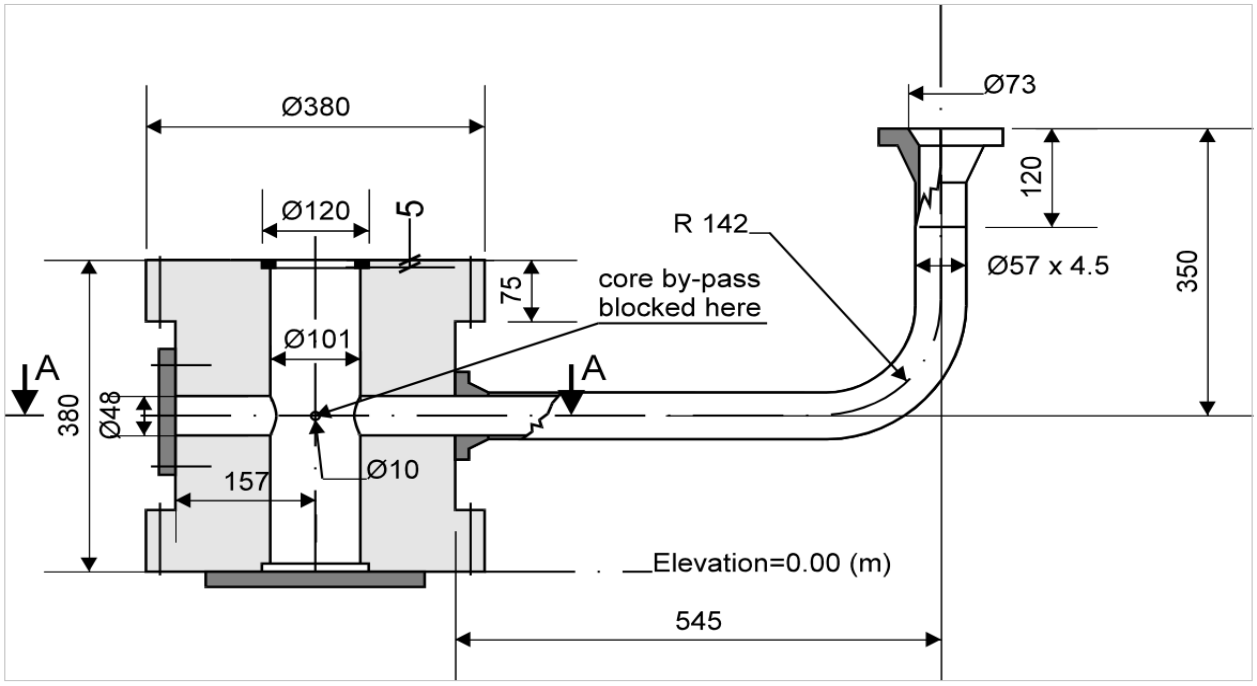

Figure A.6 Lower Plenum [1], [2]

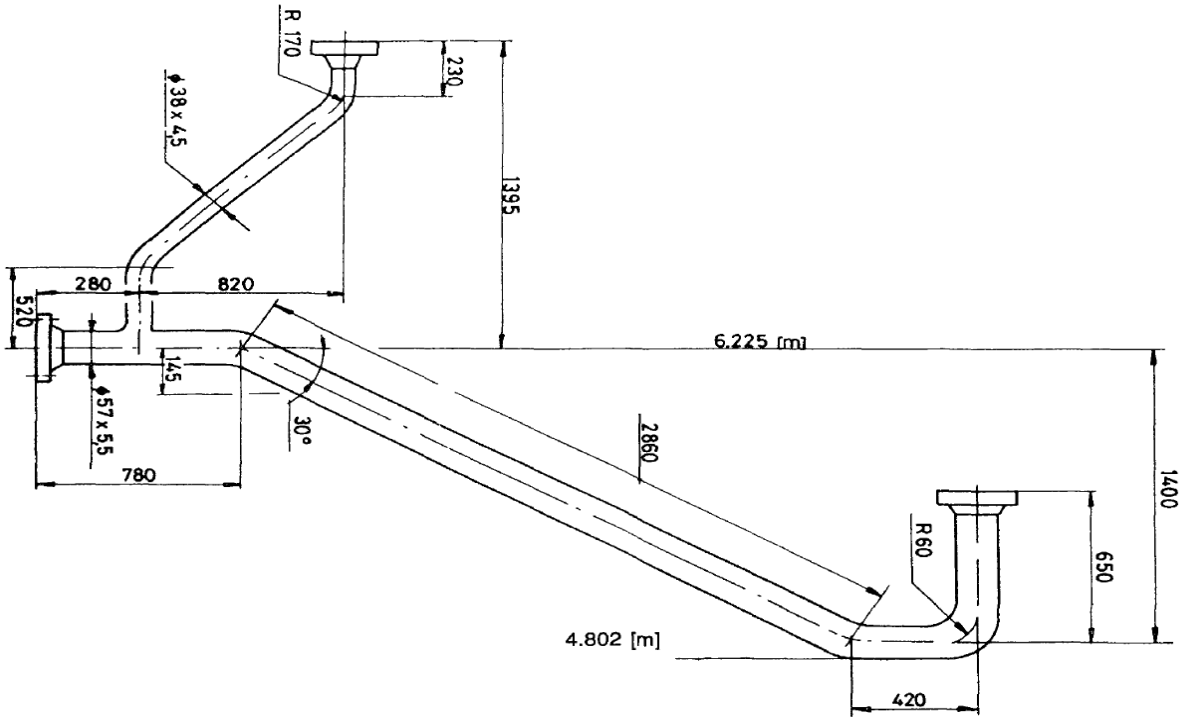

Figure A.7 Hot Leg with Pressurizer Surge Line [5]

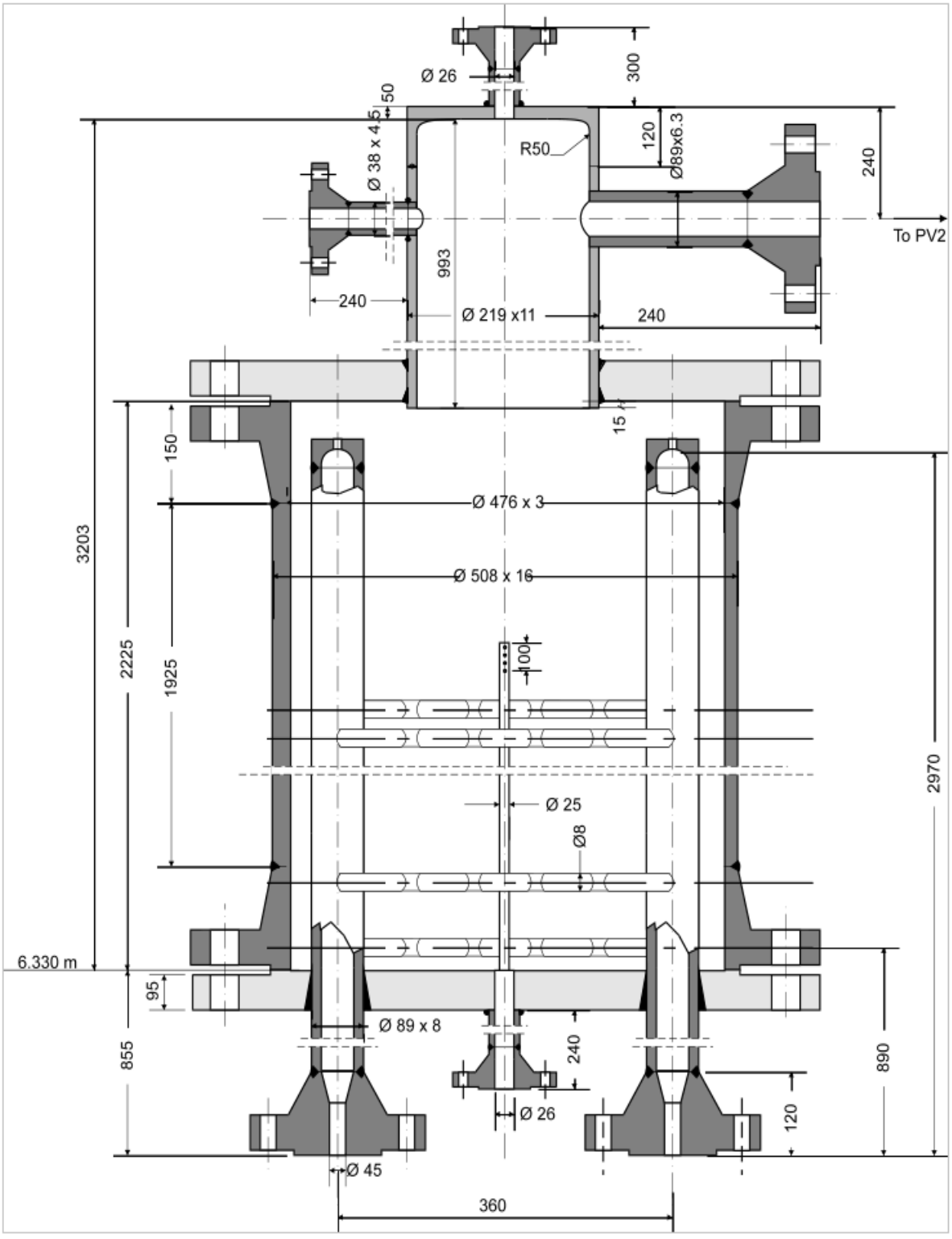

Figure A.8 Steam Generator [1], [2]

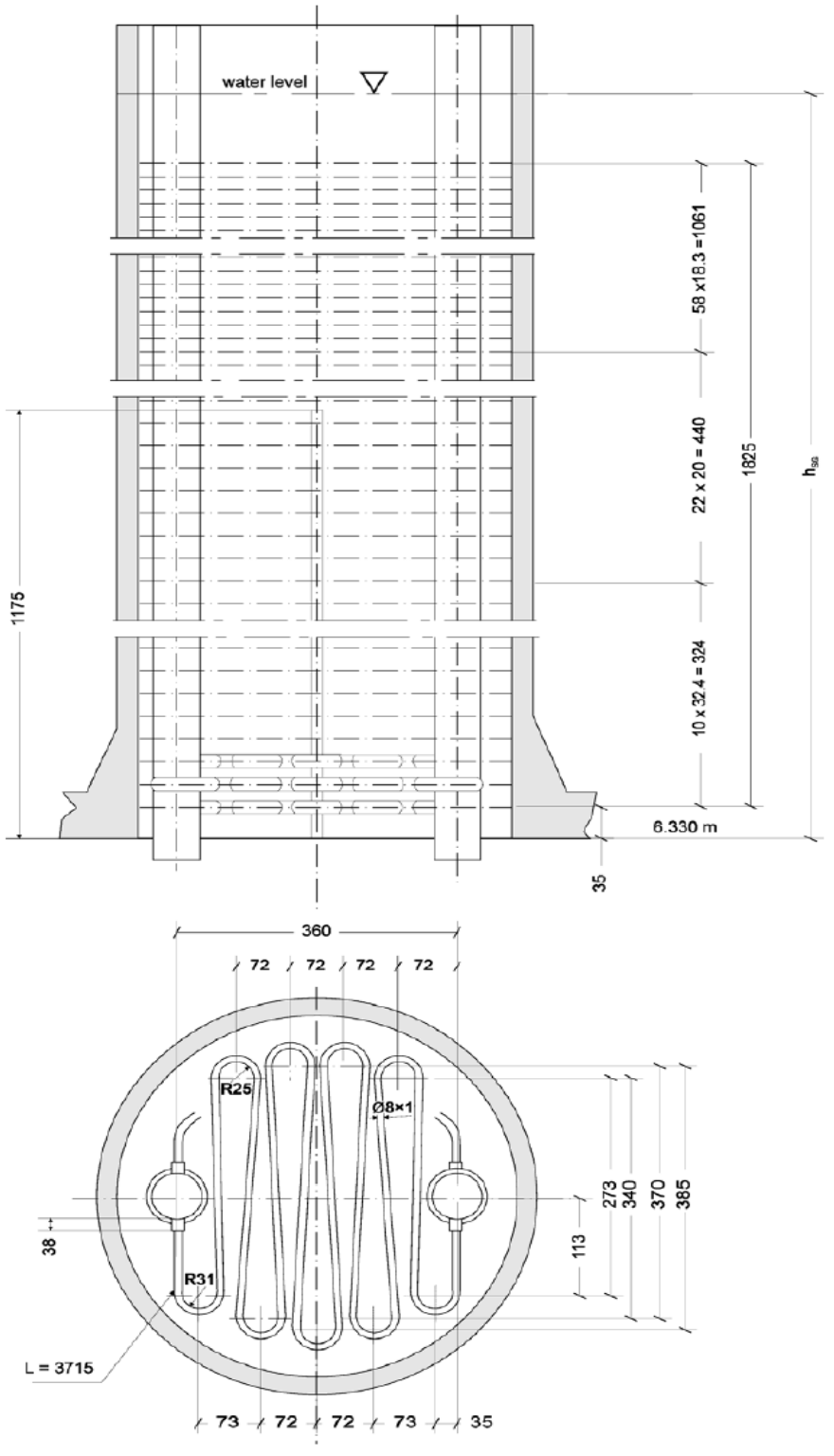

Figure A.9 Steam Generator Pipeworks [1]

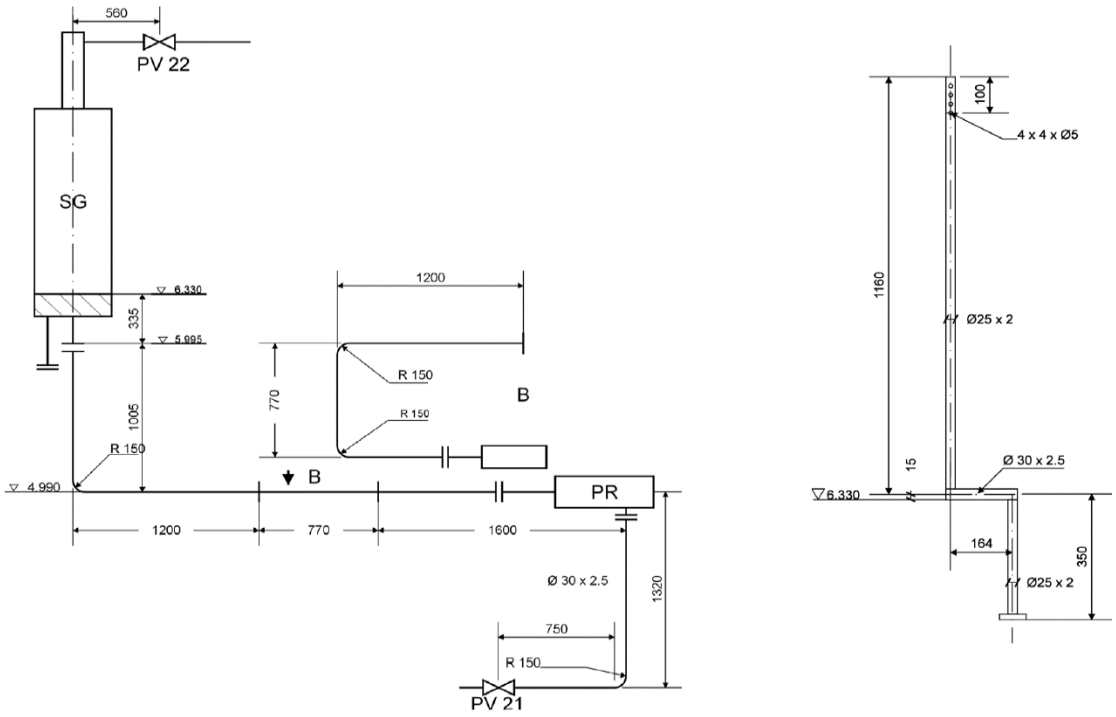

Figure A.10 Feedwater and Emergency Feedwater Lines [1]

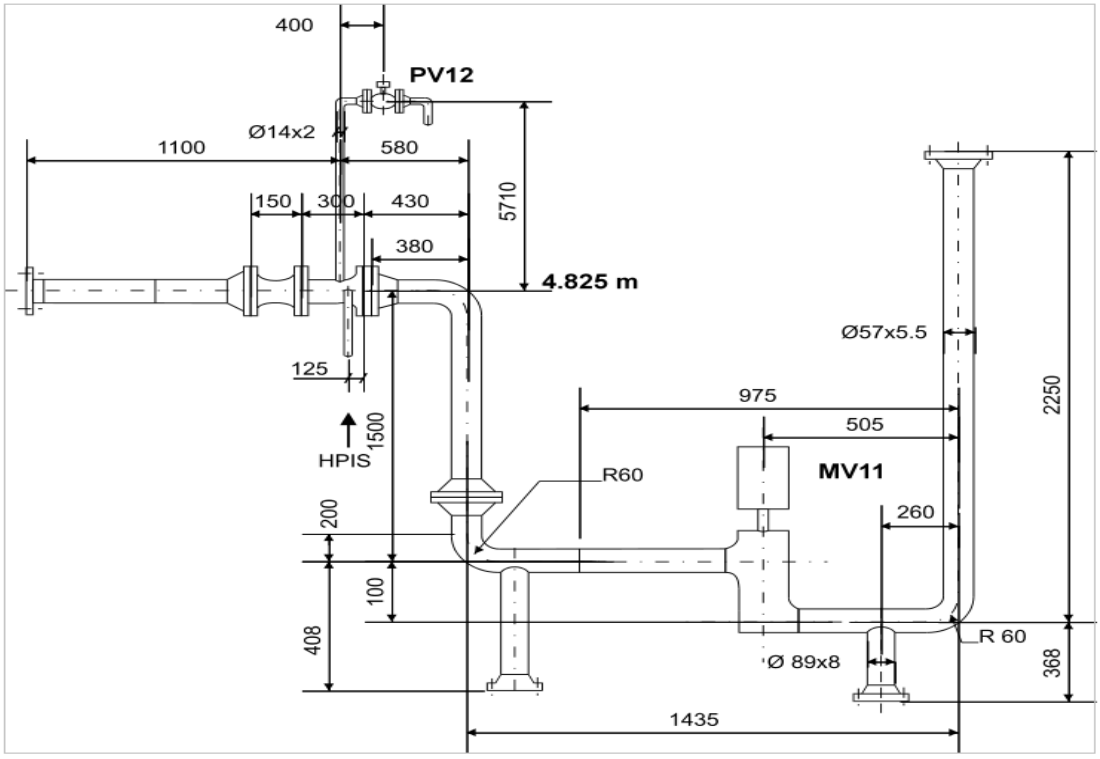

Figure A.11 Cold Leg [1], [2]

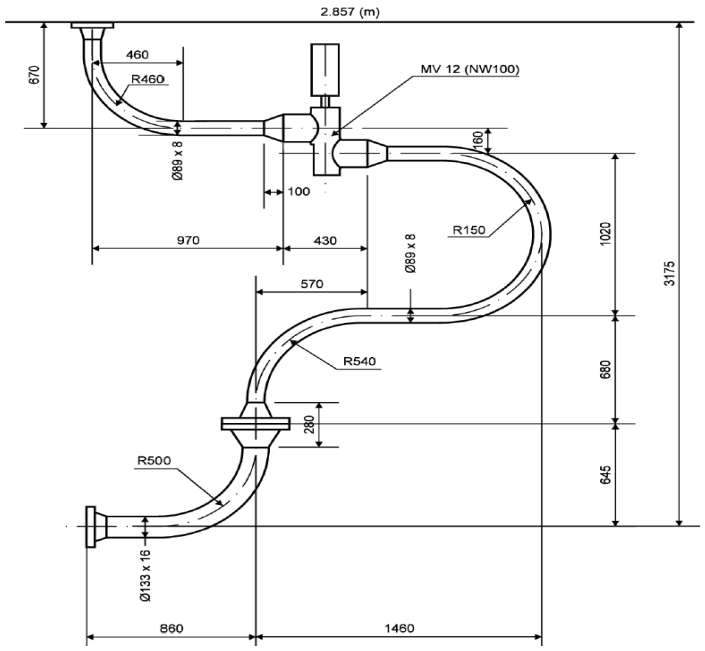

Figure A.12 Suction Side of the Pump [1]

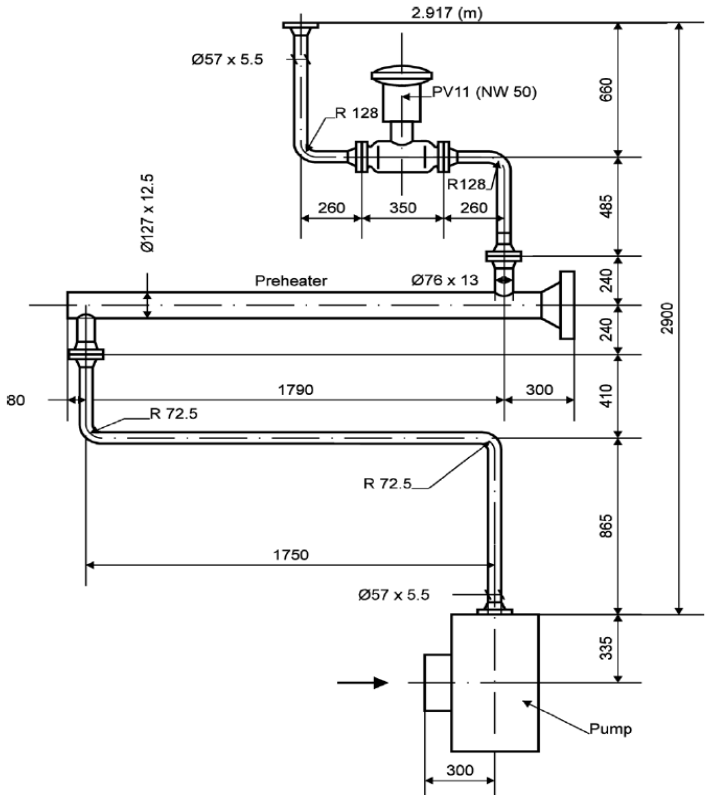

Figure A.13 Pump and Preheater [1]

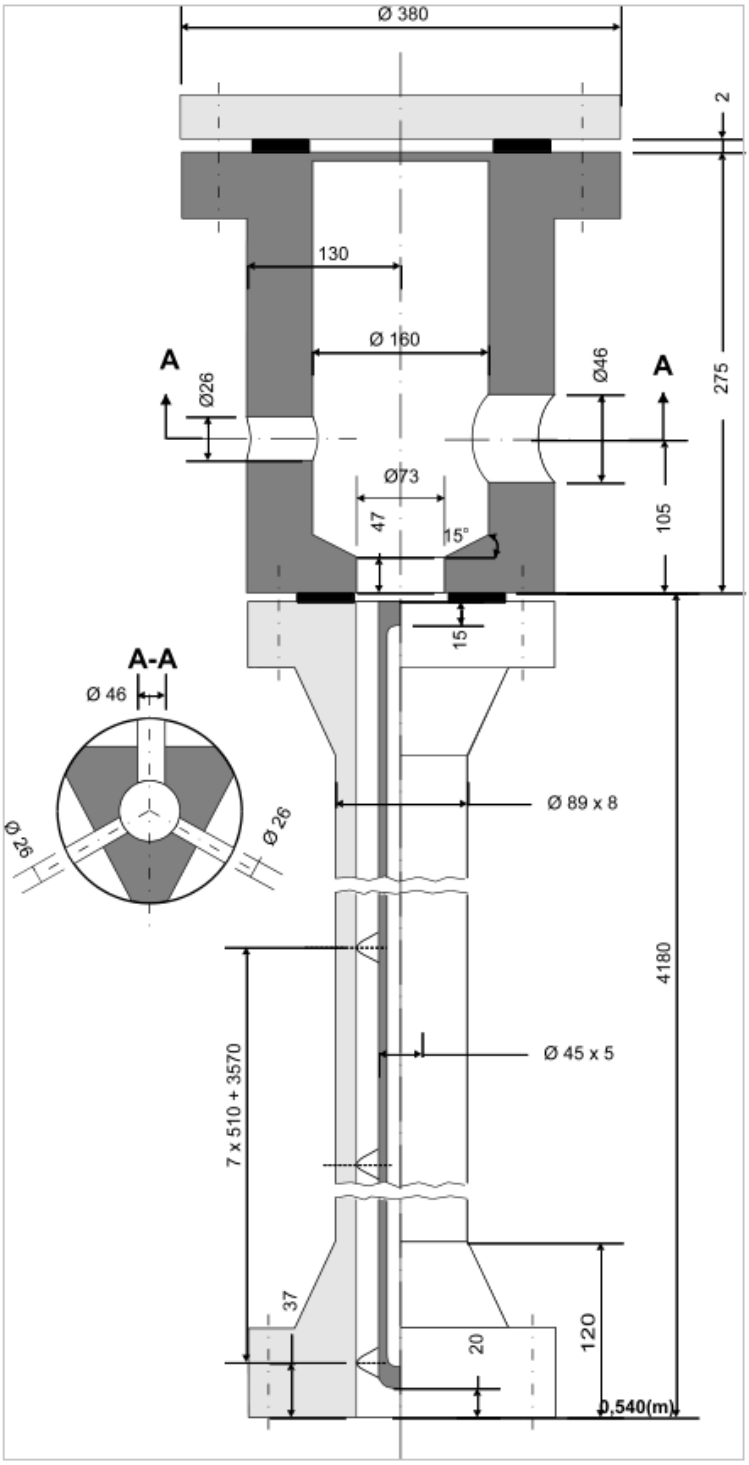

Figure A.14 External Downcomer [1], [2] (Location of the Break Flow Unit and the SIT Injection is at the Elevation A-A)

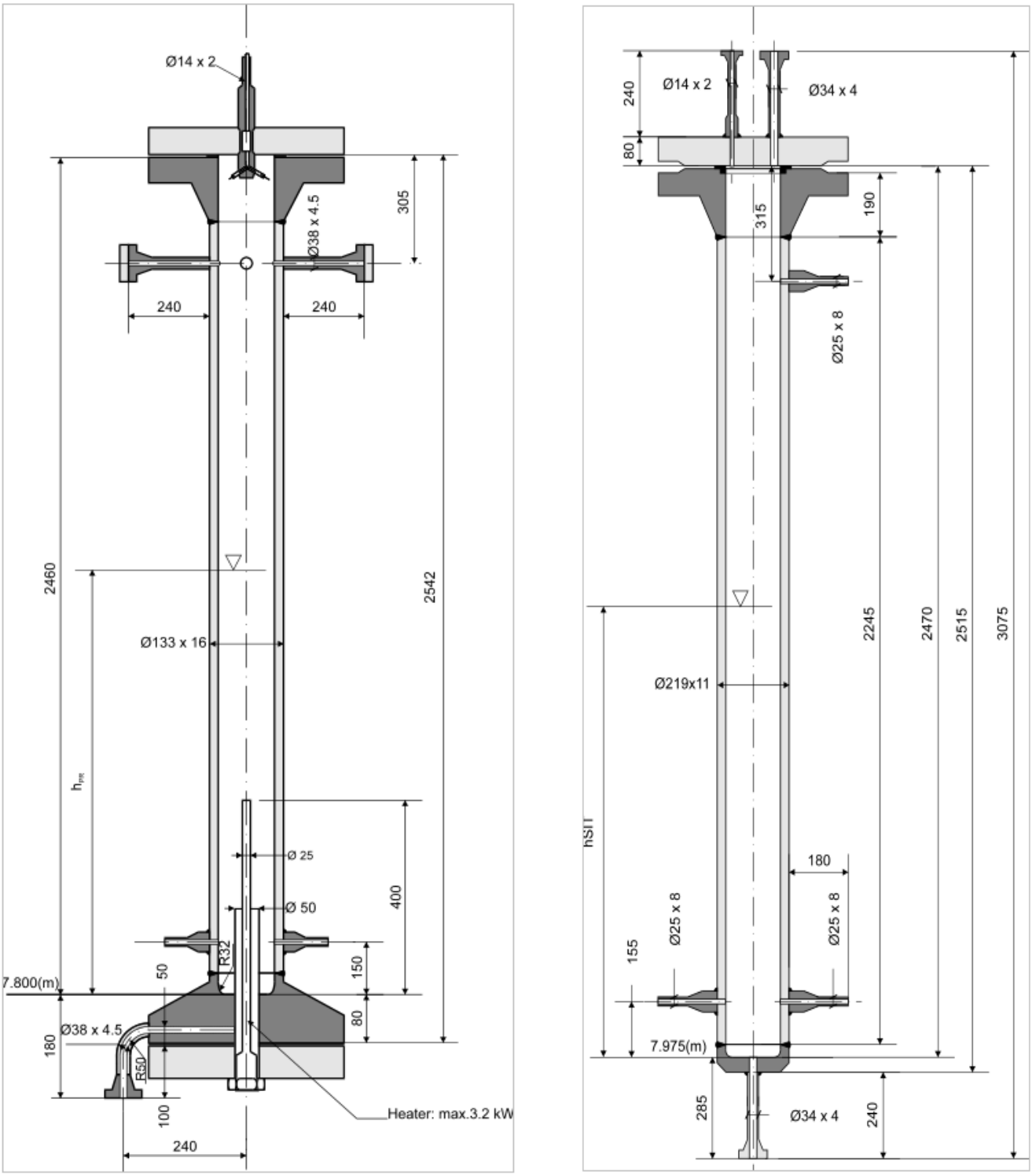

Figure A.15 Pressurizer (Left) and Hydroaccumulator (Right) [1], [2]

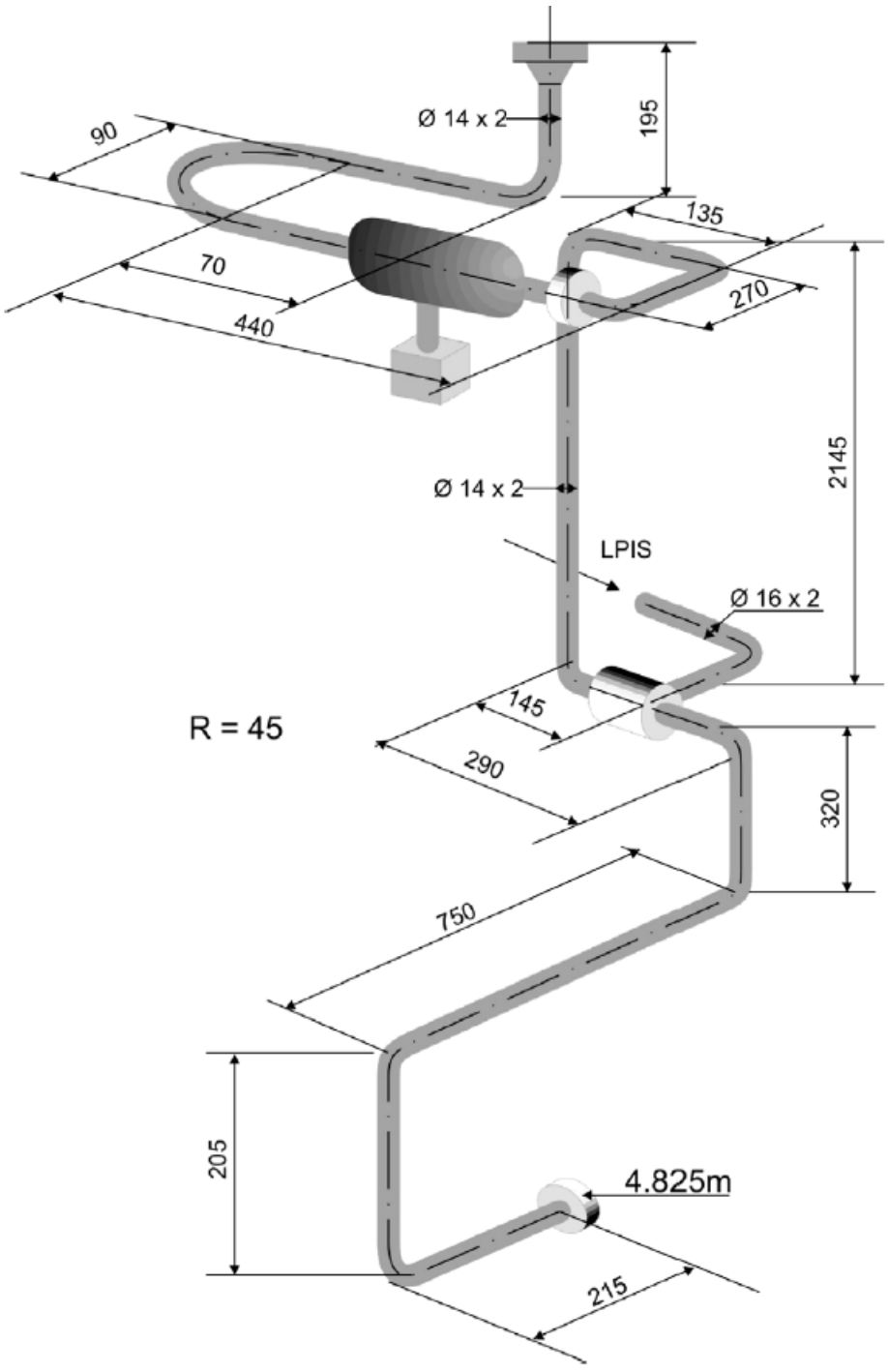

Figure A.16 Hydroaccumulator 1 Connection Line [1]

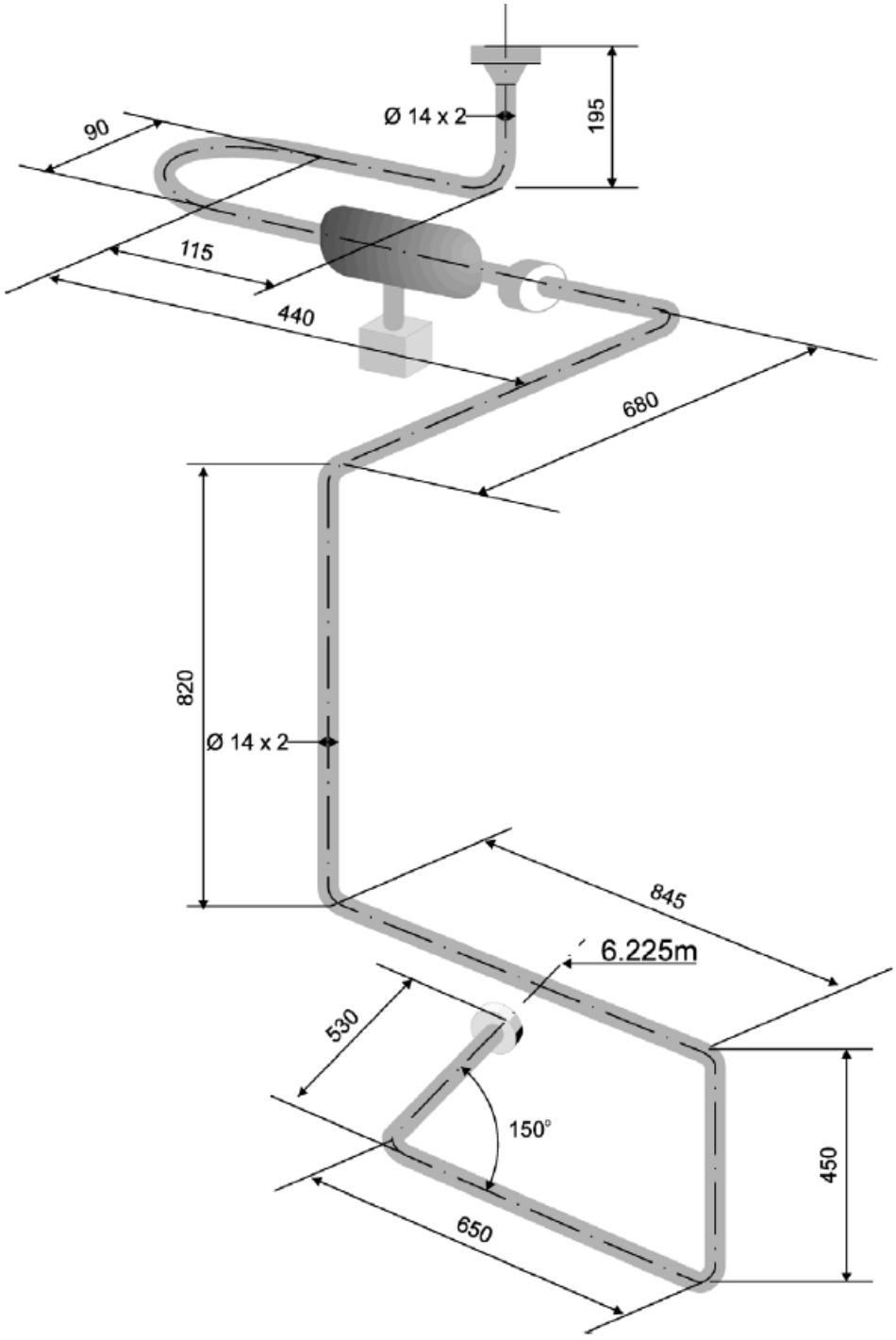

Figure A.17 Hydroaccumulator 2 Connection Line [1]

NRC FORM 335
(12-2010)
NRCMD 3.7

U.S. NUCLEAR REGULATORY COMMISSION

BIBLIOGRAPHIC DATA SHEET

(See instructions on the reverse)

1. REPORT NUMBER
(Assigned by NRC, Add Vol., Supp., Rev., and Addendum Numbers, if any.)

NUREG/IA-0533

2. TITLE AND SUBTITLE

RELAP5, TRACE and APROS Model Benchmark for the IAEA SPE-4 Experiment

3. DATE REPORT PUBLISHED

MONTH	YEAR
September	2022

4. FIN OR GRANT NUMBER

5. AUTHOR(S)

R. Orosz , T. Varju, Á. Aranyosy, V. Holl, T. Hajas & A. Aszódi

6. TYPE OF REPORT

Technical

7. PERIOD COVERED (Inclusive Dates)

8. PERFORMING ORGANIZATION - NAME AND ADDRESS (If NRC, provide Division, Office or Region, U. S. Nuclear Regulatory Commission, and mailing address; if contractor, provide name and mailing address.)

Budapest University of Technology and Economics
Institute of Nuclear Techniques
Műegyetem rkp. 3.
1111 Budapest, Hungary

9. SPONSORING ORGANIZATION - NAME AND ADDRESS (If NRC, type "Same as above", if contractor, provide NRC Division, Office or Region, U. S. Nuclear Regulatory Commission, and mailing address.)

Division of Systems Analysis
Office of Nuclear Regulatory Research
U.S. Nuclear Regulatory Commission
Washington, D.C. 20555-0001

10. SUPPLEMENTARY NOTES

K. Tien, NRC Project Manager

11. ABSTRACT (200 words or less)

One-dimensional thermal-hydraulic system codes are often used to predict and investigate different transient scenarios of NPPs. Throughout the years, numerous experimental facilities were constructed in order to simulate the accident behavior of different types of reactors. A frequently studied topic is, whether the simulation codes primarily designed to investigate western-type PWRs could describe the processes of the Russian-type reactors properly.

The main objective of this study is to investigate the SPE-4 experiment conducted on the Hungarian PMK-2 test facility with multiple system codes simultaneously. The integral test facility was operated at nominal pressures and temperatures identical of its reference plant (VVER-440/213), while the volume and power scaling ratios were 1:2070. The current experiment deals with a cold leg break of 7.4%.

The obtained results of the calculations performed with RELAP5, TRACE and the Finnish APROS codes were evaluated by comparing them to the measurement data sets. The qualitative assessment showed that each code is capable of predicting the characteristics of the major processes taking place in the reactor. In addition, a detailed quantitative analysis has also been performed with the original and improved FFT and SAR based methods. Finally, several suggestions had been made regarding the models and the methods used.

12. KEY WORDS/DESCRIPTORS (List words or phrases that will assist researchers in locating the report.)

PMK-2
SPE-4
RELAP5
TRACE
APROS
VVER
SBLOCA
FFTBM
SARBM

13. AVAILABILITY STATEMENT

unlimited

14. SECURITY CLASSIFICATION

(This Page)
unclassified

(This Report)
unclassified

15. NUMBER OF PAGES

16. PRICE

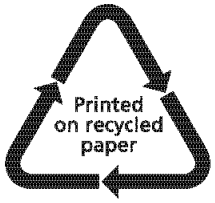

Federal Recycling Program

UNITED STATES
NUCLEAR REGULATORY COMMISSION
WASHINGTON, DC 20555-0001

OFFICIAL BUSINESS